Dispersion and dynamically one-dimensional modeling of salt transport in estuaries

Jeroen Daniëls

MSc. Thesis Hydraulic Engineering and Water Resources Management

In collaboration with:

TU Delft

NUS National University of Singapore

Deltares Enabling Delta Life

Dispersion and dynamically one-dimensional modeling of salt transport in estuaries

---

Thesis report

By Jeroen Daniëls

For the degree of Master of Science in
Hydraulic Engineering and Water Resources Management
at Delft University of Technology and National University of Singapore
To be defended on November 4 2016 at 09:00 AM in Delft, The Netherlands.

Assessment committee:

Prof. dr. ir. H.H.G. Savenije	Delft University of Technology
Prof. dr. ir. Z.B. Wang	Delft University of Technology
Ir. Z. Zhang	Delft University of Technology
Dr. ir. V.P. Chua	National University of Singapore
Dr. Y. Jing	National University of Singapore
Dr. Y. Huismans	Deltares

Key words: (alluvial) estuaries, dispersion, tidal flume experiment, mixing processes, one-dimensional numerical modeling, salinity, salt intrusion, SOBEK
Cover: Western Scheldt estuary (Satellite image by: Google maps)

Preface

This MSc thesis is the final product of my Master of Science study in Water Resources Management and Hydraulic engineering. I am glad and very grateful I was offered the opportunity to fulfill my master by participating in the double degree program organized by Delft University of Technology (TUD) and the National University of Singapore (NUS). This program did not only offer me the chance of studying at two well-known institutions, but also provided me the chance to experience what it is like to live and work in both European and Asian cultures.

Plenty of interesting topics, considering both water management and hydraulic engineering, were taught by many inspiring teachers. This provided me with valuable knowledge and an efficient work approach which was indispensable to fulfill the work needed for this thesis. One of those teachers was professor Savenije, who got me interested in the subject of salt intrusion in estuaries. His previous research provided me with a solid theoretical background. During my thesis Savenije came up with useful suggestions and ideas, wherefore I am really thankful.

Fortunately the interest in this topic is shared wider and Deltares, an independent institute of applied research in the field of water and subsurface, facilitated my research. Here I was warmly welcomed by Ymkje Huismans, who has been my daily supervisor. She really supported me with her enthusiasm and commitment. During my stay at Deltares I have had many interesting and useful discussions with Kees Kuijper, who was always willing to help me out. For this research essential adjustments to the used numerical model where made by Jan Noort, without him I would not have been able to carry out all the work I did. Some more colleagues have been involved and made some useful contributions. Ymkje, Kees, Jan and Deltares thank you a lot for your support and pleasant communion.

By reading my work and providing feedback my assessment committee allowed me to improve my work. I would like to thank professor Savenije (TUD), professor Wang (TUD), Zhilin Zhang (TUD), Vivien Chua (NUS) and Ymkje Huismans (Deltares) for taking place in my thesis assessment committee.

Intellectually my time as a TUD and NUS student was very interesting. However, my studentship would not have been the same without the people I have met over the years and became friends with. I would like to conclude this preface by thanking my parents. They always supported me and without them I would not have been able to perform my study the way I did.

Jeroen Daniëls
Delft, October 2016

Abstract

An estuary forms the transition between the ocean/sea and a river. Within its boundaries salt and fresh water mix. Fresh water intake points may be located within the reach of salt intrusion. In order to justify political and managerial decisions it is thus necessary to understand and be able to predict the process of salt intrusion in estuaries.

Within this thesis the one-dimensional modeling suite SOBEK is used to simulate salt intrusion in estuaries. Within SOBEK the one-dimensional continuity and momentum equations are used to describe hydrodynamics within the system. A state equation, relating salinity and density, is used to couple an advection-diffusion equation to the momentum equation. This advection-diffusion equation can be used to describe salt transport and makes use of a dispersion coefficient. The dispersion coefficient should capture the mixing mechanisms taking place in an estuary. Mixing mechanisms in an estuary are induced by tidal forcing, river discharge or wind and the most dominant ones are gravitational circulation and tidal pumping.

Recent validations of SOBEK have mainly focused on water levels and discharges, while less attention was payed to its capability to describe salt transport. The objective of this research is thus to obtain a better understanding of dynamic one-dimensional modeling of salt transport, validate the model and used dispersion coefficient, determine the applicability of the model and improve the dispersion coefficient based on the latest insights and recent developments.

The study is performed using two data sets. One of which is a prismatic tidal flume experiment conducted in the 60's at Delft Hydraulics. The other one is a data set considering worldwide measurements in convergent estuaries by Savenije and his students.

The nature of the considered water bodies, tidal flume and real convergent estuaries, differs much and so do the results and conclusions regarding both data sets. The first analysis performed was testing the dispersion formulation based on the one derived by Thatcher and Harleman (1972) which is currently used in SOBEK. Based on validation results for both the tidal flume experiment and real convergent estuaries and an analysis of the dispersion relation, improvements to the dispersion formulation were formulated and tested in the second phase of this research. For example, simulations for the tidal flume test showed that the model was not capable of dealing with changes in bed roughness or water depth in the tidal flume and as such terms containing those characteristics were added to the dispersion formulation.

In search of a better performing dispersion formula, the effect of the improvements to the dispersion formulation are tested. Individual adjustments were tested separately on the tidal flume simulations. More recent formulations derived by Savenije (2012), Kuijper and Van Rijn (2011), Gisen *et al.* (2015) and Zhang and Savenije (2016) are tested on the tidal flume experiment and/or real convergent estuaries . The dispersion formulations described by those researchers all contain one or more of the suggested improvements and together they contain all of the suggested improvements. For the tidal flume experiment model results using dispersion formulas derived by Thatcher and Harleman, Gisen and Kuijper and van Rijn are compared. For convergent estuaries simulations using dispersion formulas derived by Thatcher and Harleman, Gisen, Savenije, Kuijper and van Rijn and Zhang are compared.

For the tidal flume experiment the dispersion formula derived by Kuijper and van Rijn clearly performed best. This formulation relates the dispersion coefficient to the maximum flood velocity in the estuary mouth, the water depth in the estuary mouth, the estuarine Richardson number[1], the bed roughness and the relative salinity. Other formulas performed worse as they do not relate dispersion with the water depth in the estuary mouth or bed roughness.

For the convergent estuaries none of the assessed dispersion formulations performed substantially better than the others as all of them result in strong correlation between measurements and simulations. However, the simulations using the dispersion formula's described by Thatcher and Harleman (1972) and Gisen *et al.* (2015) are closer to the measurements than the other ones. The formulas described by Savenije, Kuijper and van Rijn and Zhang underestimated the salt intrusion and may potentially be improved by recalibrating the constant used.
The dispersion formulation derived by Gisen is the simplest formulation, while it performs more or less equally well than the others. Here it is therefore suggested to continue with this dispersion formula. Gisen related dispersion at the inflection point to the maximum flood velocity, the tidal excursion and the estuarine Richardson number and used the relative salinity to convert this to dispersion along an estuary. Savenije and Kuijper and van Rijn additionally included terms relating dispersion to the estuary geometry and bed roughness, however this did not lead to better results. The formulation of Thatcher and Harleman uses the estuary length, instead of the tidal excursion, as a mixing length scale. This estuary length is not well defined and lacks a physical background regarding dispersive salt transport. Therefore the formulation derived by Thatcher and Harleman is not recommended.

[1]The estuarine Richardson number is the ratio of potential energy provided by the river and the kinetic energy provided by the tide, it serves as a stratification parameter.

Nomenclature

A	is the cross-sectional area $[m^2]$
A_0	is the cross-sectional area at the estuary mouth $[m^2]$
A_1	is the cross-sectional area at the inflection point $[m^2]$
A_t	is the total cross-sectional area $[m^2]$
A_f	is the cross-sectional flow area $[m^2]$
A_{1m}	is the first order moment of the cross-section $[m^3]$
a	is the cross-sectional convergence length $[m]$
a_1	is the cross-sectional convergence length at the seaward reach of the estuary $[m]$
a_2	is the cross-sectional convergence length at the landward reach of the estuary $[m]$
$\bar{a}$	is the averaged convergence length $[m]$
B	is the estuary width $[m]$
B_0	is the estuary width at the estuary mouth $[m]$
B_1	is the estuary width at the inflection point $[m]$
B_f	is the width in the river region $[m]$
b	is the width convergence length $[m]$
b_1	is the width convergence length at the seaward reach of the estuary $[m]$
b_2	is the width convergence length at the landward reach of the estuary $[m]$
C	is the Chézy coefficient as a measure for bed roughness $[\frac{m^{\frac{1}{2}}}{s}]$
c_s	is the salt concentration $[\frac{kg}{m^3}]$
c_i	are user defined constant to chose a specific dispersion formulation $[-]$
D	is the dispersion coefficient $[\frac{m^2}{s}]$
D_0	is the salinity in the estuary mouth $[\frac{m^2}{s}]$
D_1	is the salinity at the inflection point $[\frac{m^2}{s}]$
E	is the tidal excursion ($E \approx \hat{u}T/\pi$) $[m]$
E_0	is the tidal excursion in the estuary mouth $[m]$
E_1	is the tidal excursion at the inflection point $[m]$
E_k	is the kinetic energy $[Nm]$
E_p	is the potential energy $[Nm]$
F	is the hydrostatic force $[\frac{N}{m}]$
f_1	is a constant for an additional dispersion $[\frac{m^2}{s}]$
f_2	is a constant for the dispersion coefficient $[\frac{m^3}{ppt \cdot s}]$
f_3	is a constant for the shear dispersion $[-]$
f_4	is a constant for the tidal dispersion $[-]$
g	is the gravitational acceleration $[\frac{m}{s^2}]$
H	is the tidal range $[m]$
H_0	is the tidal range at the estuary mouth $[m]$
h	is the water depth $[m]$
h_0	is the water depth in the estuary mouth $[m]$
h_1	is the water depth in the inflection point $[m]$
K	is the Van der Burgh constant $[-]$
L	is the salt intrusion length $[m]$
L_e	is the estuary length $[m]$
M	is the momentum induced by the water density and water level difference $[\frac{Nm^2}{m}]$
N_R	is the estuarine Richardson number $[-]$
P_e	is the tidal prism, the water entering the estuary from the seaside during flood $[m^3]$
Q	is the discharge $[\frac{m^3}{s}]$
Q_f	is the river water discharge $[\frac{m^3}{s}]$
R	is the hydraulic radius $[m]$

S	is the salinity in the estuary $[ppt]$
$\hat{S}$	is the maximum salinity at a certain point $[ppt]$
S_0^*	is a user defined characteristic salinity in the estuary mouth $[ppt]$
S_0	is the salinity in the estuary mouth$[ppt]$
S_1	is the salinity at the inflection point $[ppt]$
T	is the tidal period $[-]$
T_w	is the water temperature $[^\circ C]$
u	is the flow velocity $[\frac{m}{s}]$
$\hat{u}$	is the maximum flood velocity $[\frac{m}{s}]$
$\hat{u}_0$	is the maximum flood velocity in the estuary mouth $[\frac{m}{s}]$
$\hat{u}_1$	is the maximum flood velocity at the inflection point $[\frac{m}{s}]$
u_0^*	is a user defined characteristic velocity in the estuary mouth $[\frac{m}{s}]$
W	is the tidal amplitude $[m]$
x	is the distance from the estuary mouth $[m]$
x_1	is the distance the inflection point is located from the estuary mouth[2] $[m]$

α_B	is the Boussinesq constant $[-]$
α_c	is a calibration factor $[-]$
α_i	are constants $[-]$
α_G	is the mixing number at the inflection point $[m^{-1}]$
β_{rev}	is the dispersion reduction rate for reversed calculation $[-]$
δ	is the damping coefficient $[m^{-1}]$
λ	is the tidal wave length $[m]$
Φ	is a factor affecting dispersion based on estuary geometry and tidal wave propagation $[m^{-1}]$
ρ	is the water density $[\frac{kg}{m^3}]$

$\langle\rangle$	stands for tidal averaged

Abbreviations

HW	High water
HWS	High water slack
LW	Low water
LWS	Low water slack
TA	Tidal average

[2] If there is no inflection point $x_1 = 0$.

Contents

1 Introduction

The importance of the studied subject is addressed in this chapter. More specific the problem dealt with in this thesis is elaborated and the research objective is given along with the research questions. Boundaries of the research are stated and an outline of the report is given.

1.1 Background

Cameron and Pritchard (1963) defined an estuary as a semi-enclosed coastal body of water which has a free connection with the open sea and within which sea water is measurably diluted with fresh water from land drainage. As one can imagine worldwide there are many kind of estuaries. Within this research however, the focus is on alluvial estuaries and a tidal flume experiment. They are defined by Savenije (2015) as a fully alluvial estuary consisting of sediments deposited by both river and sea, in which the estuary has shaped its own bed. The main drivers affecting the characteristics of an estuary are: the tide, the river discharge, the wave conditions, the lateral sediment transport along the coast, the density difference between the fresh river and the saline sea water and the local climate (Savenije, 2015). In addition to those natural factors, mankind has a prominent influence as they regulate some systems by for example deepening the channel, dig out harbors or build constructions.

As estuaries are often densely populated and serve the needs of the inhabitants in multiple ways, local water managers and planners have to deal with conflicting interests. (Future) intake points of fresh water for different purposes may be located within the reach of salt intrusion. As those purposes require fresh water it is problematic if the water at the intake points turns saline or brackish. Human interventions (e.g. deepening of the navigation channels) and climate change (sea level rise, extremely low river discharges) can affect salt intrusion. In order to justify policy and managerial decisions it is therefore important to understand and be able to predict salt intrusion.

In order to assess changes either due to human interventions or climate change SOBEK can be used. SOBEK is the one-dimensional modeling suite of Deltares.

1.2 Problem description

SOBEK is frequently used for salt intrusion simulations, for example to evaluate the impact of changes by climate change or human interventions. At the same time the expectations of its accuracy increase. However, validations of SOBEK have mainly focused on water levels and discharge (Buschman *et al.*, 2015). That is why it is important to understand the possibilities and restrictions of this software regarding one-dimensional modeling of salt transport. In SOBEK one-dimensional advective transport is taken care of by the hydrodynamics. This leaves the one-dimensional dispersive transport as the part in need of validation.

1.3 Research objective

The objective of this thesis is to **obtain a better understanding of dynamic one-dimensional modeling of salt transport**, its possibilities and its limitations. In order to do so the model is validated for salt intrusion, its applicability is determined and the dispersion coefficient is improved based on the latest insights and recent developments.

The research questions answered in this report are:

Main question
What are the possibilities and limitations of dynamically one-dimensional modeling of salt intrusion in estuaries in SOBEK?

Sub questions

1 What are the physical processes influencing salt intrusion in estuaries?
2 What are the governing equations for one-dimensional modeling of salt intrusion in alluvial estuaries?
3 How does the dispersion formulation as derived by Thatcher and Harleman (1972)[1] perform?
4 What are possible improvements to the used dispersion formulation?
5 How do other dispersion formulations perform?

1.4 Limitations

This section clarifies the boundaries of this thesis project. This is an important aspect of the research proposal as it fits the study in a clear and outlined problem.

- The used one-dimensional software is SOBEK-3. Other software is not considered in this research.
- The focus of this thesis is on salt transportation. Hydrodynamics play a very important role herein and are therefore included in the project. Morphodynamics however act on much larger timescales (with exception of morphodynamics during flood events, but then salt intrusion is not to be concerned about) and are thus not considered within this project.
- Validation of the model is based on tidal flume experiments as performed by Rigter (1973) and measurements worldwide in real convergent estuaries by Savenije (2012).
- This research focuses on understanding the physics behind dispersive salt transport. Dispersion formulas tested are based on this physical background and originate from literature, no new dispersion formulations are derived and no calibrations are performed.
- This research focuses on salt intrusion from a sea into a river, so it is about surface water interactions.
- Within this research only cases are considered with an open connection between river and sea/ocean, in which the river discharge can flow freely in the sea/ocean and the tide can propagate in the estuary. Effects of sluices, barriers or constructions hindering flow in the estuary mouth are not part of this thesis.

[1] For some practical reasons as described by Rijkswaterstaat (1984), the formulation as used in SOBEK is edited slightly.

1.5 Outline of the report

This thesis is structured according to the research questions. After this introduction the theoretical background about salt intrusion in estuaries is given in Chapter 2. Chapter 3 explains which equations, including various dispersion formulations, are used to describe salt intrusion one-dimensionally and how those are used by SOBEK. In Chapter 4 the data and method used to assess the used software and dispersion coefficients is described. In addition a numerical sensitivity analysis is included here in order to justify the chosen time and space steps. The results using the original dispersion formula, based on Thatcher and Harleman (1972), are described in Chapter 5. In Chapter 6 is sought after an improved dispersion formulation and model results using proposed formulations are evaluated. Chapter 7 discusses the performed research and its outcomes, the possibilities and restrictions of the used model and the research limitations. In Chapter 8 conclusions and recommendations are presented.

2 Salt intrusion in estuaries

This chapter describes the main characteristics of an estuary. It is explained how the estuary is shaped, what the influence of the tide and river discharge are, which mixing processes take place within an estuary and how the salt intrudes. The chapter serves as the theoretical background of this thesis.

2.1 Estuary shape

Factors affecting the shape of an estuary are among others: tidal movement, river floods, wave action, storm action and sediment properties (Savenije, 2012). Additional to those natural factors human interventions can have a major influence on the estuary shape. Within this thesis three groups of estuary shapes are considered: prismatic, funnel and trumpet shaped estuaries (Figure 2.1). A prismatic channel has straight riverbanks, while funnel and trumpet shaped estuaries have inland converging riverbanks. The difference between the latter is that funnel shaped estuaries have only one convergence length, while trumpet shaped estuaries have a strong convergence from the estuary mouth till the inflection point and from the inflection point upstream a milder convergence.

Figure 2.1: *Left: prismatic estuary (Rotterdam Waterway), middle: funnel shaped estuary (Pungue), right: trumpet shaped estuary (ThaChin). (Google maps)*

An important factor affecting the estuary shape is the proportion between the tidal range and the river discharge and its sediments. To illustrate this imagine a prismatic channels discharging in the sea. Tidal velocities decrease in upstream direction and so erosion dominates at the downstream end of the estuary. When the river cannot compensate this erosion with its sediments, a funnel shaped estuary will form. When the river discharge and sediment load are large, it can compensate for the erosion and the prismatic channel is maintained. So, a dominant river discharges lead to channels with a long convergence length. Short convergence lengths are the result of a dominant large tidal range. It is thus the proportion between the river discharge and the tidal range which determines the shape of an estuary. In addition the mouth of an estuary can be largely affected by wave action. Waves can cause spits, bars or barrier islands to be formed, depending on the predominant direction of wave attack and on the magnitude of the waves. Strong wave action can also result in a trumpet shaped estuary, which consists of two reaches both with its own convergence lengths.

The estuary mouth is defined as the point where the estuary and ocean meet. For equations describing the estuary geometry the origin of the longitudinal axis (x=0) is located at this point and x is positive in the upstream direction. The depth of an estuary fluctuates with the meanders of flow within the estuary; it is deep in bends and shallow in crossings. However, on

average there is no bottom slope in long alluvial estuaries. There where the estuary gradually turns into a river and the river discharge becomes dominant over the tidal currents the bottom slope begins. (Savenije, 2012)

According to Savenije (2012) the geometry of an estuary can be described with Equations (2.1), (2.2) and (2.3).

$$A = A_0 e^{-x/a1} \ \ for \ \ x \leq x_1, \quad A = A_1 e^{-(x-x_1)/a_2} \ \ for \ \ x \geq x_1 \tag{2.1}$$

$$B = B_0 e^{-x/b_1} \ \ for \ \ x \leq x_1, \quad B = B_1 e^{-(x-x_1)/b_2} \ \ for \ \ x \geq x_1 \tag{2.2}$$

$$h = h_0 e^{x(a_1-b_1)/a_1 b_1} \ \ for \ \ x \leq x_1, \quad h = h_1 e^{(x-x_1)(a_2-b_2)/a_2 b_2} \ \ for \ \ x \geq x_1 \tag{2.3}$$

In which:

A	is the cross-sectional area $[m^2]$
A_0	is the cross-sectional area at the estuary mouth $[m^2]$
A_1	is the cross-sectional area at the inflection point $[m^2]$
a	is the cross-sectional convergence length[1][2] $[m]$
B	is the channel width $[m]$
B_0	is the channel width at the estuary mouth $[m]$
B_1	is the channel width at the inflection point $[m]$
b	is the width convergence length $[m]$
h	is the water depth $[m]$
h_0	is the water depth in the estuary mouth $[m]$
h_1	is the water depth in the inflection point $[m]$
x	is the distance from the estuary mouth $[m]$
x_1	is the distance the inflection point is located from the estuary mouth[3] $[m]$

An inflection point is only present in trumpet shaped estuaries, see Figure 2.1. For prismatic or funnel shaped estuaries there is no inflection point and thus $x_1 = 0$. From Equation (2.3) it follow that if a is larger than b the depth increases exponentially along the longitudinal axis, if a is smaller than b it decreases and if a equals b the depth is constant.

2.2 Tides

The cyclic fall and rise of the water level in oceans, seas and estuaries is known as the astronomical tide. The astronomical tide is the result of the complex gravitational interaction between the moon, the sun and the earth. Due to this complex interplay successive tides differ in tidal range. The tide generating capability of the Moon is twice as big as the one of the Sun, because despite that its mass is way smaller it is also significant closer to the Earth. When the Earth, Moon and Sun are in line the maximum tide occurs, which is called spring tide. When the Earth, Moon and Sun make a right angle the minimum tide occurs, which is called spring tide (see Figure 2.2). Other factors affecting tidal propagation are shoaling due to the decrease of the cross-sectional area in narrowing estuaries, damping due to friction, reflection against boundaries, deformation due to differences in tidal propagation velocities, Coriolis forces due to Earth's rotation and meteorological effects (Rijn, 2011). The difference between high water

[1] Convergence lengths are determined as the distance from the mouth at which the tangent at the mouth (x=0) intersects with the x-axis.

[2] indices 1 and 2 respectively mark before and after the inflection point.

[3] If there is no inflection point $x_1 = 0$.

(HW) and low water (LW) is known as the tidal range (H). The tide periodically fluctuates around the tidal averaged water level (TA). The time needed for one tidal wave to pass is called the tidal period (T). The occurring tides can generally be classified in three types: diurnal tides, mixed diurnal tides and semi diurnal tides. A semi-diurnal tide has almost two identical tidal cycles in a day, while a diurnal tide has just one complete tidal cycle in a day. A mixed diurnal tide has two tidal ranges in one day. Since the difference in tidal range is large, the smaller tidal range is almost insignificant when compared to the larger one (Gisen *et al.*, 2015).

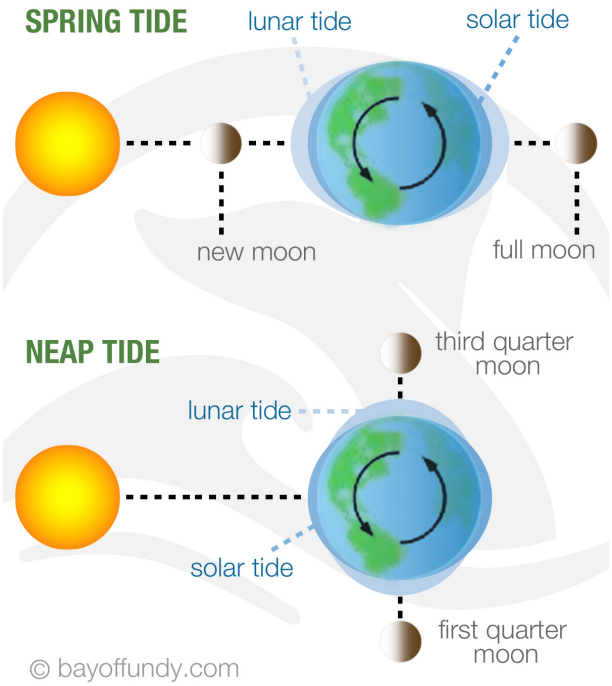

Figure 2.2: *Spring and neap tide. (Bay of Fundy, 2016)*

Next, this section continues with how the tide propagates in an estuary. Attention is paid to wave types occurring in estuaries, damping and amplification.

2.2.1 Tidal waves

The geometry strongly influences the type of tidal wave occurring in an estuary, see Figure 2.3:

- **Standing wave:** A standing wave may occur in a semi-enclosed water body (a bay or a river with closing structure). When a tidal wave enters such a water body it is reflected at its upstream end. In a standing wave HW occurs simultaneously with high water slack[4] (HWS), the same holds for LW and low water slack (LWS). The phase lag between the tidal elevation and tidal velocity is thus $\pi/2$.
- **Progressive wave:** This wave type does not occur in real estuaries as it only exists in frictionless channels with constant cross-section and infinite length. In a progressive wave high water occurs simultaneous with the maximum tidal velocity, the same holds for low water and the minimum tidal velocity. In a progressive way there is thus no phase difference between water velocity and water level.
- **Mixed wave:** In estuaries often a mixture between a progressive and standing wave occurs, a so called mixed wave. A mixed wave has a phase lag between 0 and $\pi/2$. The value of this phase lag depends on the channel geometry and the friction (Savenije, 2012).

[4] At slack tide the landward tidal current equals the seaward river current and the resulting current is zero.

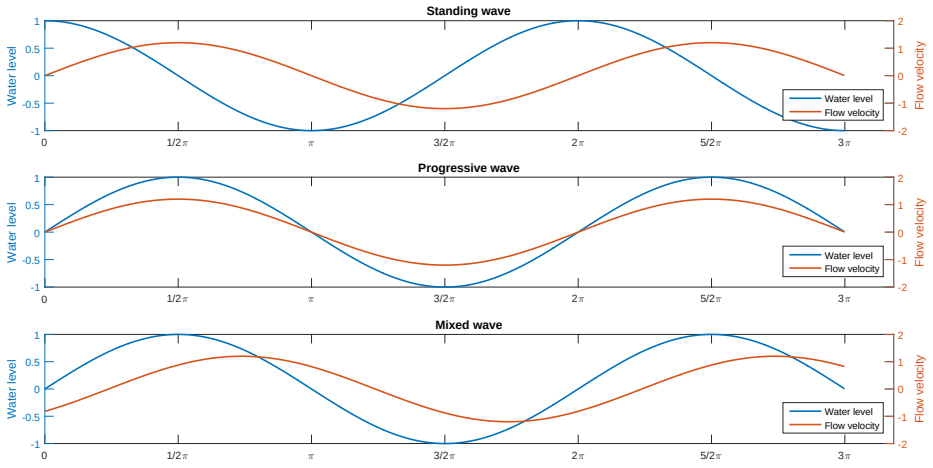

Figure 2.3: *Different tidal wave types.*

2.2.2 Damping and amplification

Jay (1991) and Savenije (1998) showed that the convergence of estuary banks and bottom friction affect the tidal range along the estuary. Convergence of estuary banks concentrates the wave energy in a smaller cross-section and thus results in an amplification of the tidal range. Friction however, dissipates wave energy and thus dampens the tidal wave. If friction is stronger than convergence the tidal range is damped. If convergence prevails over friction than the tidal range is amplified. In case the effects of convergence and friction are equal in magnitude the tidal range remains constant throughout the estuary, such an estuary is called an ideal estuary. Equation (2.4) can be used to describe the effect of damping and amplification.

$$\hat{u}_x = \hat{u}_0 e^{\delta_u x} \tag{2.4}$$

In which:

$\hat{u}_0$ is the maximum flood velocity at a certain point in the estuary $[m/s]$

$\hat{u}_x$ is the maximum flood velocity at a certain point in the estuary $[m/s]$

δ_u is the damping coefficient[5] $[m^{-1}]$

2.3 River discharge

An estuary is fed by both water from a river and a sea/ocean. During HW the ocean water flows into the estuary, resulting in a tidal velocity in upstream direction. During low water the water flows out of the estuary and the tidal velocity is in downstream direction. In addition to that there is a river discharge which results in a downstream velocity. Due to this river discharge the ebb current becomes larger and the flood current becomes smaller. If the maximum tidal current is larger than the river current, two moments of slack occur per tidal cycle. If the maximum tidal current equals the river current only one moment of slack occurs per tidal cycle. If the river current is larger than the maximum tidal current slack does not occur, here still a tidal wave is present but the flow does not changes directions anymore. Figure 2.4 illustrates the influence of river discharge for the situations mentioned above.

[5]The damping coefficient can be extracted from elevation measurements in an estuary or be extracted form a hydrodynamical model.

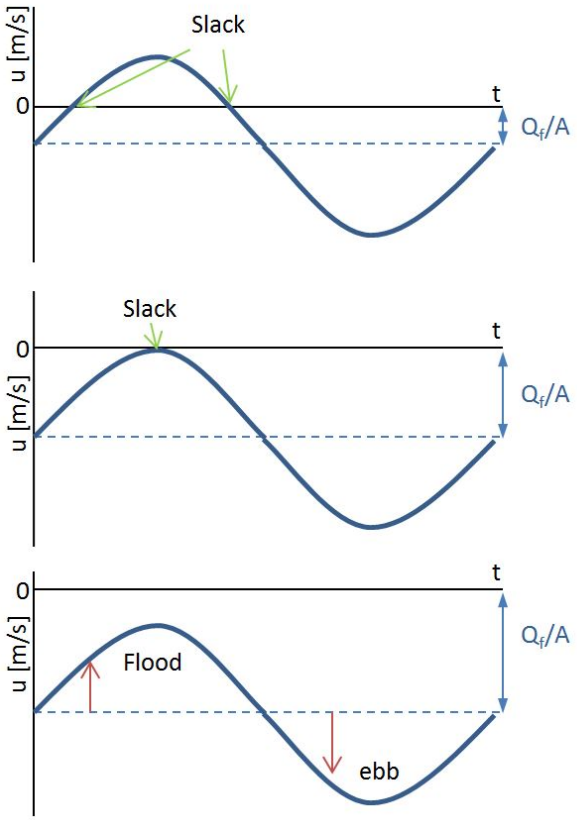

Figure 2.4: *Influence of river discharge on tidal propagation.*

2.4 Mixing processes

Here, based on the work of Fischer *et al.* (1979) and Savenije (2012), the mixing processes are classified on their driving force. Three driving forces are classified, which are mixing by the tide, river and wind. According to Savenije (2012) mixing induced by the tide and river are dominant.

2.4.1 Mixing by the tide

The tide provides the estuary with kinetic energy by rocking the water back and forward within the estuary geometry. This water movement dissipates tidal energy through mixing. Fischer *et al.* (1979) states that tidal mixing is generated in two ways: friction over the channel bottom generating turbulent mixing; and interaction of the tidal wave with the estuary bathymetry. Savenije (2012) also adds advective mixing to this list. As the tide is in most cases responsible for the dominant water movement, also the mixing processes caused by the water flow are included here. Savenije (2012) states that in most cases tidal pumping is the dominant mixing mechanism in the wider part of an estuary and in case of narrow irregular estuaries tidal trapping can be a dominant mechanism when the salinity gradient is relatively large.

2.4.1.1 Tidal trapping

Tidal trapping is the effect of side embayments and small branching channels on salt transport (Fischer *et al.*, 1979). Saline water flowing in those areas will partly remain there and mix with the estuary water at a later time. As described before, tidal waves in an estuary are of a mixed character and thus there exists a phase shift between HW and HWS. This phase shift is not significant in side embayments. When HW occurs the water in an estuary still flows upstream till HWS, in the embayment/branching channel the water starts flowing downstream from HW on. This relatively fresh water flows back in the more saline water in the main estuary channel and thus generates mixing. Tidal trapping can be an important mixing mechanism in estuaries with irregular topography, but since trapping occurs along the sides of an estuary it is relatively less important in very wide estuaries.

2.4.1.2 Residual circulation

Fischer *et al.* (1979) explains that residual circulation occurs due to averaging the velocity field at a certain point over a tidal cycle. McCarthy (1993) used a 2D-vertical model and perturbation analysis to describe the residual circulation in an estuary. He found that the buoyancy balance in an estuary is between three processes: tidal buoyancy transport (tide-driven landward transport), seaward Lagrangian tidal buoyancy transport and landward horizontal diffusive transport. McCarthy observed weak density gradients near the estuary mouth. He concluded that the density driven mixing is weak here and that the tidally driven landward buoyancy transport is dominant instead. Further upstream the density gradient increases and the density driven horizontal transport takes over to balance the Lagrangian seaward salt transport. According to Savenije (2012) the major difference between the tidal buoyancy transport and the horizontal diffusive transport is that they depend on the salinity and width and the salinity gradient respectively.

2.4.1.3 Tidal pumping

Another form of residual circulation, which was not considered by McCarthy (1993), is tidal pumping. According to Savenije (2012) it consists of two parts: residual currents over tidal flats and shallows and exchange between ebb and flood channels that meet and mix at cross-over points. In wide estuaries tidal pumping is a dominant mixing mechanism in the downstream part, where the salinity gradient is small. Below it is described in more detail.

Ebb and flood channels occur in funnel shaped estuaries if the estuary width is sufficient for those channels to develop. Savenije (2012) observed that this happens there where the estuary has a width to depth ratio of about 100 or larger. Fischer *et al.* (1979) noticed that when the estuary is wide enough and the influence of earth's rotation is noticeable due to the Coriolis[6] force currents are deflected to the right in the Northern hemisphere and to the left in the Southern hemisphere. The presence of this effect thus enhances the formation of ebb and flood channels. Figure 2.5 shows the Pungue estuary with its ebb and flood channels.
The mixing between ebb and flood channels occurs at cross-over points. According to Savenije (2012) the flood channel is significantly shorter than the ebb channel, the landward tidal velocity in the flood channel is significantly larger than in the ebb channel and the seaward tidal velocity in the ebb channel is significantly larger in the ebb channel. Due to the different travel times through both channels mixing occurs at the cross-over points. The effective longitudinal dispersion generated by this process is directly proportional to: the loop length of the ebb and flood channel system[7], the tidal excursion and the tidal pumping efficiency[8].

[6] The Coriolis effect is the effect of the turning of earth around its own axis, resulting in a curvature of flow paths.
[7] The loop length depends on the estuary width.
[8] The tidal pumping efficiency is the relative difference between flood and ebb velocities in the flood channel

Figure 2.5: *Ebb and flood channel system in the Pungue (Mozambique) (Google maps).*

2.4.1.4 Mixing in channel bends

Due to flow in a channel bend a surface slope of the water level develops, this slope drives a secondary flow which flows to the outer bend at the water surface and to the inner bend close to the bottom (Rijn, 2011). Different authors as Chant (2002), Georgas and Blumberg (2003) and Lindhart *et al.* (2015) describe the effect of stratification on this transverse mixing and come to different conclusions. What they do agree on, which should not come as a surprise, is that secondary circulation enhances transverse mixing.
Chant (2002) observed in a channel bend in the New York harbor that the strength and structure of the secondary circulation depend on the tidal forcing and river discharge. He observed that the strength of the secondary flow increases linearly with tidal forcing and that during spring tide a helical flow pattern occurs, while during neap tide a more complex flow structure consisting of two flow cells is present. For a low river flow he observes a helical flow pattern and for a high river discharge he finds that the helical flow is weaker. Chant (2002) concludes that with high river discharge or weak tidal forcing the estuary is stratified and he thus suggest that stratification reduces the strength of the secondary flow and transverse mixing.
In contradiction, Georgas and Blumberg (2003) find that stratification enhances mixing. In his three-dimensional hydrodynamic model he finds that during both flood and ebb secondary flow generates up-welling of saline water in the inner bend and down-welling of fresh water in the outer bend. This leads to a baroclinic pressure gradient directed opposite to the barotrophic gradient at the surface. During slack time, at low flow velocities the secondary flow is weak and the created baroclinic pressure gradient slowly forces the salt at the inner bend to the outer bend. Thus due to secondary circulation upwelling occurs at both the inner and outer bend at different times. Georgas and Blumberg (2003) state that this decreases the along-shore vertical steady shear dispersion of salt, and it may lead to overturning and intense vertical mixing. In addition he says that due to secondary circulation turbulent mixing is increased. Which both lead to a decrease in salt intrusion.
Lindhart *et al.* (2015) studied the secondary circulation in the Rio Magdalena (Colombia) and found that stratification has two important effects. The first is that the magnitude of secondary circulation increases in the stratified estuary due to larger transverse centrifugal acceleration as streamwise velocities increase under stratification. The second effect is the change in circulation pattern. Similar to what Chant (2002) describes she found that due to stratification two flow cells occur.

2.4.1.5 Mixing at the estuary banks

Fischer *et al.* (1979) suggests that density stratification affects transverse mixing more than vertical mixing. He based his suggestion on experiments by Sumer and Fischer (1977), who conducted two sets of stratified-flow experiments. They used a laboratory channel width a trapezoidal cross-section. In one of the experiments the channel side was smooth, while in the other one the side had a varying transverse bottom slope and thus was wavy. This waviness locally generated vertical mixing, which established transverse density gradients which induced a transverse baroclinic circulation, as is indicated by Figure 2.6. Compared to the uniform channel, the transverse mixing in the channel with the wavy slope was greatly enhanced. Fischer *et al.* (1979) state that also in real stratified estuaries transverse mixing is greatly enhanced by transverse circulation, as there bottoms also contain irregularities.

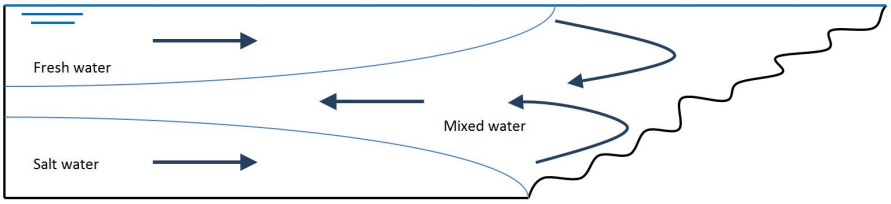

Figure 2.6: *Principle of transverse mixing due to irregular estuary banks.*

2.4.1.6 Tidal shear mixing

The water in an estuary flows in streamlines with different velocities and different directions. On top of that, they also vary in time. The water in those streamlines interact and exchange fluid, causing tidal shear mixing.

2.4.1.7 Neap-spring tide interactions

The stratification within an estuary varies between the tidal cycles. During spring tide there is more tidal energy available for mixing and the estuary is more mixed, during neap tide the estuary is more stratified. Significant mixing can be generated in the transition period between neap and spring tide.

2.4.1.8 Turbulent mixing

Along a river there is a balance between the driving forces. Those forces, friction and acceleration, are mainly components of the gravity force. The main difference is that gravity and acceleration work on all water particles, while friction only works along the bottom and estuary banks. Water flow over the bottom generates turbulence, which transfers shear stress over the cross-section and in this way affects all water particles. It is this that causes the highest flow velocities to occur at the largest distance from the estuary bed. Turbulent mixing is not a typical process occurring only in estuaries, but is present there where water flows over a bed profile. According to Savenije (2012) turbulent mixing is not an important mixing mechanism in estuaries as are gravitational mixing and other mixing mechanisms induced by the tide.

2.4.2 Mixing by the river - Gravitational circulation

In order to be in hydrostatic equilibrium the hydrostatic forces on both sides of the salt intrusion length have to be equal in magnitude, see Figure 2.7. The two balancing forces F_{saline} and F_{fresh} are described as:

$$F_s = \frac{1}{2}\rho_s g h_s^2 \tag{2.5}$$

and

$$F_f = \frac{1}{2}\rho_f g h_f^2 \tag{2.6}$$

In which[9]:

F is the hydrostatic force $[\frac{N}{m}]$
g is the gravitational acceleration $[\frac{m}{s^2}]$
h is the water depth at the riverside $[m]$
ρ is the river water density $[\frac{kg}{m^3}]$

Since $\rho_s > \rho_f$ there can only be a hydrostatic equilibrium if $h_f > h_s$. The water level difference Δh can be estimated by $\frac{\Delta\rho h}{2\rho_f}$ (Savenije, 2012). The two forces, although in balance, exert a moment (M in $[\frac{Nm^2}{m}]$) that induces the gravitational circulation, see Figure 2.7. The arm of the momentum is $\frac{1}{3}\Delta h$ and thus the moment exerted per unit volume of water and per unit width equals:

$$M = \frac{\frac{1}{3}\Delta h * \frac{1}{2}\rho g h}{\Delta x} = \frac{1}{12}\frac{\partial \rho}{\partial x} g h^2 \tag{2.7}$$

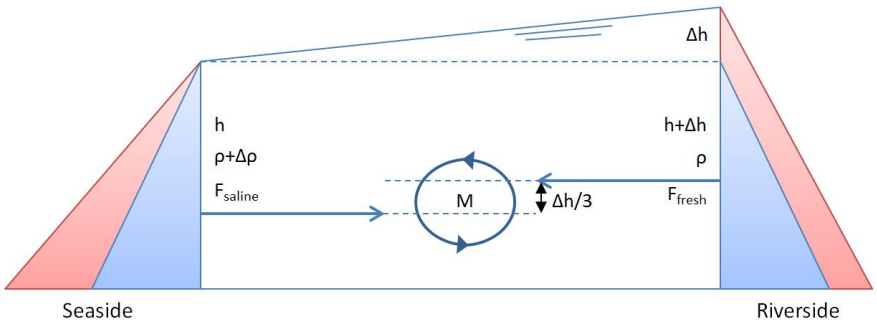

Figure 2.7: *Hydrostatic forces inducing gravitational circulation.*

According to Fischer *et al.* (1979) the potential energy provided by the river should be seen as an energy deficit which has to be overcome by the tidal energy to allow mixing. If the energy provided by the river is relatively large the estuary will be stratified. When the tide becomes more dominant, the stratification will break down and the estuary water will mix. Both for stratified and mixed estuaries a horizontal density gradient is present, and thus gravitational mixing occurs.

[9] f and s stand for fresh and salt water respectively.

Smith (1980) and West and Broyd (1981) stated that gravitational circulation is dominant in wide estuaries. According to Savenije (2012) however, gravitational circulation is dominant in near prismatic estuaries. Prismatic estuaries have recession shaped salt intrusion curve. Such an intrusion curve has relatively steep salinity gradients and thus, according to Equation (2.7), a strong gravitational circulation. In wide estuaries, with strong converging banks and a dome shaped salt intrusion curve, the salinity gradient and thus gravitational mixing only becomes strong if the estuary narrows. However, if there is a salinity gradient gravitational circulation is stronger for wide estuaries. Fischer *et al.* (1979) observed that due to a varying depth over the cross-section and that an estuary is much wider than deep, gravitational circulation drives lateral mixing rather than vertical mixing. He states that dispersion by gravitational circulation depends on the salinity gradient, the water depth and the estuary width.

2.4.3 Mixing by the wind

In estuaries wind is not a dominant driver of mixing. However, in wide estuaries it can generate both vertical and horizontal circulation. The effect wind has on the mixing process depends on the currents it induces in the vertical (Fischer *et al.*, 1979).
The shearing wind results in a surface current of relatively fresh water and a water level slope in the direction of the wind. A return flow of relatively saline water close to the bottom is induced by this water level slope. Along the interface between these two currents and through upwelling of saline water mixing occurs (Savenije, 2012).
In irregular estuaries the wind can also cause a horizontal circulation. When a wind blows over the water surface it forces to flow the water in the direction of the wind. The line of action of this force is in the centroid of the water surface. If the estuary has a irregular geometry its center of mass is shifted to the deeper side. In this case the line of action of the wind-induced force passes the center of mass of the water on the shallow side, a torque and horizontal circulation is generated (Fischer *et al.*, 1979).

2.5 Salt intrusion characteristics

This section addresses the amount of stratification in an estuary, different salinity curves and dispersive and advective salt transport.

2.5.1 Stratification

Pritchard (1955) classified estuaries into four categories, see Figure 2.8. This classification is based on vertical and lateral (in)homogeneity. The first three types are laterally homogenous, while the fourth type is laterally inhomogeneous.

- **Highly stratified**
  This type occurs when river discharge dominates the system. There is a sharp interference between the fresh and salt water in the vertical.
- **Partially mixed**
  This type occurs when both river and tide influence the system. In this case there is no sharp interference in the vertical, but a gradually changing salinity.
- **Well mixed**
  When the tidal influence dominates the system well-mixed conditions occur. The salinity is not only laterally homogeneous but also vertically.
- **Laterally inhomogeneous estuary**
  In wide estuaries the salinity distribution can be laterally inhomogeneous. The Coriolis effect and other residual circulations can gain influence resulting in lateral flows and lateral inhomogeneity.

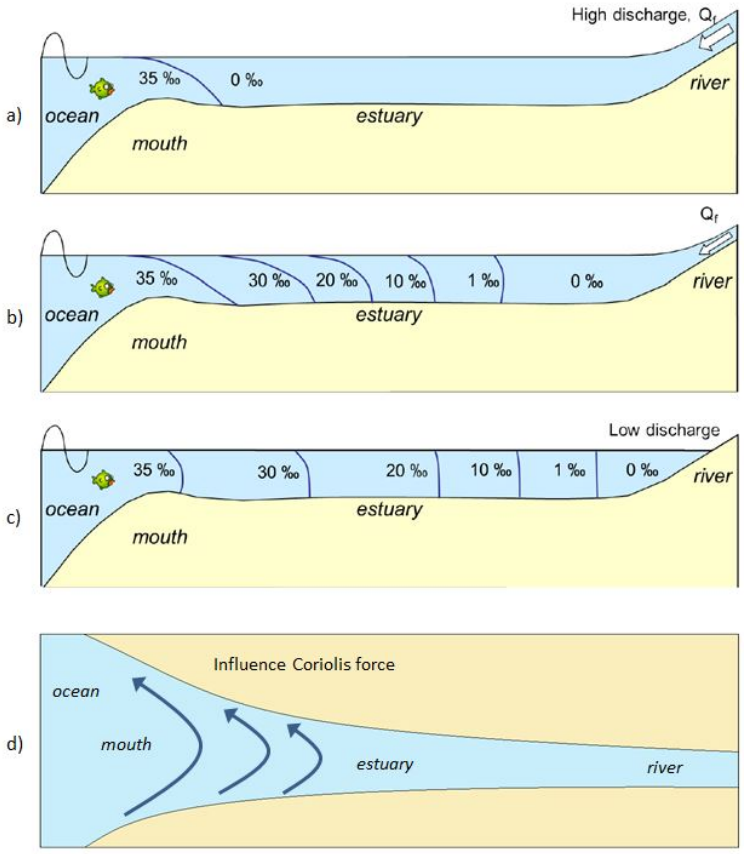

Figure 2.8: *Stratification types in estuaries: a) Highly stratified; b) partially mixed; c) well mixed (Savenije, 2012); d) laterally inhomogeneous.*

The estuarine Richardson number, Equation (2.8) is an important measure to express the amount of stratification. This number accounts for the ratio of potential energy supplied by the buoyancy of the fresh river water, $E_{p,river} = \Delta\rho g h Q_f T$, to the kinetic energy supplied by tidal movements, $E_{k,tide} = \rho u_0^2 P_e$[10]. For low numbers of N_R the estuary is well mixed, while for high numbers it is highly stratified (Table 2.1). According to Fischer *et al.* (1979) the transition occurs for N_R between 0,25 and 2,51.

Table 2.1: *Stratification and the estuarine Richardson number N_R*

Stratification	N_R
Highly stratified	>2,51
Partially mixed	0,25 < N_R < 2,51
Well mixed	<0,25

$$N_R = \frac{\Delta\rho}{\rho}\frac{gh}{\hat{u}_0^2}\frac{Q_f T}{P_e} = \frac{\Delta\rho}{\rho}\frac{g Q_f \pi}{B_0 \hat{u}_0^3} \tag{2.8}$$

[10] The tidal prism can be approximated by $P_e \approx A_0 E_0 = B_0 h_0 \hat{u}_0 T/\pi$, $E_0 = \hat{u}_0 T/\pi$.

In which:
N_R is the estuarine Richardson number $[-]$
P_e is the tidal prism, the water entering the estuary from the seaside during flood $[m^3]$
Q_f is the river water discharge $[\frac{m^3}{s}]$
T is the tidal period $[-]$

Within this study an one-dimensional approach is used and it thus is not possible to describe lateral or vertical inhomogeneous systems. Therefore the study focuses on partially to well mixed systems. However, some cases considered have a high estuarine Richardson numbers and are stratified.

2.5.2 Salinity curve

Figure 2.9 shows the salinity curve for a well mixed estuary. It contains three lines: HWS which represents the maximum salinity at a certain point along the estuary; LWS representing the minimum salinity at a certain point along the estuary and; TA representing the tidally averaged salinity. The salinity periodically varies between HWS and LWS. The horizontal distance a particle travels on average between HWS and LWS is called the tidal excursion E.

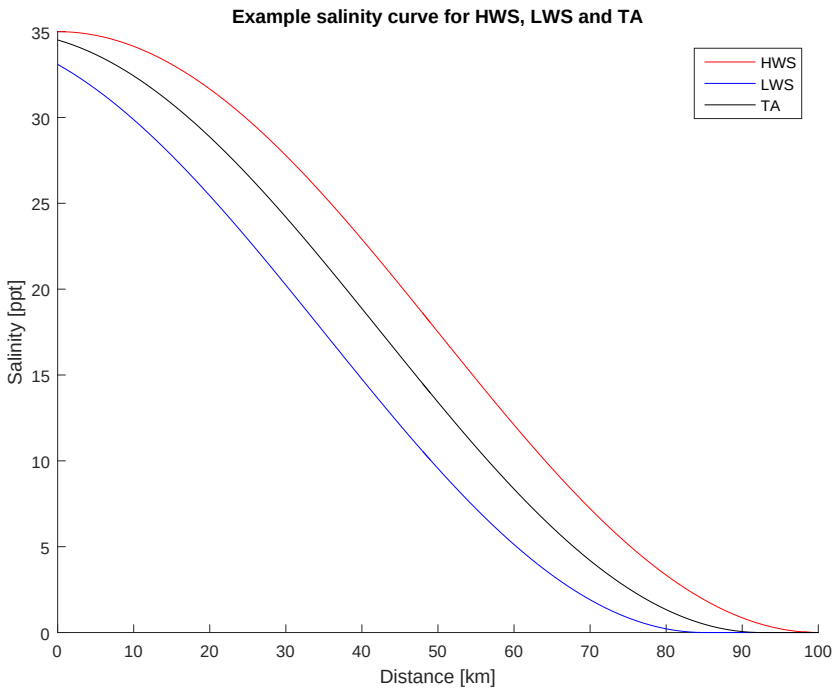

Figure 2.9: *Salinity curves for HWS, LWS and TA. The horizontal distance between HWS and LWS is the tidal excursion.*

According to Savenije (2012) four types of salinity curves can be distinguished. The key factor in which type of curve occurs is the convergence of the estuary. Figure 2.10 illustrates the different salinity curves, which are explained below.

- **Recession shaped - Type 1**
  This type of intrusion curve has a convex shape and occurs in narrow, near prismatic estuaries with high river discharges where the tidal wave dampens out. It is most common in delta's, shipping channels and riverine estuaries.
- **Bell shaped - Type 2**
  The salinity curve starts concave, but within 50% of the salt intrusion length it changes to a convex form. A bell shaped curve occurs in trumpet shaped estuaries where the convergence length close to the estuary mouth is short and long upstream of its inflection point.
- **Dome shaped - Type 3**
  This type of intrusion curve has a concave shape and occurs in funnel shaped estuaries with short convergence lengths. In those estuaries the damping of the tidal wave by friction is counteracted by the amplification of the tidal wave due to the converging geometry.
- **Humpback - Type 4**
  This is a special salinity curve which occurs if evaporation exceeds rainfall and fresh water inflow in shallow estuaries. In this case salty seawater will flow further inland. Here it evaporates, while its salt remain in the estuary and the estuary salinity increases.

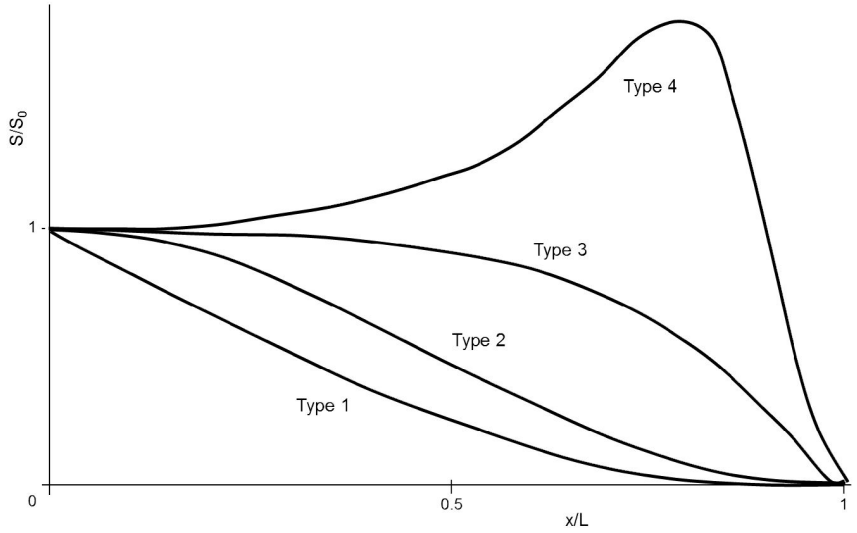

Figure 2.10: *Different types of salinity curves (Savenije, 2012).*

3 One-dimensional modeling of salt transport

Using an one-dimensional approach to describe water flow and salt transport is based on several assumptions. It is therefore not allowed to use this approach regardless. The assumptions it is based upon are according to Battjes and Labeur (2014) (Hydrodynamics) and Thatcher and Harleman (1972) (Salinity):

- The flow varies gradually in longitudinal direction. The one-dimensional approach is not valid for flow around structures/constrictions where it varies rapidly.
- The characteristic length scale is far greater than the water depth. This is valid for long waves, for example tidal waves (which are considered in this thesis), but not for short waves.
- The direction of the main flow is known beforehand by the boundary geometry and thus the main flow has a one-dimensional character.
- There is a fully hydrostatic pressure distribution[1]. This only holds when curvature of streamlines in the vertical is negligible and curvature of streamlines in bends is ignored. As a consequence of this assumption also the downstream pressure gradient is constant in a cross-section. This pressure gradient drives the water flow and thus it is feasible to work with cross-sectional averaged flow velocities.
- The salinity in the estuary is assumed to be laterally homogeneous.

In this chapter the one-dimensional hydrodynamic and salt transport equations are discussed. Special attention is given to the dispersion coefficient which is included in the salt transport equation. The chapter ends with a brief overview of the numerical software used, SOBEK-3.

3.1 Hydrodynamics

Flow in one dimension is described by the continuity and momentum equations, see Equations (3.1) and (3.2) (Deltares, 2015). Together they are known as the De Saint-Venant equations. They form a coupled set of partial differential equations which can be used to solve the two unknowns water depth h and discharge Q, given the right initial (IC's) and boundary conditions (BC's).

Continuity equation

$$\frac{\partial A_t}{\partial t} + \frac{\partial Q}{\partial x} = 0 \tag{3.1}$$

Momentum equation

$$\frac{\partial Q}{\partial t} + \frac{\partial}{\partial x}\left(\alpha_B \frac{Q^2}{A_f}\right) + gA_f \frac{\partial h}{\partial x} + \frac{gQ|Q|}{C^2 R A_f} + \frac{g}{\rho}\frac{\partial \rho}{\partial x} A_{1m} = 0 \tag{3.2}$$

[1] A fully hydrostatic pressure distribution means that all points in a cross-section have an equal piezometric level.

In which:

A_t	is the total cross-sectional area $[m^2]$
A_f	is the cross-sectional flow area $[m^2]$
A_{1m}	is the first order moment of the cross-section $[m^3]$
C	is the Chézy coefficient as a measure for bed roughness $[\frac{m^{\frac{1}{2}}}{s}]$
Q	is the discharge $[\frac{m^3}{s}]$
R	is the hydraulic radius $[m]$
α_B	the Boussinesq constant $[-]$

3.2 Salt transport

Salt transport is described by an advection-diffusion equation, see Equation (3.3). In this equation advective transport is represented by $\frac{\partial QS}{\partial x}$ and dispersive transport by $\frac{\partial}{\partial x}(A_f D \frac{\partial S}{\partial x})$. This equation is coupled to the momentum equation by a state equation which relates salinity to density. Eckart described a complex state equation which is used in SOBEK-3 (Deltares, 2015), Equation (3.4), while Kuijper and Van Rijn (2011) uses a simplified state equation, Equation (3.5). By coupling this equation to the De Saint-Venant equations, and adding an IC and BC's for salinity, the salinity S along a system can be calculated.

Salt transport equation

$$\frac{\partial A_t c_s}{\partial t} + \frac{\partial}{\partial x}\left(Q c_s - A_f D \frac{\partial c_s}{\partial x}\right) = 0 \tag{3.3}$$

Eckarts state equation relating salt concentration to density

$$\begin{aligned} \rho &= \frac{1000(Z_1 + 3S)}{0.698(Z_1 + 3S) + Z_2 - Z_3 S} \\ Z_1 &= 5890 + T_w - 0.375 T_w^2 \\ Z_2 &= 1779.5 + 11.25 T_w - 0.0745 T_w^2 \\ Z_3 &= 3.8 + 0.01 T_w \\ S &= 1000 \frac{c_s}{\rho} \end{aligned} \tag{3.4}$$

Simplified state equation used by Kuijper and Van Rijn (2011)

$$\Delta\rho \approx 0.78 S \tag{3.5}$$

In which:

c_s	is the salt concentration $[\frac{kg}{m^3}]$
D	is the dispersion coefficient $[\frac{m^2}{s}]$
S	is the salinity $[ppt]$
T_w	is the water temperature $[^\circ C]$

Dispersion and advection

The two mechanisms transporting salt in and out of an estuary are dispersion and advection. The tide and river discharge induce a movement of the water. The water along with its substances is transported land- and seaward within an estuary. This process is responsible for the advective salt transport. Thanks to the river discharge the net advective transport is in

seaward direction. On average a water particle travels with the main flow. However, due to all mixing processes described in Section 2.4 a particle may divert from this averaged tour. During this movement diluted substances, as salt, are exchanged between particles and mixing occurs, this process results in a landward dispersive transport of salt.

In a semi-steady state situation[2] the dispersive landward transport equals the advective seaward transport. Salt intrusion is thus a combination of dispersive and advective transport processes.

3.3 Dispersion coefficient

The dispersion coefficient should account for all mixing processes taking place in an estuary. In this one-dimensional approach the dispersion coefficient D should represent all processes driving dispersion, including the two- and three-dimensional processes. Defining D is not an easy task. Many researchers have tried to define an appropriate dispersion coefficient. Their work can be summarized in five categories, which are based on Prandle (1982), and the work of Savenije (2012) and Kuijper and Van Rijn (2011):

- D is a constant
- D is proportional to $\frac{\partial S}{\partial x}$
- D is proportional to $(\frac{\partial S}{\partial x})^2$
- D is proportional to S^K (Savenije (2012))
- D depends on local parameters only (Kuijper and Van Rijn (2011))

Hereafter, the in this research considered dispersion formulations are described. Those used for further calculations are limited to ones proportional to either $\frac{\partial S}{\partial x}$ or S^K. According to Savenije (2012) a dispersion coefficient proportional to $\frac{\partial S}{\partial x}$ is justified for fully density driven mixing while a proportionality to S^K is applicable for both density and tidal driven mixing. According to Preddy (1954) and Ippen and Harleman (1961) dispersion is at its maximum in the estuary mouth and decreases in upstream direction, which is in agreement with a proportionality to S^K. The other categories are not included in this research because a constant dispersion coefficient cannot represent all physical processes, the option of a dispersion coefficient dependent on local parameters only is not included in the used software and a proportionality to $(\frac{\partial S}{\partial x})^2$ would only be suitable for a case with a lateral and longitudinal density driven dispersion while here is sought after an universal formula.

3.3.1 Thatcher and Harleman

Thatcher and Harleman (1972) defined a dispersion formula based on field observations in three estuaries in the USA and on a tidal flume experiment. Within their formula they made distinction between shear dispersion which is not related to the salinity and is for example also present in rivers, first part of Equation (3.6), and tidal dispersion which is related to the salinity gradient, second part of Equation (3.6). This relation between dispersion and the salinity gradient especially represents dispersion due to gravitational circulation.

$$D(x,t) = f_3 h(x,t)\frac{\sqrt{g}}{C(x)}|u(x,t)| + f_4 L_e^2 \frac{\hat{u}_0}{\hat{S}_0} N_R^{1/4} \left|\frac{\partial S(x,t)}{\partial x}\right| \tag{3.6}$$

[2] This means that the tidal averaged salt intrusion is in steady state while the actual salt intrusion varies between HWS- and LWS-intrusion.

In which:
f_3 is a constant for the shear dispersion $[-]$
f_4 is a constant for the tidal dispersion $[-]$
L_e is the estuary length[3] $[m]$
$\hat{S}_0$ is the maximum salinity in the estuary mouth $[ppt]$
u is the flow velocity $[\frac{m}{s}]$

3.3.2 Savenije

Savenije (2012) defined a empirical dispersion formula based on a large number of real estuaries world wide. This formula is shown in Equation (3.8) and makes use of Equation (3.7) directly relating high water slack dispersion and salinity. Here the length scale is taken as the tidal excursion E as it is the length over which mixing takes place and the velocity amplitude is taken as a scale for shear and subsequent mixing. The term $\frac{h_0}{\bar{a}}$ is added to account for the estuary geometry. This formulation is not applicable in prismatic channels as for those the convergent length will go to infinity, and thus the dispersion would become zero.

$$\frac{D_x^{HWS}}{D_0^{HWS}} = \left(\frac{S_x^{HWS}}{S_0^{HWS}}\right)^K \tag{3.7}$$

$$D_0^{HWS} = 1400 u_0 E_0 N_R^{0.5} \frac{h_0}{\bar{a}} \tag{3.8}$$

In which:
$\bar{a}$ is the averaged convergence length[4]
D_0 is the salinity in the estuary mouth $[\frac{m^2}{s}]$
E_0 is the tidal excursion in the estuary mouth ($E_0 \approx \hat{u}_0 T/\pi$) $[m]$
K is the Van der Burgh constant[5] $[-]$

3.3.3 Kuijper and van Rijn

Kuijper and Van Rijn (2011) modified the equation described by Savenije (2012). What they sought after was an expression for D_0 valid for both prismatic and convergent channels and to eliminate the Van der Burgh parameter K. Based on Ippen and Harleman (1961) they added a friction parameter to account for vertical mixing related to the ratio of dissipated energy by means of bed friction and gained potential energy of the fresh river water due to an increase in density.

In their approach Kuijper and Van Rijn (2011) state that the used dispersion formula should give the same result no matter where in the estuary the mouth is defined. Using Equations (2.1), (2.2), (2.3), (2.4) and (3.5) they derived a relation between the local dispersion coefficient and the mouth dispersion coefficient as is shown in Equation (3.9). The addition of $e^{\Phi x}$ makes

[3] The estuary length is taken as the length where an estuary is closed off or where the estuary width equals the river width.

[4] the convergence length averaged over the salt intrusion length, $\bar{a} = \frac{a_1 x_1 + a_2 (L - x_1)}{L}$, in which L is the maximum salt intrusion length.

[5] Savenije (2012) estimates K by $K = 0.3 * 10^{-3} (\frac{E}{H})^{0.65} (\frac{E}{C^2})^{0.39} (1 - \delta_u b)^{-2.0} (\frac{b}{a})^{0.58} (\frac{Ea}{A_0^T})^{0.14}$, in which H is the tidal range $[m]$, δ_u the damping coefficient $[m^{-1}]$.

this relation valid locally, as this term accounts for the convergence (a and b) of the estuary geometry and the damping of the tidal wave (δ_u). It should be noticed that value of $\frac{1}{2}$ is equal to the power of N_R which is used to calculate D_0, this is in agreement with the used derivation.

$$D_x^{HWS} = e^{\Phi x} D_0^{HWS} \left(\frac{S_x^{HWS}}{S_0^{HWS}} \right)^{\frac{1}{2}}$$
$$\Phi = \frac{\delta_u}{2} + \frac{3(a-b)}{2ab} + \frac{1}{2a} \tag{3.9}$$

Kuijper and Van Rijn (2011) made a distinction between convergent and prismatic channels and came to the following relations for D_0^{HWS}.

Convergent estuaries

$$D_0^{HWS} = \alpha_c 60 \hat{u}_0 E_0 N_R^{\frac{1}{2}} \frac{h_0}{\bar{a}} \frac{C}{\sqrt{g}}$$
$$(\frac{\bar{a}}{E_0} < 10) \tag{3.10}$$

Prismatic channels

$$D_0^{HWS} = \alpha_c 6 \hat{u}_0 h_0 N_R^{\frac{1}{2}} \frac{C}{\sqrt{g}}$$
$$(\frac{\bar{a}}{E_0} \geq 10) \tag{3.11}$$

In which:
α_c is an additional calibration factor, default value $\alpha_c = 1$, and $0.7 \leq \alpha_c \leq 1.3$.

3.3.4 Gisen

Gisen (2015) used eight dimensionless parameters to form a number of dispersion coefficients which hold at the inflection point (or mouth in case of a funnel shaped or prismatic estuary). She used a multiple regression analysis to determine the coefficient in those formulations. She indicated three formulations as most promising for further investigation, of which one is selected for this research. In her analysis the other two did not result in significantly better results. In addition they had a negative correlation to C, which can be argued to be physically incorrect as a smoother channel is expected to result in more intrusion. Gisen *et al.* (2015) makes use of Equation (3.12), relating tidal averaged dispersion and salinity, and Equation (3.13) to predict the dispersion at the inflection point. When there is no inflection point, the formula can be used to predict the mouth dispersion.

$$\frac{D_x^{TA}}{D_1^{TA}} = \left(\frac{S_x^{TA}}{S_1^{TA}} \right)^K \tag{3.12}$$

$$D_1^{TA} = 0.1167 \hat{u}_1 E_1 N_R^{0.57} \tag{3.13}$$

In which:

D_1 is the salinity at the inflection point $[\frac{m^2}{s}]$
E_1 is the tidal excursion at the inflection point $[m]$
K is the Van der Burgh constant[6] $[-]$
$\hat{u}_1$ is the maximum flood velocity at the inflection point $[\frac{m}{s}]$

As in SOBEK-3 it is not possible to indicate an internal point to define dispersion along an estuary, Equation (3.14) is included here. This equation can be used to analytically calculate dispersion in the estuary mouth from the predicted dispersion at the inflection point (Gisen *et al.*, 2015). This mouth dispersion is than related to the salinity in order to calculate dispersion along the estuary.

$$
\begin{aligned}
&D_0^{TA} = D_1^{TA}\left(1 + \beta_{rev}^{TA}[1 - e^{-\frac{x_1}{a_1}}]\right) \\
&with:\ \beta_{ref}^{TA} = \frac{K a_1}{\alpha_G^{TA} A_1} \\
&and:\ \alpha_G^{TA} = \frac{D_1^{TA}}{|Q_f|}
\end{aligned}
\tag{3.14}
$$

3.3.5 Zhang

Zhang and Savenije (2016) studied the effect of residual circulations by interacting ebb and flood channels that develop in wider estuaries and how it can be combined in the regular one-dimensional advection-dispersion equation. Water particles in the middle of an estuary channel can mix longitudinally and laterally within their respective mixing lengths, the tidal excursion E and half the estuary width B. Based on the assumption that lateral exchange is proportional to longitudinal exchange (Fischer *et al.*, 1979), Zhang and Savenije (2016) derived a dispersion coefficient incorporating lateral exchange flow (Equation (3.15)).

$$
D = 0.1 \hat{u}_x E_x N_{R,x}^K \left(1 + 10\left(\frac{B_x}{E_x}\right)^2\right) \tag{3.15}
$$

In which:

B_x is the local estuary width $[m]$
E_x is the local tidal excursion $[m]$
K is the van der Burgh constant[7] $[-]$
$N_{R,x}$ is the local estuarine Richardson number
$\hat{u}_x$ is the local maximum flood velocity $[m]$

[6] Gisen *et al.* (2015) defined K as $K = 8.03 * 10^{-6}(\frac{B_f}{B_1})^{0.30}(\frac{g}{C^2})^{0.09}(\frac{E_1}{H_1})^{0.97}(\frac{h_1}{b_2})^{0.11}(\frac{H_1}{h_1})^{1.10}(\frac{\lambda_1}{E_1})^{1.68}$, in which B_f is the river width $[m]$, λ is the length of the tidal wave $[m]$ with boundary condition at the inflection point. E_1 $[m]$ is estimated by $\hat{u}_1 T/\pi$, where $\hat{u}_1 = 1m/s$

[7] Zhang and Savenije (2016) state that when information is lacking K can be taken as 0,58 as a good starting value. If more data is available $K = \frac{2+w}{3+2w}$ can be used to calculate K, in which $w = \frac{7{,}2E|Q_f|}{7{,}7*10^{-4}\sqrt{g}H^2 A_1 CT}\frac{L}{S_1}$. Calculated values range between $\frac{1}{2}$ and $\frac{2}{3}$. It should be noticed that in their predictive equation for K it depends on the river discharge and is thus not constant for an estuary.

It should be noticed that this formulation does not predict a value for the dispersion coefficient at the estuary mouth or inflection point which can be converted to dispersion at a certain point in the estuary by relating it to the salinity. It predicts dispersion at every point along an estuary based on its local values.

3.4 SOBEK

SOBEK-3, the one-dimensional modeling suite of Deltares, has been used to simulate the salt intrusion process. The equations it uses are described previously in this chapter. As SOBEK-3 uses a numerical approach the equations are discretized in space and time.

3.4.1 Numerical routine

Figure 3.1 shows the computational routine which is used by SOBEK-3 (Noort, 2016). In order to describe the system hydrodynamics the De Saint-Venant equations, Equations (3.1) and (3.2), are solved in the first box of the routine. After that the dispersion coefficient is calculated based on the hydrodynamics of the current time step and the salinity of the previous time step. With the known hydrodynamics and dispersion coefficient at the considered time step the salt transport Equation (3.3) is solved and a new salinity profile is calculated. For the next time step the same routine is used, starting with hydrodynamics, then dispersion and finally salt transport and so on.

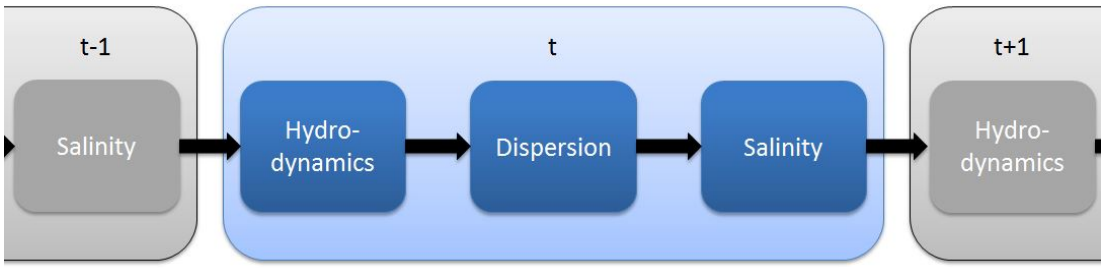

Figure 3.1: *Routine used for numerical calculations.*

In order to solve the set of equations the right IC's and BC's have to be provided. The IC's which have to be specified are:

- Water level in the entire channel
- Discharge in the entire channel
- Salinity profile

The BC's which have to be specified are:

- Downstream water level
- Upstream discharge
- Downstream salinity
- Upstream salinity

3.4.2 Dispersion coefficients

SOBEK-RE, an older version of SOBEK, had several options for the dispersion coefficient. Among which an slightly adjusted form of the Thatcher and Harleman formulation. In a beta-version of SOBEK-3 a new dispersion formula is included offering more degrees of freedom. Below the options both versions of the software offered are explained.

3.4.2.1 SOBEK-RE

The dispersion formulation in SOBEK-RE consisted of four parts, see Equation (3.16), which can be used in different configurations (Deltares, 2012).

$$D(x,t) = f_1(x,t) + f_2(x,t)\left|\frac{\partial S(x,t)}{\partial x}\right| + f_3(x,t)h(x,t)\frac{\sqrt{g}}{C(x)}|u(x,t)| + f_4(x,t)L_e^2\frac{u_0^*}{S_0^*}\left(\frac{\Delta\rho}{\rho}\frac{gh_0}{\hat{u}_0^2}\frac{Q_f T}{P_e}\right)^{1/4}\left\langle\left|\frac{S(x)}{S_0}\frac{\partial S(x)}{\partial x}\right|\right\rangle \tag{3.16}$$

In which:

f_1 till f_4	are user defined constants. Those could be chosen as a constant, defined locally or changing in time.
u_0^*	is a user defined characteristic velocity in the estuary mouth $[\frac{m}{s}]$
S_0^*	is a user defined characteristic salinity in the estuary mouth $[ppt]$
$\langle\rangle$	stands for tidally averaged.

The options which the user has are, using:

- f_1: using a spatial or time dependent distribution.
- f_1 and f_2: extension of the first option with a linear dependency on the salinity gradient.
- f_1, f_3 and f_4: a formulation based on the dispersion equation defined by Thatcher and Harleman (1972).

Of those the last option has most physical background and therefore more attention is payed to this option. As mentioned this formulation is based on the one as derived by Thatcher and Harleman (1972). For practical reasons some adaptations have been included in the dispersion coefficient used in SOBEK-RE. The differences are that in the part containing f_3 the Chézy coefficient is used instead of Mannings n, a term $\frac{S(x,t)}{S_0(t)}$ is added to make the dispersion coefficient decrease faster as this improved model results, and Thatcher and Harleman define u_0^* equal to $\hat{u}_0$ while in SOBEK-RE it has a fixed value since it was discovered that otherwise it would not physically represent the processes going on in the tidal flume test (Rijkswaterstaat, 1984). This last point follows from the analysis that for increasing tidal amplitude the dispersive salt transport in the flume decreased. As is seen in Section 6.1.9, this is only simulated when the fixed value u_0^* is used.

3.4.2.2 New formula

In SOBEK-3 a new dispersion formula (Equation (3.17)) is implemented which can be transformed in the previously mentioned dispersion formulas of Thatcher and Harleman, Savenije, Kuijper and van Rijn, Gisen and Zhang, by choosing the right coefficients. This formula is pretty long and may cause suspicions of data fitting. That is not the case as different terms in the formula can be "switched" off by setting the respective coefficient as 0. All terms included are based on a physical background which will be explained later.

$$D = c_1 u(x,t) h(x,t) \frac{\sqrt{g}}{C} + c_2 \hat{u}_0^{c_3} E_0^{c_4} N_R^{c_5} \left(\frac{C}{\sqrt{g}}\right)^{c_6} \left(\frac{h_0}{a}\right)^{c_7} \left(\frac{h_0}{E_0}\right)^{c_8} \left(1 + c_9 \left(\frac{B_0}{E_0}\right)^2\right) \left\langle \frac{S}{S_0} \right\rangle^{c_{10}} \left\langle \left| \frac{\partial S}{\partial x} \right| \right\rangle^{c_{11}} \tag{3.17}$$

In which:
c_1 till c_{10} are user defined constant, which should be chosen according to the dispersion formula used.

4 Methodology

This chapter addresses the data used for this research. After explaining which data is used, it is explained how it is used to simulate salt intrusion and how model results are evaluated. The final part of this chapter includes a numerical sensitivity analysis which justifies the chosen time and space steps.

4.1 Data

This research is based upon two data sets. The first data set used is the one obtained by Rigter (1973) in a tidal flume experiment. The second data set is set up by Savenije and considers real convergent estuaries.

4.1.1 Tidal flume test

Rigter (1973) studied the intrusion of seawater in estuaries at the Delft Hydraulics Laboratory. For his study he used a tidal flume. This flume had a rectangular cross-section, 0,672 meter wide and 0,50 meter high, and was 100 meter long. At the upstream end of the flume a fresh water discharge was supplied. Downstream of the flume a sea basin with a periodic tidal movement of the water level was located (Figure 4.1). The water level in the basin was regulated by a controlled spillway and at the bottom of the basin saline water was pumped in to control the salinity. The exact salinity in the flume mouth is not known, therefore it is assumed that the fresh water discharge is not directly flushed away and the salinity in the mouth behaves following a sinus profile.

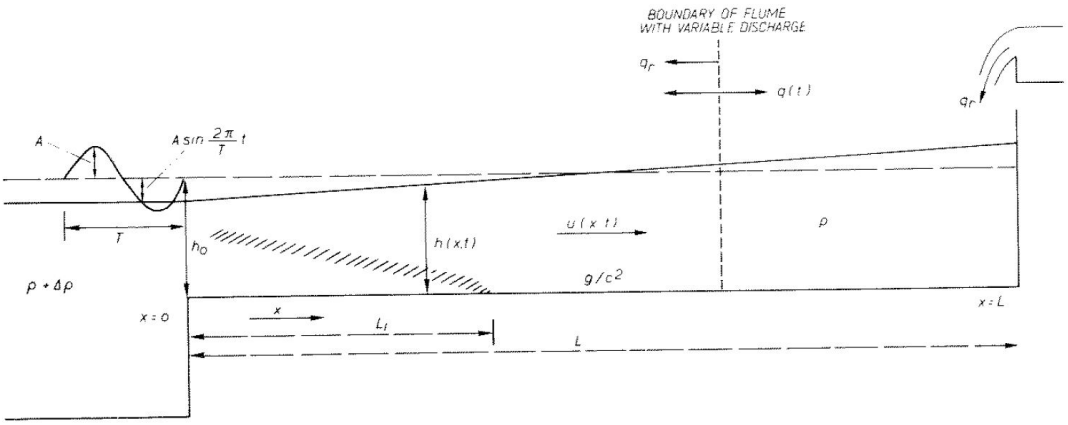

Figure 4.1: *Set up of the tidal salinity flume. (Rigter, 1973)*

In his study, Rigter (1973) investigated the effect on the salt water intrusion length by changing some variables in the model setup. The variables Rigter changed were the tidal amplitude W, the Chézy coefficient C, the water depth h, the flume length L_e[1], the fresh water discharge Q and the relative density difference between the fresh- and saline water $\Delta\rho/\rho$. Rigter started with a reference test and studied the effect of all variables separately by both increasing and decreasing them. For calculations the dimensions of the flume test were scaled to prototype (see Appendix A), the prototype width was 430 meters and the tidal period 44700 seconds.

[1] Rigter (1973) was not able to actually change the flume length. In order to test the effect of a changing flume length he had to be inventive. What he did was supplying a variable discharge at the upstream end of the tidal flume. This made it possible to imitate tidal movements which would occur in flumes with another length.

Table 4.1 shows the prototype values used for the different variables in the flume test, the values in bold style are the ones describing the reference case. Appendix A includes the full data set used for the tidal flume tests. In order to validate the model the maximum and minimum salt intrusion lengths are used as a measure. It is preferable to have some kind of longitudinal salinity profile to check the fit of the modeled salinity curve, but for the tidal flume test those data is not available.

Table 4.1: *Prototype values for the flume test variables*

Variable	**W**	**C**	**h**	L_e	**Q**	$\Delta\rho/\rho$
Units	m	$m^{1/2}/s$	m	m	m^3/s	$-$
				67.859		
	0,4			72.538	473	0,0045
	0,5	40	9,98	86.579	592	0,0066
	0,6	50	12,03	100.621	711	0,0137
Reference case	**0,8**	**60**	**13,82**	**114.662**	**949**	**0,0215**
	1,2	70	16,00	128.698	1896	0,0290
	1,6	80	17,02	161.459	2845	0,0355
	2,4	90	19,98	194.221	3801	

4.1.2 Real convergent estuaries

Savenije, and his students, did field surveys in many estuaries all over the world. The data he collected can be separated in geometry data and water flow data. Below a list is presented which shows which data is used for this research, in Appendix B Savenije's data set used is included. It should be noted that the geometry of the estuaries is idealized in this approach.

- Geometry:
  - A_0: The cross-sectional area in the estuary mouth [m^2]
  - a: The cross-sectional convergence length [m]
  - B_0: The channel width in the estuary mouth [m]
  - B_f: The channel width in the river region [m]
  - b: The width convergence length [m]
  - h: The water depth along the estuary [m]
  - h_0: The water depth in the estuary mouth [m]
  - x_1: The inflection point (in case of a trumpet shaped estuary, in this case the convergence lengths have to be determined for both sections before and after the inflection point) [m]
- Water flow:
  - H_0: The tidal range [m]
  - C: Chezy coefficient[2] [$m^{\frac{1}{2}}/s$]
  - Q_f: The fresh water discharge [m^3/s]
  - S_x: The salinity along the estuary [ppt]
  - T: The tidal period [s]

Additionally, water levels along the estuary have to be measured. From those elevations damping or amplification of the tidal wave can be calculated and it can be used to calibrate a hydrodynamic model to find the bed roughness. From the same hydrodynamic model the maximum flood velocity at the estuary mouth or inflection point can be estimated.

[2] Another coefficient for the bed roughness would also suffice.

4.2 Method

In this section the steps one should follow simulating salt intrusion in estuaries using SOBEK-3 are included. After that the criteria to quantify the quality of the model results are explained.

4.2.1 Model setup

The first step in simulating salt intrusion in estuaries is building up the SOBEK-3 model. In order to do so the following steps have to be executed:

- **Define estuary boundaries**
  One should indicate where the estuary mouth is located (downstream boundary) and where the river section starts (upstream boundary).
- **Define cross-sections**
  SOBEK linearly interpolates between known cross-sections. For prismatic channels two, or even one, defined cross-section suffice. However, the cross-section of a convergent estuary changes gradually and so more cross-sections have to be defined. In the most downstream part, where the cross-section varies most, a cross-section is defined every 500 meter, between those points it is linearly interpolated. In this research the distance between two defined cross-sections gradually increased in upstream direction.
- **Define bed roughness**
  The bed roughness of the main channel and flood plains have to be defined. As it is hard to measure, the bed roughness can be found in literature or by calibrating a hydrodynamic model. In this research the bed roughness is based on Savenije (2012) and Kuijper and Van Rijn (2011).
- **Define initial conditions**
  The initial water level, discharge and salinity along the estuary have to be defined.
- **Define boundary conditions**
  At the upstream boundary a discharge and background salinity have to be defined. At the downstream boundary the water level and salinity have to be defined, both of them are fluctuating with the tide. The water level can simply be taken equal to the tide. The boundary condition for salinity is more complex and it uses the so called Thatcher Harleman time-lag (Deltares, 2015). If the outflow concentration is different from the concentration at inflow there is a discontinuity in the concentration at the return of the flow. The transition from one to the other condition requires some time and is dependent on the replacement of the water in the boundary region. To account for this time a half-cosine variation is used, when the water starts flowing into the estuary the concentration increases according to this half-cosine function. Then it remains constant until the water flow turns again.
- **Chose dispersion coefficient and define constants**
  One should chose the right dispersion coefficient and define the corresponding constants in Equation (3.17). The dispersion formulations used in this research are elaborated in Chapter 2. The first dispersion formula used is the one based on Thatcher and Harleman (1972) Based on the analysis of those model results adjustments to the dispersion formulation are proposed, other dispersion formulas are selected and tested.
- **Define grid**
  The grid cell size has to be defined. In this research for the prismatic channels a grid cell size of 500 meter is used, while for convergent estuaries the distance between two grid cells was 100 meter.
- **Define simulation length and time step**
  The simulation length should be chosen sufficiently long to allow a semi-steady state to develop. Also a computational time step has to be defined. If this time step is taken to large and will lead to unstable results, SOBEK-3 itself will reduce it.
- **Select output parameters**
  The modeler should select what output parameters are needed for further analysis.
- **Run the model**

4.2.2 Evaluate and analyze model results

One should check whether the model results are reliable. If the results are reliable the salt intrusion length and, only if longitudinal salinity data is available, salinity curves have to be extracted from the model data. In order to do so, Matlab is used. The maximum and minimum salinities at a certain point in the estuary can be transformed in a maximum and minimum intrusion curve. The salt intrusion length is defined as the first grid point where the salinity is below a certain threshold value. For the tidal flume test this value is chosen to be 0,38 ppt[3], for convergent estuaries the threshold value is chosen to be 0,01 ppt as such salinity is considered negligible. To validate the model, the measured and simulated values are compared.

The quality of the model results are quantified by the criteria below. For the tidal flume test the R^2, $RMSE$ and σ are used for the minimum and maximum salt intrusion. For the maximum salt intrusion of the real convergent estuaries the R^2, $RMSE$ and σ are used. For the salinity profiles of the real convergent estuaries B_e and σ are used.

- **Coefficient of determination (R^2)** $[-]$: is a measure for correlation between simulations and observations.

$$R^2 = \left(\frac{1}{m-1} \sum_{i=1}^{m} \left(\left(\frac{y_{simulation} - \bar{y}_{simulation}}{\sigma_{y_{simulation}}} \right) \left(\frac{y_{observation} - \bar{y}_{observation}}{\sigma y_{observation}} \right) \right) \right)^2 \tag{4.1}$$

- **Root mean squared error (RMSE)** $[-]$: is a measure for the average error, which amplifies and severely punishes large errors. Here it is taken for relative errors, as the absolute error in case of long intrusion lengths can be large compared to the absolute error for small intrusion lengths.

$$RMSE = \sqrt{\frac{1}{m} \sum_{i=1}^{m} \left(y_{simulation} - y_{observation} \right)^2} \tag{4.2}$$

- **Standard deviation (σ)**: is a measure for the spreading of the simulations. σ_L $[-]$ for the minimum and maximum intrusion lengths considers the relative errors, while σ_p $[ppt]$ for the salinity curves considers actual errors.

$$\sigma = \sqrt{\frac{1}{m-1} \sum_{i=1}^{m} \left(y_{diff} - \bar{y}_{diff} \right)^2} \tag{4.3}$$

- **Bias (B_e)** $[ppt]$: is the mean difference of measured and computed salinity curves.

$$B_e = \frac{\sum_{i=1}^{m} \left(y_{simulation} - y_{observation} \right)}{m} \tag{4.4}$$

[3] According to Kuijper (2016) the accuracy of the measurement in the tidal flume test was about 0,3 kg/m^3, using formula (3.5) this results in a tress-hold value of 0,38 ppt.

In which:

m	is the number of observations/simulations
y_{diff}	are the differences between simulated and observed values
$\bar{y}_{diff}$	is the mean of the differences between simulated and observed values
$y_{observation}$	are the observed values
$\bar{y}_{observation}$	are the averaged observed values
$y_{simulation}$	are the simulated values
$\bar{y}_{simulation}$	are the averaged simulated values

4.3 Numerical sensitivity analysis

This analysis justifies the chosen space step ($\Delta x = 500m$) and time step ($\Delta t = 300s$) used to simulate the tidal flume tests. The numerical sensitivity analysis has only been performed for the reference case of the tidal flume tests. It is assumed that the space step used for the convergent estuaries ($\Delta x = 100m$) and its corresponding time step are sufficiently small. In the tables below the cases with the used space and time step are expressed in a bold letter type. The space or time step changed are expressed in an italic letter type. **Note:** the estimated intrusion lengths have an accuracy of the used space step and the dispersion formulation used is the one described in Section 3.4.2.1.

As SOBEK cannot cope with a combination of a time step of 300 s and a space step of 250 m and smaller, this analysis is extended with a space step analysis with a time step of 150 s. From Tables 4.2 and 4.3 it can be seen that the simulated maximum intrusion length fluctuates around 27 km and the simulated minimum intrusion length is just above 14 km. If the accuracy corresponding to the used space step is taken into account, it is concluded that for this research a space step of $\Delta x = 500m$ is sufficiently accurate.

Table 4.2: *Space step analysis*

Discretization		SOBEK-3, TH	
dt	*dx*	L_{max}	L_{min}
[s]	*[m]*	[km]	[km]
300	***500***	**27,04**	**14,52**
300	*1000*	26,92	14,96
300	*2000*	28,16	16,09

Table 4.3: *Space step analysis, for time step of 150 seconds*

Discretization		SOBEK-3, TH	
dt	*dx*	L_{max}	L_{min}
[s]	*[m]*	[km]	[km]
150	*250*	26,73	14,24
150	*500*	26,54	14,52
150	*1000*	26,92	14,96

The time step analysis is included in Table 4.4. Here one can observe that the simulated maximum and minimum intrusion lengths converge to 26,54 km and 14,52 km respectively. The used time and space step combination results in simulated maximum and minimum intrusion lengths of 27,04 km and 14,52 km respectively and is considered sufficiently accurate for the purpose of this thesis.

Table 4.4: *Time step analysis*

Discretization		SOBEK-3, TH	
dt	dx	L_{max}	L_{min}
[s]	[m]	[km]	[km]
50	500	26,54	14,52
75	500	26,54	14,52
150	500	26,54	14,52
300	**500**	**27,04**	**14,52**
600	500	27,04	15,52
1200	500	27,54	15,02

5 Testing the Thatcher and Harleman dispersion formulation

The model results obtained by using the dispersion formula based on the one derived by Thatcher and Harleman (1972), which is repeated in Equation (5.1), are presented in this chapter. In SOBEK-RE which is used frequently to simulate salt intrusion in estuaries, this was the most physically grounded dispersion formula and therefore it serves as a base for this research. For the simulations SOBEK-3 is used.

$$D(x,t) = f_3 h(x,t)\frac{\sqrt{g}}{C(x)}|u(x,t)|+ \\ f_4 L_e^2 \frac{u_0^*}{S_0^*}\left(\frac{\Delta\rho}{\rho}\frac{g h_0}{\hat{u}_0^2}\frac{Q_f T}{P_e}\right)^{1/4}\left\langle\left|\frac{S(x)}{S_0}\frac{\partial S(x)}{\partial x}\right|\right\rangle \tag{5.1}$$

As is shown in Appendix C and stated by Winterwerp (1980), the shear dispersion is negligible with respect to the tidal dispersion. Shear dispersion thus had a negligible contribution to the total dispersion and therefore it was excluded from further analysis. By elaborating the second part of Equation (5.1) and neglecting the first part, it can be rewritten in Equation (5.2)[1]. This equation directly shows the dependency of D with the parameters influencing it. This way, it can be easier assessed what the influences of different system characteristics are.

$$D = \alpha u_0^{-\frac{3}{4}}\left(\frac{\Delta\rho}{\rho}\right)^{\frac{1}{4}} Q_f^{\frac{1}{4}} B_0^{-\frac{1}{4}}\left\langle\left|\frac{S}{S_0}\frac{\partial S}{\partial x}\right|\right\rangle \\ \alpha = f_4\frac{u_0^*}{S_0^*}L_e^2(g\pi)^{\frac{1}{4}} \tag{5.2}$$

5.1 Results tidal flume test

As explained in Chapter 3 with the tidal flume test the effect of different variables on the salt intrusion length is researched. In this section the measured and computed salt intrusion are compared. The used constants are:

- $f_3 = 25$ (Thatcher and Harleman, 1972)
- $f_4 = 0.006$ (Winterwerp, 1980)[2]

5.1.1 Tidal amplitude

For low tidal amplitudes W the estuary is strongly stratified as there is no energy available for tidal mixing. Van Os and Abraham (1992) state that for low W the system is more stratified. In those situations the dispersive landward salt transport is relatively large as there is little energy available for tidal mixing. When W increases more energy is available for tidal mixing, the estuary becomes more mixed and thus the dispersive salt transport decreases. With increasing W also the tidal excursion increases. Figure 5.1 shows that indeed for low W the salt intrudes relatively far and the distance between minimum and maximum intrusion is

[1] In order to rewrite this equation the definition for the tidal prism $P_e = A_0 E_0 = B_0 h_0 \hat{u}_0 T/\pi$ is used.

[2] Winterwerp (1980) found another value for f_4 than Thatcher and Harleman (1972) did, as the geometry of the Nieuwe Waterweg changed and the sea boundary was located at another position.

relatively small. When W increases the dispersive transport decreases and the fluctuation around it increases. From a certain W on this movement around the tidally averaged situation is dominant in determining the maximum intrusion length.

The SOBEK simulations show a similar behavior, see Figure 5.1. The correct relationship between salt intrusion and increasing W is explained by the proportionality of D to $\hat{u}_0^{-\frac{3}{4}}$. When the tidal amplitude increases, so does the maximum flood velocity and thus the dispersive salt transport decreases with increasing W. At the same time when W increases the tidal excursion increases and, as a result of the advective transport, so does the fluctuation around the averaged intrusion. It should be noticed that the maximum salt intrusion is underestimated for both small and large W. The error is largest for small W, when stratification is strongest.

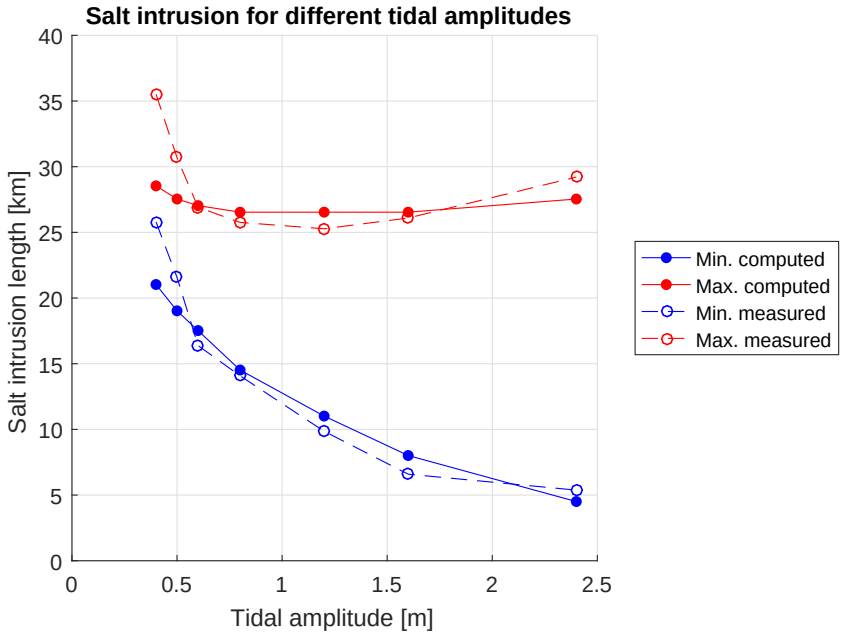

Figure 5.1: *Measured and computed salt intrusion lengths for varying tidal amplitudes.*

5.1.2 Bed roughness

According to Uittenbogaard (2016) turbulent mixing breaks down stratified flow. Van Os and Abraham (1992) agree and state that for a smooth bed, high C[3], there is little turbulent mixing and thus the estuary is more stratified. In addition it is expected that gravitational circulation increases as the flow over the channel bed is less hindered. On the other hand, if the channel becomes smoother and flow velocities increase, the tidal energy available for mixing increases. If all those effects are summed up, it can be expected that if C increases also the dispersive salt transport increases. With increasing C also the tidal excursion increases and thus the distance between maximum and minimum intrusion increases. This is exactly what Rigter (1973) observed in his tidal flume experiment, see Figure 5.2.

The simulations show another behavior, if C increases the simulations show a decrease in dispersive salt transport. This can be explained by looking at the maximum flood velocity in the estuary mouth $\hat{u}_0$, Figure 5.3. For increasing C also $\hat{u}_0$ increases, and according to the

[3]The bed roughness is parametrized by the Chézy coefficient C. When the bed becomes rougher the Chézy coefficient becomes smaller, when the bed becomes smoother the Chézy coefficient becomes larger. It should be noticed that Thatcher and Harleman (1972) have not experimented with different bed roughness when formulating their dispersion coefficient. They worked with a fixed bed roughness or calibrated the bed roughness for the hydraulic model they were using.

proportionality of D to $\hat{u}_0^{-\frac{3}{4}}$ the dispersive salt transport decreases. The simulated distance the water travels up and down the estuary over a tidal cycle increases with increasing C, which is in agreement with the observations.

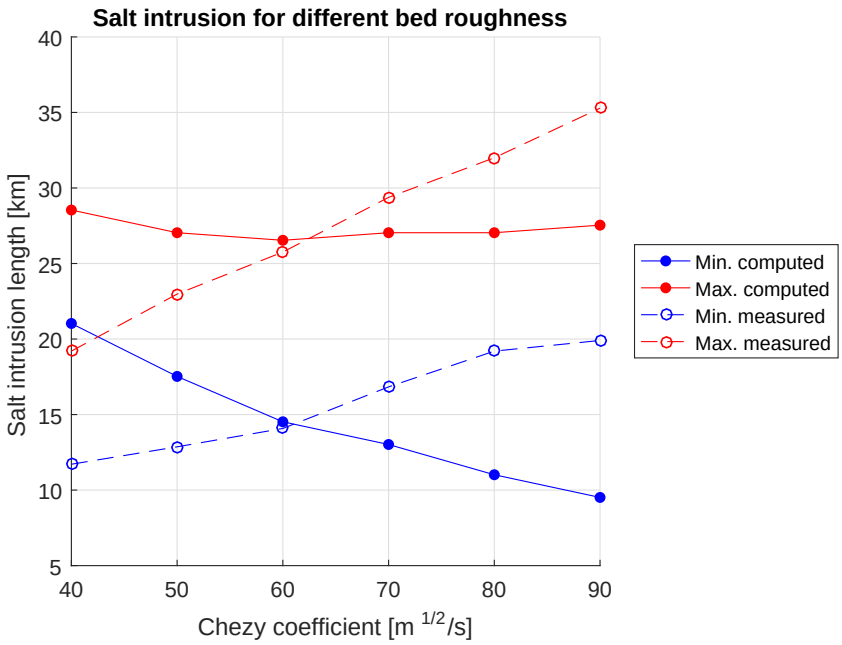

Figure 5.2: *Measured and computed salt intrusion lengths for varying bed roughness.*

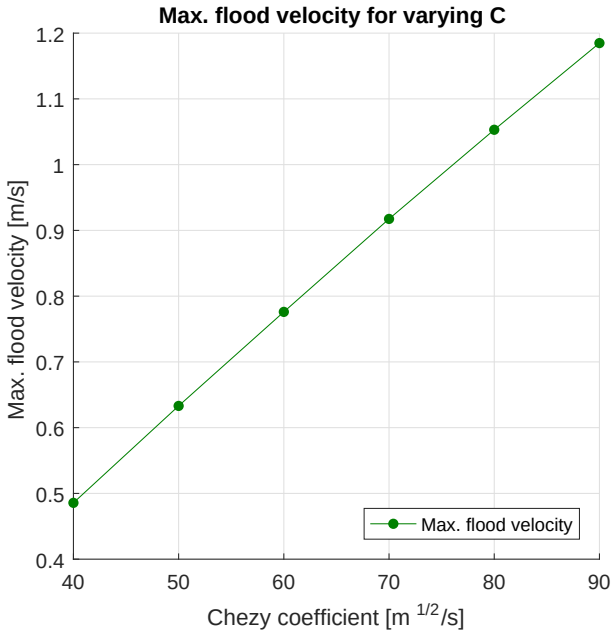

Figure 5.3: *Maximum flood velocity in the estuary mouth for varying C.*

5.1.3 Water depth

If the water depth h increases so does the gravitational circulation. In addition when h increases the maximum flood velocity increases (Figure 5.5) while the fresh water velocity decreases as the fresh water discharge is spread over a larger cross-section (Q_f/A). For large h the river discharge is thus less powerful in pushing the salt water out. Both effects lead to an increased

salt intrusion for increasing h. The tidal excursion stays more or less constant for increasing h. This agrees with what Rigter (1973) observed, see Figure 5.4, both the maximum and minimum intrusion length increase with increasing h with more or less equal strength.

The modeled intrusion length does not increase significantly for increasing h as can be seen in Figure 5.4. This can be explained by the proportionality of D with $\hat{u}_0^{-\frac{3}{4}}$ and the last term in Equation (3.3). With an increasing water depth, the flood velocity increases (Figure 5.5) and thus the dispersion coefficient decreases. However, with h increasing so does the cross-sectional area A. The combination of D decreasing and A increasing in Equation (3.3) results in more or less constant maximum and minimum salt intrusion lengths. The difference between simulated minimum and maximum intrusion lengths stays, similar to what is seen in observations, more or less constant.

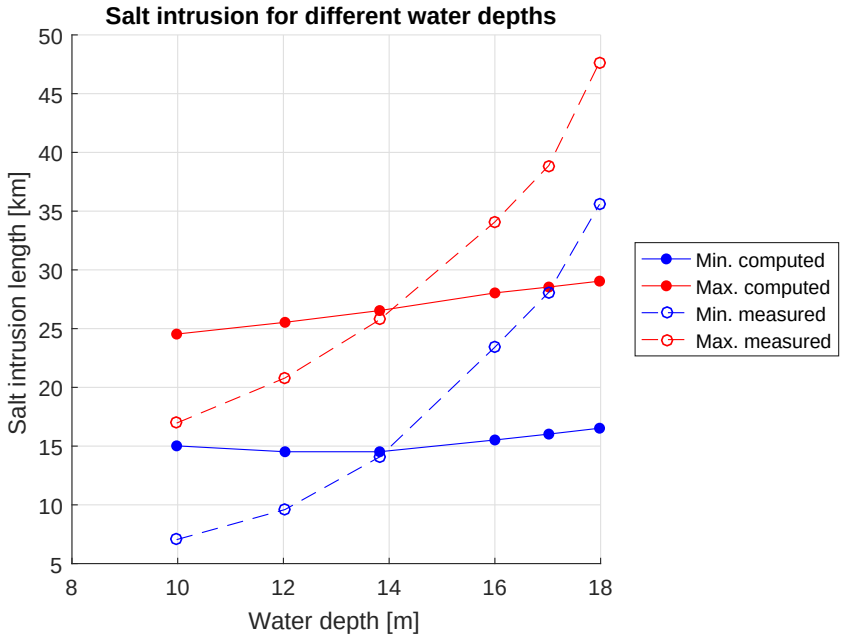

Figure 5.4: *Measured and computed salt intrusion lengths for varying water depths.*

5.1.4 Flume length

In a prismatic channel, like the tidal flume, a tidal wave dampens out due to friction while traveling upstream through the channel. When the wave reaches the closed upstream end of the flume it is reflected. The incoming and reflected waves together determine the hydraulic conditions in the system. The length of the flume influences where and when the wave is reflected. When the tidal flume has a length of a quarter of the wave length resonance occurs, reflection is at its maximum and the maximum flood velocity in the estuary mouth is at its peak. In this situation there is a lot of energy available for tidal mixing, salt water does not intrude far into the estuary and the water will travel great distances land- and seaward within the estuary. When the flume length deviates from the resonance length the maximum flood velocity in the estuary mouth decreases, see Figure 5.6, and so do the mixing capacity and the tidal excursion. Figure 5.7 includes observations by Rigter (1973) which show the behavior explained.

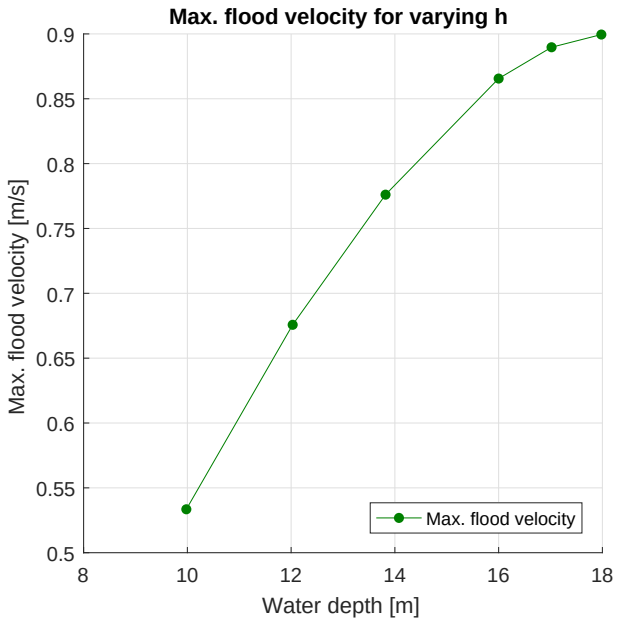

Figure 5.5: *Maximum flood velocity in the estuary mouth for varying h.*

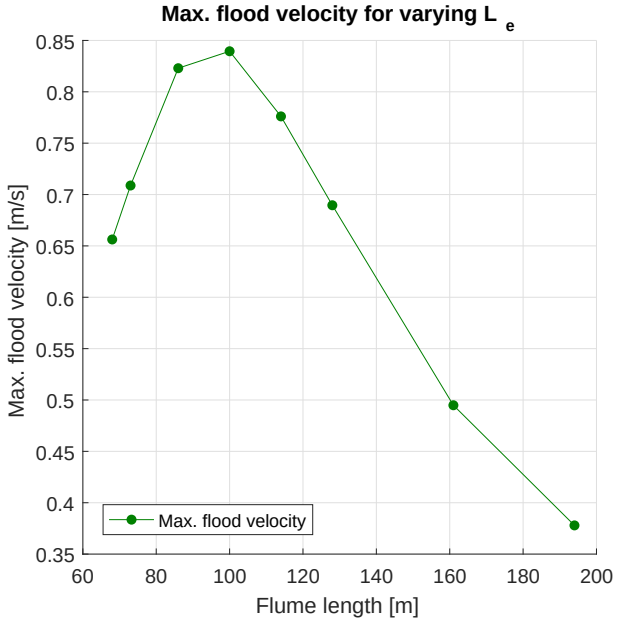

Figure 5.6: *Maximum flood velocity in the estuary mouth for varying L_e.*

α, and thus D in Equation (5.2) depend quadratically on the estuary length. However, here it is taken constant at 100 km (Rijkswaterstaat, 1984). When the actual flume length would be used, dispersive salt transport would increase with increasing flume length, which does not represent reality as is shown in Figure 5.7. Therefore the estuary length does not seem to be the right length scale to be included in the dispersion coefficient. In the simulations the increase in dispersive salt transport is, when deviating from the reference case, underestimated. The simulated movement of the salt intrusion between HWS and LWS is captured for changing flume lengths.

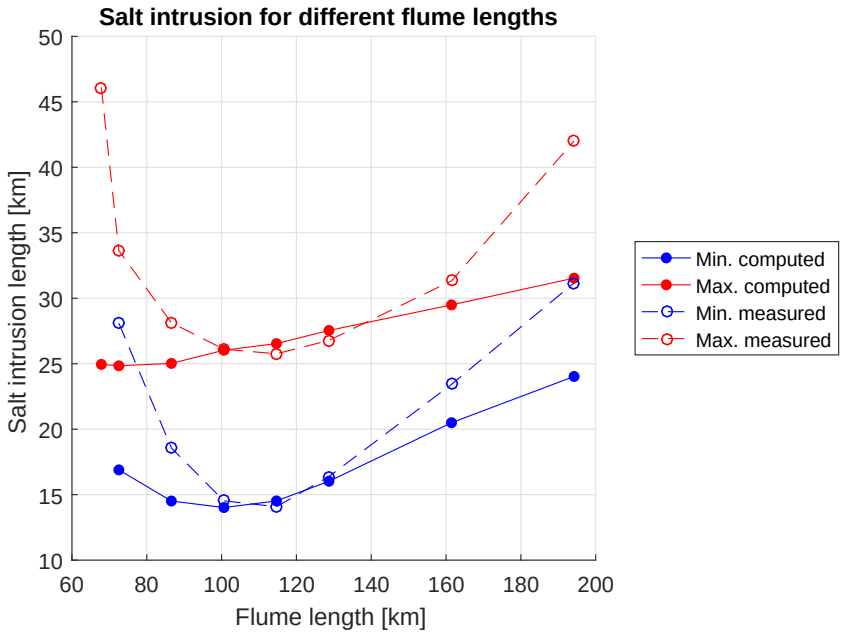

Figure 5.7: *Measured and computed salt intrusion lengths for varying flume lengths.*

5.1.5 River discharge

According to Van Os and Abraham (1992) the system becomes more stratified with increasing river discharge Q_f. For low river discharges the kinetic energy provided by the tide prevails over the potential energy provided by the river and the system is mixed. When the river discharge increases the potential energy which has to be overcome to break down stratification increases and the estuary becomes more and more stratified. With increasing river discharge also the advective seaward salt transport increases. For low river discharges there is little advective salt transport out of the estuary and salt intrusion is dominated by dispersion. For high river discharges advection dominates salt transport. As Rigter (1973) observed, the net effect is that for increasing Q_f the salt intrusion decreases, see Figure 5.8. The tidal excursion stays more or less constant for a changing Q_f.

For low Q_f the simulation slightly underestimates the salt intrusion, but the general behavior is approached. From a certain discharge on the simulated salt intrusion does not decrease as fast as the measured salt intrusion. The minimum salt intrusion length even increases, the distance between maximum and minimum intrusion is therefore underestimated. When the discharge increases even further both maximum and minimum salt intrusion drop to nearly zero. This might be explained by the proportionality of D to $\hat{u}_0^{-\frac{3}{4}}$ and Q_f. When Q_f increases $\hat{u}_0$ decreases and thus D increases. When Q_f becomes sufficiently large $\hat{u}_0$ may drop below 0 m/s, and only outflows occurs (which is the case in the test with $Q_f = 3801 m^3/s$). If $\hat{u}_0$ becomes sufficiently small, but remains positive, D will explode and result in extremely high landward dispersive transport, see $Q_f = 2845 m^3/s$ in Figure 5.8. In case of extremely high discharges with only outflow, the BC used is not representative anymore as it does not allow salt to intrude in the estuary.

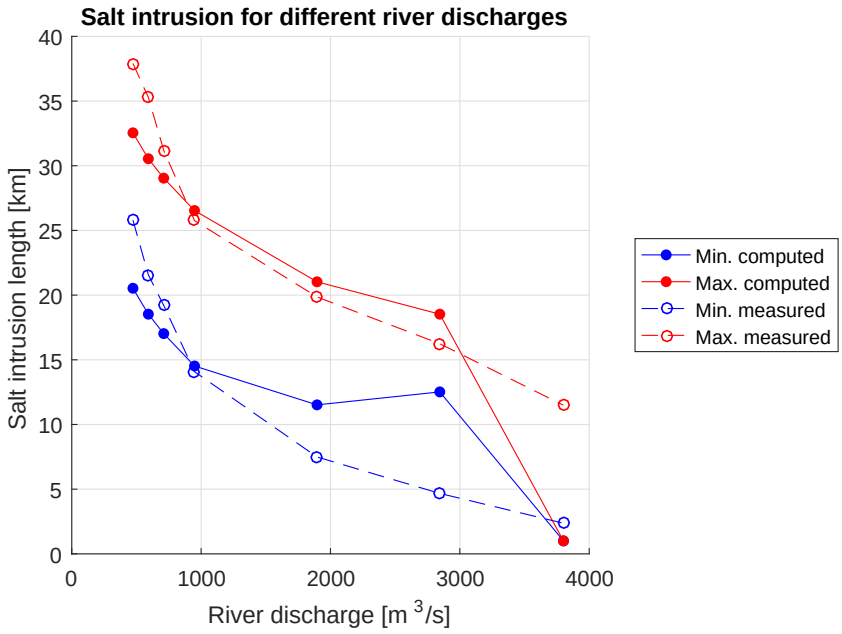

Figure 5.8: *Measured and computed salt intrusion lengths for varying river discharges.*

5.1.6 Relative density difference

When the relative density difference $\Delta\rho/\rho$ increases so does gravitational circulation. For increasing $\Delta\rho/\rho$ the salt travels further upstream as can be seen from Figure 5.9. Rigter (1973) observed a strong, and nearly linear, increase of the salt intrusion for increasing $\Delta\rho/\rho$. The simulations show a slight increase in salt intrusion for increasing $\Delta\rho/\rho$, due to the dependency on $(\Delta\rho/\rho)^{\frac{1}{4}}$. The slope of this increase is to mild compared too the observed slope. The tidal excursion, remains more or less constant for both the measurements and the simulations as the tidal amplitude does not change its magnitude.

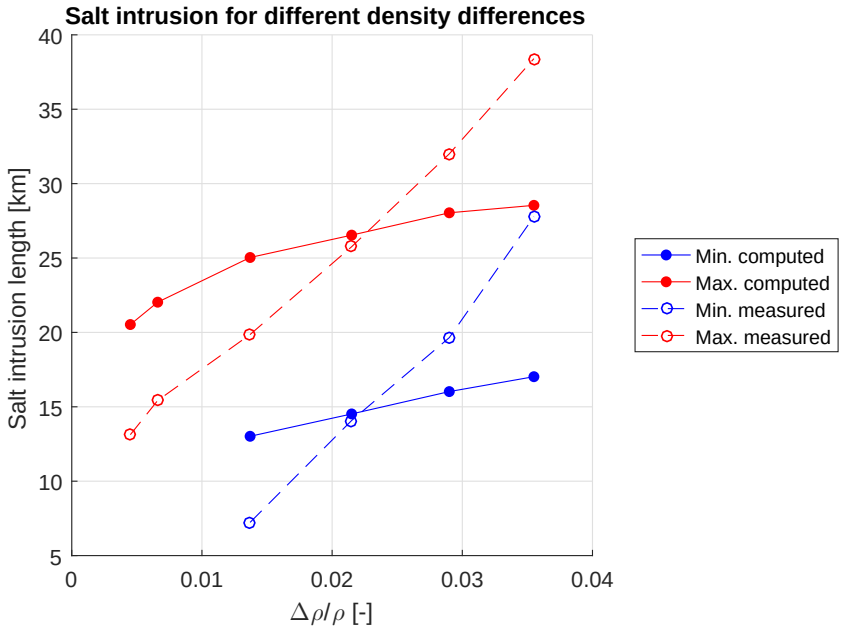

Figure 5.9: *Measured and computed salt intrusion lengths for varying relative density differences.*

5.1.7 Overall performance

Figure 5.10 shows the minimum and maximum computed intrusion lengths to their respective measured intrusion lengths. As can be seen from this figure in general the model is not sensitive enough to capture changes in system variables. Some notable observations are that the minimum intrusion for changing W does follow the line of perfect agreement quite well, the values for minimum intrusion with varying C are almost perpendicular to the line of perfect agreement and the observations for varying Q do follow the line of perfect agreement quite well except for high river discharges. The most remarkable simulation is the one with the highest river discharges, here the water does not flow into the estuary anymore, as an artifact the boundary condition does not allow salt to intrude in the estuary and thus salt does not intrude.

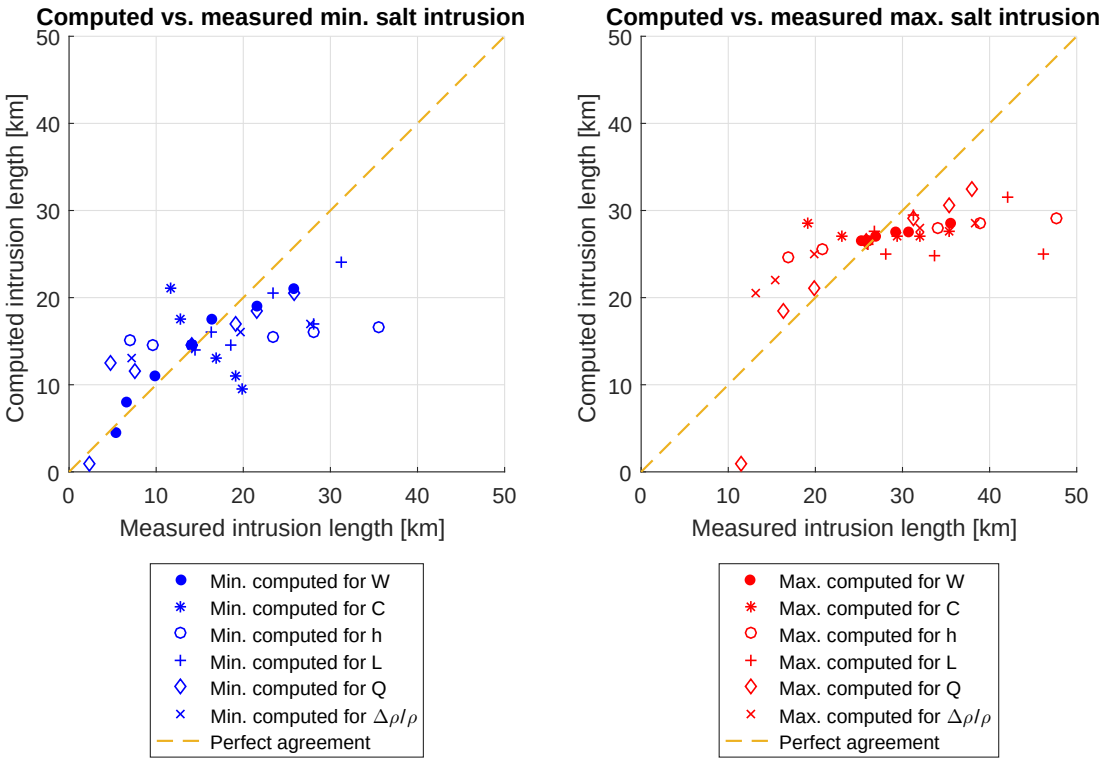

Figure 5.10: *Measured vs. computed salt intrusion lengths for the tidal flume experiment.*

Table 5.1 includes the values for R^2, $RMSE$ and σ. As there is some doubt about the model results for $Q = 2845 \frac{m^3}{s}$ and $Q = 3801 \frac{m^3}{s}$ the values are presented again, not considering those respective tests. In addition salt intrusion is not the main concern in cases of such a high discharge and attention should be payed to flood defense instead. The values for R^2 reveals the correlation between measurements and observations is not strong. While the values for $RMSE$ and σ show that the averaged error and spreading are significant.

Table 5.1: *Quality criteria for model results*

	All cases	Reduced set
R^2	0,60	0,58
$RMSE$	0,38	0,31
σ	0,38	0,31

5.2 Results real convergent estuaries

Simulations of salt intrusion in real convergent estuaries have been compared for both the maximum salt intrusion length and the salinity profiles along an estuary. In order to simulate salt intrusion in real convergent estuaries the f_3 and f_4 terms are taken, as suggested by Thatcher and Harleman (1972), 75 and 0,0015 respectively. Figure 5.11 shows the computed maximum salt intrusion lengths against the measured maximum salt intrusion lengths and Figure 5.12 shows an example of a salinity curve along the Maputo estuary, in Appendix D all salinity curves are included. The R^2, $RMSE$, σ_L, B_e and σ_p values for the simulations using dispersion formulation (5.1) are given in Table 5.2.

Table 5.2: *Quality criteria for model results, in which σ_L and σ_p concern maximum intrusion and salinity profiles respectively.*

Criteria	Value	Units
R^2	0,87	-
$RMSE$	0,23	-
σ_L	0,20	-
B_e	0,01	ppt
σ_p	3,33	ppt

From Figure 5.11 and the R^2 value it can be seen that there is quite some correlation between computed and measured maximum salt intrusion. However, from Figure 5.12, all the other salinity curves and σ_p it can be seen that the computed and measured salinity profiles deviate significantly. The value B_e is approximately zero, indicating that the averaged error for the simulated salinity curve is small.

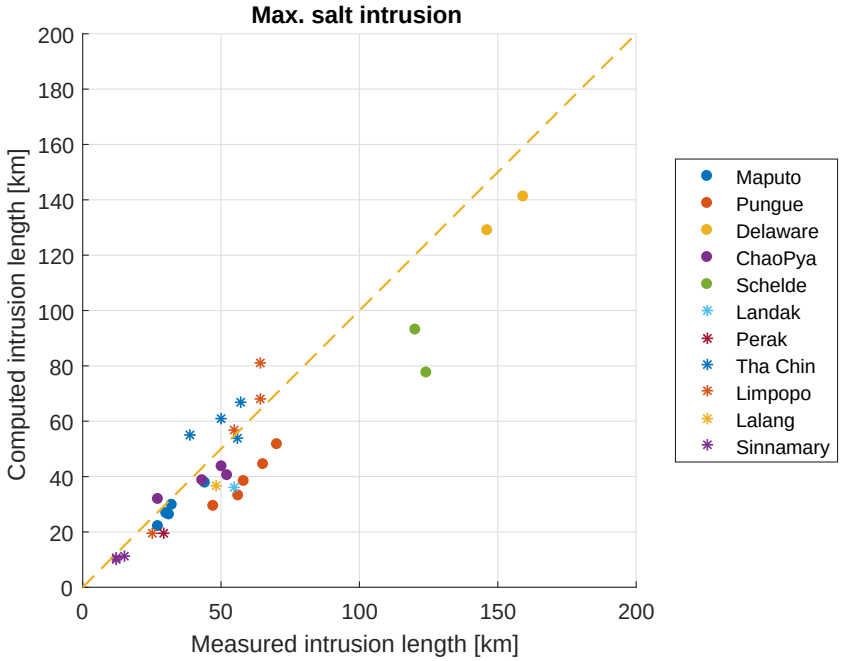

Figure 5.11: *Measured and computed salt intrusion lengths for real convergent estuaries.*

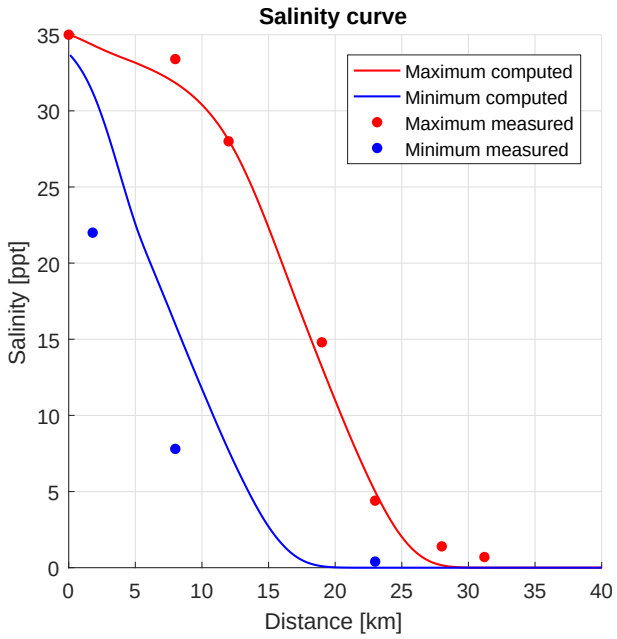

Figure 5.12: *Salinity profile for the Maputo estuary.*

5.3 Discussion

The results above indicate that the simulations of salt intrusion in the tidal flume using the Thatcher and Harleman dispersion formula do not physically represent all processes going on. Table 5.3 shows which physical processes affect salt intrusion by changing the system variables, what is the observed effect and what happens in the simulations. The last column in Table 5.3 concludes if the observed behavior is captured (✓) or not (✗). However sometimes the right behavior for a physical process is captured its effect is underestimated, which for example happens for L_e and $\Delta\rho/\rho$. The main shortcomings are that the simulations are off for changing C and h.

For real convergent estuaries there is strong correlation between measurements and simulations. However, from the salinity profiles it is seen that there are still significant differences between measurements and observations.

Table 5.3: *Effect of changing variables in the tidal flume experiment on advective transport A, the predicted dispersion in the estuary mouth D_0 and the tidal excursion E. Note that a * is added to indicate an under- or overestimation of the effect. $\uparrow$ means increase, $\downarrow$ means decrease, $\downarrow\uparrow$ means first decrease then increase, - means no effect.*

Increasing parameter	Physical process	Effect	Thatcher and Harleman	Conclusion
W	More tidal mixing	$D_0 \downarrow$	$\hat{u}_0 \uparrow \rightarrow D_0 \downarrow$	✓*
	Higher tidal excursion	$E \uparrow$	$E \uparrow$	✓
C	Less turbulent mixing	$D_0 \uparrow$	-	✗
	More gravitational circulation	$D_0 \uparrow$	-	✗
	More tidal mixing	$D_0 \downarrow$	$\hat{u}_0 \uparrow \rightarrow D_0 \downarrow$	✓
	Higher tidal excursion	$E \uparrow$	$E \uparrow$	✓
h	More gravitational circulation	$D_0 \uparrow$	$\hat{u}_0 \uparrow \rightarrow D_0 \downarrow$	✗
	Spreaded discharge less powerfull in pushing water out	$A \downarrow$	Salt transport equation	✓
	No effect on tidal excursion	$E-$	$E-$	✓
L_e	Reflection, max. mixing at resonance length	$D_0 \uparrow$	$\hat{u}_0 \uparrow\downarrow \rightarrow D_0 \downarrow\uparrow$	✓*
	Tidal excursion max. when L_e is the resonance length	$E \downarrow\uparrow$	$E \downarrow\uparrow$	✓
Q_f	Less tidal mixing	$D_0 \uparrow$	$Q_f \uparrow + \hat{u}_0 \downarrow \rightarrow D_0 \uparrow$	✓*
	More advective transport out the estuary	$A \uparrow$	$A \uparrow$	✓
	No effect on tidal excursion	$E-$	$E \downarrow$	✗
$\Delta\rho/\rho$	More gravitational circulation	$D_0 \uparrow$	$\Delta\rho/\rho \uparrow \rightarrow D_0 \uparrow$	✓*
	No effect on tidal excursion	$E-$	$E-$	✓

6 Towards an improved dispersion formula

Within this chapter is sought after a better performing dispersion formula. In order to do so first adjustments to the dispersion formula are proposed and assessed. After that dispersion formulations as described by Gisen *et al.* (2015), Savenije (2012), Kuijper and Van Rijn (2011) and Zhang and Savenije (2016) are tested. This is a logical follow up step as the formulations as described by these authors make use of the disclosed adjustments and have never been tested in a dynamic model. Within the assessment of those dispersion formulations again distinction is made between the tidal flume experiment and real convergent estuaries.

Please note that the observations and physical background considering the tidal flume experiment are described in Chapter 5 and are not repeated here. In Appendix D the salinity profiles generated for the used dispersion formulations are included. Those are used in this chapter to judge model performance.

6.1 Adjustments to the dispersion formulation

Based on the results for the tidal flume experiment and real convergent estuaries a number of possible improvements are be suggested. This section describes those improvements and its effects. The adjustments are based on the results described in Chapter 5. After explaining the proposed adjustments, they are linked with physical processes going on in estuaries, the newly formed dispersion formula is presented and the effect of the individual adjustments are addressed.

6.1.1 Estuary length and tidal excursion

As is seen before the estuary length L_e is not an ideal length scale to describe dispersive salt transport. It is not well defined and inclusion in the dispersion formulation does not result in realistic results for simulations of the tidal flume test. Many authors, like Savenije (2012), Kuijper and Van Rijn (2011) and Gisen *et al.* (2015), use the tidal excursion E instead of L_e as a length scale. Savenije (2012) states that E is the correct length scale to be included as it is the length over which mixing in convergent estuaries actually takes place.

6.1.2 Characteristic flood velocity and maximum flood velocity

The maximum flood velocity in the estuary mouth used for scaling the dispersion coefficient is taken constant in Equation (5.1) based on research done by Rijkswaterstaat (1984). According to Savenije (2012) the velocity amplitude, or maximum flood velocity in the estuary mouth, is the scale for shear dispersion. Therefore it should not be taken constant.

6.1.3 Estuarine Richardson number

As the simulations show salt intrusion is not sensitive enough to changes in seawater density, taking the estuarine Richardson number N_R to a higher power might improve the dispersion formula. Savenije (2012), Kuijper and Van Rijn (2011) and Gisen *et al.* (2015) typically take N_R to a power ranging between 0,5 and 0,6. Increasing the power of N_R also affects the sensitivity of D to P_e, Q_f and $\hat{u}_0$ and thus the simulations for all series of the tidal flume experiment.

6.1.4 Friction

The simulated behavior of salt intrusion for different bed roughness deviated from observations in the tidal flume. Therefore adding the term $\frac{C}{\sqrt{g}}$ should improve the model results. It should be noted that in real scenarios the bed friction does not occur in such a wide range as is tested in the tidal flume.

6.1.5 Water depth

The salt intrusion simulations are insensitive for changes in water depth h, while model observations show an increased salt intrusion for increased water depths. Therefore a term containing h should improve the simulations. In prismatic channels the convergence length goes to infinity and thus is not feasible to use in the dispersion formulation. Therefore in prismatic estuaries the term $\frac{h}{E}$ can be used, while for convergent estuaries $\frac{h}{\bar{a}}$ should be used.

6.1.6 Wide estuaries

Based on recent research by Zhang and Savenije (2016) it is expected that in very wide parts of an estuary dispersion is underestimated by currently used dispersion formula's. That is why they suggested to add an extra term to account for this extra dispersion. By multiplying D with $(1 + 10(\frac{B_x}{E_x})^2)$ the dispersion increases particularly in wide parts of the estuary, while in smaller parts of an estuary its effect is negligible.

6.1.7 Salinity and salinity gradient

Relating the dispersion coefficient to $\langle \frac{S}{S_0} \rangle^K$ instead of $\langle \frac{S}{S_0} \frac{\partial S}{\partial x} \rangle$ should improve the simulations particularly in (parts of) estuaries where dispersion is dominated by the tide, while maintaining its ability to simulate dispersive salt transport in density dominated dispersion regions.

By using $\langle \frac{S}{S_0} \frac{\partial S}{\partial x} \rangle$ the effect of the salinity profile on the dispersion coefficient is reduced. In case of a long intrusion length $\langle \frac{S}{S_0} \rangle$ remains high for a relative long distance, while $\langle \frac{\partial S}{\partial x} \rangle$ is relatively small. The two effects partly neutralize each other. If $\langle \frac{S}{S_0} \rangle^K$ is used instead dispersion is highest in the estuary mouth and will decrease in upstream direction.

6.1.8 Linking physical processes and the new dispersion formula

Table 6.1 shows the link between physical processes and parameters in the dispersion formula. As one read attentively through the mixing processes described before one should notice not all mixing processes are included in the table. It is true that mixing induced by tidal trapping, in channel bends, at estuary banks and by the wind are not captured in the dispersion formula. Fortunately, in most cases the mixing processes captured by the dispersion formula are the dominant mixing processes.

Table 6.1: *Linking formula to physical processes*

Parameter	Dispersive processes
$uh\frac{\sqrt{g}}{C}$	Shear dispersion
$\hat{u}_0$	Velocity scale for shear mixing
E_0	Mixing length scale for convergent estuaries
N_R	Gravitational circulation, stratification
$\frac{C}{\sqrt{g}}$	Turbulent mixing
$\frac{h_0}{a}$	Gravitational circulation, geometry factor (convergent estuaries)
$\frac{h_0}{E_0}$	Mixing length scale (prismatic estuaries), gravitational circulation
$(1+c_9(\frac{B_x}{E_x})^2)$	Tidal pumping, residual circulation in wide estuaries
$\langle\frac{S}{S_0}\rangle$	Residual circulation, gravitational circulation, neap-spring neap tide
$\langle\frac{\partial S}{\partial x}\rangle$	Gravitational circulation, neap-spring tide

Here the newly suggested dispersion formula is presented in Equation (6.1). Based on the suggested improvements new dispersion formulas, which originate from literature, are proposed. Those and the individual adjustments are tested hereafter in this chapter.

$$D = c_1 u(x) h(x) \frac{\sqrt{g}}{C} + c_2 \hat{u}_0^{c_3} E_0^{c_4} N_R^{c_5} \left(\frac{C}{\sqrt{g}}\right)^{c_6} \left(\frac{h_0}{\bar{a}}\right)^{c_7} \left(\frac{h_0}{E_0}\right)^{c_8} \left(1 + c_9 \left(\frac{B_x}{E_x}\right)^2\right) \left\langle \frac{S}{S_0} \right\rangle^{c_{10}} \left\langle \left| \frac{\partial S}{\partial x} \right| \right\rangle^{c_{11}} \tag{6.1}$$

6.1.9 Individual adjustments

The effect of the individual adjustments proposed have been assessed individually on the tidal flume simulations. In order to do so only the salinity dependent part of the dispersion coefficient is used. This analysis led to some useful conclusions which are presented here. In Appendix E the corresponding figures are included. The individual adjustments assessed are:

- Multiplying D with $\frac{C}{\sqrt{g}}$, makes the dispersion depend on C.
- Multiplying D with $\frac{h_0}{E_0}$, includes an h_0 and extra $\hat{u}_0^{-1}$.
- Changing L_e by E_0, as $E_0 \propto \hat{u}_0$ the proportionality of D to $\hat{u}_0$ changes.
- Change the power of N_R to $\frac{1}{2}$, the proportionality of D with $\hat{u}_0$, $\frac{\Delta\rho}{\rho}$ and Q_f changes.
- Replace u_0^* by $\hat{u}_0$, this adds an extra $\hat{u}_0$ to the proportionality of D.
- Change $\langle\frac{S}{S_0}\frac{\partial S}{\partial x}\rangle$ to $\langle\frac{S}{S_0}\rangle^K$, changes the proportionality of D to the salinity.

The changes above can be categorized. Conclusions per category are:

- **Change in the power of $\hat{u}_0$**
  Best results are obtained when taking $\hat{u}_0$ to a negative power, especially considering the tidal amplitude series. For the C- and h-series results are better with a positive power. However, those effects can also be achieved using other parameters. When D is proportional to $\hat{u}_0$ to a negative power the model results are off for high Q_f.
- **Change in the power of Q_f and $\frac{\Delta\rho}{\rho}$**
  By increasing the power of N_R the relation of D to Q_f and $\frac{\Delta\rho}{\rho}$ changes. This increase

significantly improves model results for the $\Delta\rho/\rho$-series. By increasing the power of N_R also the proportionality of D to $\hat{u}_0$ changes, which deteriorates the results for the Q_f-series.

- **Adding terms containing C and/or h**
  Adding an extra C or h improves the simulations for the corresponding series. The added parameter tested here was $\frac{h_0}{E_0}$ and also contains an E_0 which undoes the effect of the extra h_0. The effect of an extra h_0 itself does improve the model results.
- **Change the dependency of the salinity from $\langle \frac{S}{S_0}\frac{\partial S}{\partial x}\rangle$ to $\langle \frac{S}{S_0}\rangle^{\frac{1}{4}}$**
  Improves model results for W, h, L_e, Q_f and $\Delta\rho/\rho$, while the results for C slightly deteriorate.

Based on this analysis it is expected that better results for the tidal flume experiment are obtained when D is inversely proportional to $\hat{u}_0$, h, N_R is taken to a power higher than $\frac{1}{4}$, C and $\langle \frac{S}{S_0}\rangle$. The formulation derived by Kuijper and Van Rijn (2011) has those characters and it is thus expected to generate good simulations for the tidal flume experiment. For real convergent estuaries it is expected that best results are obtained using E_0 as a length scale instead of L_e and relating dispersion to $\langle \frac{S}{S_0}\rangle$ instead of $\langle \frac{S}{S_0}\frac{\partial S}{\partial x}\rangle$.

6.2 Gisen

Here, in Equation (6.2), the dispersion formula described by Gisen *et al.* (2015) is repeated. In case there is an inflection point the predictive dispersion first has to be converted to dispersion in the estuary mouth by using Equation (3.14) before it can be used to simulate salt intrusion in SOBEK. In Appendix B the van der Burgh constants (K-values) used are included.

$$\begin{aligned} D_1^{TA} &= 0.1167\hat{u}_1 E_1 N_R^{0.57} \\ \frac{D_x^{TA}}{D_1^{TA}} &= \left(\frac{S_x^{TA}}{S_1^{TA}}\right)^K \end{aligned} \tag{6.2}$$

Equation (6.2) can be rewritten into Equation (6.3) which directly shows the proportionality of the dispersion coefficient to the parameters influencing it.

$$\begin{aligned} D_1 &= \alpha \hat{u}_1^{0.29} \left(\frac{\Delta\rho}{\rho}\right)^{0.57} Q_f^{0.57} B_1^{-0.57} T \\ \alpha &= 0.1167 g^{0.57} \pi^{-0.43} \end{aligned} \tag{6.3}$$

6.2.1 Tidal flume test

In this section the behavior of the simulated salt intrusion using dispersion formulation (6.2) is accessed. As in general the measured and computed tidal excursions agree, in this section not much attention is payed to advective salt transport carrying the salty water land- and seaward within the estuary. As there is no inflection point in the tidal flume the dispersion formula is applied directly in the estuary mouth. So here $\hat{u}_1$ is taken as $\hat{u}_0$.

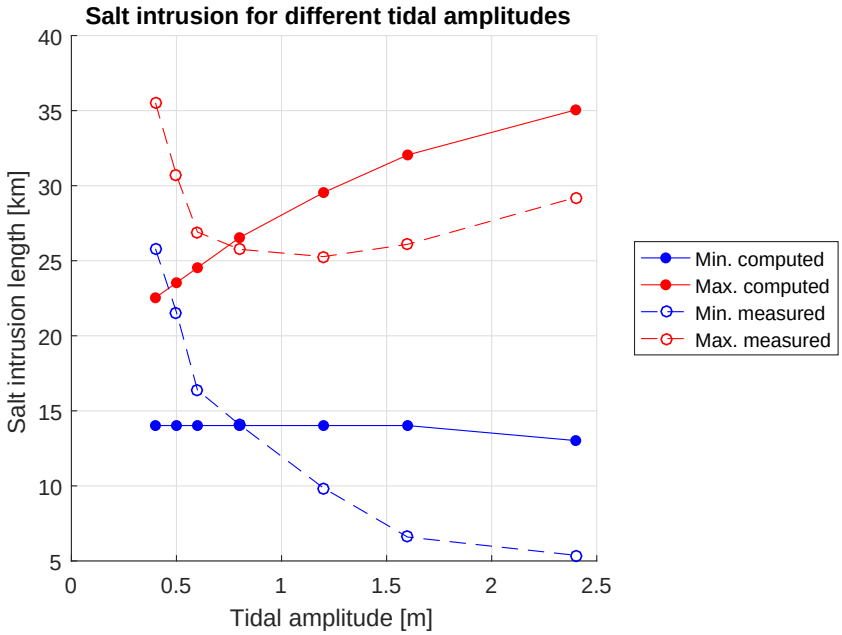

Figure 6.1: *Measured and computed salt intrusion lengths for varying tidal amplitudes.*

6.2.1.1 Tidal amplitude

As is seen from Figure 6.1 the simulated salt intrusion behavior does not agree with the observed salt intrusion. With increasing tidal amplitude, tidal energy for mixing increases. As tidal energy for mixing increases salt intrusion decreases. However, using Equation (6.2) dispersive salt transport will increase for increasing W. This is due to the proportionality of D to $\hat{u}_0^{0.29}$, which increases for an increasing tidal amplitude.

6.2.1.2 Bed roughness

For increasing C salt intrusion increases. As is shown in Figure 5.3 $\hat{u}_0$ increases with increasing C. Now due to the proportionality of D to $\hat{u}_0^{0.29}$ also the dispersive salt transport increases with increasing C, see Figure 6.2. However, the simulated increase in intrusion with increasing C is slightly underestimated.

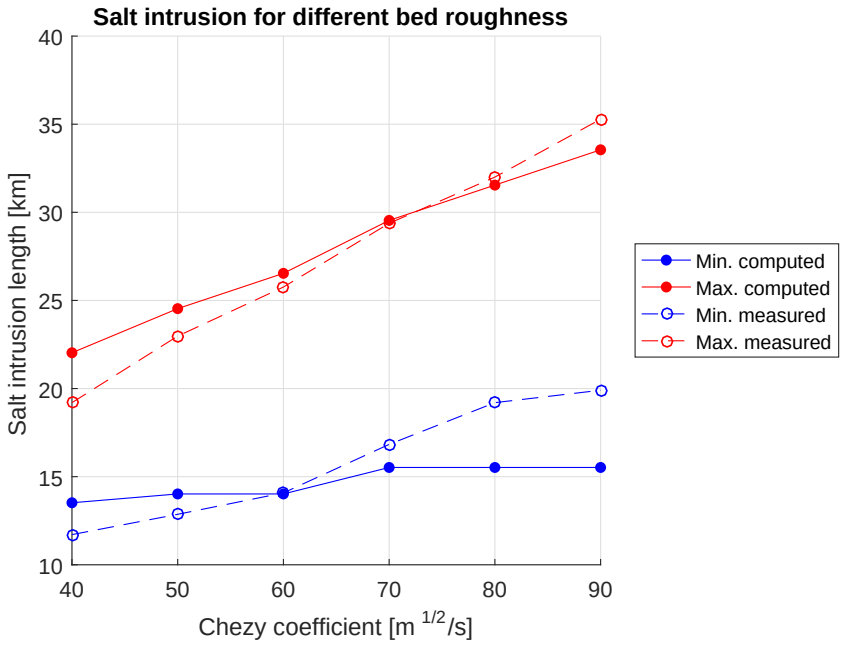

Figure 6.2: *Measured and computed salt intrusion lengths for varying bed roughness.*

6.2.1.3 Water depth

Both measured and computed salt intrusion increase for increasing h. For increasing h also $\hat{u}_0$ increases, see Figure 5.5. Due to the proportionality of D to $\hat{u}_0^{0.29}$ also the computed salt intrusion increases with increasing h. However, the measured intrusion seams to increase according to a power law, while the simulated intrusion increases approximately linear.

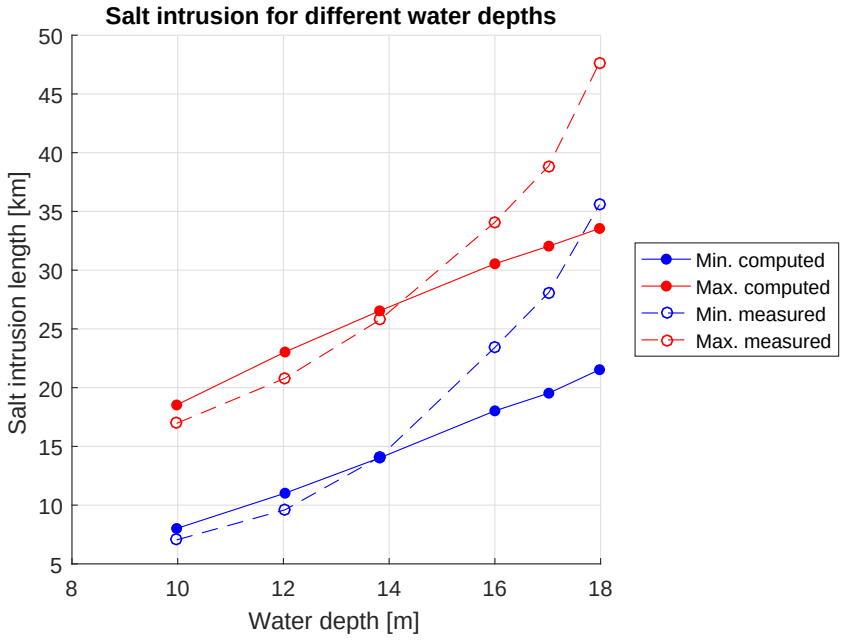

Figure 6.3: *Measured and computed salt intrusion lengths for varying water depth.*

6.2.1.4 Flume length

The measured salt intrusion increases when the flume length deviates from the resonance length. The simulated intrusion length does not show this behavior. When resonance occurs $\hat{u}_0$ is at its maximum (Figure 5.6), most tidal energy is available for mixing and thus dispersive salt transport is relatively small. Due to the proportionality of D to $\hat{u}_0^{0.29}$ the computed dispersive transport decreases with an intrusion length deviating from the resonance length and thus the dispersive salt transport does not react correctly on changes in flume length.

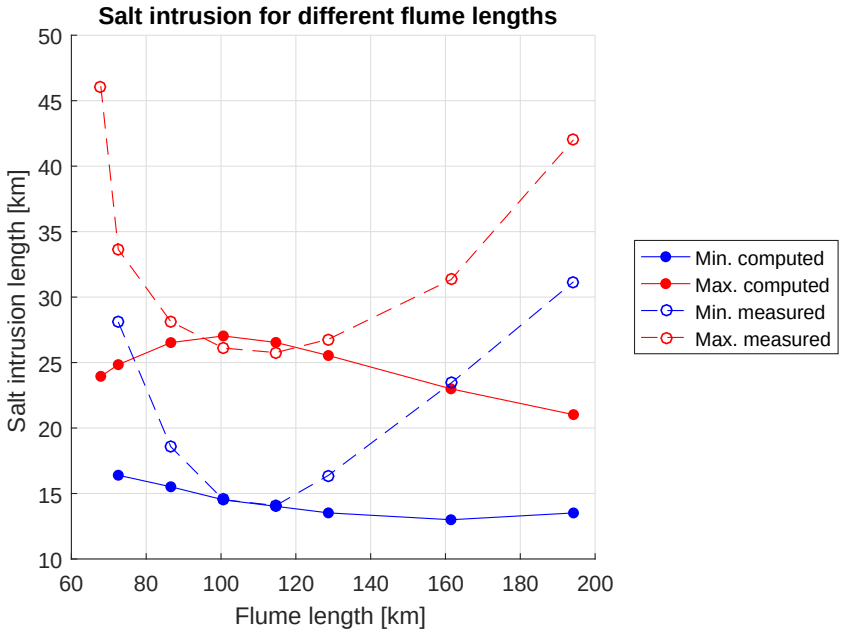

Figure 6.4: *Measured and computed salt intrusion lengths for varying flume length.*

6.2.1.5 River discharge

For discharges up till 2000 m^3/s the simulated salt intrusion follows the behavior of the computed salt intrusion. When the discharge becomes higher the tidal excursion, distance between maximum and minimum salinity, is underestimated. When the discharge reaches a point were the flow direction is always seaward the BC used in SOBEK prevents the salt from entering the estuary and there is no intrusion anymore. With Q_f increasing $\hat{u}_0$ decreases and the advective seaward transport increases. The dispersive landward transport increases due to the proportionality of D to $Q_f^{0.57}$, despite being counteracted by the proportionality of D to $\hat{u}_0^{0.29}$. So both advective seaward and dispersive landward salt transport increase. The net effect is that the salt intrudes less far when Q_f increases.

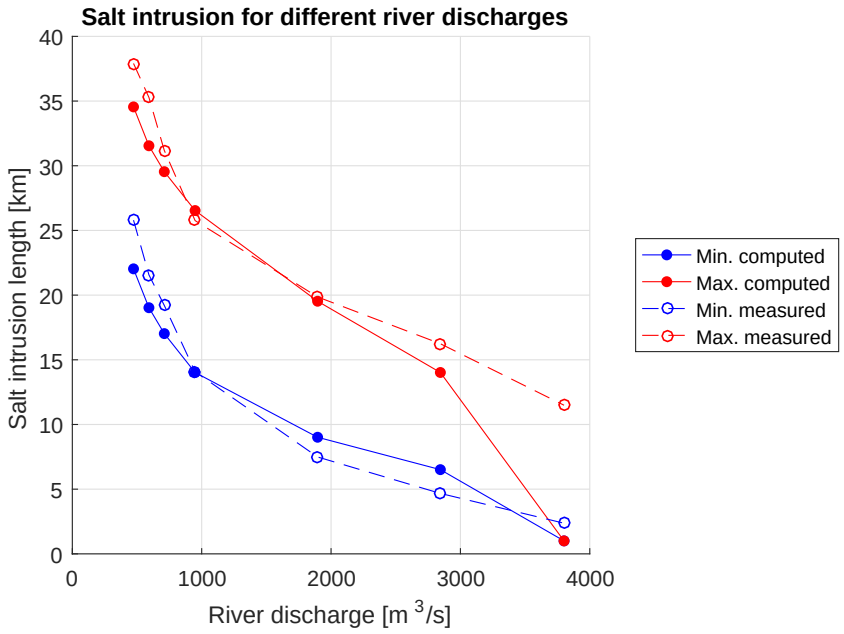

Figure 6.5: *Measured and computed salt intrusion lengths for varying river discharge.*

6.2.1.6 Relative density difference

The measured salt intrusion increases when the relative density difference increases. D is proportional to $(\frac{\Delta\rho}{\rho})^{0.57}$ and so the simulated salt intrusion also increases when $\frac{\Delta\rho}{\rho}$ increases. The increase in salt intrusion with increasing $\frac{\Delta\rho}{\rho}$ is slightly underestimated.

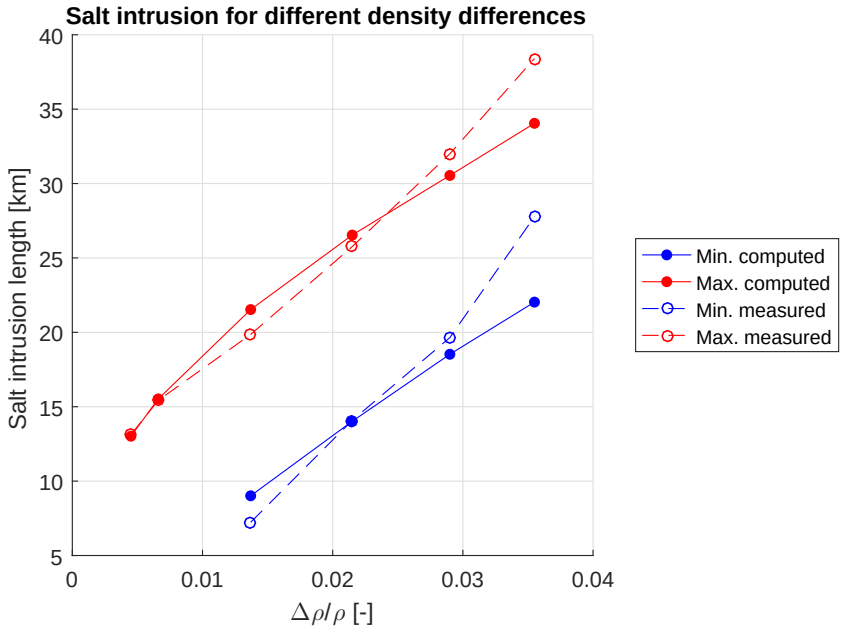

Figure 6.6: *Measured and computed salt intrusion lengths for varying relative density differences.*

6.2.1.7 Overall performance

Figure 6.7 shows the minimum and maximum computed intrusion lengths to their respective measured intrusion lengths. As can be seen from this figure in general the simulations are not sensitive enough to capture changes in system variables. Some notable observations are that the line of perfect agreement is nicely approached for the Q-series (except for $Q = 3801m^3/s$) for both minimum and maximum intrusion, the $\frac{\Delta\rho}{\rho}$ series closely follows the line of perfect agreement, while series W and L deviate clearly from the line of perfect agreement.

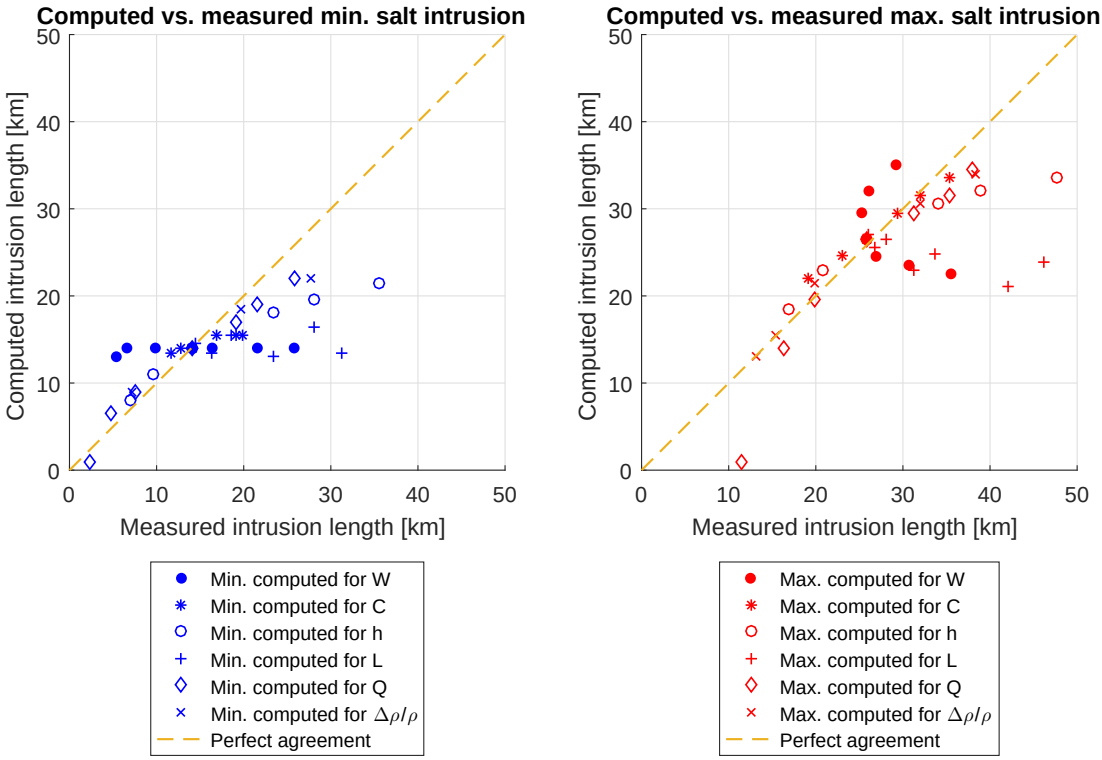

Figure 6.7: *Measured vs. computed salt intrusion lengths for the tidal flume experiment.*

Table 5.1 shows the values for R^2, $RMSE$ and σ obtained using the dispersion formula derived by Gisen *et al.* (2015). As can be seen from Figure 6.7 and R^2 there is correlation, although it is not strong.

Table 6.2: *Quality criteria for model results*

	All cases	Reduced set	Units
R^2	0,65	0,62	-
$RMSE$	0,32	0,30	-
σ	0,31	0,30	-

6.2.2 Real convergent estuaries

As stated before Gisen *et al.* (2015) described a predictive dispersion formula for the inflection point. In the schematized estuaries and the used software (SOBEK-3) the predicted dispersion has to be defined in the estuary mouth. That is why the predicted dispersion at the inflection point is converted to dispersion in the estuary mouth using Equation (3.14). As the dispersion formula derived by Gisen gave an underestimation for wide estuaries as for example the Delaware and Schelde (see Figure 6.8) additionally dispersion formula (6.4) is tested. This

formulation combines dispersion formulas described by Gisen *et al.* (2015) and Zhang and Savenije (2016). The difference with the formulation described by Zhang is that Gisen related the tidal averaged dispersion to a predicted dispersion at the inflection point and the salinity, while Zhang described a predictive dispersion coefficient based on local conditions only.

$$D_x^{TA} = 0.1167\hat{u}_0 E_0 N_R^{0.57}\left(1 + 10\left(\frac{B_x}{E_x}\right)^2\right)\left\langle\frac{S_x^{TA}}{S_0^{TA}}\right\rangle \tag{6.4}$$

Simulations of salt intrusion in real convergent estuaries have been compared for both the maximum salt intrusion length and the salinity profiles along an estuary. Figures 6.8 and 6.9 show the computed maximum salt intrusion lengths against the measured maximum salt intrusion lengths and Figures 6.10 and 6.11 show an example of a salinity curve along the Maputo estuary. From the latter figures the effect of the additional term accounting for the width can be seen as the salinity near the estuary mouth is higher when the additional term is used in predicting the dispersion coefficient. The R^2, $RMSE$, σ_L, B_e and σ_p values for the simulations using dispersion formulation (6.2) and (6.4) are given in Table 6.3.

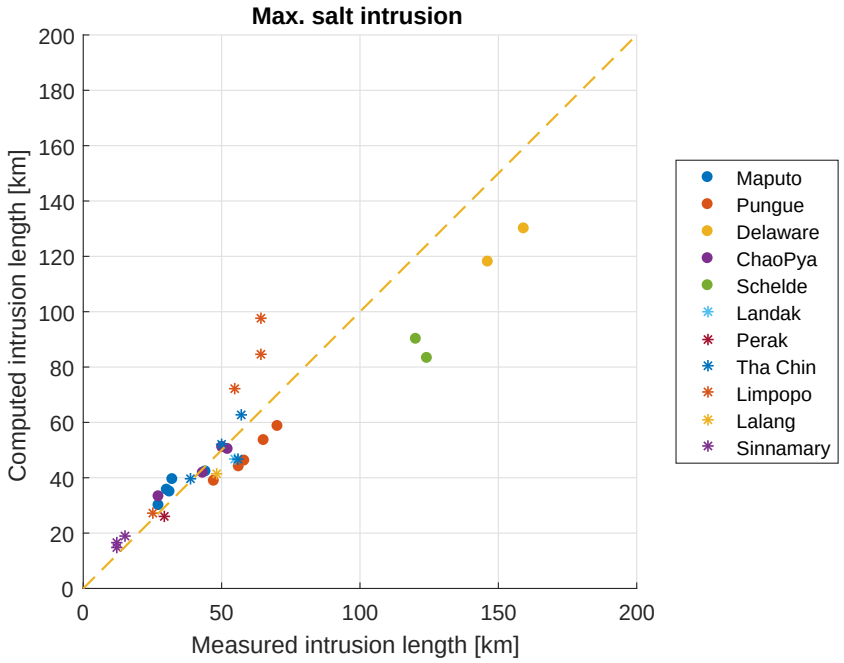

Figure 6.8: *Measured vs. computed salt intrusion lengths for real convergent estuaries. Dispersion is calculated with the dispersion formula described by Gisen et al. (2015).*

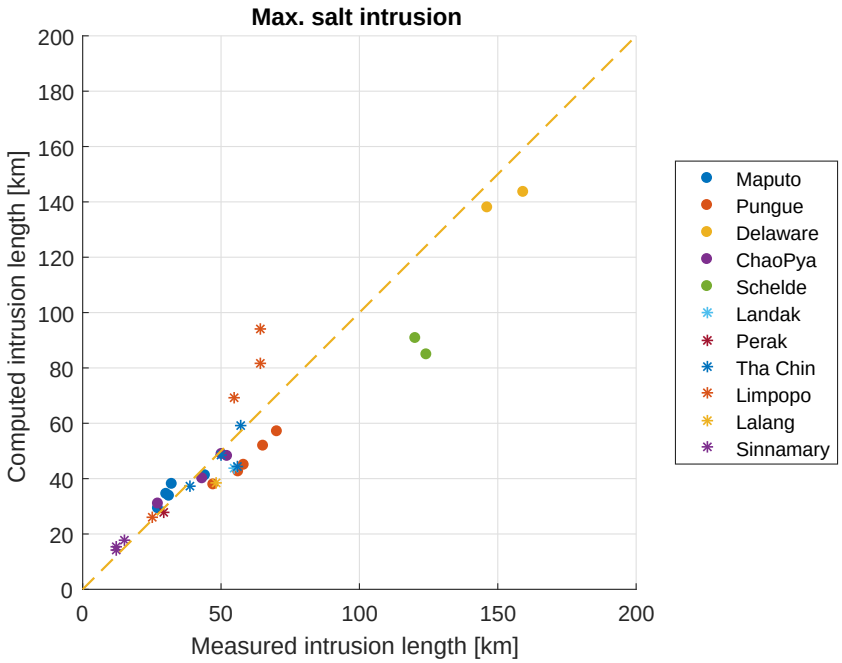

Figure 6.9: *Measured vs. computed salt intrusion lengths for real convergent estuaries. Dispersion is calculated with the dispersion formula described by Gisen et al. (2015) with the additional term* $(1 + 10(B_x/E_x)^2)$.

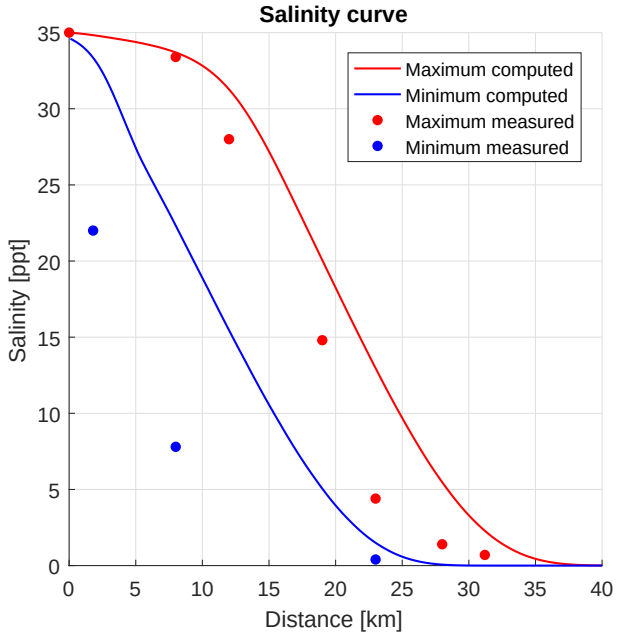

Figure 6.10: *Salinity profile for the Maputo estuary. Dispersion is calculated with the dispersion formula described by Gisen et al. (2015).*

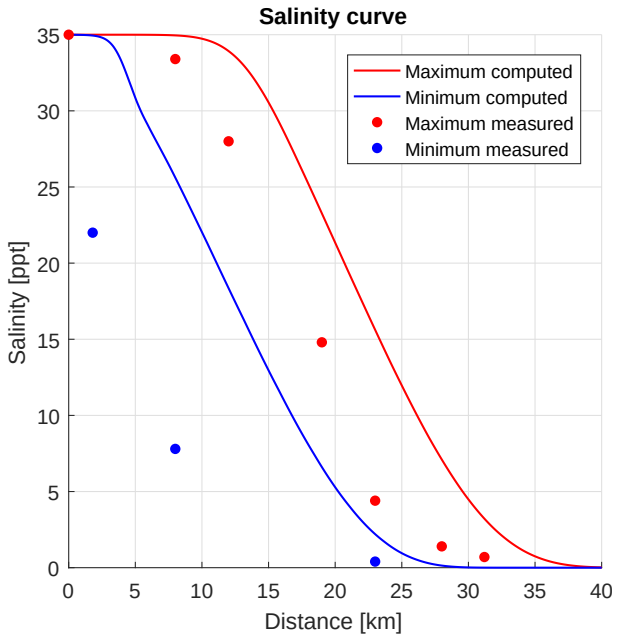

Figure 6.11: *Salinity profile for the Maputo estuary. Dispersion is calculated with the dispersion formula described by Gisen et al. (2015) with the additional term* $(1 + 10(B_x/E_x)^2)$.

Table 6.3: *Quality criteria for model results, in which* σ_L *and* σ_p *concern maximum intrusion and salinity profiles respectively.*

Criteria	Gisen	Gisen + width	units
R^2	0,85	0,88	-
$RMSE$	0,21	0,19	-
σ_L	0,21	0,19	-
B_e	0,35	1,34	ppt
σ_p	2,94	3,23	ppt

From the figures of maximum measured and computed intrusion and R^2 can be seen that there is quite some correlation between observed and simulated maximum intrusion length. Due to the improvement for the Delaware estuary using the extra term accounting for wide estuaries the correlation is slightly better when the term accounting for wide estuaries is added. In Figure 6.9 the Schelde and Limpopo estuary deviate significantly more than the other estuaries from the line of perfect agreement. The simulations using the original dispersion formulation described by Gisen *et al.* (2015) are close to the line of perfect agreement especially for low intrusion lengths, up to $60km$. From Figure 6.10, the other salinity profiles and σ_p it is seen that the simulated salinity curves can deviate significantly from the observed salinity curves. The averaged deviation is small, as can be seen from the value for B_e. The values for B_e and σ_p are slightly better for the original formulation.

6.3 Savenije

Equation (6.5) repeats the dispersion formulation derived by Savenije (2012). As D depends on $\bar{a}$ it cannot be applied in case of prismatic estuaries, for which $\bar{a}$[1] would go to infinity and D to zero. Therefore, here it is only applied for real convergent estuaries. The disadvantage of this formulation is that the intrusion length is used to calculated $\bar{a}$ and thus an iterative process has to be used. First a predicted value for $\bar{a}$ has to be used, then L_{max} is calculated, then a new $\bar{a}$ is found, a new L_{max} is calculated and so on. In Appendix B the van der Burgh constants (K-values) used are included.

$$\begin{aligned} D_0^{HWS} &= 1400 u_0 E_0 N_R^{0.5} \frac{h_0}{\bar{a}} \\ \frac{D_x^{HWS}}{D_0^{HWS}} &= \left(\frac{S_x^{HWS}}{S_0^{HWS}} \right)^K \end{aligned} \tag{6.5}$$

6.3.1 Real convergent estuaries

Simulations of salt intrusion in real convergent estuaries have been compared for both the maximum salt intrusion length and the salinity profiles along an estuary. Figure 6.12 shows the computed maximum salt intrusion lengths against the measured maximum salt intrusion lengths and Figure 6.13 shows an example of a salinity curve along the Maputo estuary. The R^2, $RMSE$, σ_L, B_e and σ_p values for the simulations using dispersion formulation (6.5) are given in Table 6.4.

The simulations using this dispersion equation show quite some correlation for the maximum intrusion length, as is indicated by R^2 and can be seen from Figure 6.12. The simulated maximum intrusion does however underestimate the measured intrusion as can be seen from Figure 6.12 and B_e. When looking to σ_p it is seen that there is also significant deviation around the salinity curves.

It is interesting to note that the simulations for the Schelde estuary go quite well. This estuary is dredged for navigation purposes and thus deeper than what it would be in natural equilibrium. The inclusion of the term $\frac{h}{\bar{a}}$ might thus result in this improved behavior for dredged estuaries.

Table 6.4: *Quality criteria for model results, in which σ_L and σ_p concern maximum intrusion and salinity profiles respectively.*

Criteria	Value	Units
R^2	0,86	-
$RMSE$	0,30	-
σ_L	0,27	-
B_e	-1,50	ppt
σ_p	3,12	ppt

[1] Remember, the salt intrusion length L is used to calculate the convergence length averaged over the salt intrusion length $\bar{a}$, $\bar{a} = \frac{a_1 x_1 + a_2 (L - x_1)}{L}$.

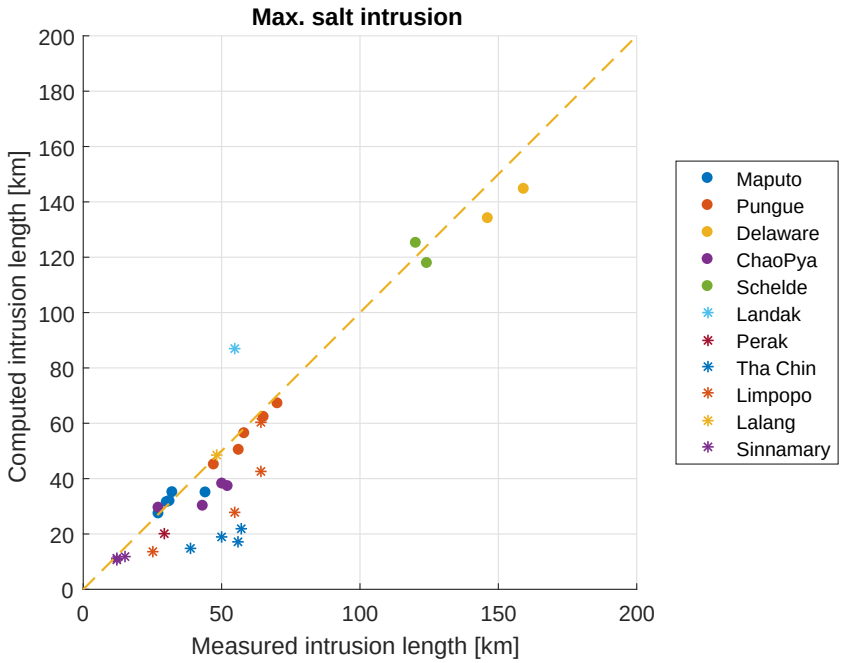

Figure 6.12: *Measured vs. computed salt intrusion lengths for real convergent estuaries. Dispersion is calculated with the dispersion formula described by Savenije (2012).*

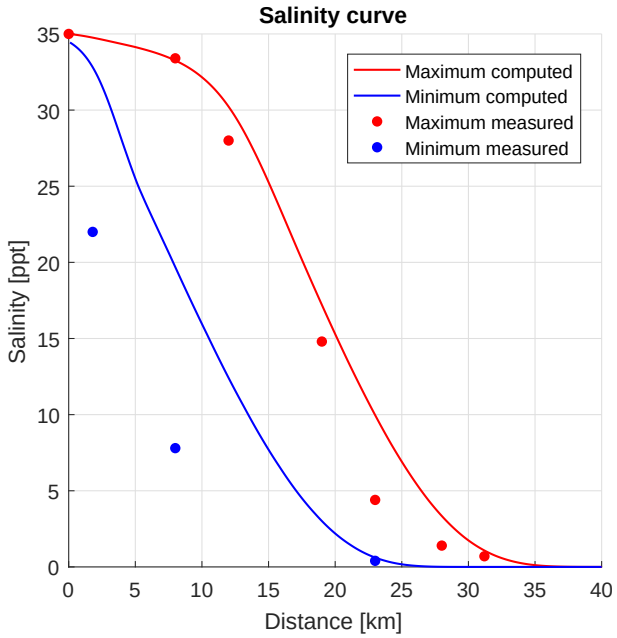

Figure 6.13: *Salinity profile for the Maputo estuary. Dispersion is calculated with the dispersion formula described by Savenije (2012).*

6.4 Kuijper and van Rijn

Kuijper and Van Rijn (2011) used Equation (6.6) to define the dispersion coefficient along the channel. The factor $e^{\Phi x}$ was added in order to allow the estuary mouth to be located anywhere along the estuary, it accounts for convergence, damping and amplification. It was not numerically possible to use $e^{\Phi x}$[2] within this thesis, therefore relation (6.7) is used instead.

[2]Remember, $\Phi = \frac{\delta_u}{2} + \frac{3(a-b)}{2ab} + \frac{1}{2a}$.

As Kuijper and Van Rijn (2011) defined separate dispersion coefficients for prismatic and convergent channels they will be addressed separately in the corresponding section. For the tidal flume test neglecting $e^{\Phi x}$ does not affect the results much as the convergence lengths go to infinity and the influence of damping/amplification is small. Dispersion in real convergent estuaries can be significantly affected by this term. For the considered estuaries Φ is in the range of $5,0 \cdot 10^{-6}$ and $4,8 \cdot 10^{-4}$. As those values are larger than zero, inclusion of $e^{\Phi x}$ would increase the simulated dispersive transport and the results presented here are underestimated.

$$D_x^{HWS} = e^{\Phi x} D_0^{HWS} \left(\frac{S^{HWS}}{S_0^{HWS}} \right)^{\frac{1}{2}} \tag{6.6}$$

$$D_x^{HWS} = D_0^{HWS} \left(\frac{S^{HWS}}{S_0^{HWS}} \right)^{\frac{1}{2}} \tag{6.7}$$

6.4.1 Tidal flume test

The flume used in this experiment was a prismatic channel and thus Equation (6.8) is used to describe dispersive salt transport. However, in these simulations tidal averaged values are used instead of HWS values for D and S. In this section simulation results are presented.

$$\begin{aligned} D_0^{HWS} &= \alpha_c 6 \hat{u}_0 h_0 N_R^{\frac{1}{2}} \frac{C}{\sqrt{g}} \\ \alpha_c &= \frac{5}{6} \\ (\frac{\bar{a}}{E_0} &> 10) \end{aligned} \tag{6.8}$$

Equation (6.8) is rewritten into Equation (6.9) which directly shows the proportionality of the dispersion coefficient to the parameters influencing it.

$$\begin{aligned} D_0^{HWS} &= \alpha \hat{u}_0^{-\frac{1}{2}} \left(\frac{\Delta \rho}{\rho} \right)^{\frac{1}{2}} Q_f^{\frac{1}{2}} B_0^{-\frac{1}{2}} h_0 C \\ \alpha &= 5\sqrt{\pi} \end{aligned} \tag{6.9}$$

6.4.1.1 Tidal amplitude

From Figure 6.14 can be seen that simulated salt intrusion shows the same behavior as the observed salt intrusion for changing tidal amplitude. Using Equation (6.8) the dispersive salt transport decreases with increasing $\hat{u}_0$, due to the proportionality of D to $\hat{u}_0^{-\frac{1}{2}}$. With increasing tidal amplitude the energy for tidal mixing and $\hat{u}_0$ increase and thus the behavior of observations and simulations agree. Also the movement of the salt water land- and seaward is nicely simulated. For large tidal amplitudes this advective salt transport is dominant over dispersive salt transport.

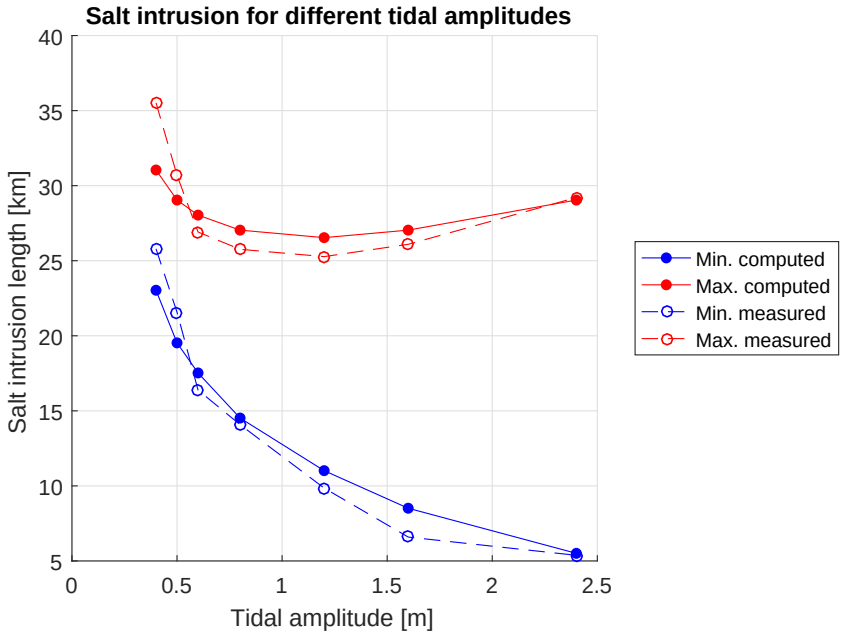

Figure 6.14: *Measured and computed salt intrusion lengths for varying tidal amplitudes.*

6.4.1.2 Bed roughness

Both the observed and simulated minimum and maximum salt intrusion increase for increasing C. The increase of the simulated intrusion with increasing C is slightly underestimated. Despite being, justly, counteracted by the proportionality of D to $\hat{u}_0^{-\frac{1}{2}}$, still the right trend is observed for a changing bed roughness. The increase in simulated salt intrusion with increasing C is due to the inclusion of $\frac{C}{\sqrt{g}}$ in the dispersion formulation.

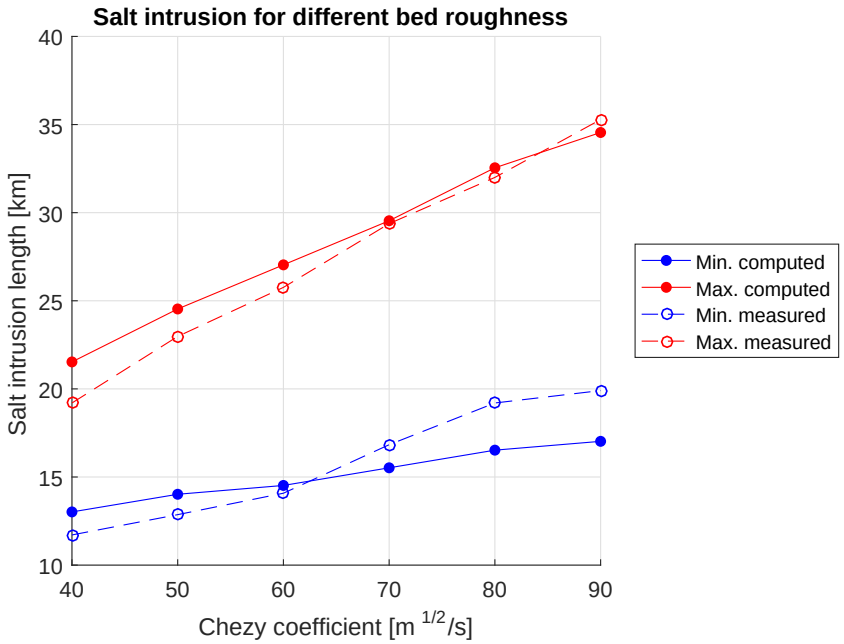

Figure 6.15: *Measured and computed salt intrusion lengths for varying bed roughness.*

6.4.1.3 Water depth

The simulated salt intrusion approaches the observed intrusion. However, for deeper waters the simulated intrusion length underestimates the observed intrusion length. As is seen before with increasing h also $\hat{u}_0$ increases. Now D increases due to a proportionality to h, while it decreases due to a proportionality to $\hat{u}_0^{-\frac{1}{2}}$. The combined effect is an increasing D with h increasing, as the proportionality to h is dominant in this case.

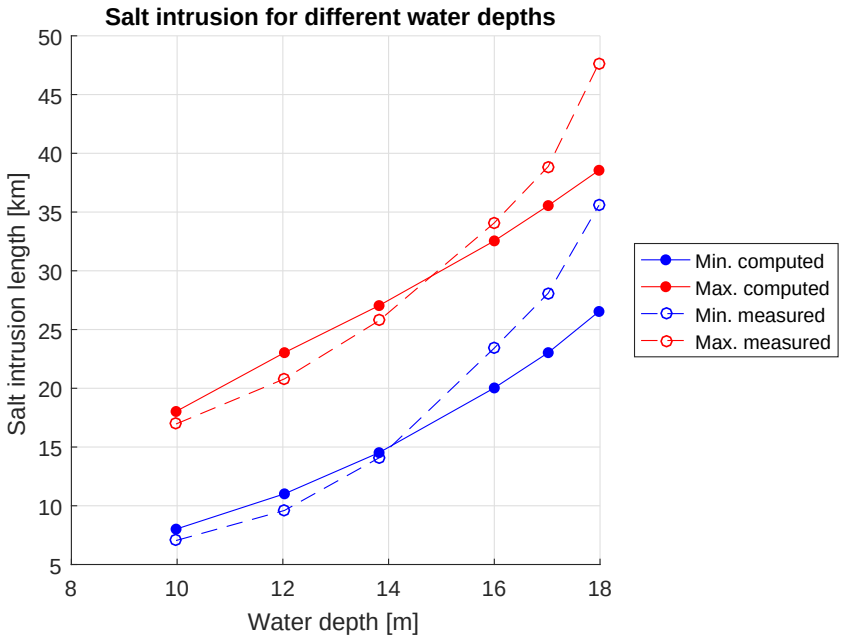

Figure 6.16: *Measured and computed salt intrusion lengths for varying water depth.*

6.4.1.4 Flume length

The observed salt intrusion increases when the flume length deviates from the resonance length. The simulated intrusion length also shows this behavior, see Figure 6.17. Only it underestimates changes in intrusion length significantly when the flume length deviates from the reference test. The effect of changing flume length is captured by the proportionality of D to $\hat{u}_0^{-\frac{1}{2}}$.

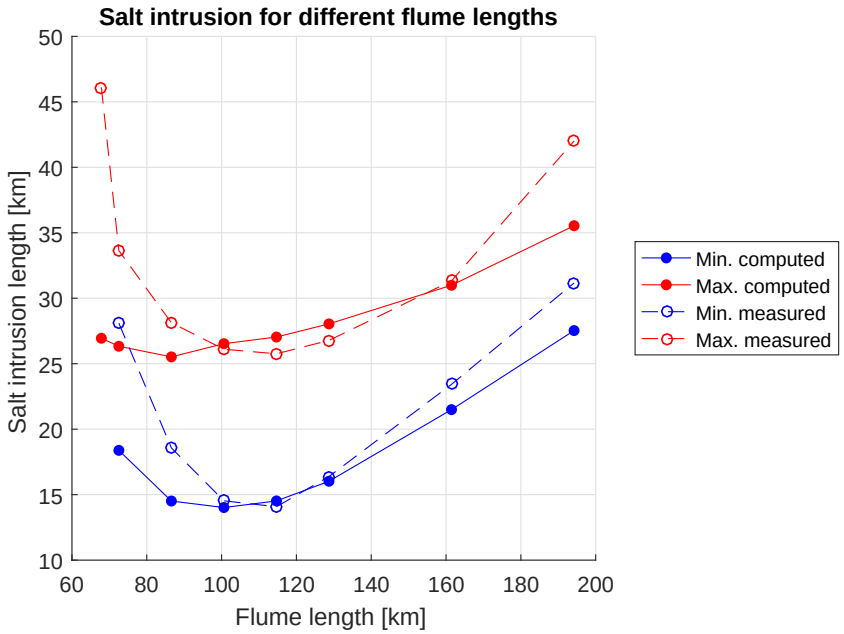

Figure 6.17: *Measured and computed salt intrusion lengths for varying flume length.*

6.4.1.5 River discharge

For low river discharges the simulated intrusion approaches the observed intrusion. For $Q_f > 1000 \frac{m^3}{s}$ the simulated intrusion starts to deviate from the observed intrusion. It is seen that the dispersion coefficient explodes for high discharges which is due to a proportionality of D to $\hat{u}_0^{-\frac{1}{2}}$, in which $\hat{u}_0$ is not defined correctly as is discussed in Chapter 7. As in case of high river discharges flooding is much more of a concern than salt intrusion also an assessment excluding river discharges of $Q_f = 2845 \frac{m^3}{s}$ and $Q_f = 3801 \frac{m^3}{s}$ is included to compare model results using different dispersion formulas.

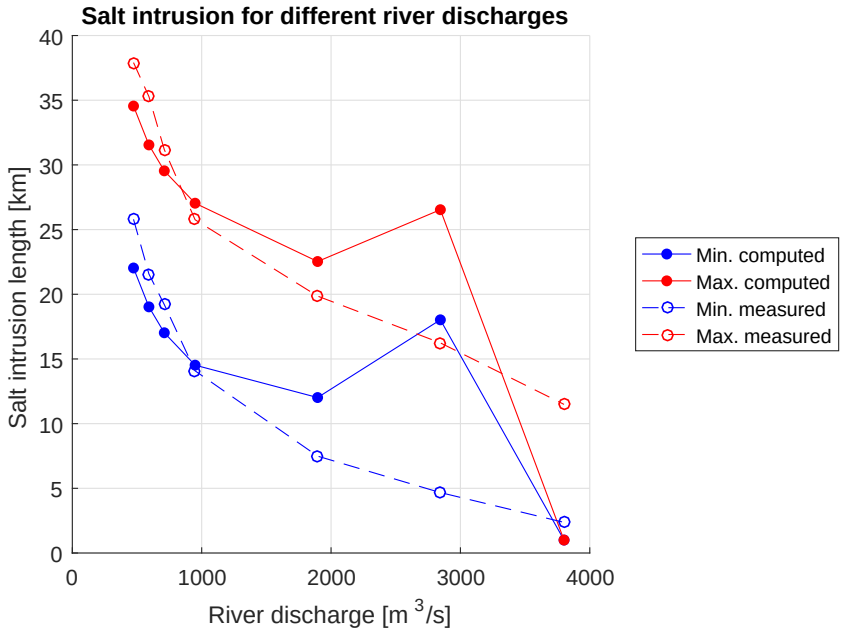

Figure 6.18: *Measured and computed salt intrusion lengths for varying river discharge.*

6.4.1.6 Relative density difference

The measured salt intrusion increases when the relative density difference increases, which agrees with the observed intrusion. D is proportional to $(\frac{\Delta\rho}{\rho})^{\frac{1}{2}}$ and so the simulated salt intrusion also increases when $\frac{\Delta\rho}{\rho}$ increases. The increase in salt intrusion with increasing $\frac{\Delta\rho}{\rho}$ is slightly underestimated.

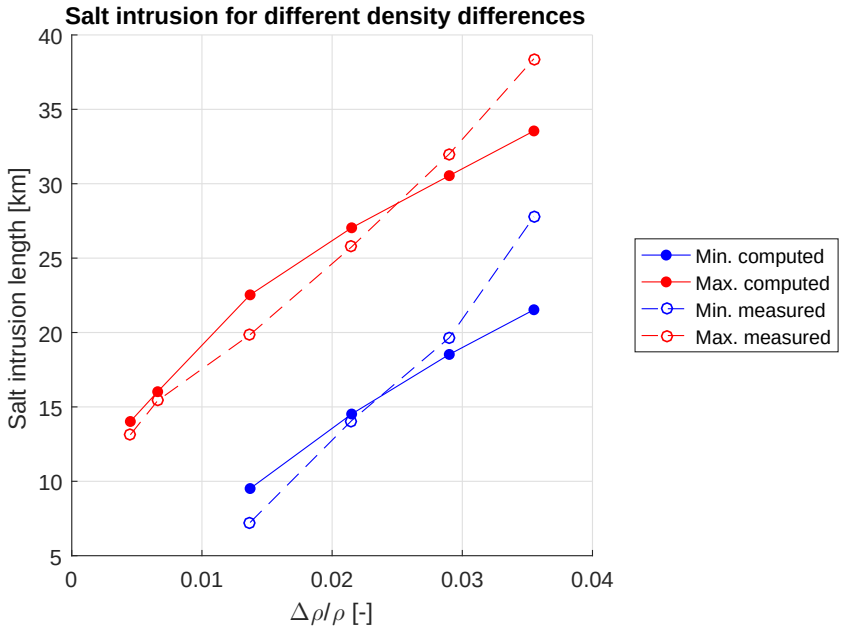

Figure 6.19: *Measured and computed salt intrusion lengths for varying relative density differences.*

6.4.1.7 Overall performance

Figure 6.20 shows the minimum and maximum computed versus observed intrusion lengths. As can be seen from this figure the simulations show quite some correlation with the observations. Most points are close to the line of perfect agreement. However, some points deviate from this general behavior. The points for high river discharges (the ones most to the left) and for high water depths (the ones most to the right) deviate much. Most deviations are seen for the series considering the flume length.

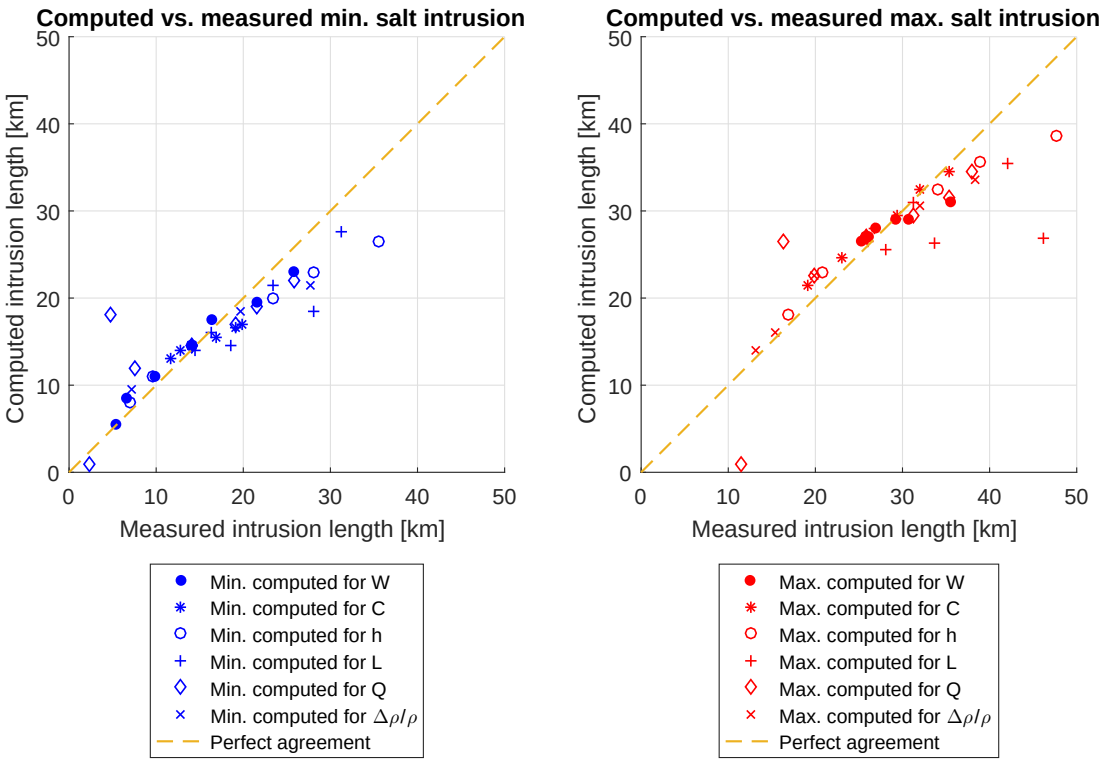

Figure 6.20: *Measured vs. computed salt intrusion lengths for the tidal flume experiment.*

Table 6.5 shows the values for R^2, $RMSE$ and σ obtained using the dispersion formula derived by Kuijper and Van Rijn (2011). From Figure 6.20 and R^2 it is seen that there is strong correlation between simulations and observations, especially when the cases with high Q_f are neglected.

Table 6.5: *Quality criteria for model results*

	All cases	Reduced set	Units
R^2	0,82	0,87	-
$RMSE$	0,38	0,15	-
σ	0,39	0,15	-

6.4.2 Real convergent estuaries

Equation (6.10) repeats the dispersion formula Kuijper and Van Rijn (2011) use for convergent estuaries. The salt intrusion simulations in real convergent estuaries have been compared for both the maximum salt intrusion length and the salinity profiles along an estuary. Figure 6.21 shows the computed maximum salt intrusion lengths against the measured maximum salt intrusion lengths and Figure 6.22 shows an example of a salinity curve along the Maputo estuary. The R^2, $RMSE$, σ_L, B_e and σ_p values for the simulations using dispersion formulation (6.10) are given in Table 6.6.

$$
\begin{aligned}
&D_0 = \alpha_c 60 \hat{u}_0 E_0 N_R^{\frac{1}{2}} \frac{h_0}{\bar{a}} \frac{C}{\sqrt{g}} \\
&\alpha_c = 1 \\
&(\frac{\bar{a}}{E_0} < 10)
\end{aligned}
\tag{6.10}
$$

From the R^2 value and Figure 6.21 it can be seen that there is strong correlation between measured and computed maximum salt intrusion. Again, in general the computed intrusion underestimates the measured intrusion. This can be seen from Figure 6.21 and the bias B_e. The underestimation may be (partly) due to the effect of neglecting $e^{\Phi x}$ in calculating the dispersion, which when accounted for results in more dispersion. Especially in the Maputo, Perak, ThaChin and Sinnamary estuaries this effect is significant. It is again seen that the simulations for the Schelde estuary are close to the line of perfect agreement and that the dispersion formulation contains a h.

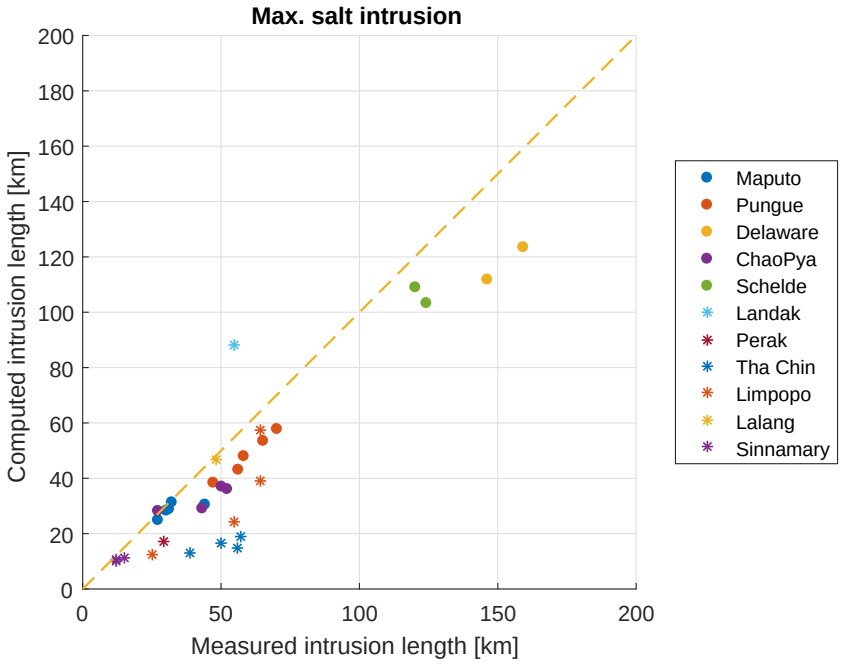

Figure 6.21: *Measured vs. computed salt intrusion lengths for real convergent estuaries. Dispersion is calculated with the dispersion formula described by Kuijper and Van Rijn (2011).*

Table 6.6: *Quality criteria for model results, in which σ_L and σ_p concern maximum intrusion and salinity profiles respectively.*

Criteria	Value	units
R^2	0,83	-
$RMSE$	0,35	-
σ_L	0,26	-
B_e	-2,62	ppt
σ_p	3,64	ppt

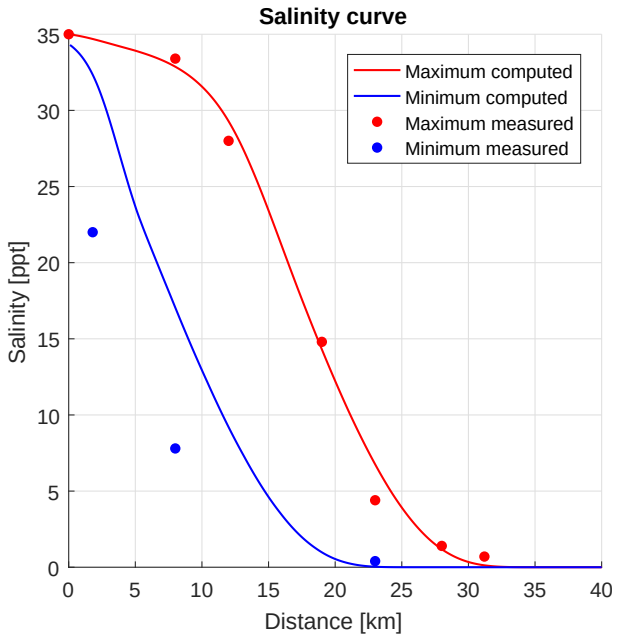

Figure 6.22: *Salinity profile for the Maputo estuary. Dispersion is calculated with the dispersion formula described by Kuijper and Van Rijn (2011).*

6.5 Zhang

Equation (6.11) repeats the dispersion formulation as defined by Zhang and Savenije (2016). This equation is only tested for the real convergent estuaries as it is derived to account for the effects only present in very wide estuaries. Using Equation (6.11) the dispersion is calculated based on local values only. However, this local calculation is not available in SOBEK-3. That is why here Equation (6.12) is used instead. The effect of relating the dispersion to the mouth dispersion depends on the width convergence and damping/amplification[3].

$$D = 0.1\hat{u}_x E_x N_{R,x}^K \left(1 + 10\left(\frac{B_x}{E_x}\right)^2\right) \tag{6.11}$$

$$D = 0.1\hat{u}_0 E_0 N_{R,0}^K \left(1 + 10\left(\frac{B_x}{E_x}\right)^2\right) \left\langle \frac{S^{TA}}{S_0^{TA}} \right\rangle^K \tag{6.12}$$

[3]If local values are estimated by Equations (2.2) and (2.4) a term $e^{(\delta_u + \frac{1}{b})Kx}$ should be added to Equation (6.12).

6.5.1 Real convergent estuaries

Zhang and Savenije (2016) determined a starting value for K ($K = 0.58$) and defined a formula to calculate K for the specific case. Here both methods are tested, in Appendix B the predicted van der Burgh constants (K-values) used are included. Simulations of salt intrusion in real convergent estuaries have been compared for both the maximum salt intrusion length and the salinity profiles along an estuary. Figures 6.23 and 6.24 show the computed maximum intrusion lengths against the measured ones. Figures 6.25 and 6.26 show a salinity curve in the Maputo estuary. The R^2, $RMSE$, σ_L, B_e and σ_p values are given in Table 6.7.

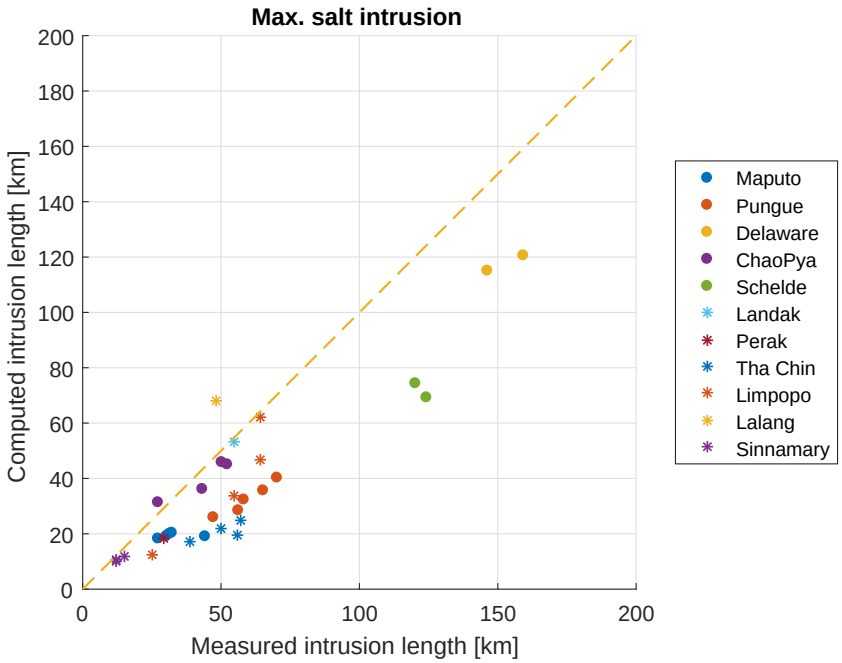

Figure 6.23: *Measured vs. computed salt intrusion lengths for real convergent estuaries. Dispersion is calculated with the dispersion formula described by Zhang and Savenije (2016) using K=0,58.*

Both simulations, using $K = 0,58$ and the predictive equation for K, show quite some correlation for the maximum intrusion length as is indicated by the R^2-value and can be seen from Figures 6.23 and 6.24. The correlation is just gently stronger in case the predictive equation for K is used. In both model series the simulated intrusion underestimates the measured intrusion as can be seen from Figures 6.23 and 6.24 and the values for B_e. There is also quite some deviation around the salinity profiles as the σ_p-values indicate. The salinity profiles are slightly better approached when a fixed value of 0,58 is used for K.

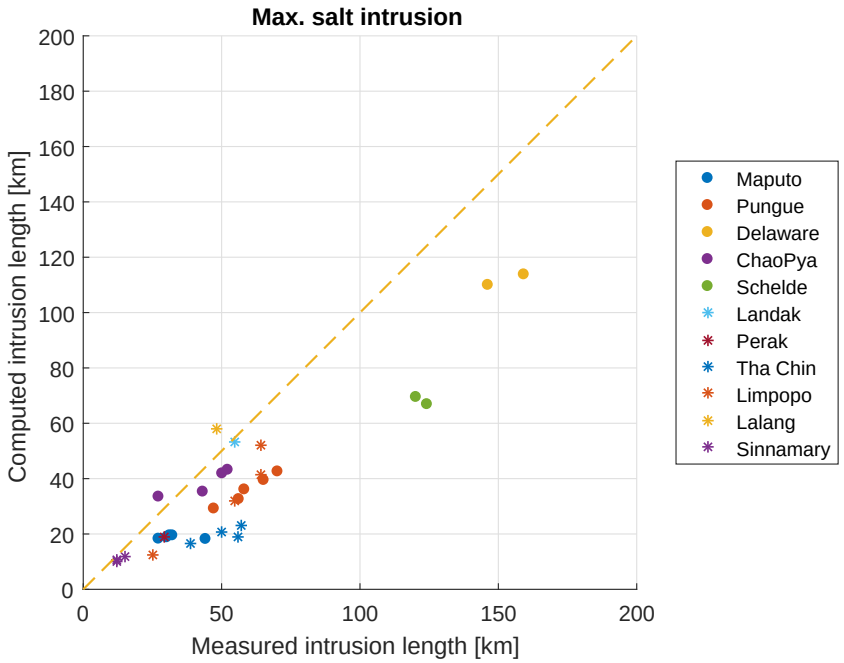

Figure 6.24: *Measured vs. computed salt intrusion lengths for real convergent estuaries. Dispersion is calculated with the dispersion formula described by Zhang and Savenije (2016) using K-predicted.*

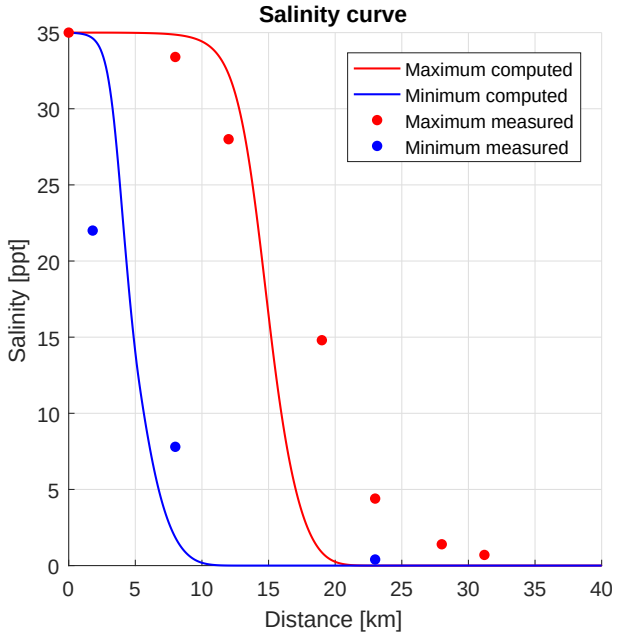

Figure 6.25: *Salinity profile for the Maputo estuary. Dispersion is calculated with the dispersion formula described by Zhang and Savenije (2016), using K=0,58.*

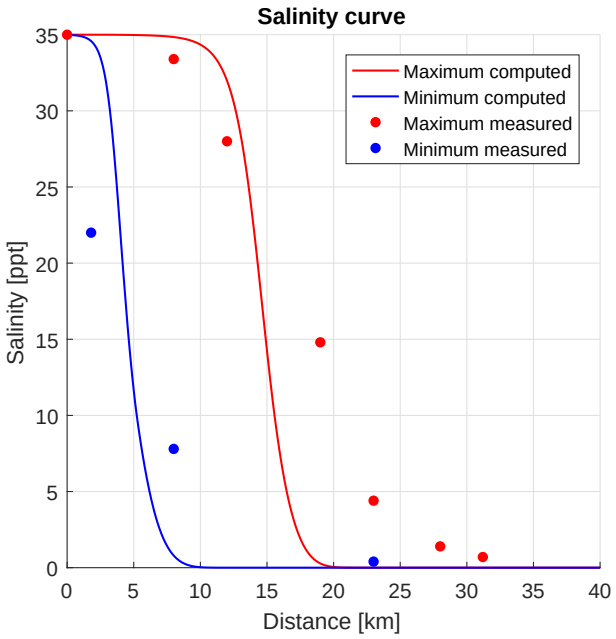

Figure 6.26: *Salinity profile for the Maputo estuary. Dispersion is calculated with the dispersion formula described by Zhang and Savenije (2016), using the predictive equation for K.*

Table 6.7: *Qualtiy criteria for model results, in which σ_L and σ_p concern maximum intrusion and salinity profiles respectively.*

Criteria	Zhang $K = 0.58$	Zhang $K_{predicted}$	Units
R^2	0,82	0,85	-
$RMSE$	0,38	0,38	-
σ_L	0,23	0,21	-
B_e	-2,24	-2,45	ppt
σ_p	4,09	4,21	ppt

7 Discussion

Within this chapter the results are discussed. First the best performing dispersion formulations for both prismatic and convergent estuaries are pointed out. After that their possibilities and restrictions are discussed. Finally the limitations which have to be taken into account interpreting the outcomes are presented.

7.1 Best performing dispersion formulation

The most important discussion is why different dispersion formulations are used for the tidal flume experiments and the real convergent estuaries. The main difference between those is the channel geometry. The tidal flume experiment used a flume in which the depth was in the same order of magnitude as the width, while real convergent estuaries (and real prismatic channels) are much wider than deep. In addition all irregularities occurring in reality, such as side embayments or side channels, are not present in the tidal flume. As those differences might have significant effects on the salt intrusion process here the tidal flume experiment and the real convergent estuaries are treated separately.

In the tidal flume it is observed that with an increasing tidal amplitude the dispersive landward salt transport decreases. Which is explained by the increase of tidal mixing and less stratification. This agrees with an inversely proportionality of the dispersion coefficient with the maximum flood velocity. Such a relation is present in the formulations described by Thatcher and Harleman (1972) (which uses the estuary length as a length scale) and Kuijper and Van Rijn (2011) (which uses the depth as a length scale for prismatic channels). However, Savenije (2016) questions the applicability of this relation in real cases and argues that the dispersion coefficient should be related to the maximum flood velocity, tidal excursion and the estuarine Richardson number. This way the dispersive landward salt transport increases when the tidal amplitude increases. As an argument he states that the tidal excursion is the length over which different tidal mixing processes can take place and should therefore be taken as the mixing length scale. As the tidal excursion depends on the maximum flood velocity the dispersion coefficient is proportional to the maximum flood velocity. This agrees with the dispersion formulations described by Gisen *et al.* (2015), Savenije (2012), Kuijper and Van Rijn (2011) (for convergent estuaries) and Zhang and Savenije (2016).

Tidal flume experiment

There is no doubt which tested dispersion formulation performs best for the tidal flume experiments. This is the formulation as derived for prismatic channels by Kuijper and Van Rijn (2011), which is repeated in Equation (7.1). In this equation the velocity and length scale used are $\hat{u}_0$ and h_0 respectively, which result in the inversely proportionality of D with $\hat{u}_0$, N_R is the stratification parameter and $\frac{C}{\sqrt{g}}$ accounts for the effect of friction. In Table 7.1 the R^2, $RMSE$ and σ values for the assessed dispersion formulations are included. The simulations using the dispersion formulation derived by Kuijper and Van Rijn (2011) has a strong, and by far strongest, correlation. When the unreliable simulations, the ones for high discharges, are excluded from the analysis the $RMSE$ and σ are by far smallest using this equation.

$$D_0^{HWS} = 5\hat{u}_0 h_0 N_R^{\frac{1}{2}} \frac{C}{\sqrt{g}}$$
$$\frac{D_x}{D_0} = \left(\frac{S_x}{S_0}\right)^{\frac{1}{2}} \tag{7.1}$$

Table 7.1: *Quality criteria for model results for all dispersion formulations regarding the tidal flume experiment. Kuijper and van Rijn (improved) made use of improved P_e and $\hat{u}_0$ values which is commented on later.*

Dispersion formula	Thatcher and Harleman		Gisen	
	All cases	Reduced set	All cases	Reduced set
R^2 $[-]$	0,60	0,58	0,65	0,62
$RMSE$ $[-]$	0,38	0,31	0,32	0,30
σ $[-]$	0,38	0,31	0,31	0,30
Dispersion formula	**Kuijper and van Rijn**		**Kuijper and van Rijn (improved)**	
	All cases	Reduced set	All cases	Reduced set
R^2 $[-]$	0,82	0,87	0,86	0,87
$RMSE$ $[-]$	0,38	0,15	0,14	0,14
σ $[-]$	0,39	0,15	0,14	0,14

Overall the reaction to changes in the system variables is captured using this dispersion formulation, which was seen in Figure 6.21. However, for large h the salt intrusion is underestimated, the simulations are not sensitive enough for changes in L_e, for large Q_f salt intrusion is overestimated and for extremely large Q_f where water flows only out of the estuary no salt intrudes in the estuary anymore.

Real convergent estuaries

In contradiction to what is observed for the tidal flume there is no dispersion formulation that performs substantially better than the others for real convergent estuaries. However, if one had to be selected it would be the dispersion formula described by Gisen *et al.* (2015), which in case of wide estuaries can be extended for lateral mixing, as it scores relatively good on all criteria (see Table 7.2). There is strong correlation between measured and simulated maximum intrusion for all formulations. In Table 7.2 also the results for the dispersion formula for prismatic channels derived by Kuijper and Van Rijn (2011) is included. Although this formula is not derived for convergent estuaries, it is tested on those in Appendix G. This is done as this dispersion formula gave such good results for the tidal flume test that it is worth testing its applicability on real convergent estuaries. It is noticeable that the simulations do not significantly perform different, despite that there is a variety of mixing length scales used (h_0, E_0 and L_e).

The formulations as described by Thatcher and Harleman (1972) and Gisen *et al.* (2015) have a small B_e and relatively small σ_p. While the formulations derived by Kuijper and Van Rijn (2011) and Zhang and Savenije (2016) have a rather large B_e and σ_p. The formulation derived by Savenije (2012) has a relative small value for σ_p and a moderate B_e-value. Kuijper and Van Rijn (2011) used the term $e^{\Phi x}$ to account for geometry convergence and damping/amplification of the tidal wave, which would increase the dispersion and salt intrusion. In this research, this term is neglected and the simulations underestimate the salt intrusion to a certain degree. The equation described by Zhang and Savenije (2016) makes use of local quantities to define the dispersion coefficient, while in this research it is related to the mouth dispersion. This adjustments affects the simulations, its exact effect depend on the width convergence and damping/amplification of the tidal wave.

Table 7.2: *Quality criteria for model results for all dispersion formulations regarding real convergent estuaries. (KR stands for Kuijper and van Rijn)*

Dispersion formula	Thatcher and Harleman	Gisen	Gisen + width term	Savenije
$R^2\ [-]$	0,87	0,85	0,88	0,86
$RMSE\ [-]$	0,23	0,21	0,19	0,30
$\sigma_L\ [-]$	0,20	0,21	0,19	0,27
$B_e\ [ppt]$	0,01	0,35	1,34	-1,50
$\sigma_p\ [ppt]$	3,33	2,94	3,23	3,12
Dispersion formula	$KR_{convergent}$	$KR_{prismatic}$	Zhang $K = 0,58$	Zhang $K_{predicted}$
$R^2\ [-]$	0,83	0,84	0,82	0,85
$RMSE\ [-]$	0,35	0,37	0,38	0,38
$\sigma_L\ [-]$	0,26	0,19	0,23	0,21
$B_e\ [ppt]$	-2,62	-3,49	-2,24	-2,45
$\sigma_p\ [ppt]$	3,64	3,91	4,09	4,21

Inclusion of the parameters $\frac{h}{a}$ and/or $\frac{C}{\sqrt{g}}$, which Savenije (2012) and Kuijper and Van Rijn (2011) did, did not lead to significant changes in model performance (see Table 7.2). However, the Schelde estuary is dredged and it the formulations including $\frac{h}{a}$ resulted in the best simulations. When the additional term $(1 + 10(B_x/E_x)^2)$ is included in the simulations best results are obtained if it is added to Gisen's formulation, which scores better on all criteria in Table 7.2 than the formulation described by Zhang and Savenije (2016). Dispersion formulas underestimating salt intrusion can be improved by calibrating (increasing) the c_2 value.

7.2 Possibilities and restrictions

For the tidal flume experiment there is one formula which performs best. Here its possibilities and restrictions are discussed. The dispersion formulas assessed for the real convergent estuaries perform more or less equally well[1]. Therefore here there practical value is discussed.

Tidal flume experiment

The model using the dispersion formula (7.1) is capable of estimating the maximum intrusion length for changing tidal amplitudes, bed roughness, water depth, low to moderate river discharges and sea water salinity. However one should be careful applying the model to extreme situations, the general behavior of salt intrusion is captured. In case of changing flume lengths and high river discharges, the model does not seem to be too trustworthy. The overestimation in case of high river discharges is explained by the taken $\hat{u}_0$ and P_e. Both are underestimated in the current version of SOBEK as one can see in figure 7.1. In Appendix F a later performed analysis of the dispersion formulation for prismatic channels derived by Kuijper and Van Rijn (2011) is included. There it is seen that by using the adjusted values for $\hat{u}_0$ and P_e the model results improve (see grey values in Table 7.1) and the overestimation for high river discharges disappears.

Real convergent estuaries

In dispersion formula (6.1) the scale factors for shear mixing and the mixing length are included. Dispersion induced by the most dominant mixing mechanisms, like gravitational circulation and tidal pumping, are captured. However, some mixing mechanisms which can induce dispersive transport in specific cases are not captured in the formula. Those mechanisms are tidal trapping, mixing in channel bends, mixing at the estuary banks and mixing by the wind.

In addition there are some practical remarks for all dispersion formulations used.

[1] If one bears in mind that some formulations need some further calibration.

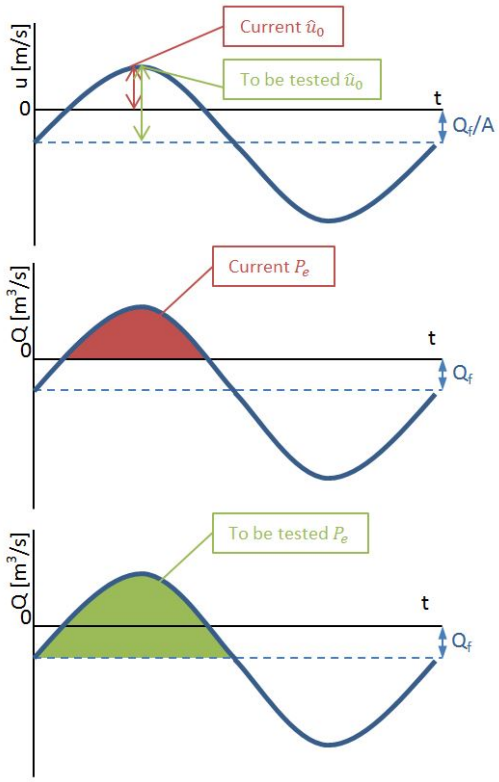

Figure 7.1: *Used and to be tested $\hat{u}_0$ and P_e.*

- **Thatcher and Harleman:**
  It makes use of many user defined constants. The most questionable one is the estuary length L_e. This length is not well defined and does not have a physical meaning in the dispersive process.
- **Gisen:**
  In order to estimate the value for c_{10} one needs to know the value for C. When it is known the dispersion in the estuary mouth has to be calculated manually from the manually calculated dispersion at the inflection point, for which the value for $\hat{u}_1$ has to be known[2].
- **Gisen with $(1 + 10(B_x/E_x)^2)$:**
  The same comment as for the original formula described by Gisen *et al.* (2015) holds. The extra term can be included when lateral mixing plays an important role, this choice has to be made by the user.
- **Savenije:**
  The formulation makes use of parameters which are not known before calculation starts. From a hydrodynamic model u_0, C and δ_u can be extracted in order to estimate c_{10}. To predict dispersion this formulation makes use of $\bar{a}$, which is a scaled convergence length over the salt intrusion length. As we are looking after the intrusion length it is unknown beforehand and some iterative process has to be applied. Additionally when this formula is applied dynamically under changing conditions the intrusion length and thus $\bar{a}$ changes constantly.
- **Kuijper and van Rijn:**
  Similar to the formula derived by Savenije this formulation makes use of $\bar{a}$. In their derivation Kuijper and Van Rijn (2011) found that the term $e^{\Phi x}$ has to be included in the dispersion formulation. As this term is not easy implemented numerically it is neglected. By neglecting $e^{\Phi x}$, Φ is in general positive, the dispersive transport is underestimated.

[2]When no literature is available on the bed roughness, one calibrate a hydrodynamic model for C. This model could then also be used to estimate $\hat{u}_1$.

- **Zhang:**
  Zhang and Savenije (2016) describe a dispersion formula which has to be applied locally. In SOBEK however, this is not (yet) possible. That is why dispersion along the estuary is related to the dispersion in the estuary mouth here. As this formula is not calibrated for this application it should be calibrated again or applied locally in a possible future version of SOBEK.

7.3 Limitations

The outcomes of this research have to been read considering the limitations below.

Tidal flume experiment

- There was no longitudinal salinity data available and thus validations are purely based on the maximum and minimum intrusion lengths.
- The Nieuwe Waterweg was the prototype for the tidal flume test.
- No field observations are used to validate the model.
- The salinity BC at the seaside is based upon the maximum salinity and TH-time lag.

Real convergent estuaries

- In reality the estuary might lag behind steady state due to changing BC's. In this research it is assumed that the salinity distribution in the estuaries is in steady state.
- The salinity BC at the seaside is based upon the maximum salinity and TH-time lag. This approximation may divert from reality.
- The shape of the estuary is strongly schematized by Equations (2.1) till (2.3).
- The estuaries are schematized as single branched channels. In real estuaries some significant tributaries which should be accounted for might be present.
- Determining the mouth salinity, which is used in this research, is not an easy task. It is easier to determine the salinity at the inflection point.
- Due to time considerations in this research only 11 of the 33 estuaries have been used to validate SOBEK-3 and the used dispersion formulations.

8 Conclusions and recommendations

This chapter addresses conclusions based upon the research carried out. After that attention is payed to recommendations for further research and the use of the model.

8.1 Conclusions

Within this thesis is sought after a better understanding of dynamic one-dimensional modeling of salt transport, with a focus on dispersive transport. Here the most important findings are addressed following the research questions as defined in Chapter 1.

An estuary is the transition from a river to a sea or ocean. It is thus physically affected by both the river, via discharge, and the sea, via tide. The shape of an estuary is strongly influenced by the ratio between tidal range and river discharge. When the tide gains influence with respect to the river the estuary will have a stronger converging shape. The geometry of an estuary affects the hydrodynamics within it and therefore salt transport. Within estuary boundaries mixing of fresh and saline water occurs. The most dominant mechanisms are gravitational circulation, induced by the density differences of fresh river water and saline sea water, and tidal pumping induced by tidal currents which occurs in wide parts of the estuary.

The hydrodynamics of an estuary are described by the one-dimensional momentum and continuity equation. The salt transport equation is coupled to the hydrodynamics, using a state equation linking salinity and density. The part in need of validation is the dispersion coefficient D which is used in the one-dimensional salt transport equation. D accounts for salt transport induced by mixing processes taking place in an estuary.

Previously calculations of salt intrusion using SOBEK-RE made use of the dispersion formulation based on the one as described by Thatcher and Harleman (1972). However, in this research it is found that this dispersion formulation cannot cope with all changes in system characteristics. Using the tidal flume experiment exercised by Rigter (1973) it is seen that using this formulation the model is not sensitive enough to capture changes induced by varying tidal amplitude, flume length, river discharge and relative density differences. In addition the results are quite off for changing bed roughness and water depth. However simulations for real converging estuaries show quite some correlation with the measurements, the use of the estuary length as a length scale for dispersive salt transport is not convenient and can be argued to be physically incorrect.

Based on the results obtained using the adapted formulation as described by Thatcher and Harleman it is tried to improve the dispersion formulation. Equation (8.1) shows the new formulation. This formulation makes it possible to test a wide range of dispersion formulations. It allows users to chose the maximum flood velocity and tidal excursion as dispersion scaling factors, it allows users to chose the power of the estuarine Richardson number, it includes improvements to account for the affect of changing water depth and bed roughness, it includes a term which increases dispersion only in wide parts of the estuary and it allows the user to chose the dependency on the salinity and/or salinity gradient. Equation (8.1) includes many parameters and looks like some form of data fitting. However, by taking the right set of constants dispersion formulas as described by Savenije (2012), Kuijper and Van Rijn (2011), Gisen *et al.* (2015) and Zhang and Savenije (2016) can be used and by choosing a constant as zero the respective term falls out of the equation. As the tidal flume experiment differs from the real convergent estuaries by its smooth geometry and width to depth ratio those are addressed

separately in the remainder of this section.

$$D = c_1 u(x) h(x) \frac{\sqrt{g}}{C} + c_2 \hat{u}_0^{c_3} E_0^{c_4} N_R^{c_5} \left(\frac{C}{\sqrt{g}}\right)^{c_6} \left(\frac{h_0}{\bar{a}}\right)^{c_7} \left(\frac{h_0}{E_0}\right)^{c_8} \left(1 + c_9 \left(\frac{B_x}{E_x}\right)^2\right) \left\langle \frac{S}{S_0} \right\rangle^{c_{10}} \left\langle \left| \frac{\partial S}{\partial x} \right| \right\rangle^{c_{11}} \tag{8.1}$$

The tidal flume experiment served as a test to assess the performance of the numerical model in prismatic channels. Here it is found that the dispersion formula defined by Kuijper and Van Rijn (2011) performs best for the tidal flume experiment. This formula performs best because it relates D_0 to $\hat{u}_0$, h_0, $N_R^{\frac{1}{2}}$, $\frac{C}{\sqrt{g}}$ and $\left\langle \frac{S}{S_0} \right\rangle^{\frac{1}{2}}$, while in others the dependency on changing h_0 and C were not included. Using this formula the right relation is approached to represent tidal mixing capacity and gravitational circulation. One should be careful applying this formula under extreme conditions as very low tidal amplitude and deep waters, as errors increased in those situations.

For real convergent estuaries model simulations using dispersion formulations as described by Thatcher and Harleman (1972), Gisen *et al.* (2015), Savenije (2012), Kuijper and Van Rijn (2011) and Zhang and Savenije (2016) are compared. None of the assessed dispersion formulations performed substantially better than the others. However, the formulation described by Gisen *et al.* (2015) scored relatively good on all assessment criteria and some practical notes make this formulation the one most easy to apply. Gisen *et al.* (2015) related D_1 to $\hat{u_1}$, E_1, $N_R^{0.57}$ and $\left\langle \frac{S_x}{S_1} \right\rangle^K$. Especially for intrusion lengths up to 60 km the formulation leads to good approximations of the maximum intrusion length and when the term $(1 + 10(B_x/E_x)^2)$ is used the results improved for wide estuaries in which lateral mixing plays an important role. Savenije (2012) and Kuijper and Van Rijn (2011) included the terms $\frac{h}{\bar{a}}$ and/or $\frac{C}{\sqrt{g}}$ in their formulas, which did not result in significant differences in the simulations. However, simulations of the Schelde estuary, which is dredged, improved by including $\frac{h}{\bar{a}}$. Simulations for dredged estuaries might thus improve when this term is included, within this research this could not be proven due to a little number of observations in dredged estuaries.

At the beginning of this project there were only a limited options of dispersion formulas included in SOBEK, of which only one was physically grounded. During this project a new dispersion formula was implemented giving the user many more options. This new formula always relates dispersion along an estuary to the dispersion in the estuary mouth, and as such it is not possible to use local characteristics to define the dispersion coefficient. When using the dispersion formula derived by Kuijper and Van Rijn (2011) for the tidal flume test and one of the dispersion formulas described by Thatcher and Harleman (1972), Gisen *et al.* (2015), Savenije (2012), Kuijper and Van Rijn (2011) or Zhang and Savenije (2016) for the real convergent estuaries, the simulated intrusion lengths show strong correlation with the measured intrusion lengths. However, the observed and simulated salinity curves in an estuary can still deviate much. It should be noted that the downstream boundary only allows salt to intrude in the estuary when the flow is directed into the estuary. As a consequence the model does not allow salt to intrude with extremely high river discharge when the flow is always directed seawards.

8.2 Recommendations

Within this section recommendations are given. They are categorized recommendations in general, for prismatic channels and for convergent estuaries.

General recommendations:

- Test the effect of changing BC's, as for example the transition from spring to neap tide and a discharge series, in order to find out if the model is capable to react appropriately to those dynamic conditions.
- Test a dispersion formulation where all parameters used are defined locally. This would look something like equation (8.2)[1]. By doing so the same results should be obtained, no matter where the estuary mouth is defined.

$$\begin{aligned} D_x &= \alpha_1 \hat{u}_x E_x N_{R,x}^{\alpha_2} \left(1 + \alpha_3 \left(\frac{B_x}{E_x}\right)^2\right) \left\langle \frac{S_x}{S_0} \right\rangle^K \\ &= \alpha_1 \hat{u}_x E_x \left(\frac{\Delta\rho_x}{\rho} \frac{g h_x}{\hat{u}_x^2} \frac{Q_f T}{P_{e,x}}\right)^{\alpha_2} \left(1 + \alpha_3 \left(\frac{B_x}{E_x}\right)^2\right) \left\langle \frac{S_x}{S_0} \right\rangle^K \end{aligned} \tag{8.2}$$

Recommendations for tidal flume experiment:

- Use the dispersion formulation as defined by Kuijper and Van Rijn (2011) for prismatic channels to describe salt intrusion in estuaries.
- The maximum flood velocity and tidal prism are underestimated in the current version of SOBEK as is illustrated by Figure 7.1. This especially results in errors during high river discharge. By using the for river discharge adjusted values for $\hat{u}_0$ and P_e the problem is solved, see Appendix F. It is thus recommended to use the improved version.
- Use longitudinal salinity profiles to validate model results. As currently no longitudinal data is available field measurements should be carried out or a three-dimensional model could be used as a measure.
- Validate the model results with field observations, for example for the Nieuwe Waterweg.
- As the prototype used in this research is based on the Nieuwe Waterweg one should be careful applying the model regardless to other real prismatic channels. It is recommended to validate the model first for some other prismatic channels.

Real convergent estuaries:

- Try to find a case in a real convergent estuary or real prismatic channel in which all conditions but the tidal amplitude remain the same. This case can than be used to assess the effect of a changing tidal amplitude. It can than be used to support the decision of the used mixing length scale and thus the relation of the dispersion with the maximum flood velocity.
- Calibrate the models of Savenije (2012), Kuijper and Van Rijn (2011) and Zhang and Savenije (2016). After calibration, the results of all formulas should be evaluated again.
- Use more estuaries to validate the model. Now eleven estuaries with 32 cases have been used. However in the data base of Savenije there are 33 estuaries and 86 cases. For 22 estuaries there are longitudinal salinity profiles available.
- Look after an universal value for K. This would make the model more practical for inexperienced users.

[1] In equation (8.2) α_1, α_2 and α_3 are previously defined constants and K is the van der Burgh constant.

- Zhang and Savenije (2016) revised the data used and made an updated data set containing the geometric characteristics of the estuaries. It is recommended to use this data set for further research.
- Analyze the salinity curves to gain more insight in which situation which dispersion formula performs best and why.
- Use the dispersion formulation described by Gisen *et al.* (2015) for salt intrusion predictions. Only when it is known or expected that lateral mixing processes play an important role in the salt intrusion the term $(1 + 10(B_x/E_x)^2)$ should be added to improve model results.
- Use the inflection point as the downstream model boundary when the dispersion formula described by Gisen *et al.* (2015) is used. By doing so the manual conversion of the predicted dispersion at the inflection point to dispersion in the estuary mouth is avoided.

References

Battjes, J. and R. Labeur, 2014. *Open Channel flow*. TU Delft.

Bay of Fundy, 2016. "Bay of fundy tides: The highest tides in the world!" URL http://www.bayoffundy.com/about/highest-tides/, accessed: 2016-05-02.

Buschman, F., Y. Huismans, W. Kranenburg, C. Wesselius, R. Uittenbogaard and K. Kuijper, 2015. "Plan of action, validating SOBEK and salt intrusion."

Cameron, W. and D. Pritchard, 1963. *Estuaries, The Composition of sea-water : comparative and descriptive oceanography*, vol. 2. Wiley, New York.

Chant, R., 2002. "Secondary circulation in a region of flow curvature: Relationship with tidal forcing and river discharge." *Journal of Geophysical Research* 107 (C9): 14-1-14-11. DOI 10.1029/2001JC001082.

Deltares, 2012. *Salt Intrusion, Technical Reference SOBEK-RE*.

Deltares, 2015. *SOBEK Suite, Technical Reference Manual SOBEK 3*.

Fischer, H., E. List, R. Koh, J. Imberger and N. Brooks, 1979. *Mixing in inland and coastal waters*. Academic Press, New York.

Georgas, N. and A. Blumberg, 2003. "The influence of centrifugal and Coriolis forces on the circulation in a curving estuary." *Estuarine and Coastal modeling* pages 541-558.

Gisen, J., 2015. *Prediction in ungauged estuaries*. Delft University of Technology.

Gisen, J., H. Savenije, R. Nijzink and A. Abd Wahab, 2015. "Testing a 1-D Analytical Salt Intrusion Model and its Predictive Equations in Malaysian Estuaries." *Hydrological Sciences Journal* 60 (1).

Google maps. "Google maps." URL http://www.google.nl/maps/, accessed: 2016-05-02.

Ippen, T. and D. Harleman, 1961. *One-dimensional analysis of salinity intrusion in estuaries*. Tech. rep., U.S. Army Corps of Engineers.

Jay, D., 1991. "Green law revisited - tidal long-wave propagation in channels with strong topography." *Journal of Geophysical Research-Oceans* 96 (C11): 20585-20598. DOI 10.1029/91JC01633.

Kuijper, K., 2016. personal communication.

Kuijper, K. and L. van Rijn, 2011. "Analytical and numerical analysis of tides and salinities in estuaries." *Ocean Dynamics* DOI 10.1007/s10236-011-0454-z.

Lindhart, M., E. Mosselman and H. Avila, 2015. "Stratified secondary circulation in the Rio Magdalena, Colombia." .

McCarthy, R., 1993. "Residual currents in tidally dominated, well-mixed estuaries." *Journal of the Hydraulic Division* 45A: 325-340.

Noort, J., 2016. personal communication.

Os, A. van and G. Abraham, 1992. *Density currents and salt intrusion*. Tech. rep., Delft Hydraulics.

Prandle, D., 1982. “Estuarine circulation patterns.” *Journal of Physical Oceanography* 11: 1311-1324.

Preddy, W., 1954. “The mixing and movement of water in the estuary of the Thames.” *Journal of of the Marine Biological Association of the United Kingdom* 33: 645-662.

Pritchard, D., 1955. “Estuarine circulation patterns.” *Proceedings of the American Society of Civil Engineers* 81 (717): 1-11.

Rigter, B., 1973. “Minimum Length of Salt Intrusion in Estuaries.” *Journal of the Hydraulic Division* pages 1475-1496.

Rijkswaterstaat, 1984. *IJking chloridedeel ZWENDL Noordelijk Deltabekken*. Tech. rep., Rijkswaterstaat.

Rijn, v. L., 2011. *Principles of fluid flow and surface waves in rivers, estuaries, seas and oceans*. Aqua Publications.

Savenije, H. “Salinity and tides.” URL https://salinityandtides.com/, accessed: 2016-09-12.

Savenije, H., 1998. “Analytical expression for tidal damping in alluvial estuaries.” *Journal of Hydraulic Engineering-Asce123* 124 (6): 615-618.

Savenije, H., 2012. *Salinity and Tides in Alluvial Estuaries*. Delft University of Technology.

Savenije, H., 2015. “Prediction in ungauged estuaries: An integrated theory.” *Water Resources Research* 51. DOI 10.1002/2015WR016936.

Savenije, H., 2016. personal communication.

Smith, R., 1980. “Buoyancy effects upon longitudinal dispersion in wide well-mixed estuaries.” *Philosophical Transactions of the Royal Society of London Series a-Mathematical Physical and Engineering Sciences* 296: 467-496.

Sumer, S. and H. Fischer, 1977. “Transverse mixing in partially stratified flow.” *Journal of the Hydraulic Division* 103 (6): 587-600.

Thatcher, M. and D. Harleman, 1972. *A mathematical model for the prediction of unsteady salinity intrusion in estuaries*. Tech. rep., Massachusetts Institute of Technology.

Uittenbogaard, R., 2016. personal communication.

West, J. and T. Broyd, 1981. “Dispersion coefficients in estuaries.” *Proceedings of the Institution of Civil Engineers Part 2-Research and Theory* 71: 721-737.

Winterwerp, J., 1980. *Eén-dimensionale beschrijving van de zoutverdeling in de Rotterdamse Waterweg en Nieuwe Maas m.b.v. het dispersie-concept van Thatcher-Harleman*. Tech. rep., Delft Hydraulics.

Zhang, Z. and H. Savenije, 2016. “The physics behind Van der Burgh’s empirical equation, providing a new predictive equation for salinity intrusion in estuaries.”

List of Figures

List of Tables

A Data tidal flume experiment

In Table A.1 the characteristics of the tidal flume experiment are shown. In order to test the effect of those characteristics Rigter (1973) changed the system in the following way:

- **Tidal amplitude**
  Rigter adapted the amplitude of the spillway which moved up and down to imitate the tidal movements.
- **Bed roughness**
  Rigter used vertical bars (0.5 cm by 0.5 cm) arranged diagonally to obtain the desired roughness. Those bars always stuck out above the water level.
- **Water depth**
  Rigter adapted the height of the spillway.
- **Flume length**
  As Rigter was not able to actually change the flume length, he adapted the upstream supplied fresh water discharge. By supplying a variable discharge it was possible to imitate tidal movements which would occur in flumes with another length.
- **Varying river discharge**
  Rigter adapted the amount upstream supplied fresh water.
- **Relative density difference**
  Rigter adapted the salinity of the supplied saline water at the sea basin.

Table A.1: *Data tidal flume experiment by Rigter (1973), the changed prototype variables are shown in red.*

Data tidal flume experiment		
General		
Tidal period:	44700	s
Gravitational acceleration	9.81	$\frac{m}{s^2}$
Flume width	430	m
Scaling		
Horizontal:	640	
Vertical:	64	
Velocity:	8	
Time:	80	
Bed roughness:	3.16	

Variable	W	C	h	L	Q	$\Delta\rho/\rho$	L_{min}	L_{max}
Units	$[m]$	$[\frac{m^{\frac{1}{2}}}{s}]$	$[m]$	$[m]$	$[\frac{m^3}{s}]$	$[-]$	$[m]$	$[m]$
Case								
Tidal amplitude W								
1	0,4	60	13,82	114662	949	0,0215	25792	35520
2	0,5	60	13,82	114662	949	0,0215	21568	30688
3	0,6	60	13,82	114662	949	0,0215	16384	26912
4	**0,8**	**60**	**13,82**	**114662**	**949**	**0,0215**	**14080**	**25760**
5	1,2	60	13,82	114662	949	0,0215	9856	25274
6	1,6	60	13,82	114662	949	0,0215	6592	26093
7	2,4	60	13,82	114662	949	0,0215	5376	29210
Bed roughness C								
8	0,8	40	13,82	114662	949	0,0215	11712	19200
9	0,8	50	13,82	114662	949	0,0215	12864	22976
4	**0,8**	**60**	**13,82**	**114662**	**949**	**0,0215**	**14080**	**25760**
10	0,8	70	13,82	114662	949	0,023	16832	29376
11	0,8	80	13,82	114662	949	0,023	19200	32000
12	0,8	90	13,82	114662	949	0,023	19904	35283
Water depth h								
13	0,8	60	9,98	114662	949	0,0215	7040	16960
14	0,8	60	12,03	114662	949	0,0215	9600	20800
1	**0,8**	**60**	**13,82**	**114662**	**949**	**0,0215**	**14080**	**25760**
15	0,8	60	16,00	114662	949	0,0215	23424	34080
16	0,8	60	17,02	114662	949	0,0215	28096	38880
17	0,8	60	17,98	114662	949	0,0215	35584	47680
Flume length L								
18	0,8	60	13,82	67859	949	0,0215		46112
19	0,8	60	13,82	72538	949	0,0215	28096	33638
20	0,8	60	13,82	86579	949	0,0215	18752	28128
21	0,8	60	13,82	100621	949	0,0215	14528	26106
4	**0,8**	**60**	**13,82**	**114662**	**949**	**0,0215**	**14080**	**25760**
22	0,8	60	13,82	128698	949	0,0215	16384	26778
23	0,8	60	13,82	161459	949	0,0215	23424	31328
24	0,8	60	13,82	194221	949	0,0215	31168	42010
River discharge Q_f								
25	0,8	60	13,82	114662	473	0,0215	25792	37907
26	0,8	60	13,82	114662	592	0,0215	21568	35283
27	0,8	60	13,82	114662	711	0,0215	19200	31181
4	**0,8**	**60**	**13,82**	**114662**	**949**	**0,0215**	**14080**	**25760**
28	0,8	60	13,82	114662	1896	0,0215	7488	19859
29	0,8	60	13,82	114662	2845	0,0215	4672	16243
30	0,8	60	13,82	114662	3801	0,0215	2368	11488
Density difference $\Delta\rho/\rho$								
31	0,8	60	13,82	114662	949	0,0045		13126
32	0,8	60	13,82	114662	949	0,0066		15424
33	0,8	60	13,82	114662	949	0,0137	7232	19859
4	**0,8**	**60**	**13,82**	**114662**	**949**	**0,0215**	**14080**	**25760**
34	0,8	60	13,82	114662	949	0,0290	19648	32000
35	0,8	60	13,82	114662	949	0,0355	27776	38400

B Data real convergent estuaries

Table B.1: *Geometry and bed roughness of real convergent estuaries*

	A_0	A_1	a_1	a_2	B_0	B_1	B_f	b_1	b_2	h_0	h_1	h_f	x_1	C
	$[m^2]$	$[m^2]$	$[m]$	$[m]$	$[m]$	$[m]$	$[m]$	$[m]$	$[m]$	$[m]$	$[m]$	$[m]$	$[m]$	$\frac{m^{\frac{1}{2}}}{s}$
Maputo	47500	4700	2200	16000	11700	1150	100	2200	16000	4,06	4,06	4,06	5100	60
Pungue	14500	-	18500	-	5200	-	50	18500	-	2,79	-	2,79	0	52,5
Delaware	255000	-	41000	-	37655	-	120	42000	-	6,77	-	5,88	0	60
ChaoPhya	4600	3084	30000	130000	860	472	200	20000	130000	5,35	6,53	6,53	12000	55
Schelde	150000	-	27000	-	16000	-	50	27000	-	9,38	-	9,38	0	57,5
Landak	2000	-	60000	-	230	-	100	60000	-	8,7	-	8,7	0	60
Perak	20500	9210	5000	37000	9100	2068	130	2700	21000	2,25	4,45	14,74	4000	60
ThaChin	20000	1439	1900	87000	3600	259	45	1900	8700	5,56	5,56	5,56	5000	45
Limpopo	1700	1143	50400	115000	550	181	90	18000	115000	3,09	6,31	6,31	20000	57,5
Lalang	2880	-	167000	-	360	-	130	94000	-	8	-	12,5	0	60
Sinnamary	3300	1121	2500	39000	2300	470	95	1700	12000	1,43	2,39	7,23	2700	50

Table B.2: *Tidal range, river discharge, seawater salinity, tidal period, maximum intrusion length and predicted K values.*

Estuary	Date	H	Q_f	$\hat{S}_0$	T	L_{max}	K_{Gisen}	$K_{Savenije}$	K_{Zhang}
	$dd-mm-yyyy$	$[m]$	$[\frac{m^3}{s}]$	$[ppt]$	$[s]$	$[km]$	$[-]$	$[-]$	$[-]$
Maputo	28-04-1982	2,8	25	35	44400	32	0,32	0,38	0,70
Maputo	15-07-1982	1,5	8	35	44400	44	0,32	0,38	0,69
Maputo	19-04-1984	3,3	120	28	44400	27	0,32	0,38	0,57
Maputo	17-05-1984	3,3	50	30	44400	31	0,32	0,38	0,65
Maputo	29-05-1984	2,8	40	31	44400	30	0,32	0,38	0,63
Pungue	26-05-1982	5	50	32	44400	58	0,22	0,30	0,52
Pungue	22-09-1982	5,2	26	34	44400	65	0,22	0,30	0,53
Pungue	31-01-2002	6,2	262	25	44400	47	0,22	0,30	0,50
Pungue	01-03-2002	6,7	150	27	44400	56	0,22	0,30	0,50
Pungue	12-10-1993	3,8	10	36	44400	70	0,22	0,30	0,55
Delaware	23-08-1932	1,7	120	32	44400	146	0,09	0,22	0,63
Delaware	04-10-1932	1,7	72	32	44400	159	0,09	0,22	0,64
ChaoPhya	05-06-1962	2,2	63	28,5	86400	50	0,71	0,75	0,65
ChaoPhya	16-01-1987	2,5	180	16	86400	27	0,71	0,75	0,51
ChaoPhya	23-02-1983	1,6	100	27	86400	43	0,71	0,75	0,62
ChaoPhya	29-01-1983	2,4	90	32	86400	52	0,71	0,75	0,62
Schelde	01-07-1987	3	90	34	44400	120	0,10	0,25	0,64
Schelde	02-11-2000	4	220	34	44400	124	0,10	0,25	0,61
Landak	15-09-2009	1,6	10	18	86400	55	0,69	0,69	0,58
Perak	13-03-2013	2,5	316	24	44400	29	0,24	0,24	0,54
ThaChin	16-04-1981	1,6	55	25	86400	50	0,31	0,35	0,51
ThaChin	27-02-1986	2,6	40	31	44400	56	0,31	0,35	0,45
ThaChin	01-03-1986	1,8	40	32	86400	57	0,31	0,35	0,45
ThaChin	13-08-1987	2	39	25	44400	39	0,31	0,35	0,45
Limpopo	04-04-1980	1,1	150	29	44400	25	0,38	0,5	0,58
Limpopo	31-12-1982	1,1	2	37	44400	64	0,38	0,5	0,72
Limpopo	24-07-1994	0,9	5	37	44400	55	0,38	0,5	0,61
Limpopo	10-08-1994	1	3	36	44400	64	0,38	0,5	0,64
Lalang	20-10-1989	2,6	120	26	86400	48	0,57	0,65	0,74
Sinnamary	12-11-1993	2,6	168	26	44400	12	0,46	0,45	0,52
Sinnamary	27-04-1994	2,9	148	22	44400	12	0,46	0,45	0,54
Sinnamary	03-11-1994	2,9	112	27	44400	15	0,46	0,45	0,52

C Influence f_3 term in Thatcher-Harleman dispersion for the tidal flume test

The analysis carried out in this Chapter 5 focused mainly on the f_4 part in the dispersion formulation. In order to show that the f_3 term is of minor importance to salt intrusion, the models also have been run without the f_3 term. Figure C.1 shows that there are no significant differences in maximum and minimum salt intrusion lengths between both settings. Therefore it can be concluded that the effect of the f_3 term is negligible with respect to the f_4 term regarding salt intrusion in estuaries and thus can be neglected in the analysis.

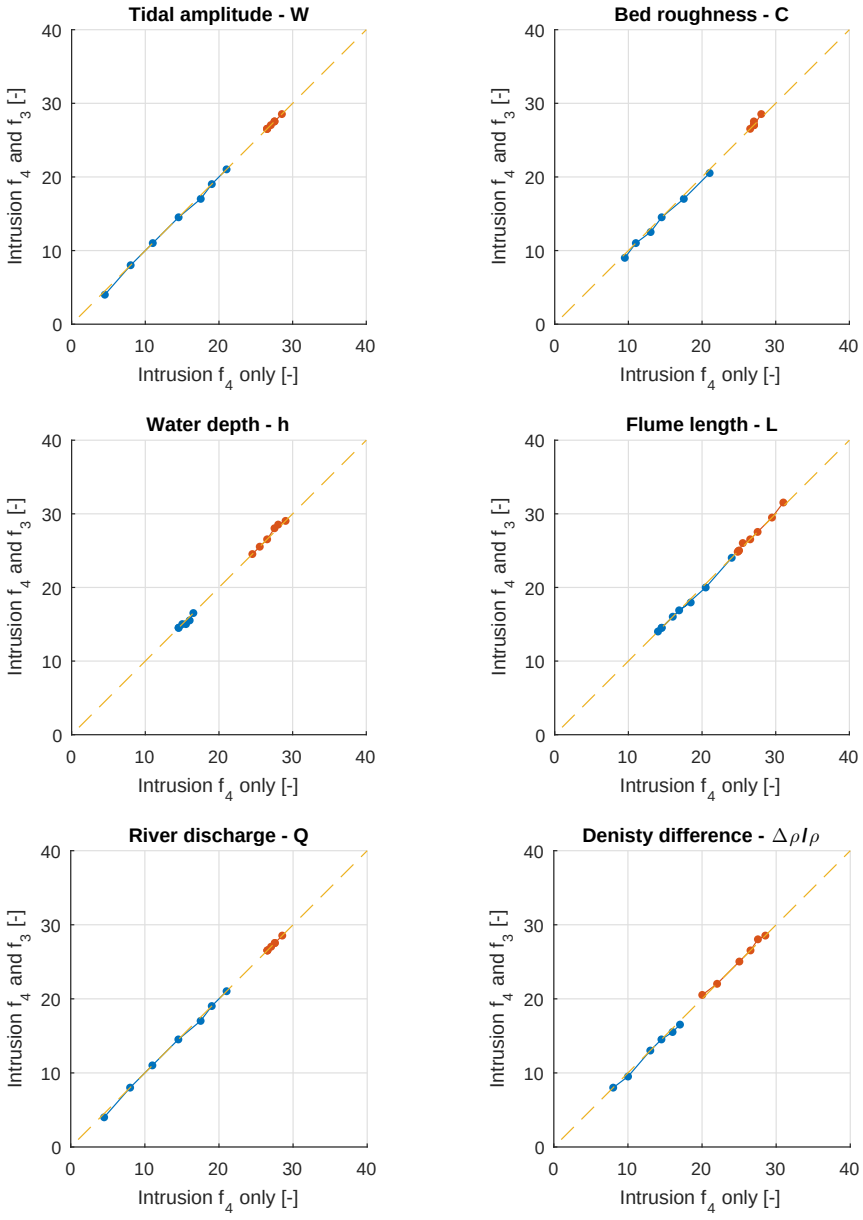

Figure C.1: *Maximum (red) and minimum (blue) intrusion for a model using both f_3 and f_4 terms compared to a model using only the f_4 term. The yellow striped line indicates perfect agreement between model results.*

D Salinity curves

This appendix includes the salinity profiles for all model runs for the real convergent estuaries. They are categorized based upon with which dispersion formula they are generated. The lines represent the model outcomes and the dots represent the measurements. Blue indicates salinity at LWS and red indicates salinity at HWS.

D.1 Thatcher and Harleman

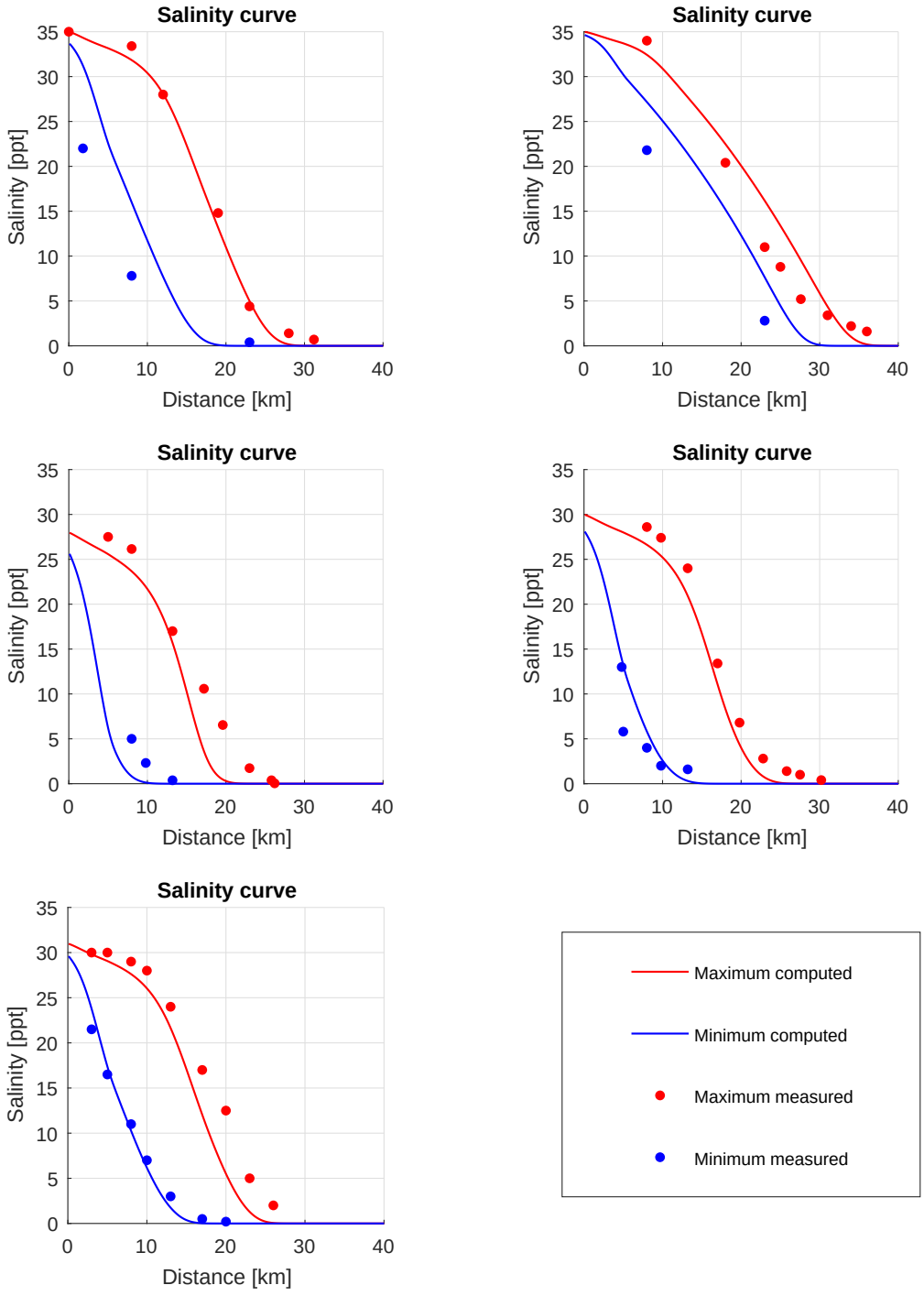

Figure D.1: *Salinity profile for the Maputo estuary*

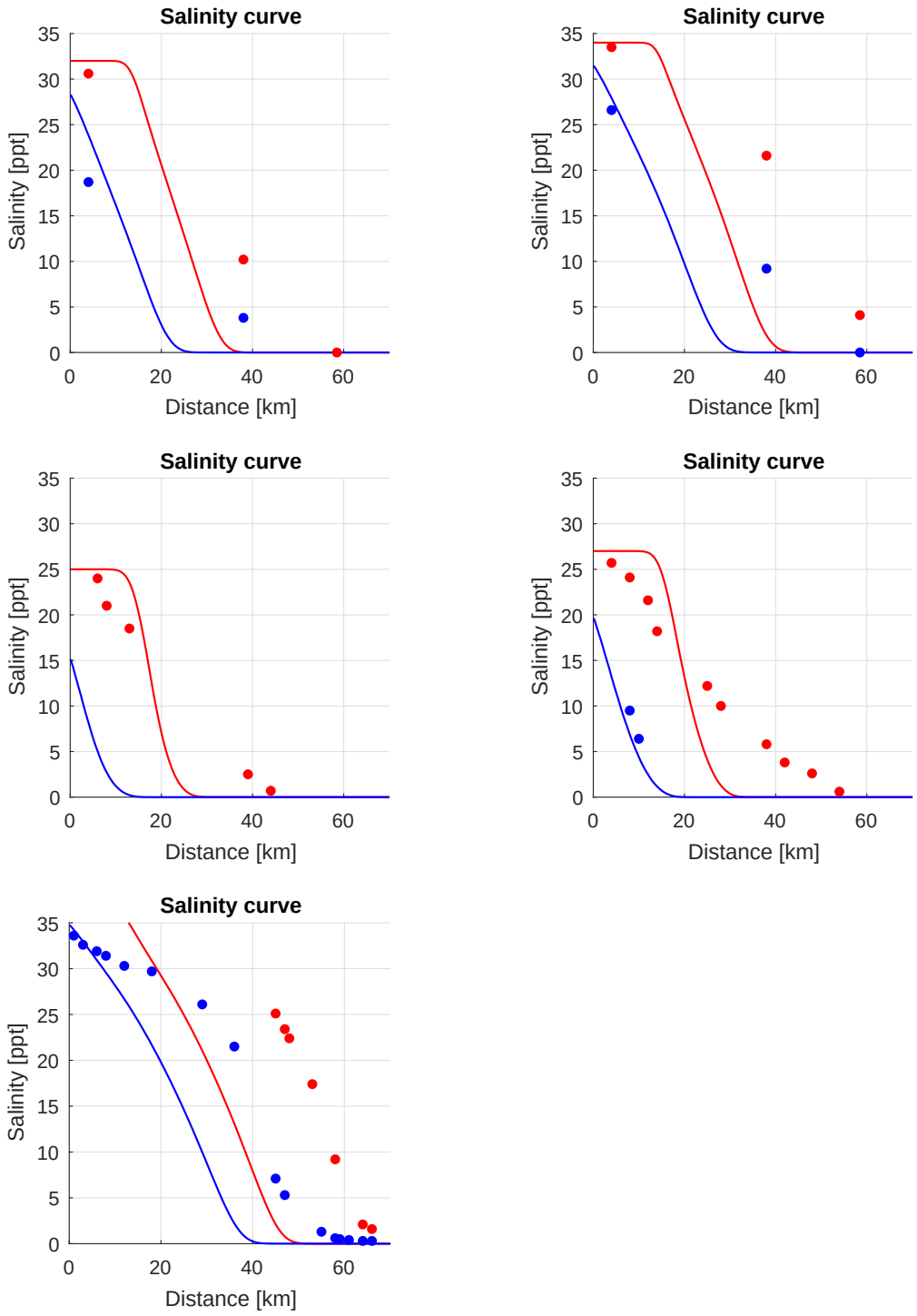

Figure D.2: *Salinity profile for the Pungue estuary*

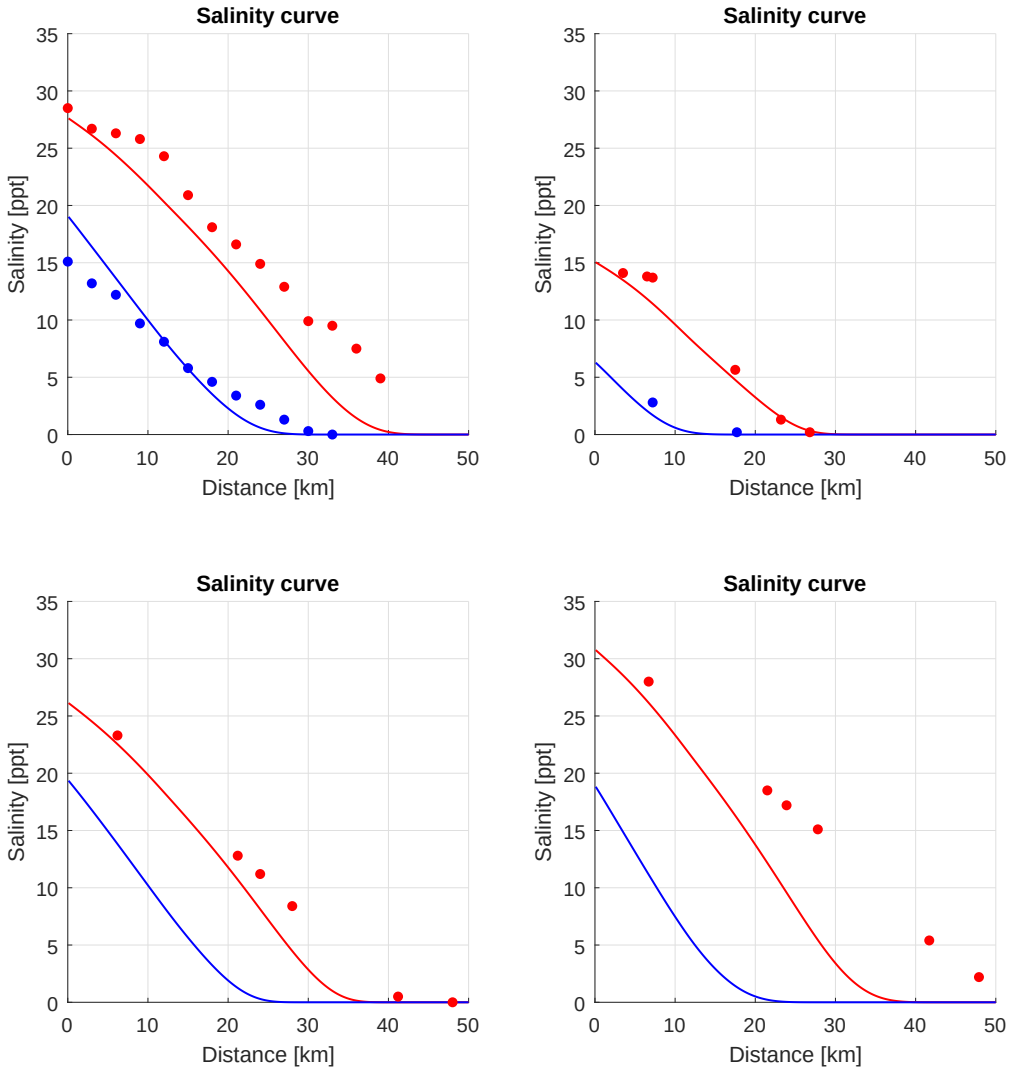

Figure D.3: *Salinity profile for the ChaoPhya estuary*

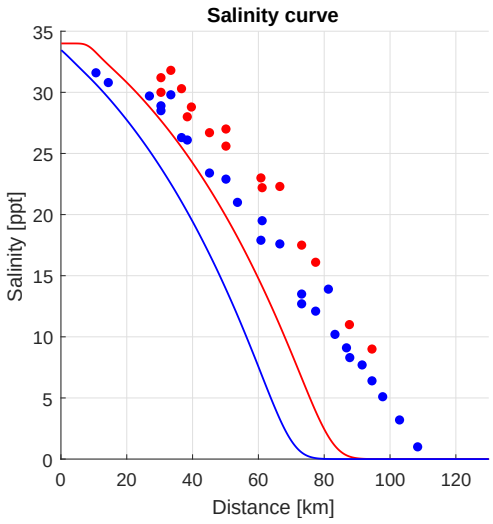

Figure D.4: *Salinity profile for the Westerschelde estuary*

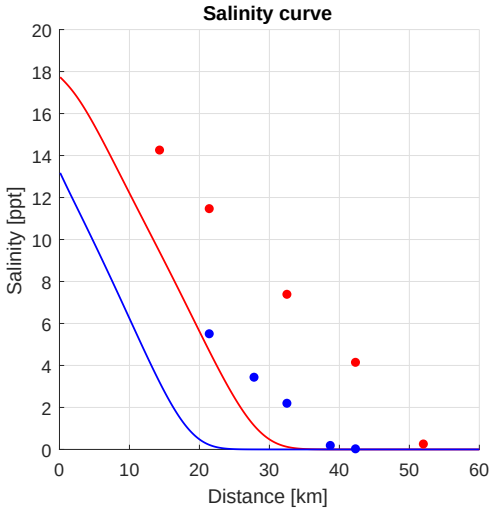

Figure D.5: *Salinity profile for the Landak estuary*

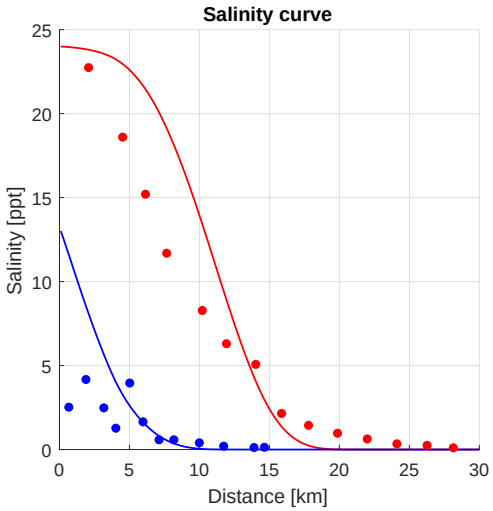

Figure D.6: *Salinity profile for the Perak estuary*

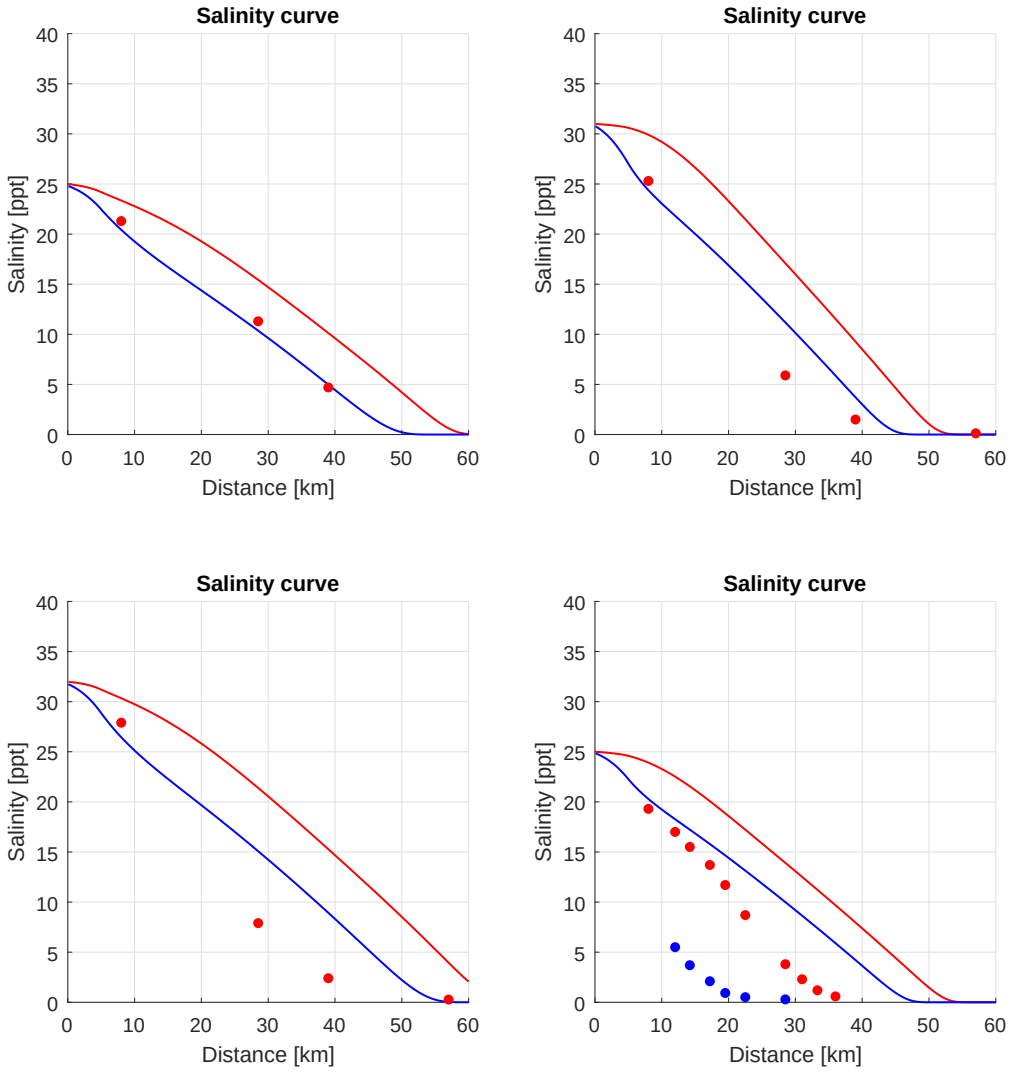

Figure D.7: *Salinity profile for the ThaChin estuary*

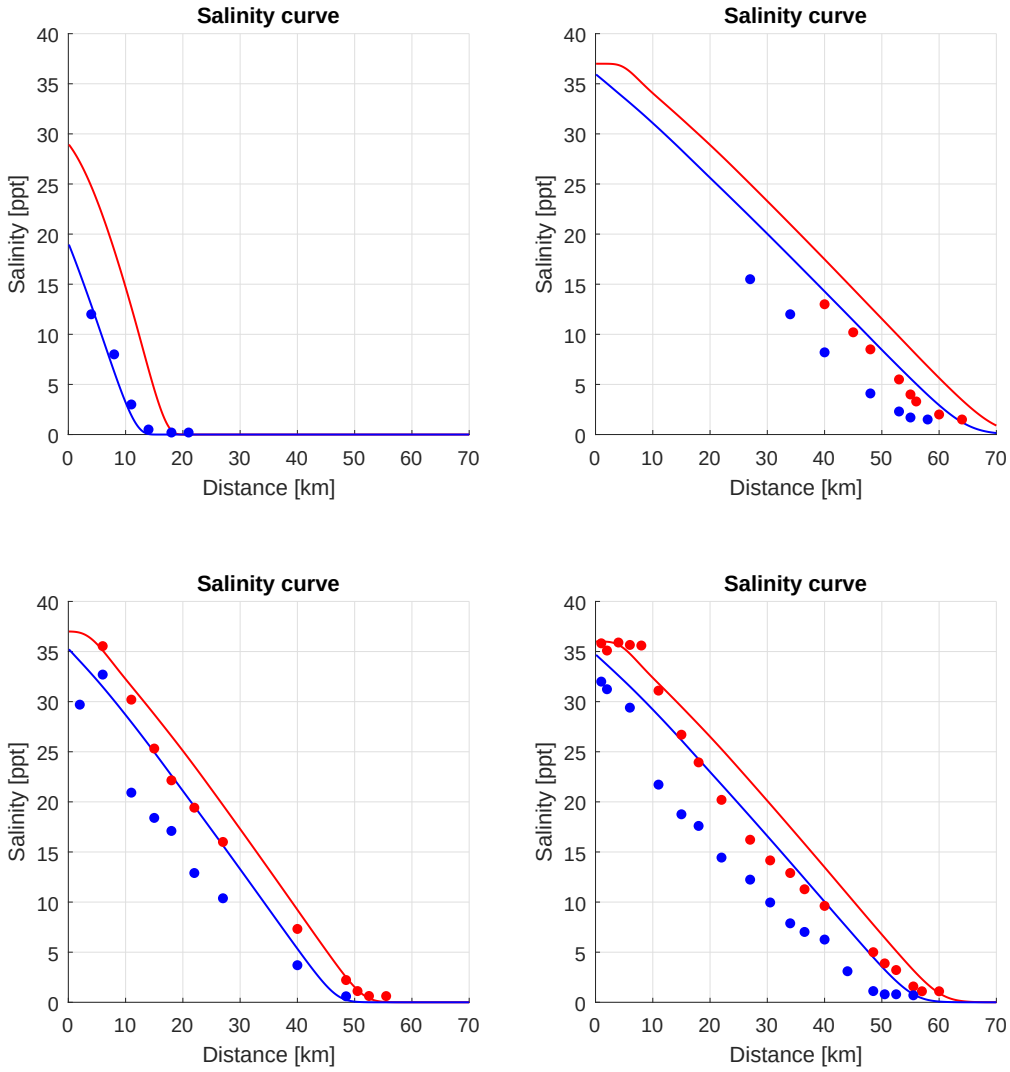

Figure D.8: *Salinity profile for the Limpopo estuary*

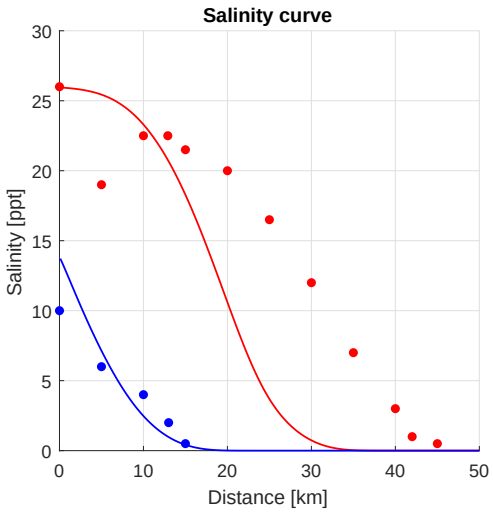

Figure D.9: *Salinity profile for the Lalang estuary*

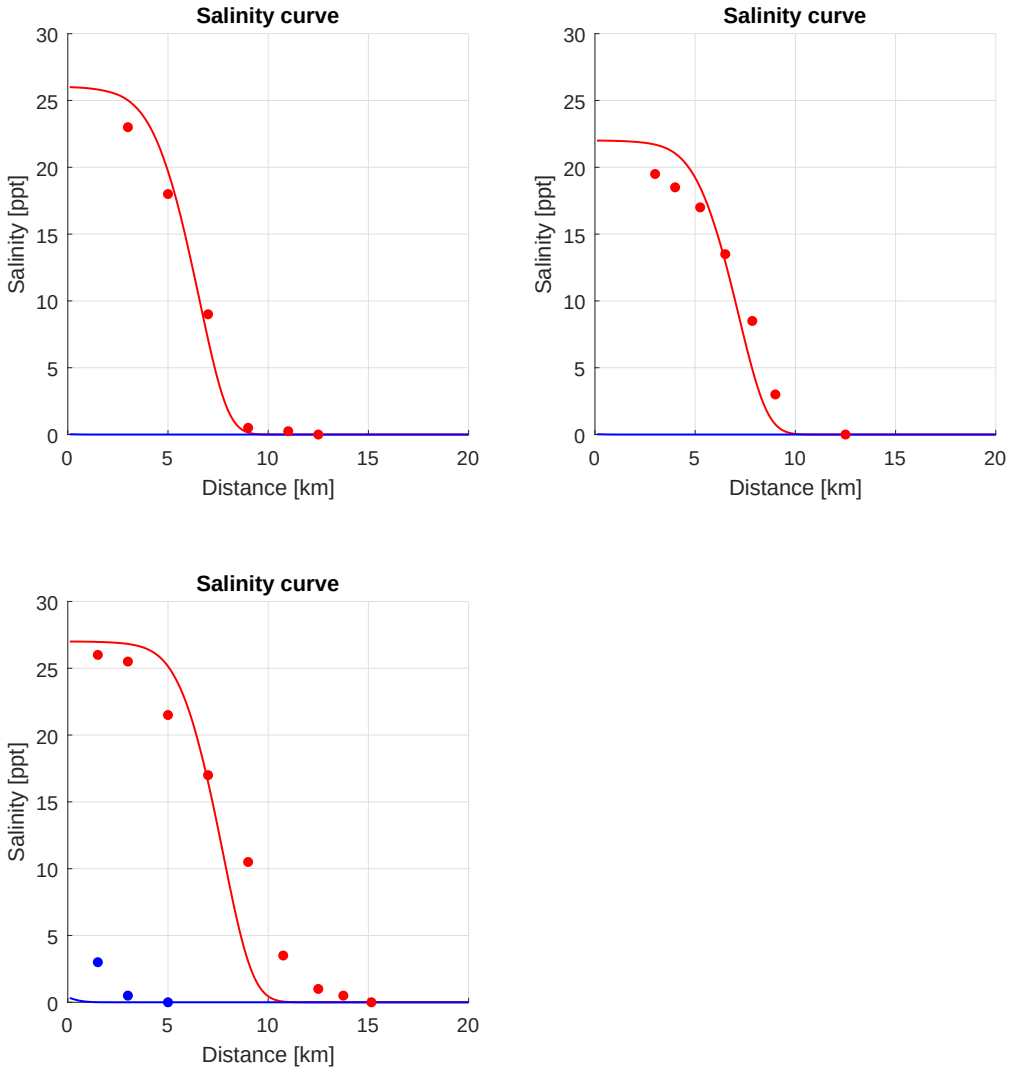

Figure D.10: *Salinity profile for the Sinnamary estuary*

D.2 Gisen

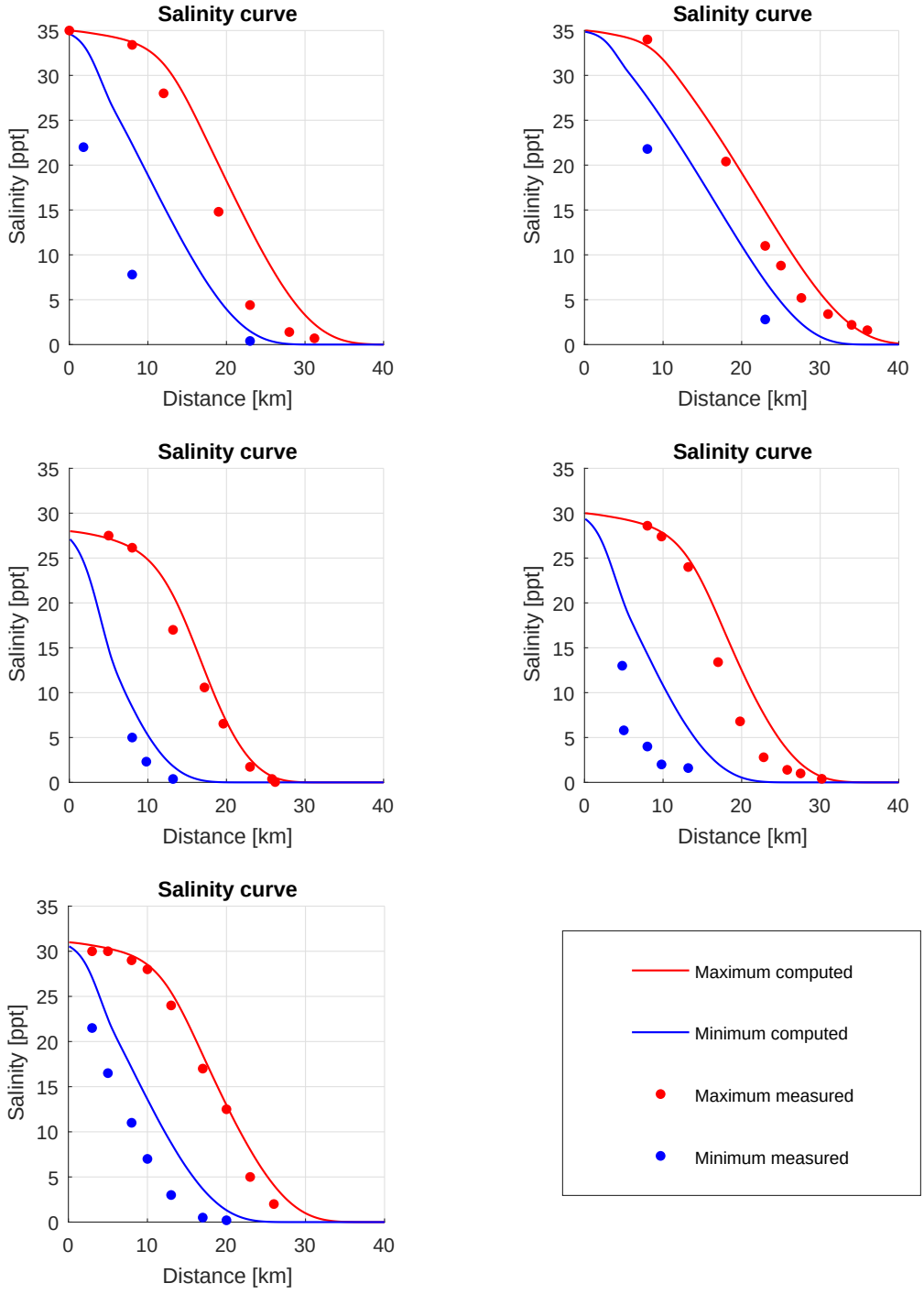

Figure D.11: *Salinity profile for the Maputo estuary*

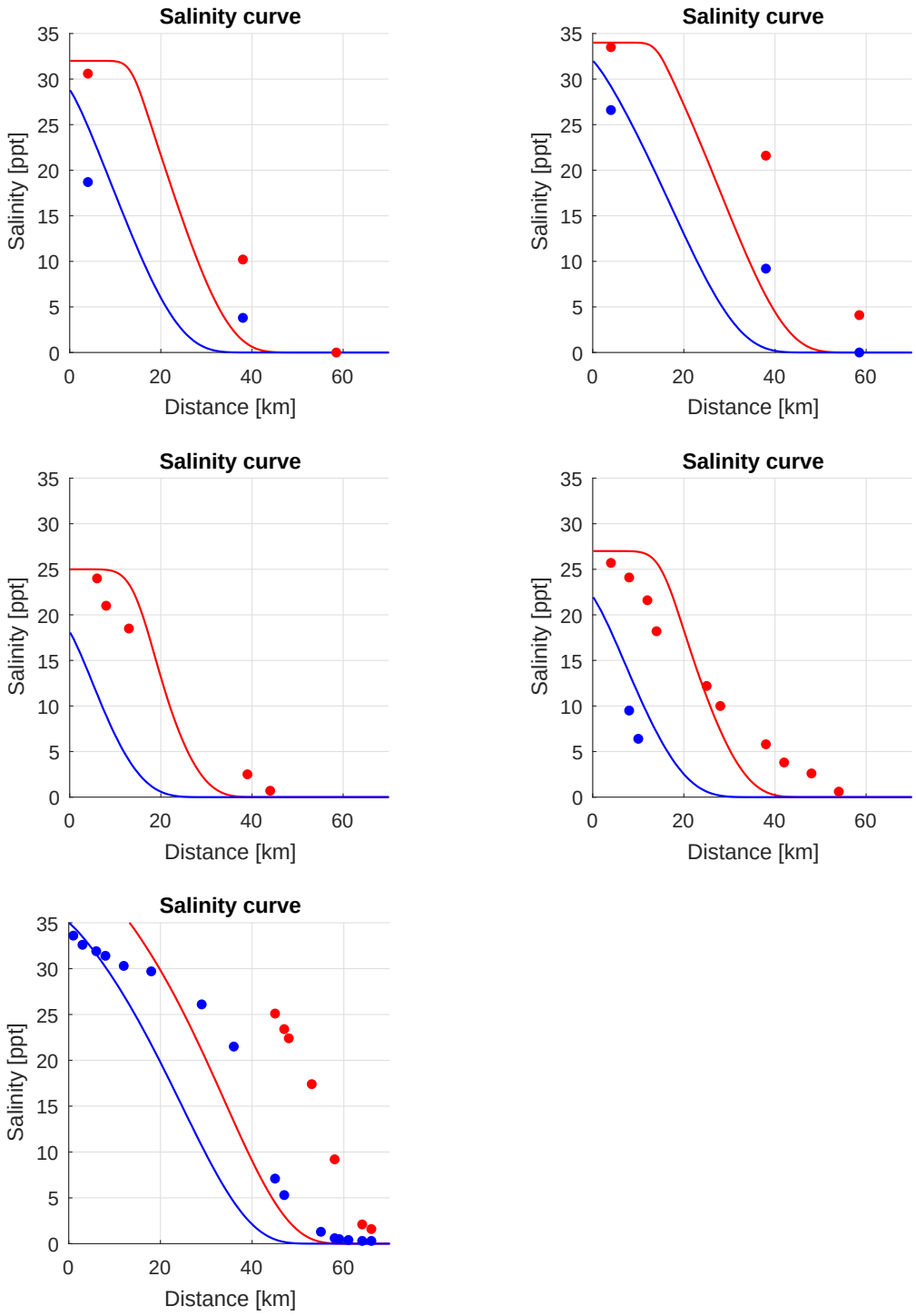

Figure D.12: *Salinity profile for the Pungue estuary*

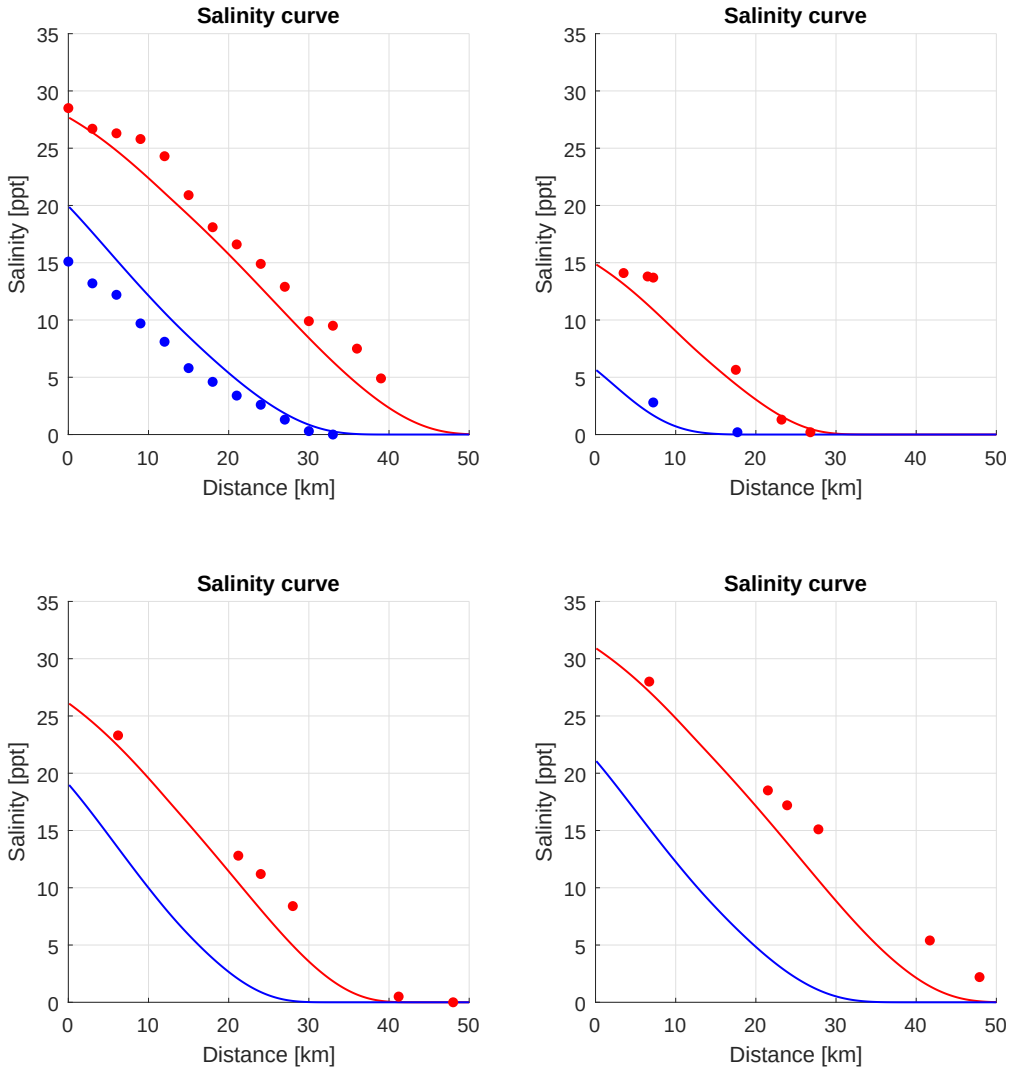

Figure D.13: *Salinity profile for the ChaoPhya estuary*

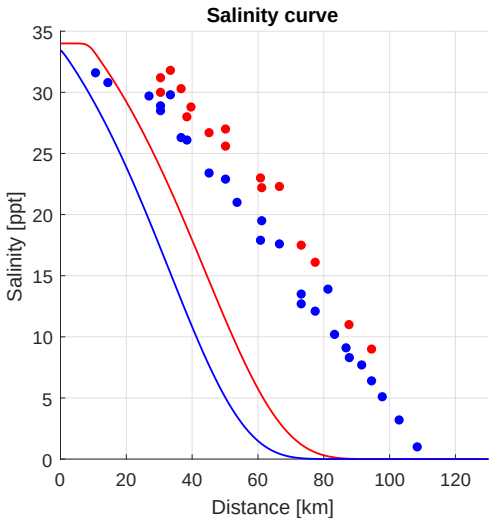

Figure D.14: *Salinity profile for the Westerschelde estuary*

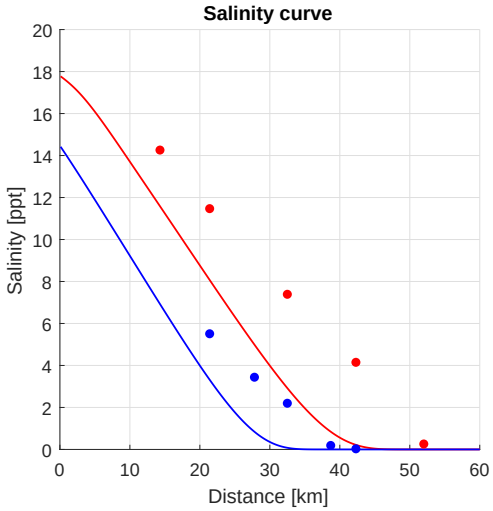

Figure D.15: *Salinity profile for the Landak estuary*

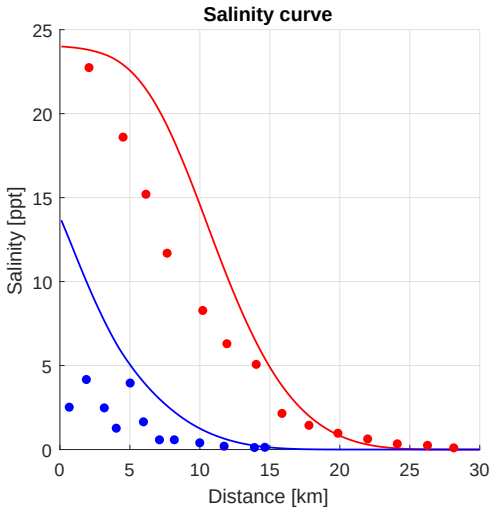

Figure D.16: *Salinity profile for the Perak estuary*

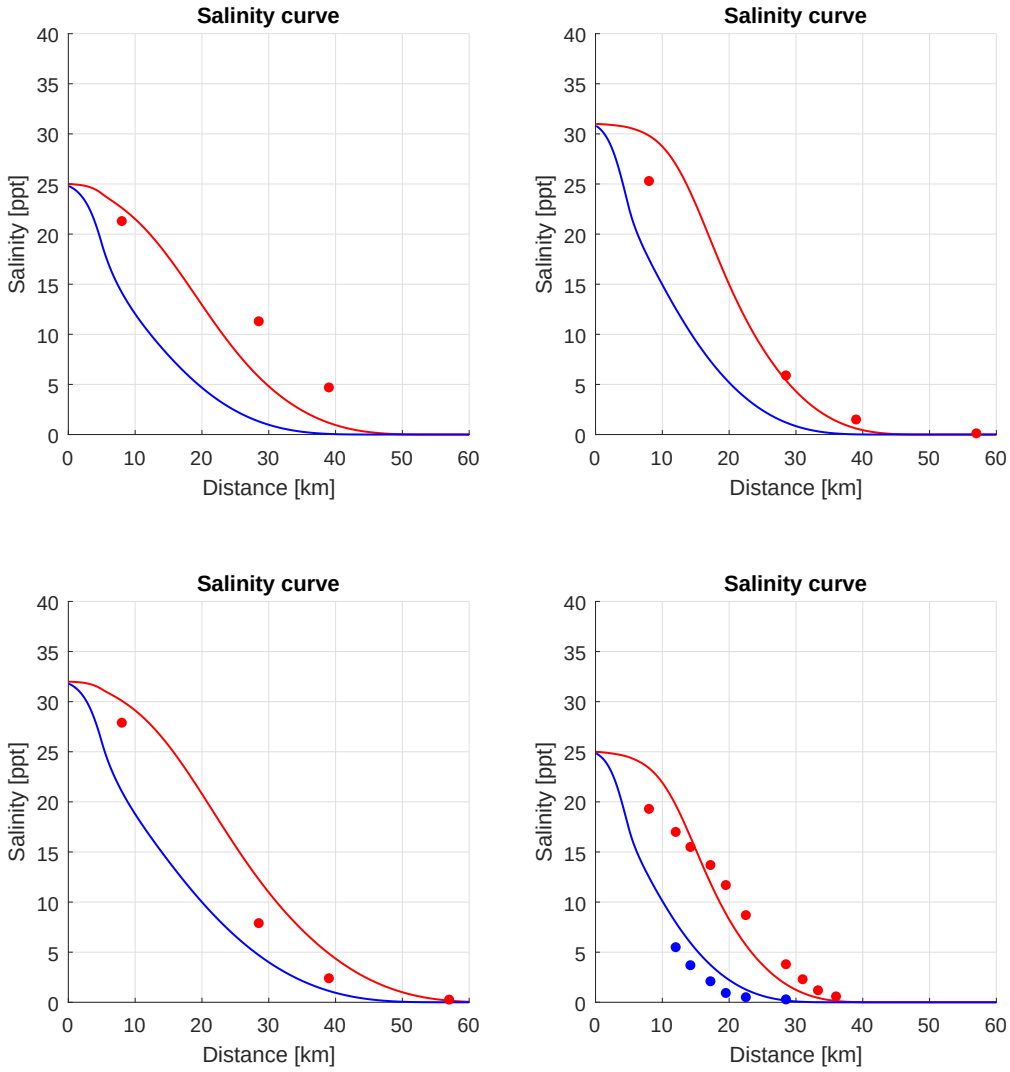

Figure D.17: *Salinity profile for the ThaChin estuary*

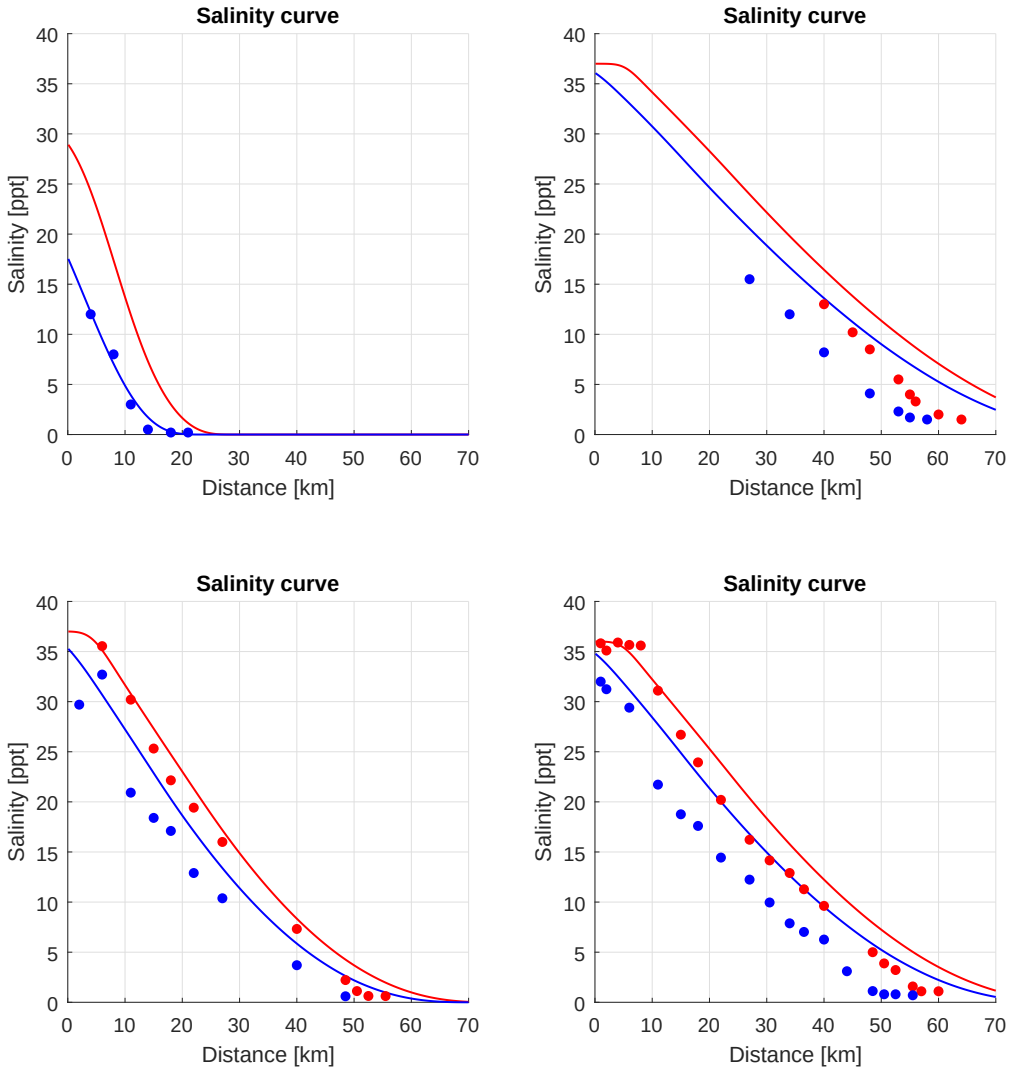

Figure D.18: *Salinity profile for the Limpopo estuary*

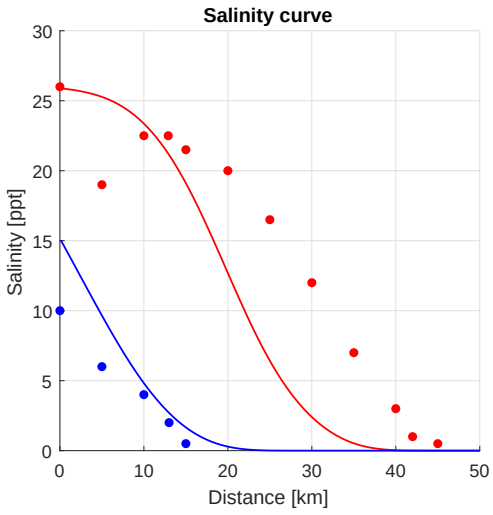

Figure D.19: *Salinity profile for the Lalang estuary*

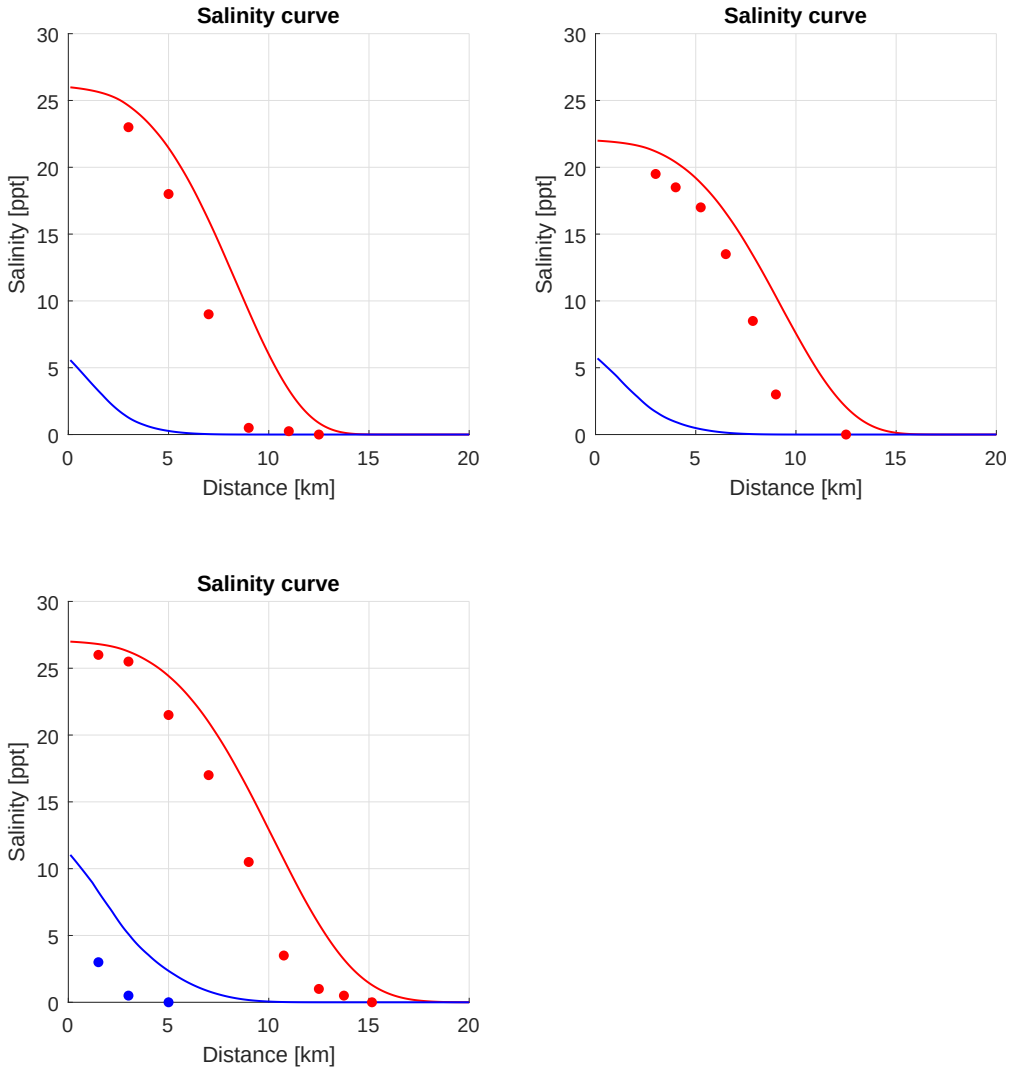

Figure D.20: *Salinity profile for the Sinnamary estuary*

D.3 Gisen with $(1 + 10(B_x/E_x)^2)$

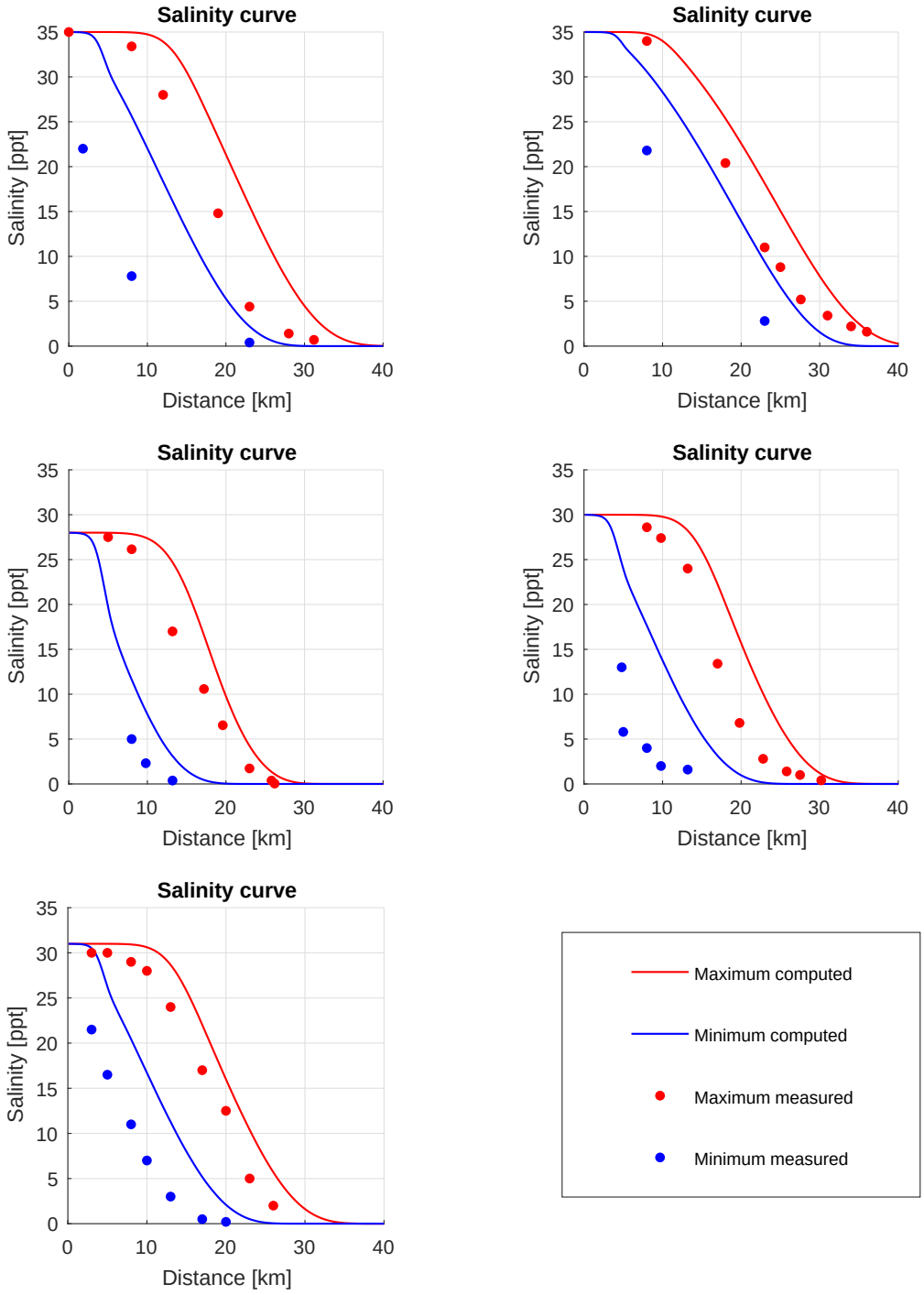

Figure D.21: *Salinity profile for the Maputo estuary*

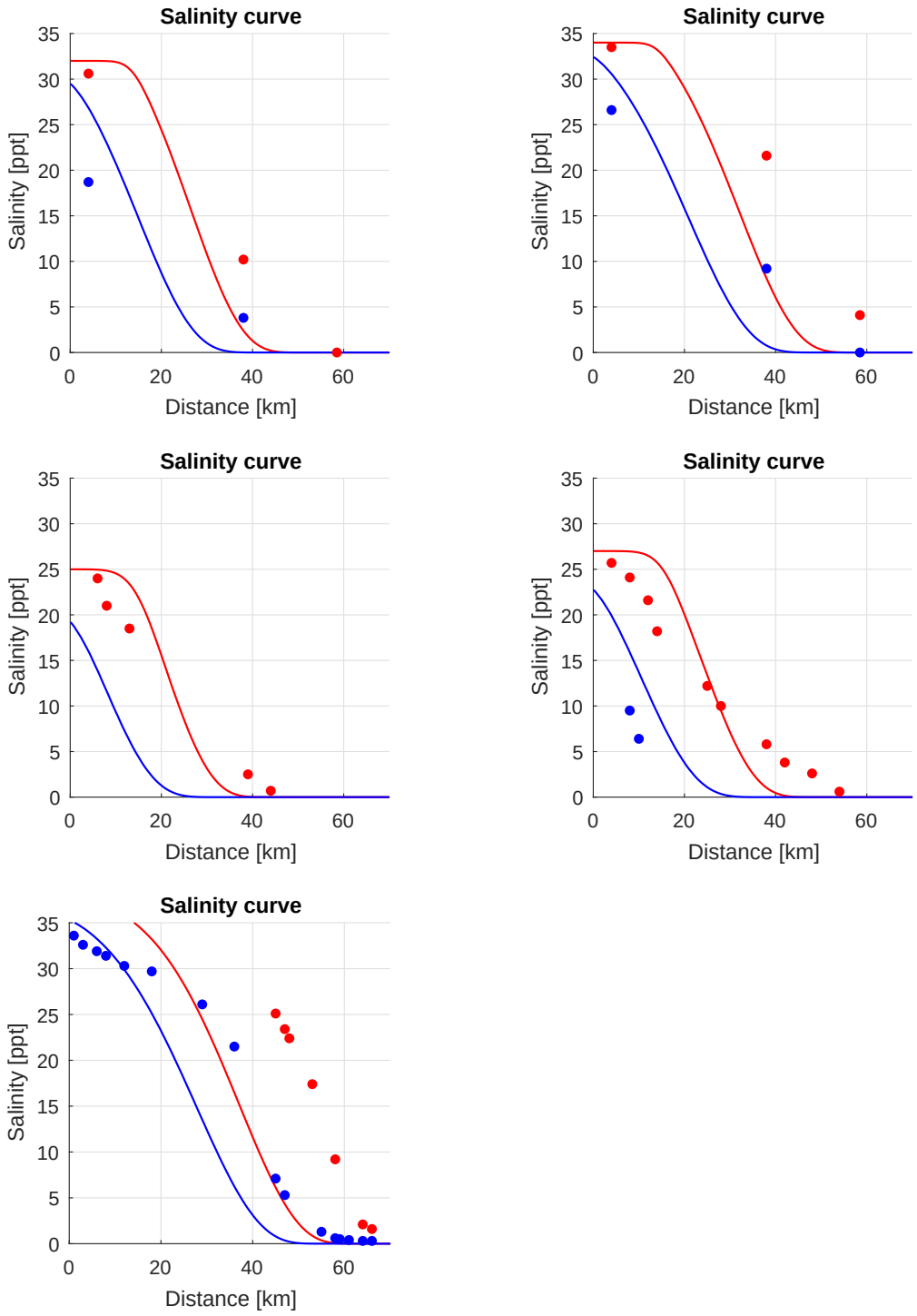

Figure D.22: *Salinity profile for the Pungue estuary*

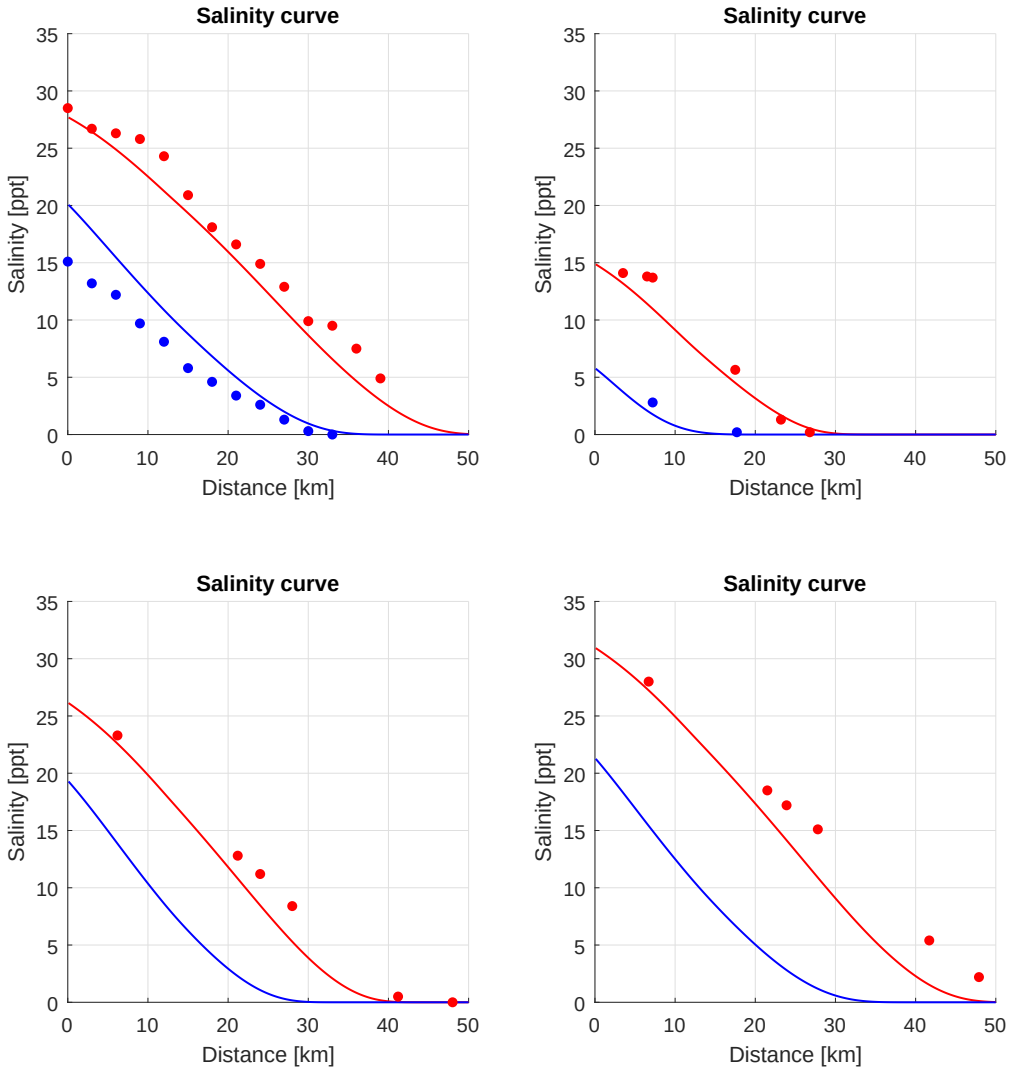

Figure D.23: *Salinity profile for the ChaoPhya estuary*

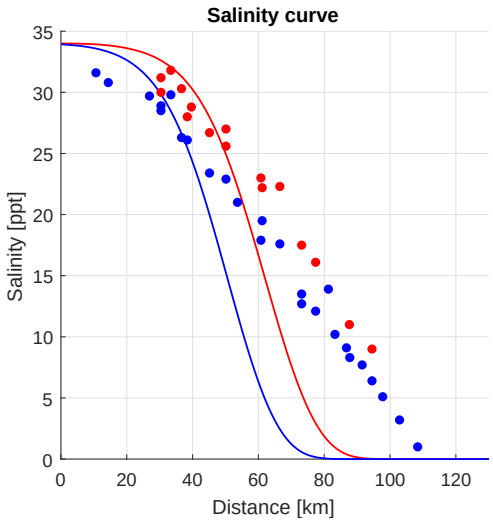

Figure D.24: *Salinity profile for the Westerschelde estuary*

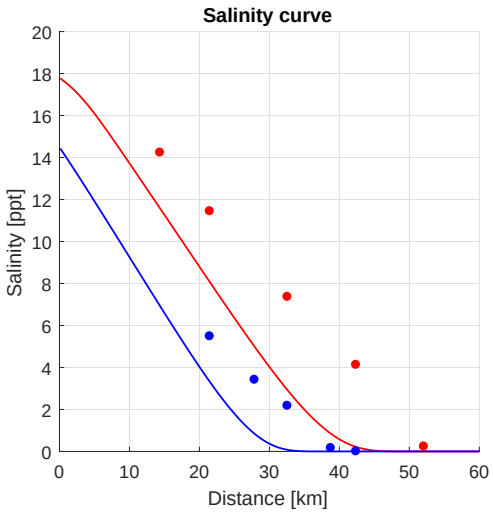

Figure D.25: *Salinity profile for the Landak estuary*

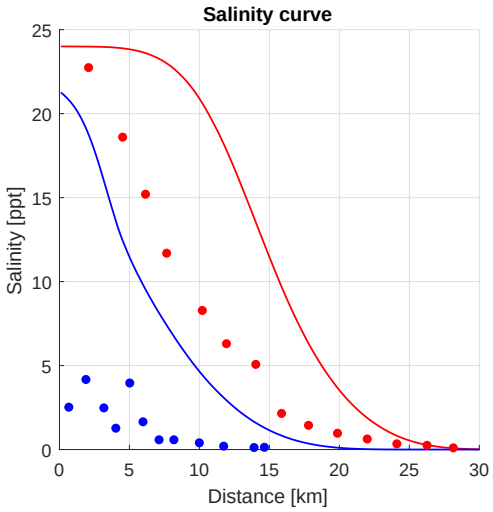

Figure D.26: *Salinity profile for the Perak estuary*

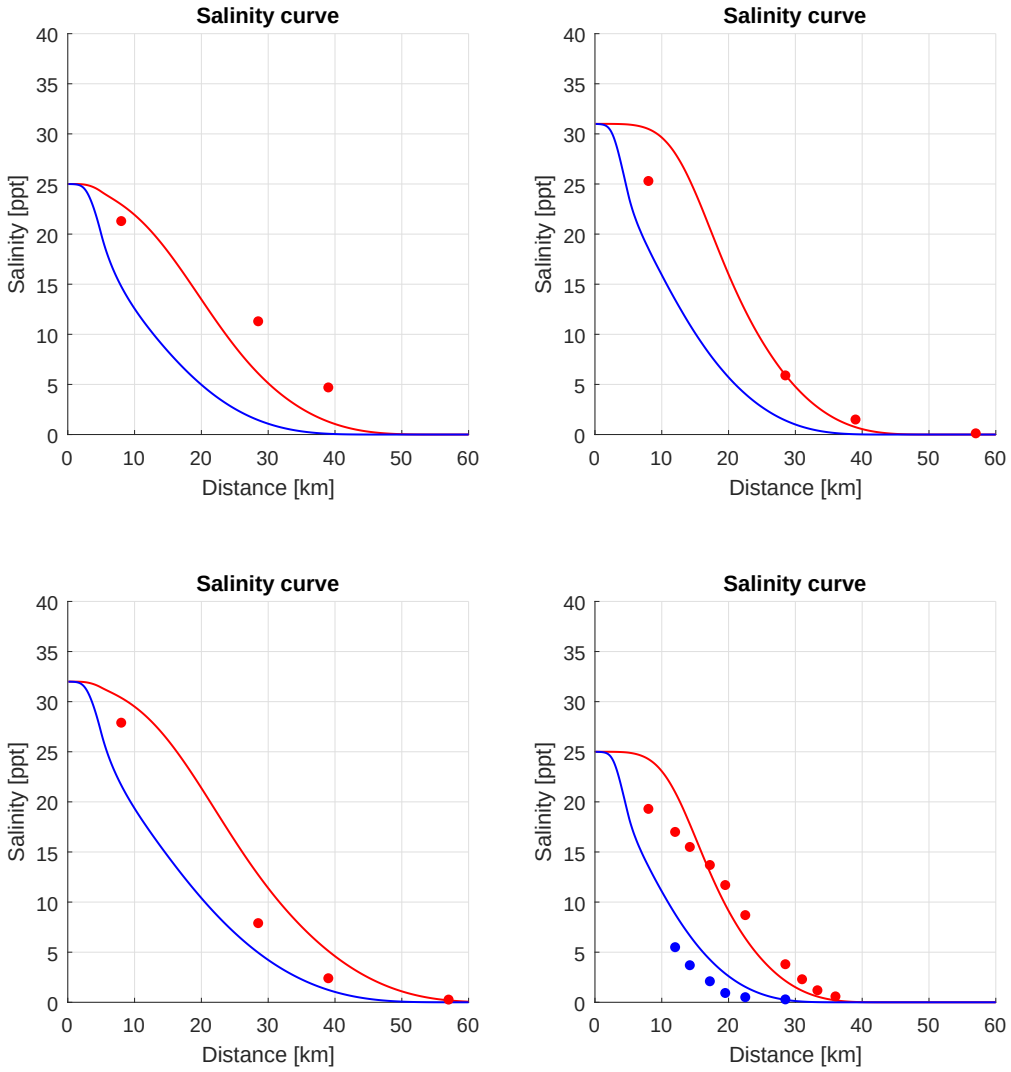

Figure D.27: *Salinity profile for the ThaChin estuary*

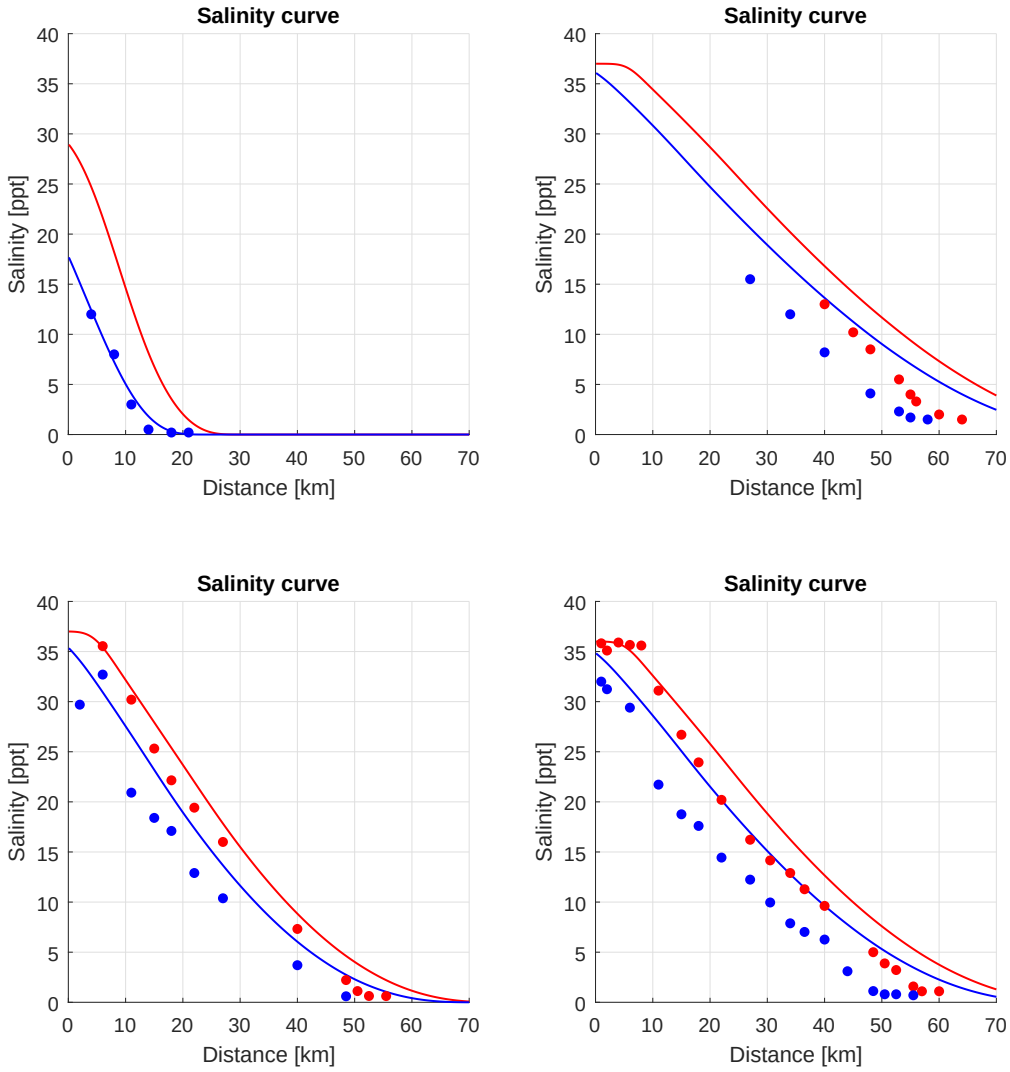

Figure D.28: *Salinity profile for the Limpopo estuary*

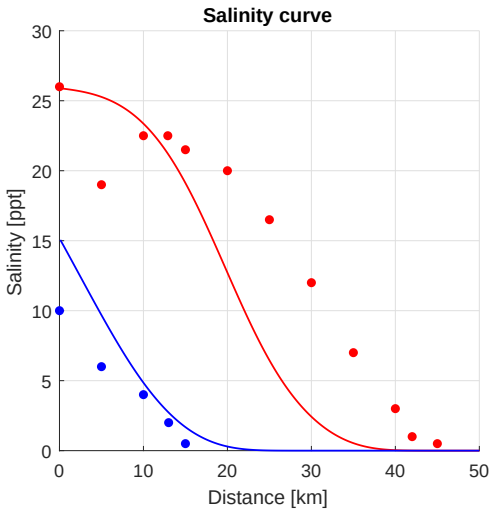

Figure D.29: *Salinity profile for the Lalang estuary*

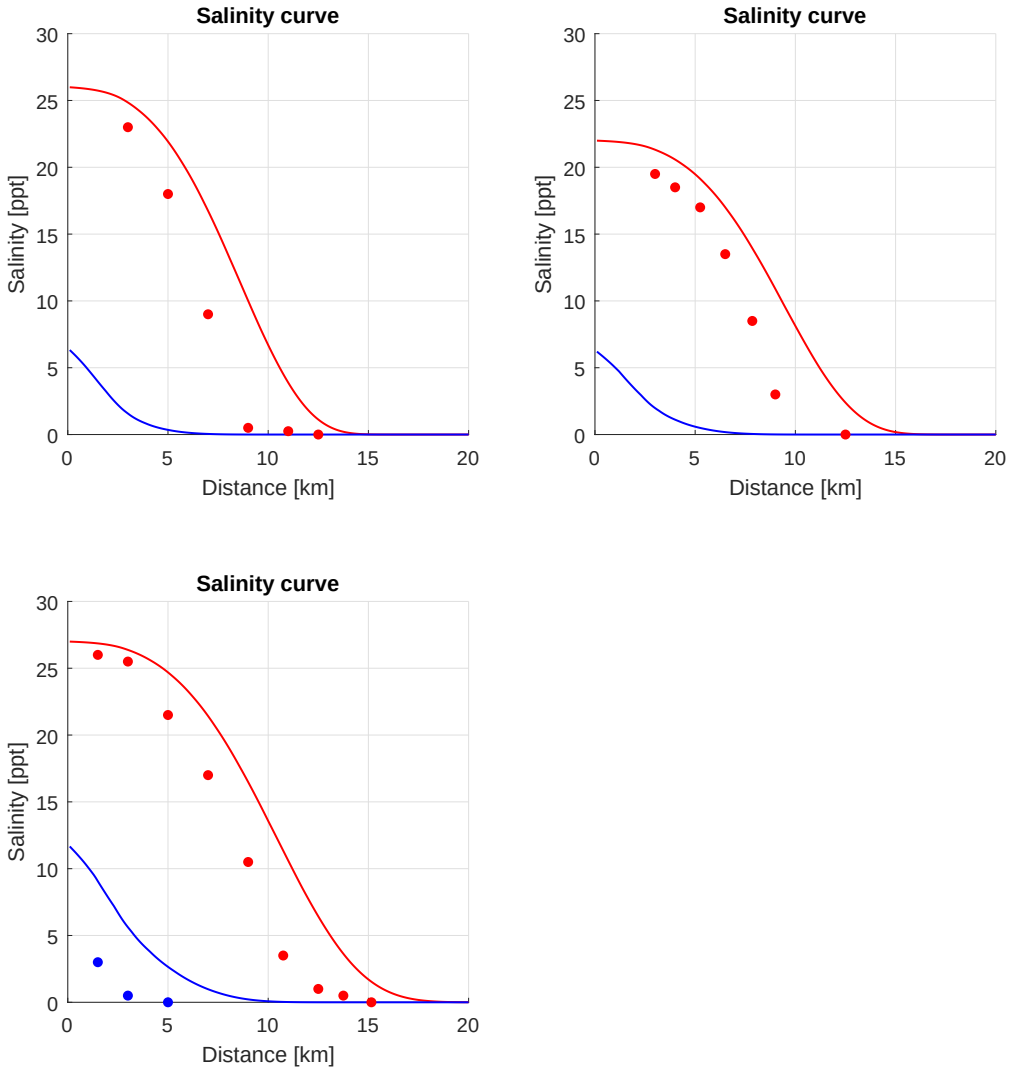

Figure D.30: *Salinity profile for the Sinnamary estuary*

D.4 Savenije

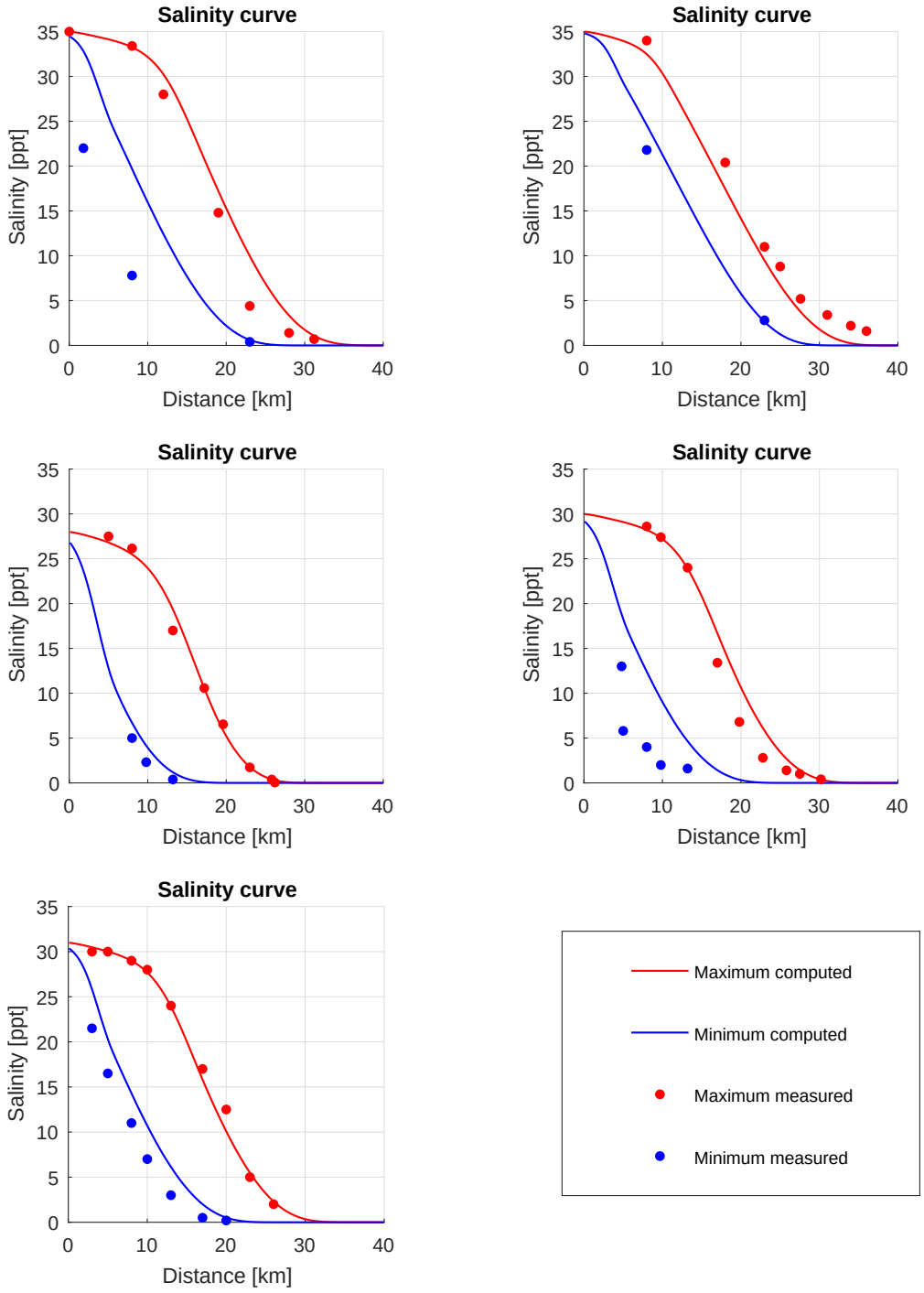

Figure D.31: *Salinity profile for the Maputo estuary*

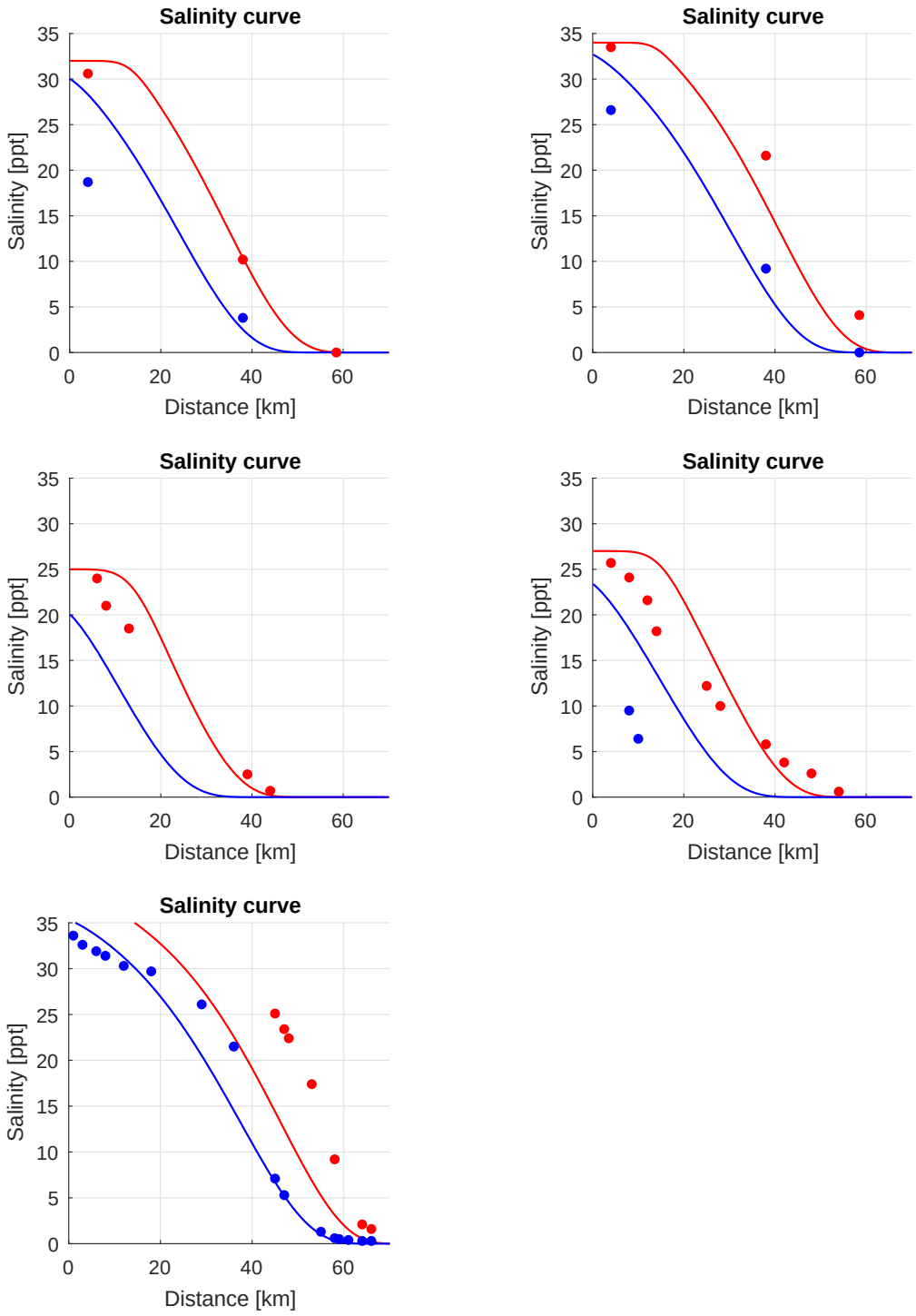

Figure D.32: *Salinity profile for the Pungue estuary*

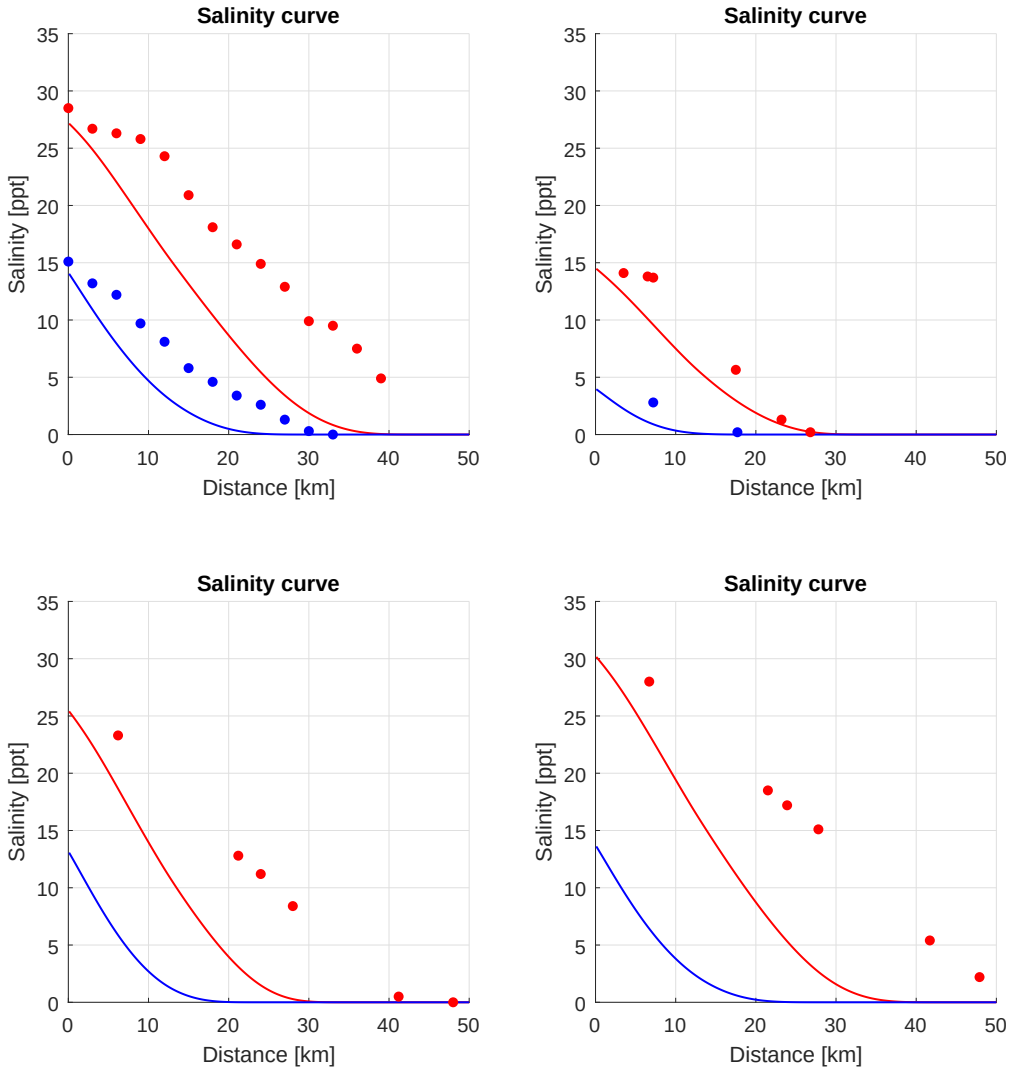

Figure D.33: *Salinity profile for the ChaoPhya estuary*

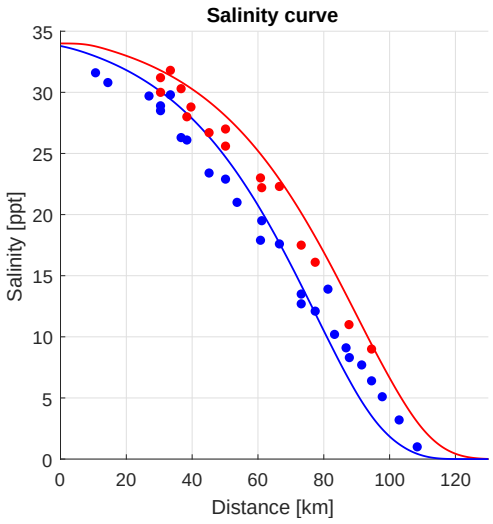

Figure D.34: *Salinity profile for the Westerschelde estuary*

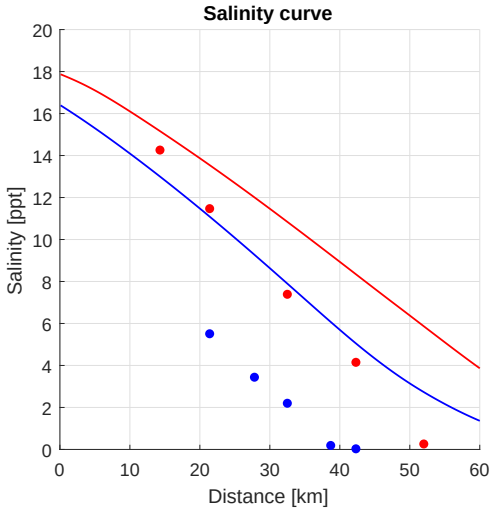

Figure D.35: *Salinity profile for the Landak estuary*

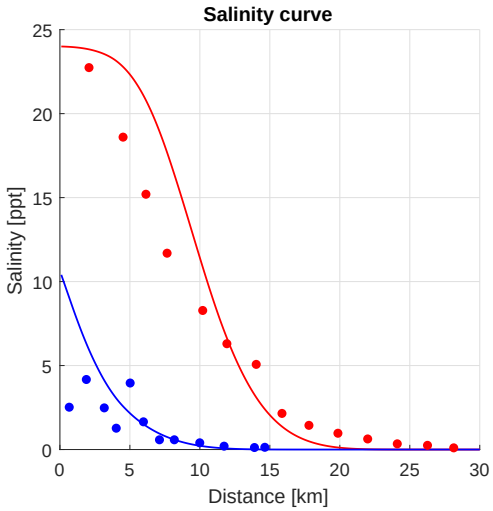

Figure D.36: *Salinity profile for the Perak estuary*

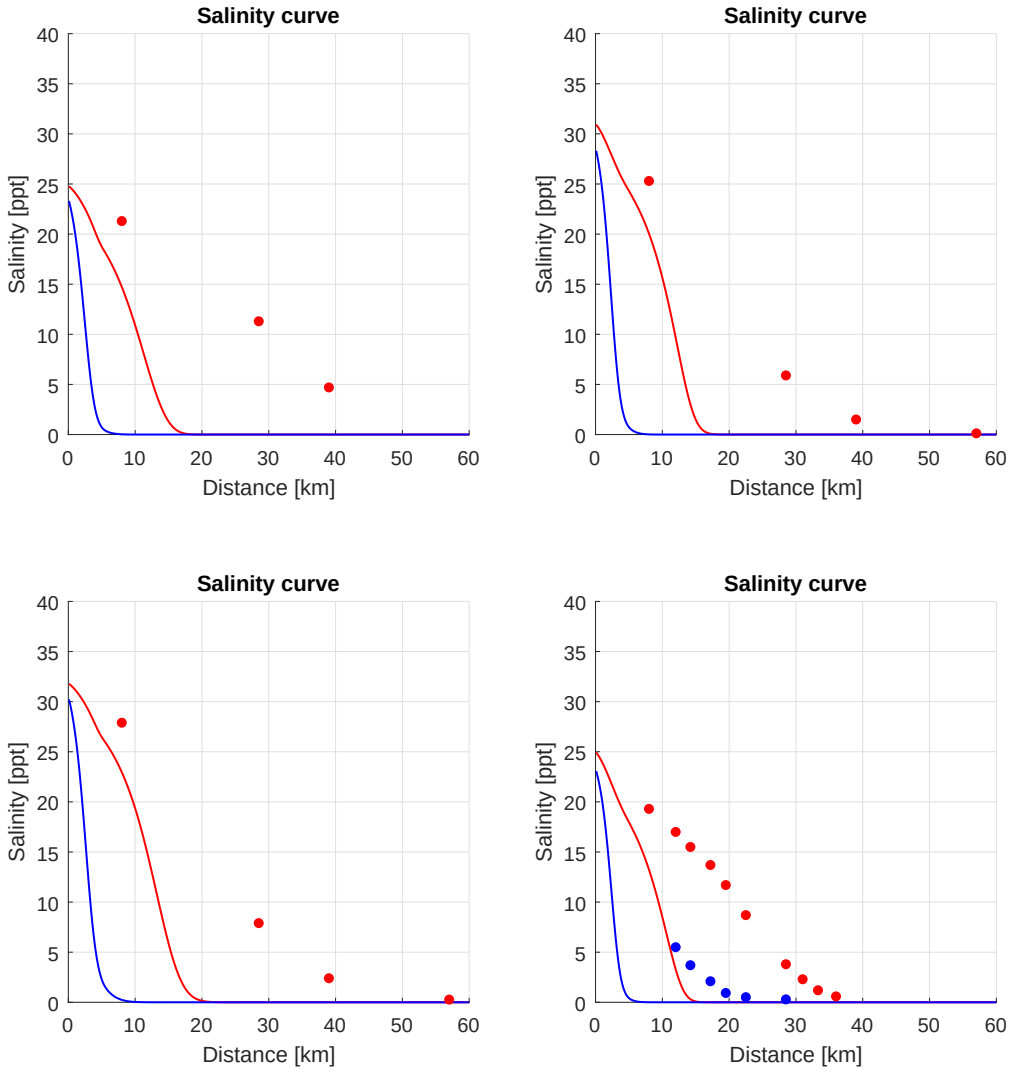

Figure D.37: *Salinity profile for the ThaChin estuary*

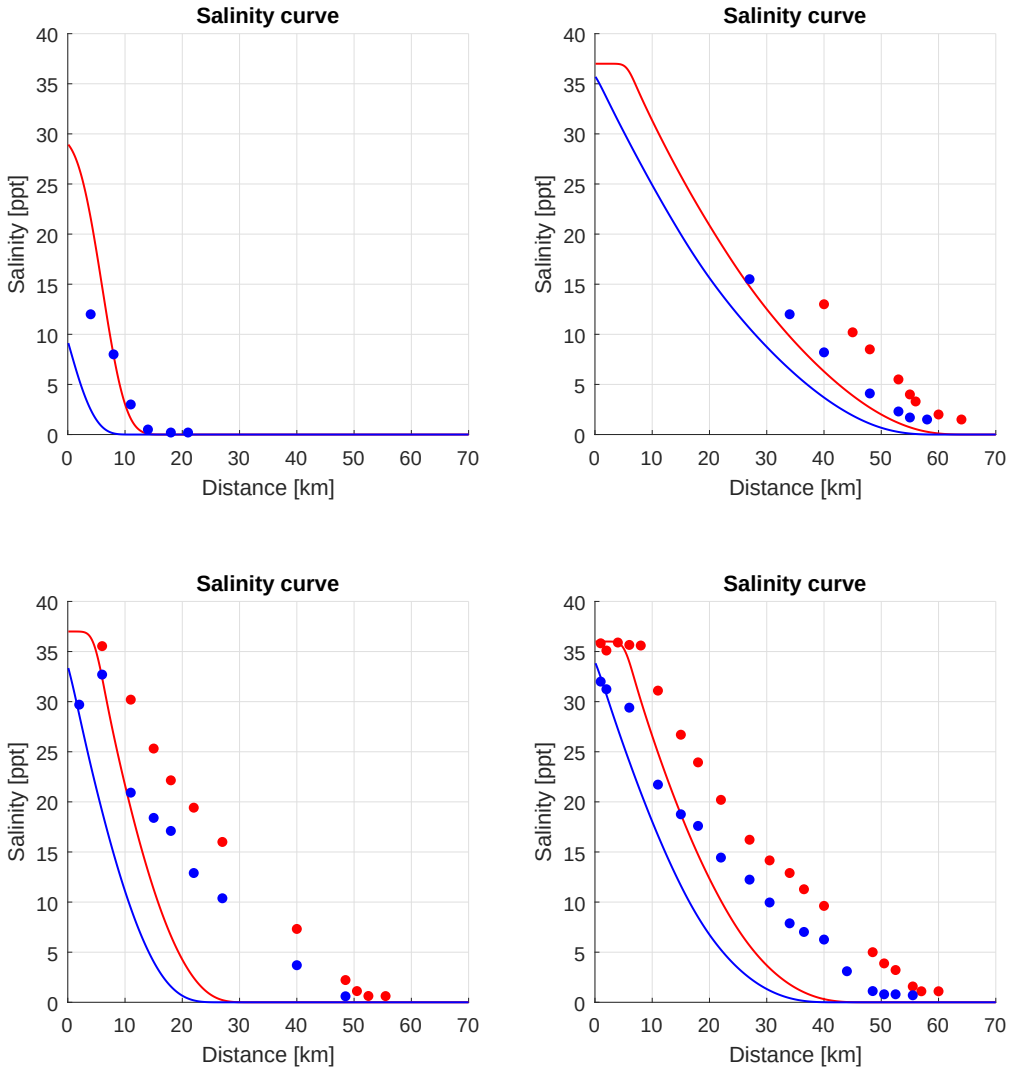

Figure D.38: *Salinity profile for the Limpopo estuary*

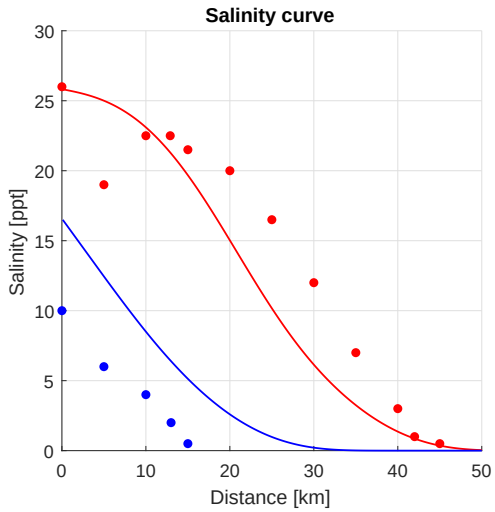

Figure D.39: *Salinity profile for the Lalang estuary*

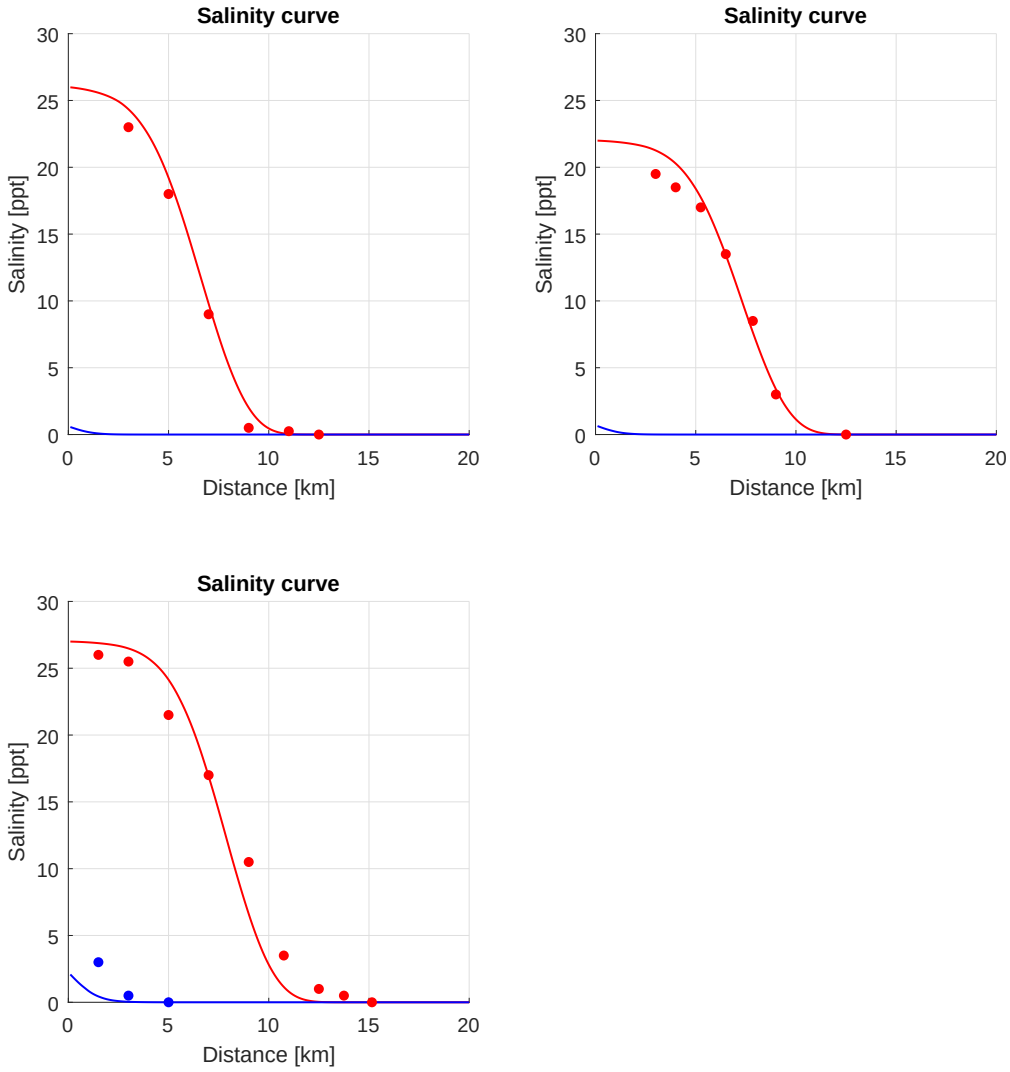

Figure D.40: *Salinity profile for the Sinnamary estuary*

D.5 Kuijper and van Rijn

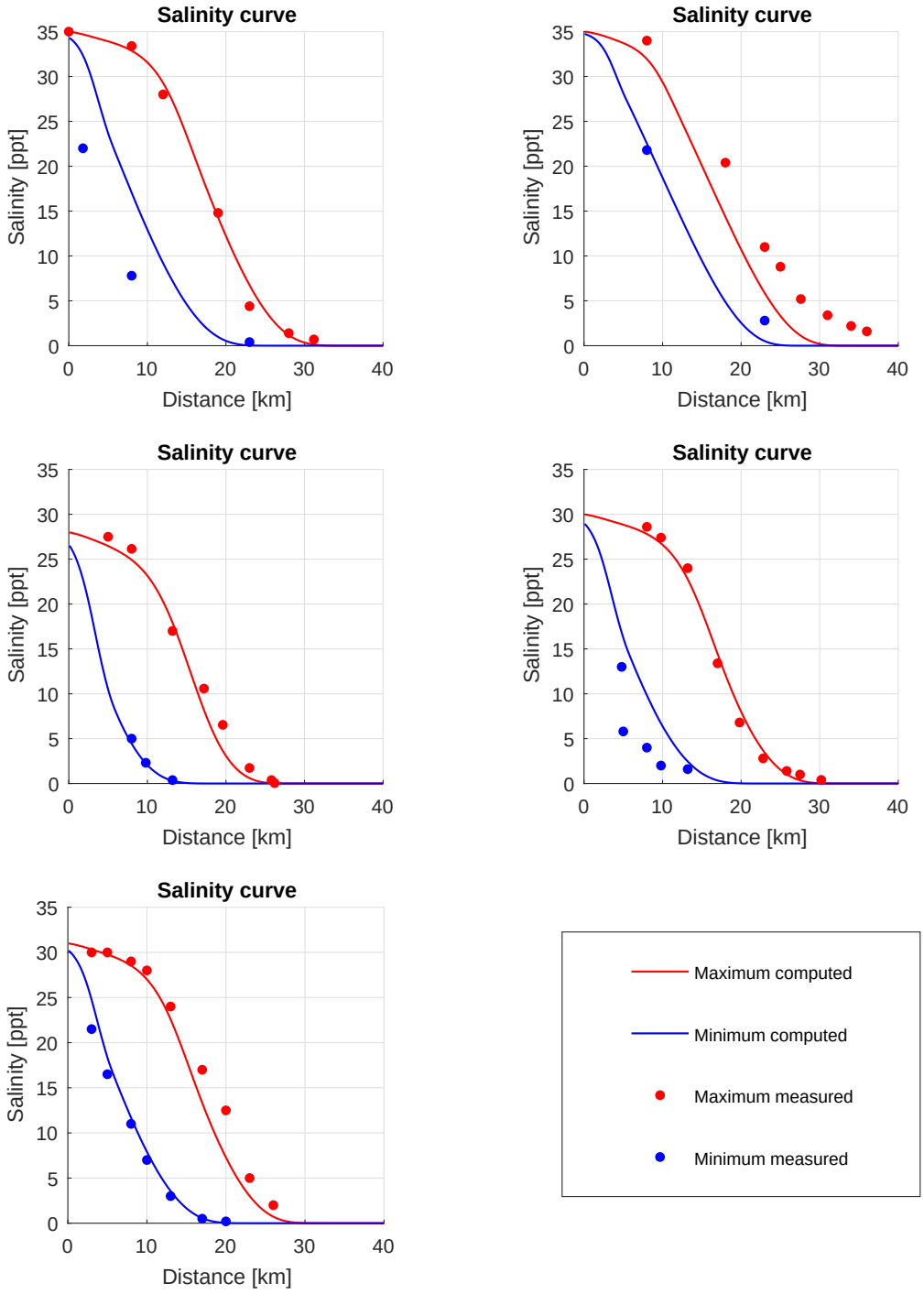

Figure D.41: *Salinity profile for the Maputo estuary*

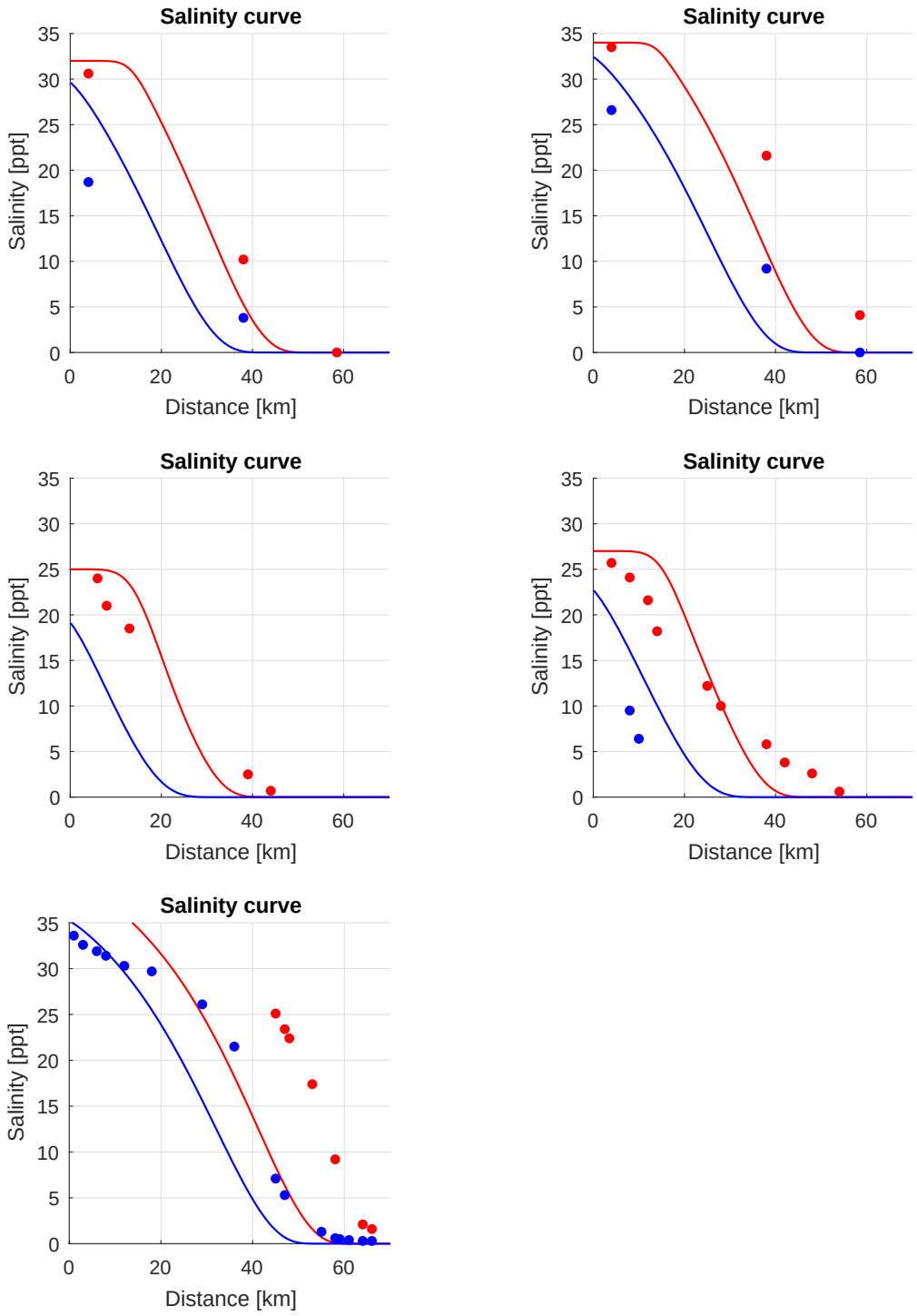

Figure D.42: *Salinity profile for the Pungue estuary*

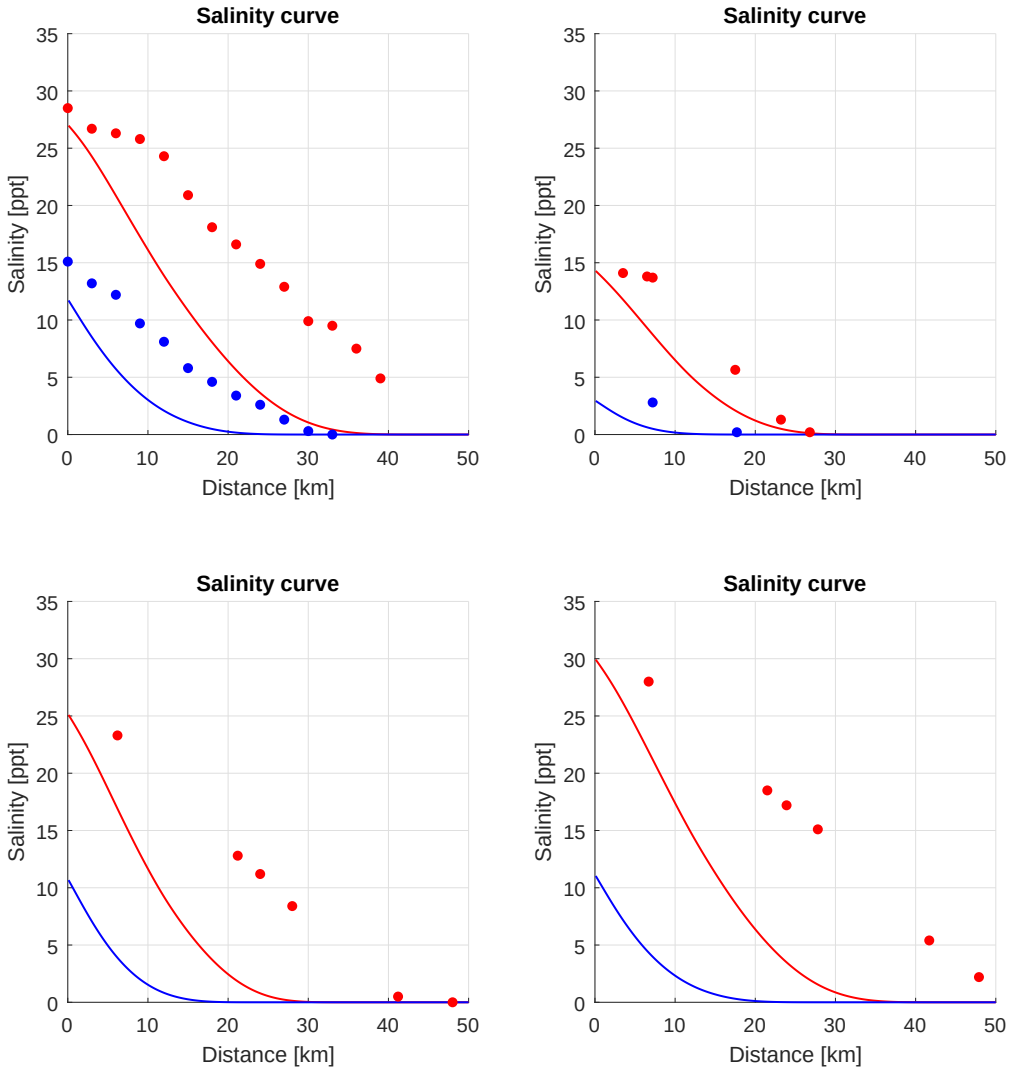

Figure D.43: *Salinity profile for the ChaoPhya estuary*

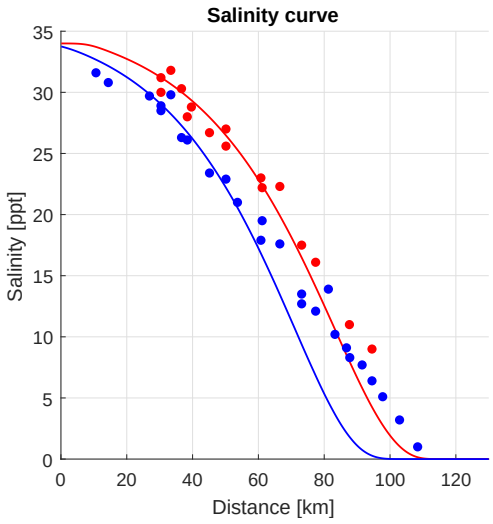

Figure D.44: *Salinity profile for the Westerschelde estuary*

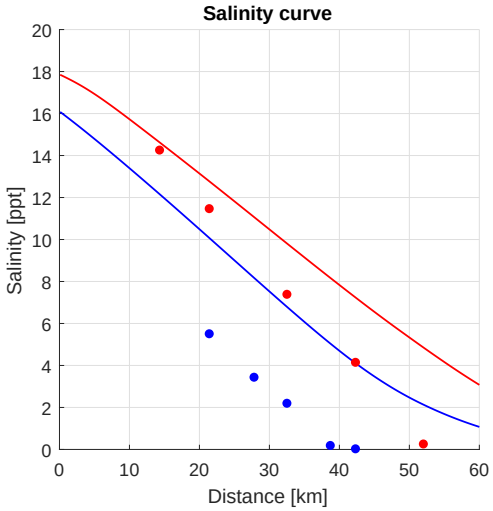

Figure D.45: *Salinity profile for the Landak estuary*

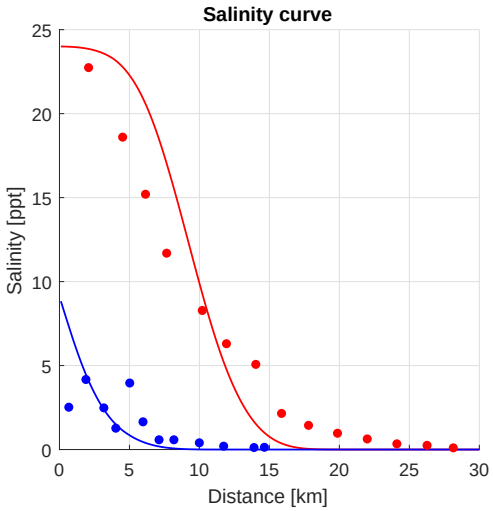

Figure D.46: *Salinity profile for the Perak estuary*

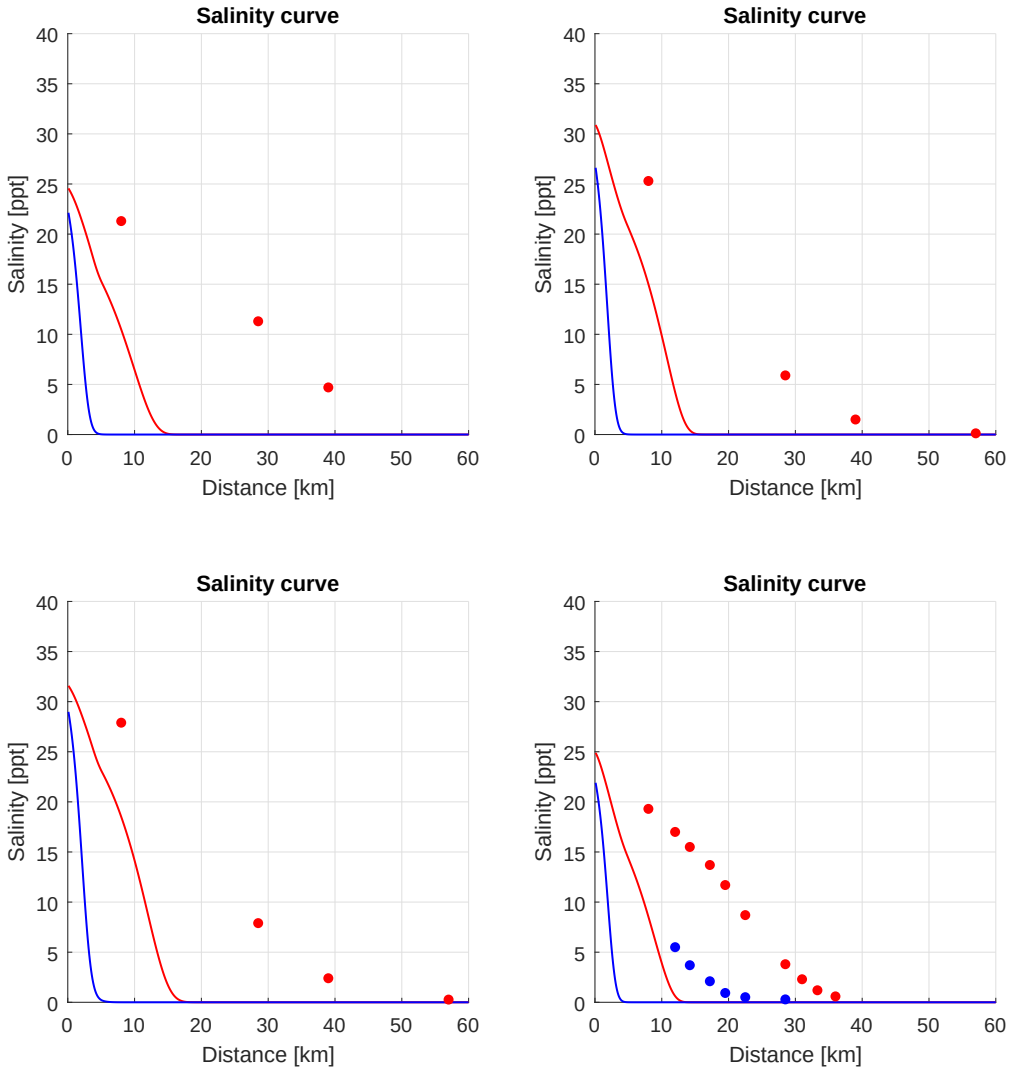

Figure D.47: *Salinity profile for the ThaChin estuary*

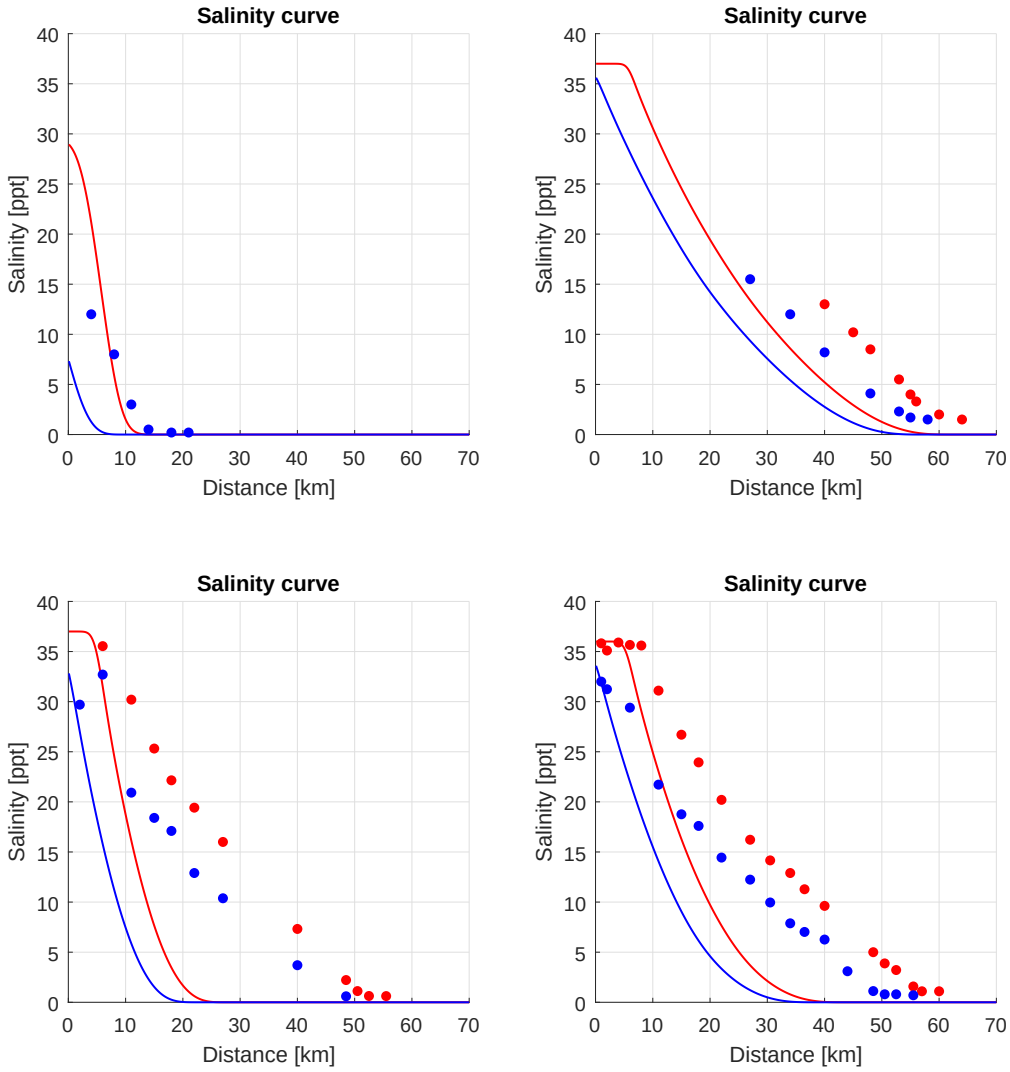

Figure D.48: *Salinity profile for the Limpopo estuary*

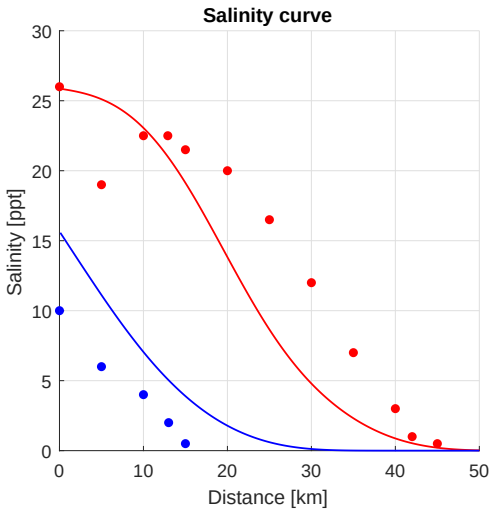

Figure D.49: *Salinity profile for the Lalang estuary*

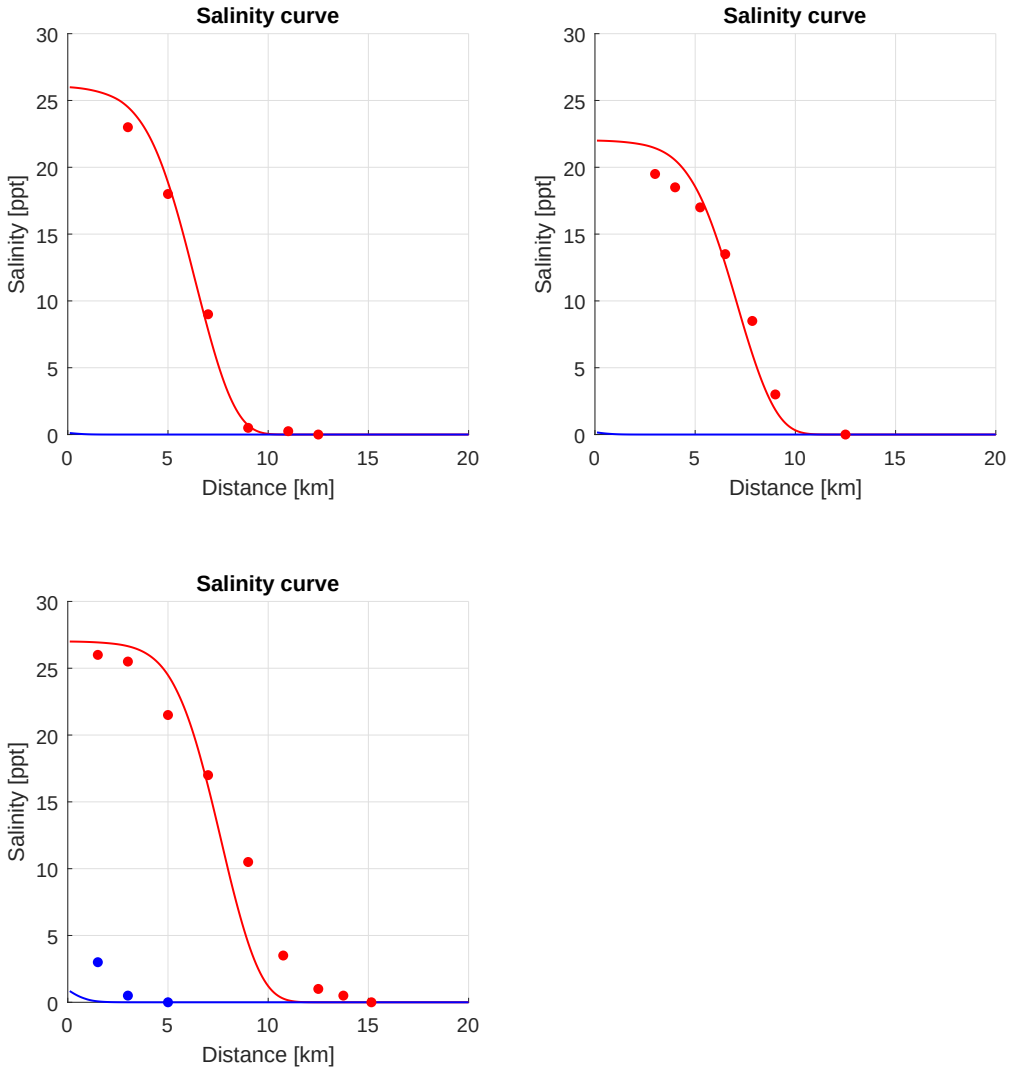

Figure D.50: *Salinity profile for the Sinnamary estuary*

D.6 Zhang, $K = 0.58$

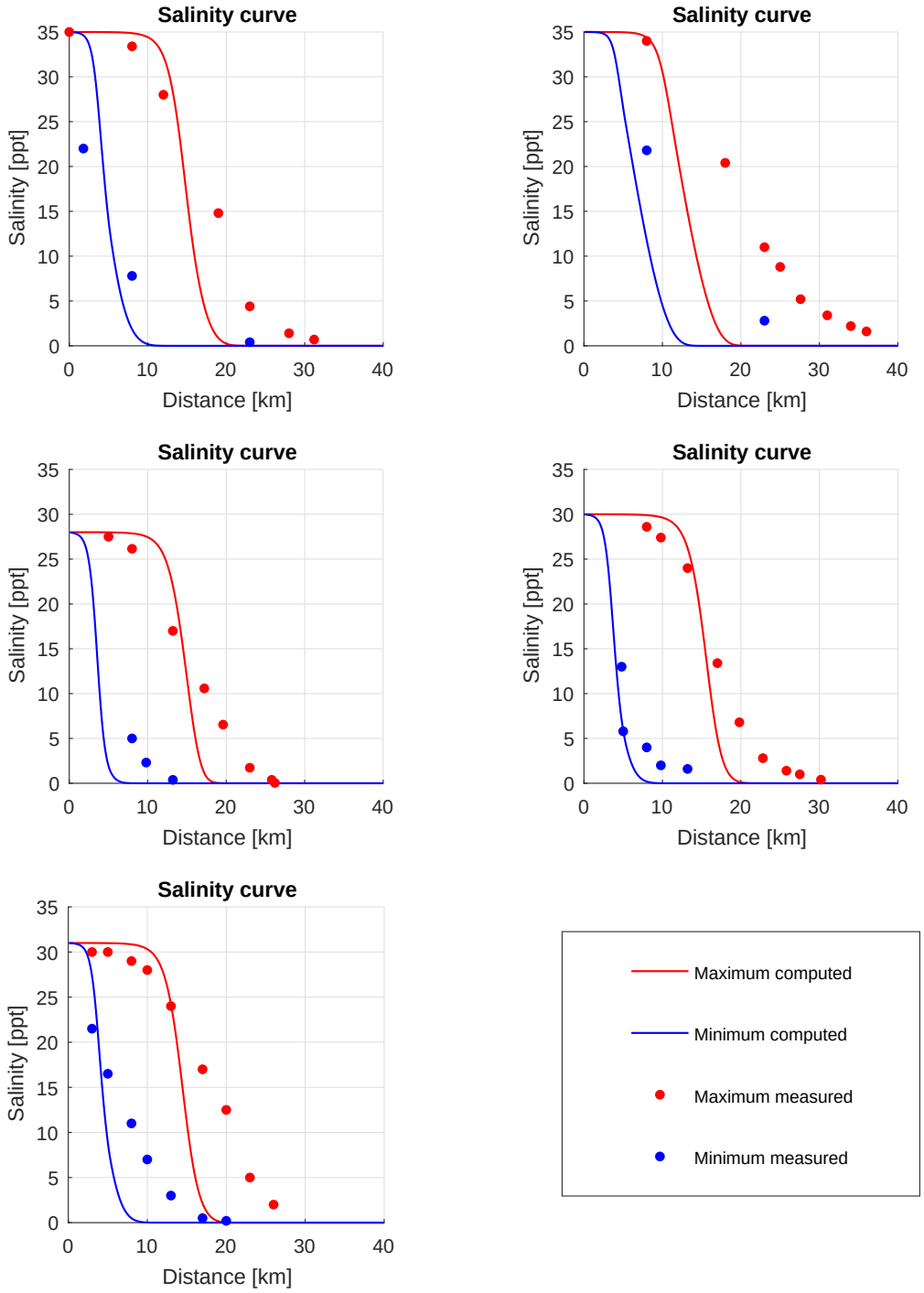

Figure D.51: *Salinity profile for the Maputo estuary*

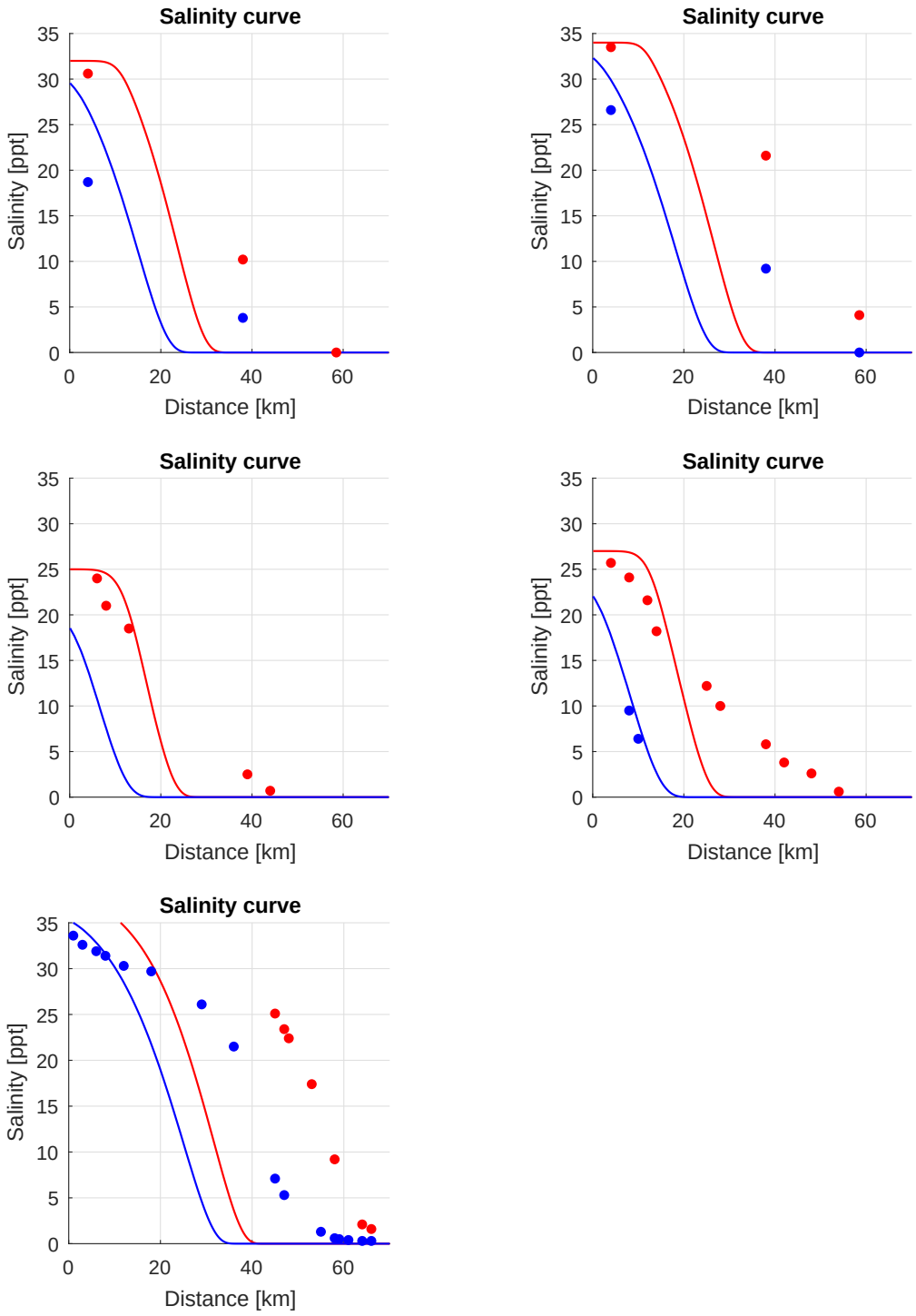

Figure D.52: *Salinity profile for the Pungue estuary*

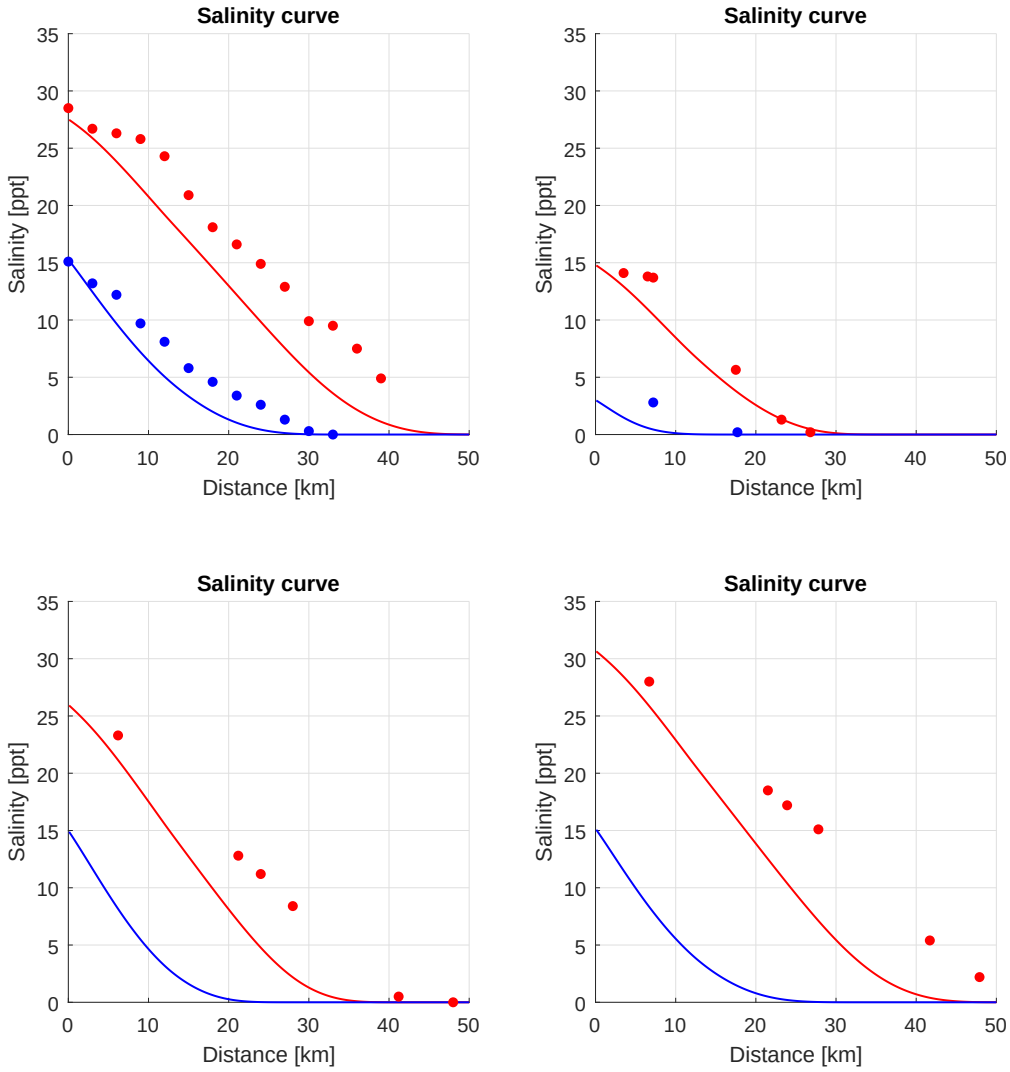

Figure D.53: *Salinity profile for the ChaoPhya estuary*

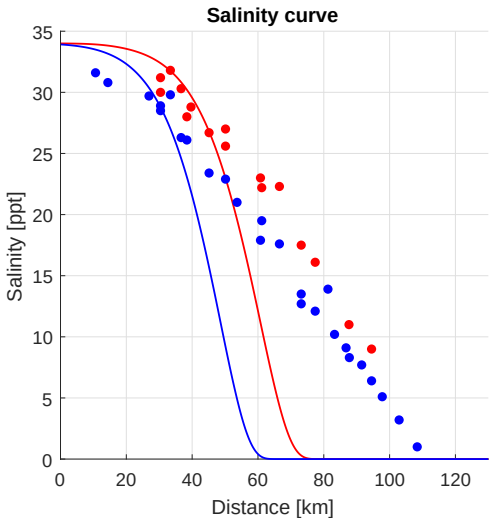

Figure D.54: *Salinity profile for the Westerschelde estuary*

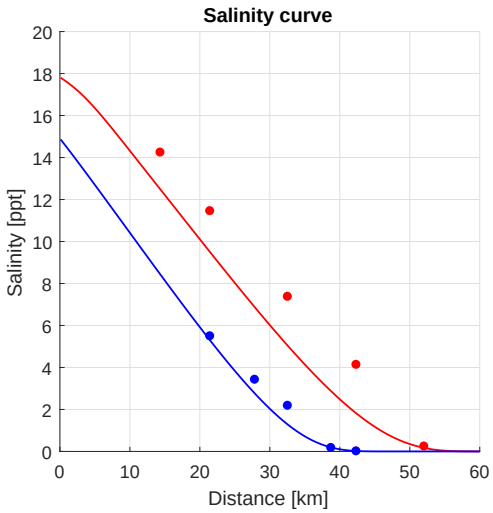

Figure D.55: *Salinity profile for the Landak estuary*

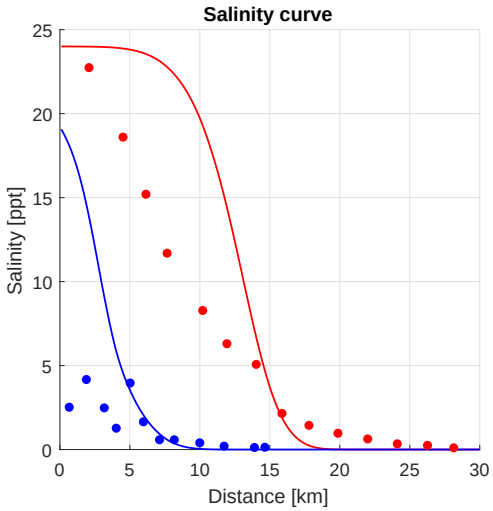

Figure D.56: *Salinity profile for the Perak estuary*

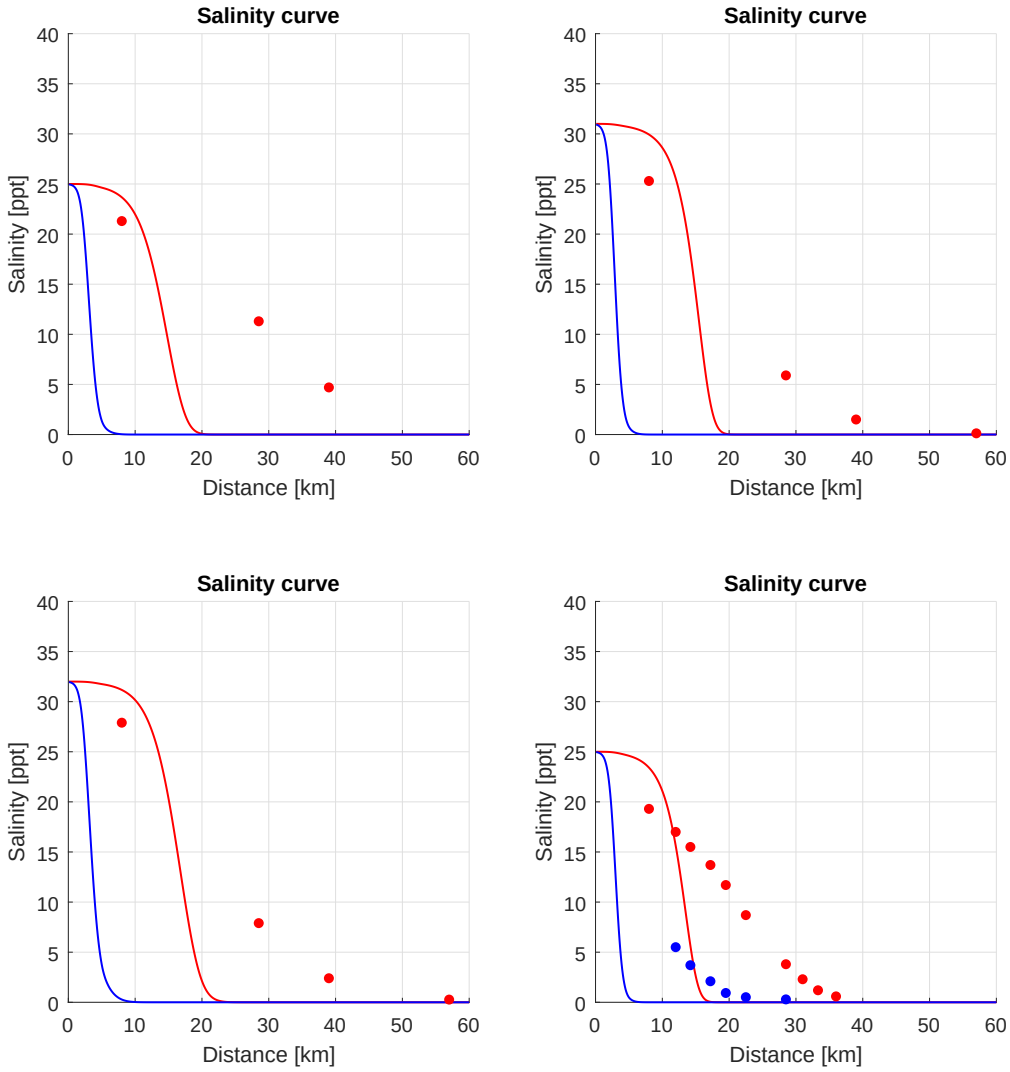

Figure D.57: *Salinity profile for the ThaChin estuary*

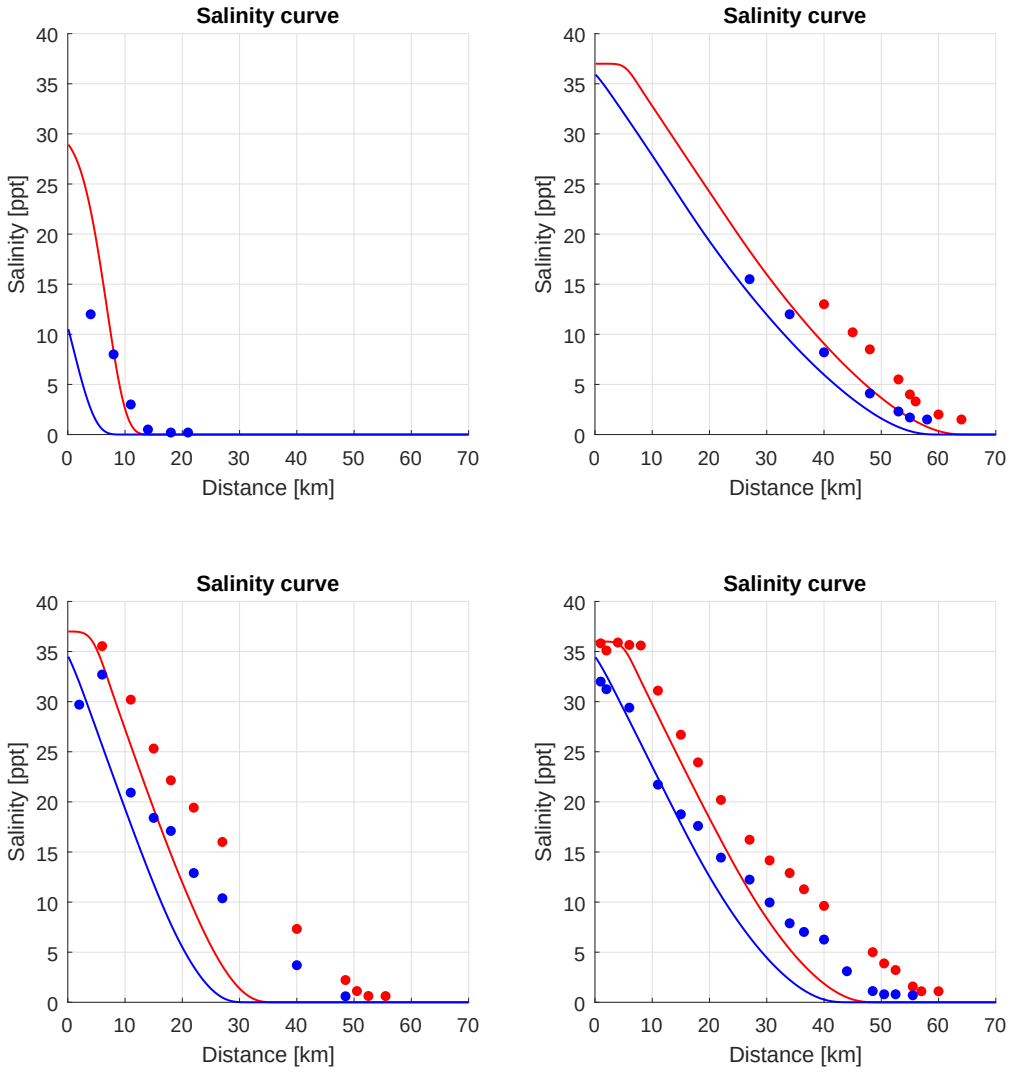

Figure D.58: *Salinity profile for the Limpopo estuary*

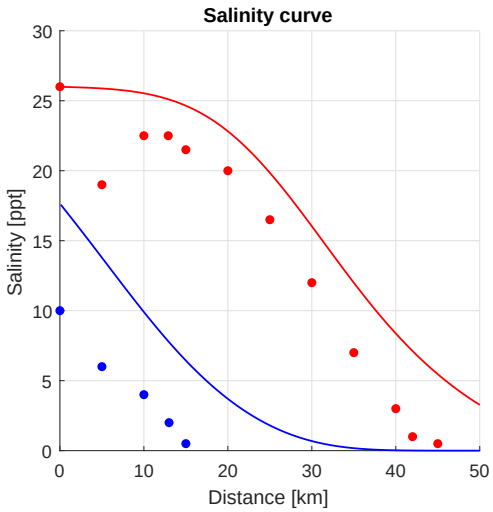

Figure D.59: *Salinity profile for the Lalang estuary*

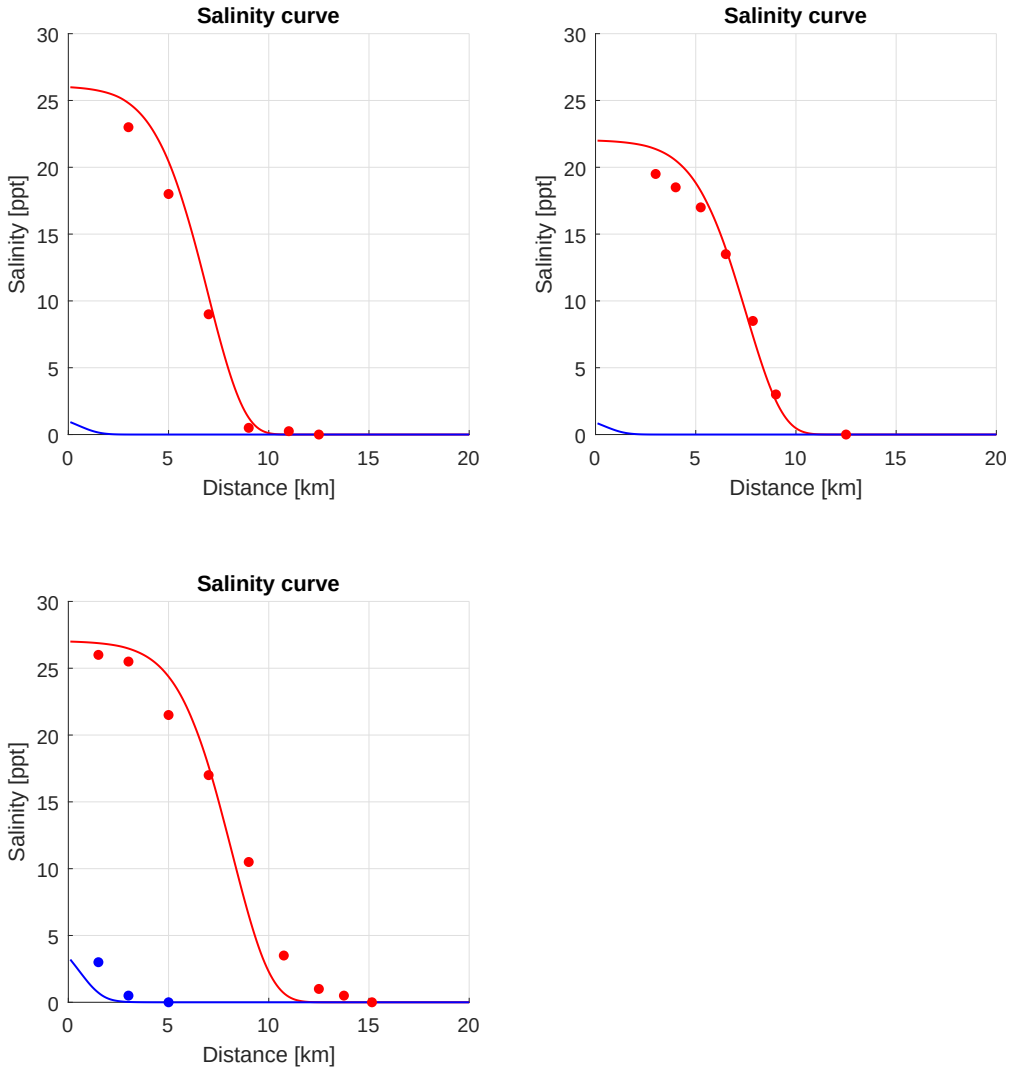

Figure D.60: *Salinity profile for the Sinnamary estuary*

D.7 Zhang, $K_{predicted}$

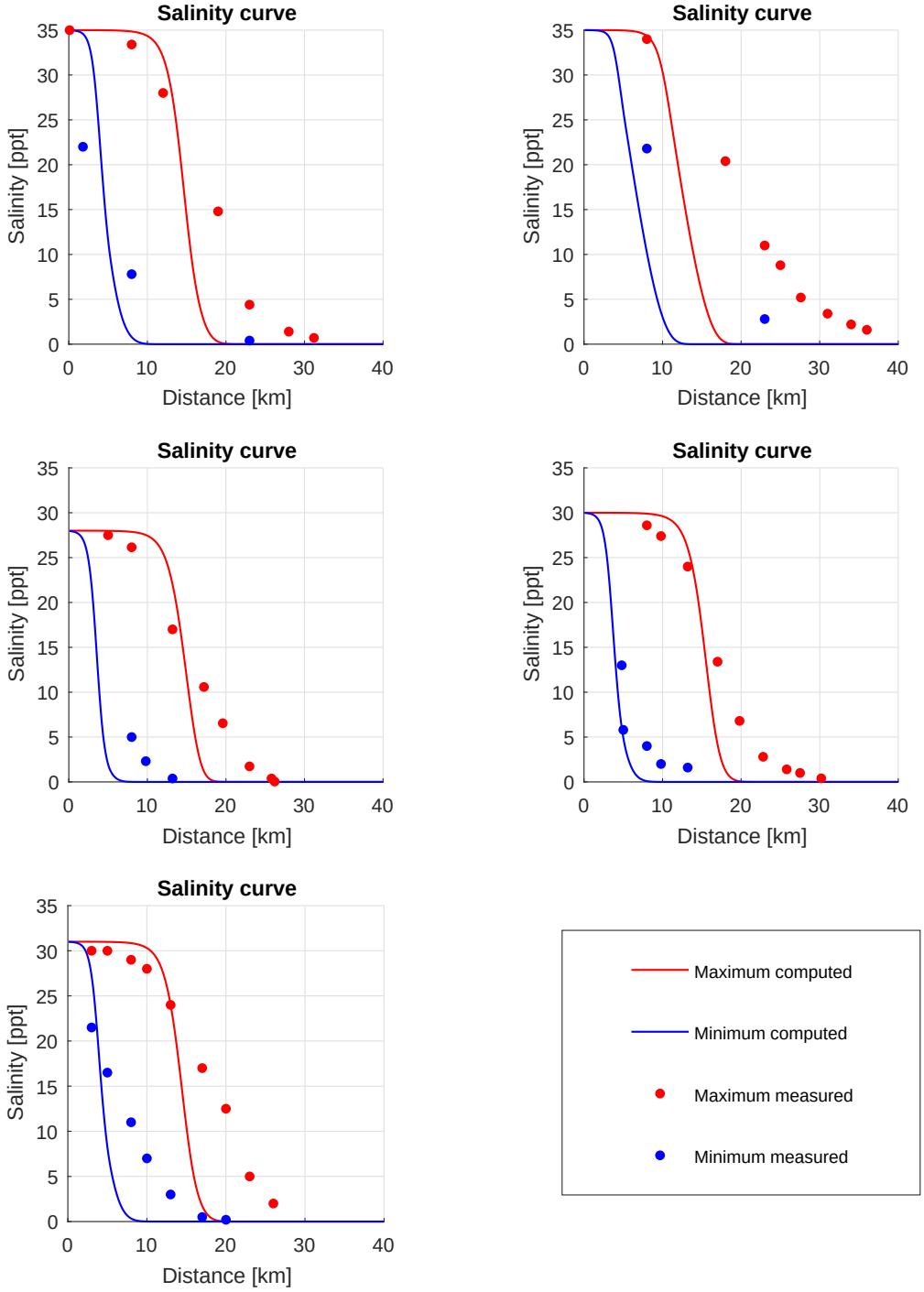

Figure D.61: *Salinity profile for the Maputo estuary*

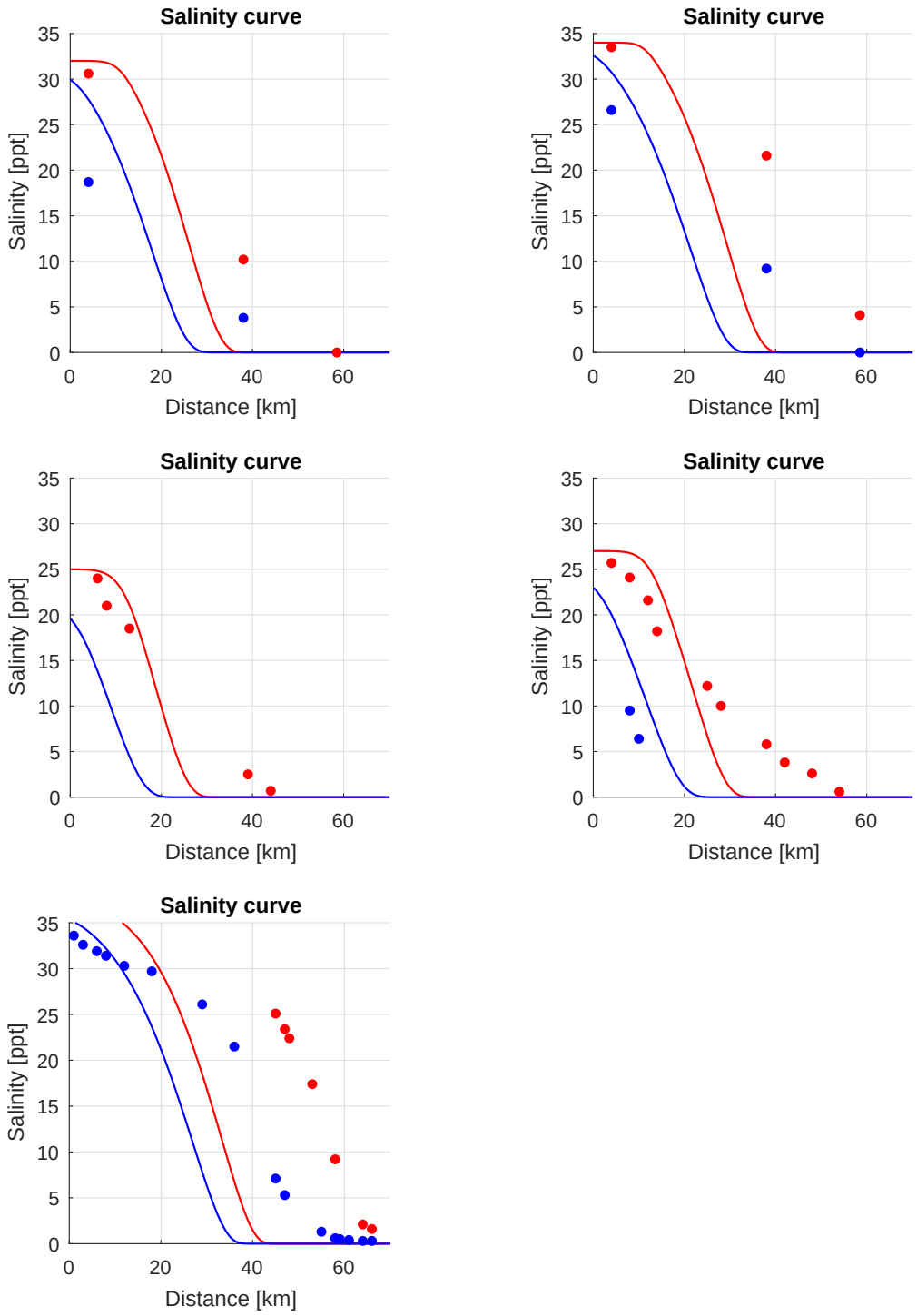

Figure D.62: *Salinity profile for the Pungue estuary*

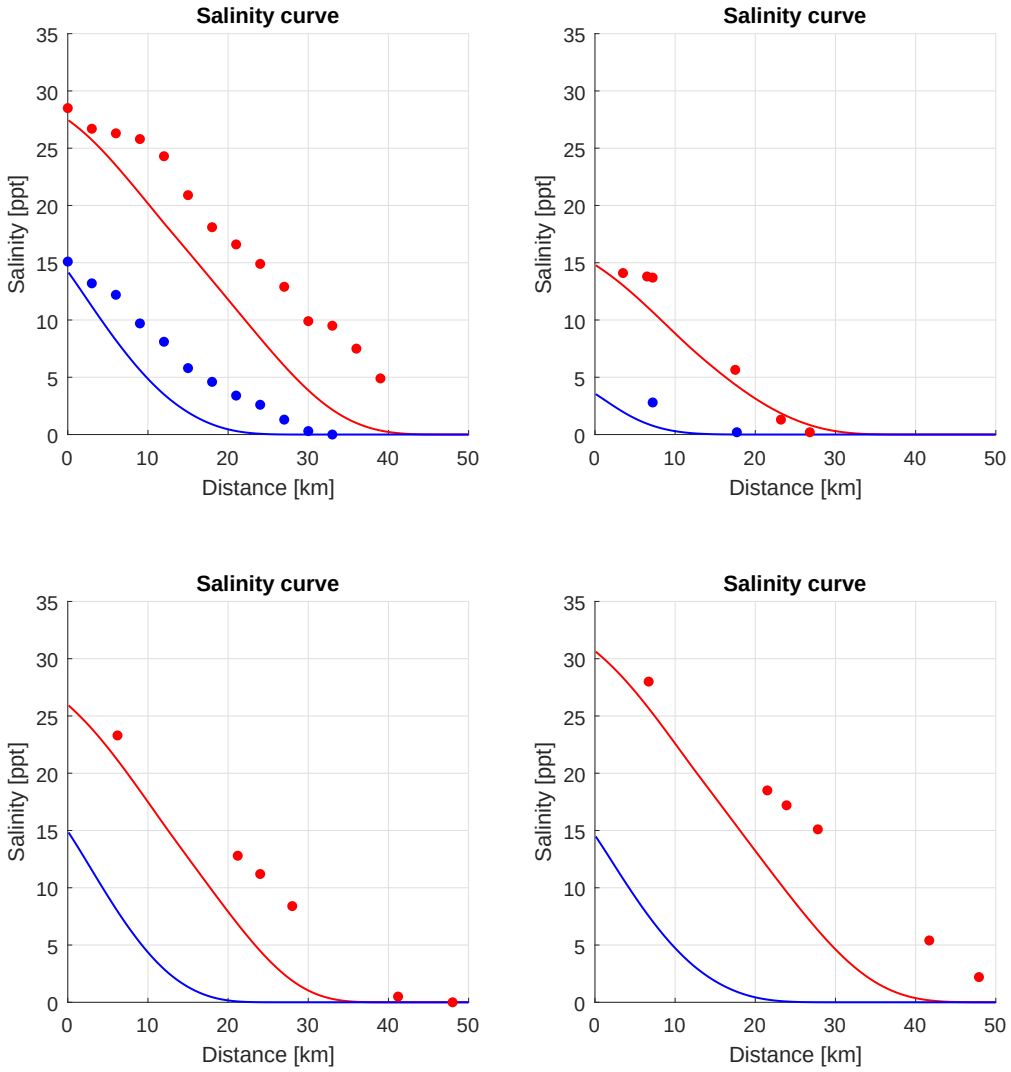

Figure D.63: *Salinity profile for the ChaoPhya estuary*

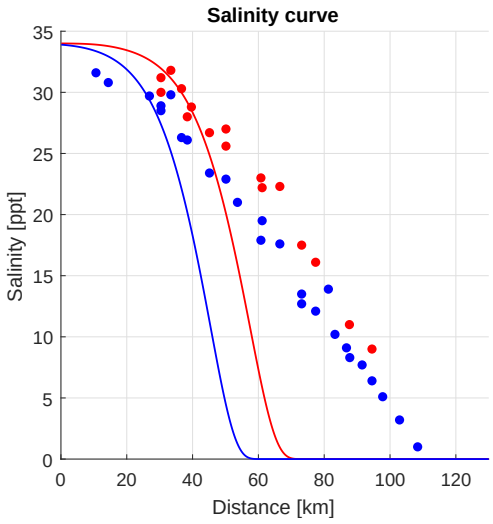

Figure D.64: *Salinity profile for the Westerschelde estuary*

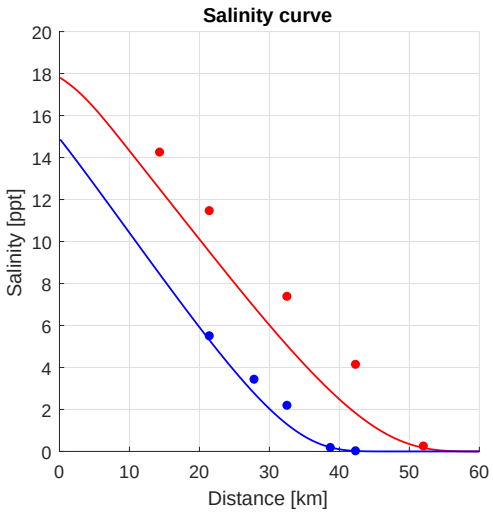

Figure D.65: *Salinity profile for the Landak estuary*

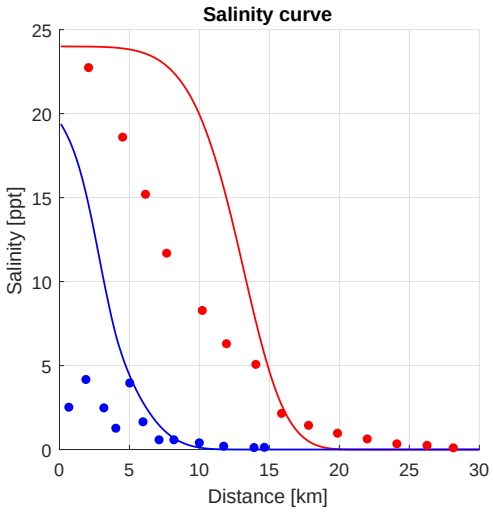

Figure D.66: *Salinity profile for the Perak estuary*

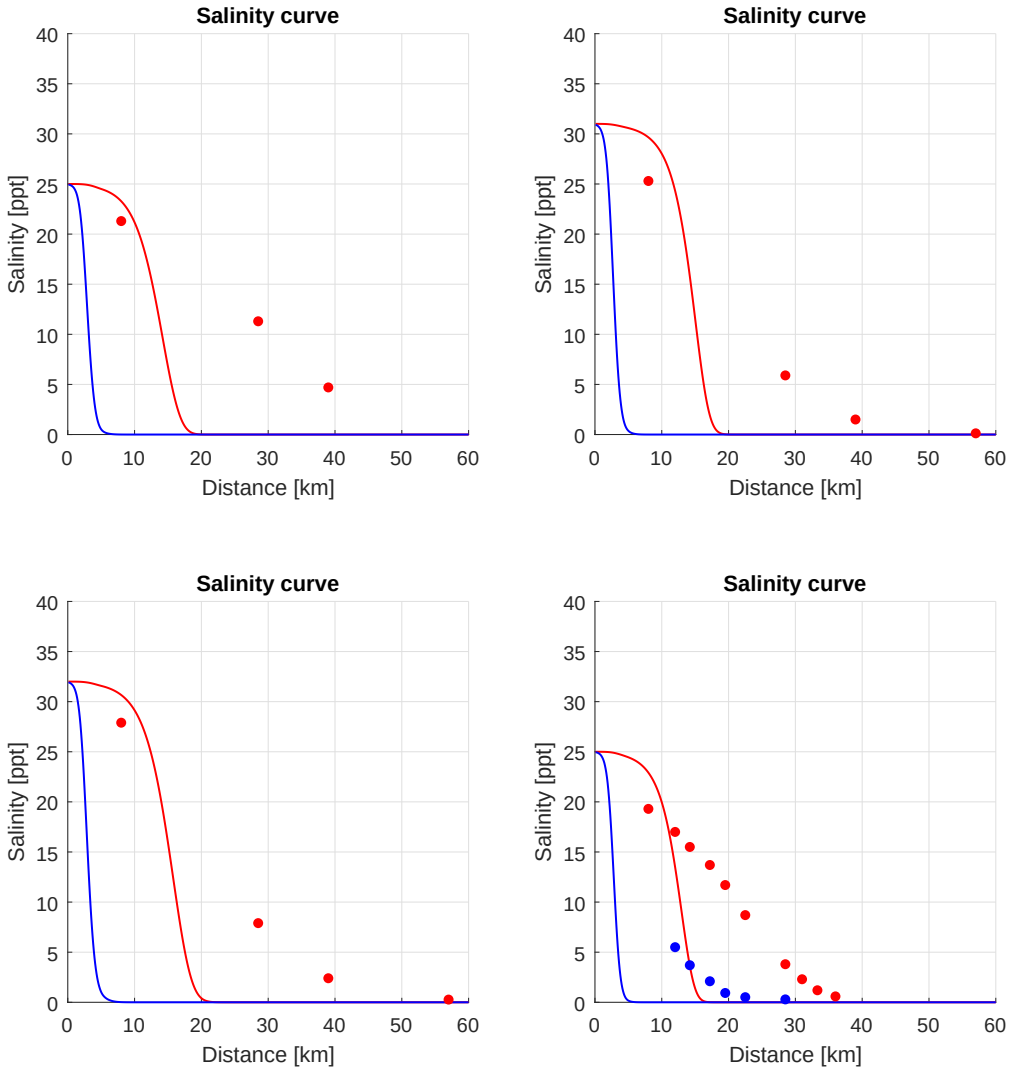

Figure D.67: *Salinity profile for the ThaChin estuary*

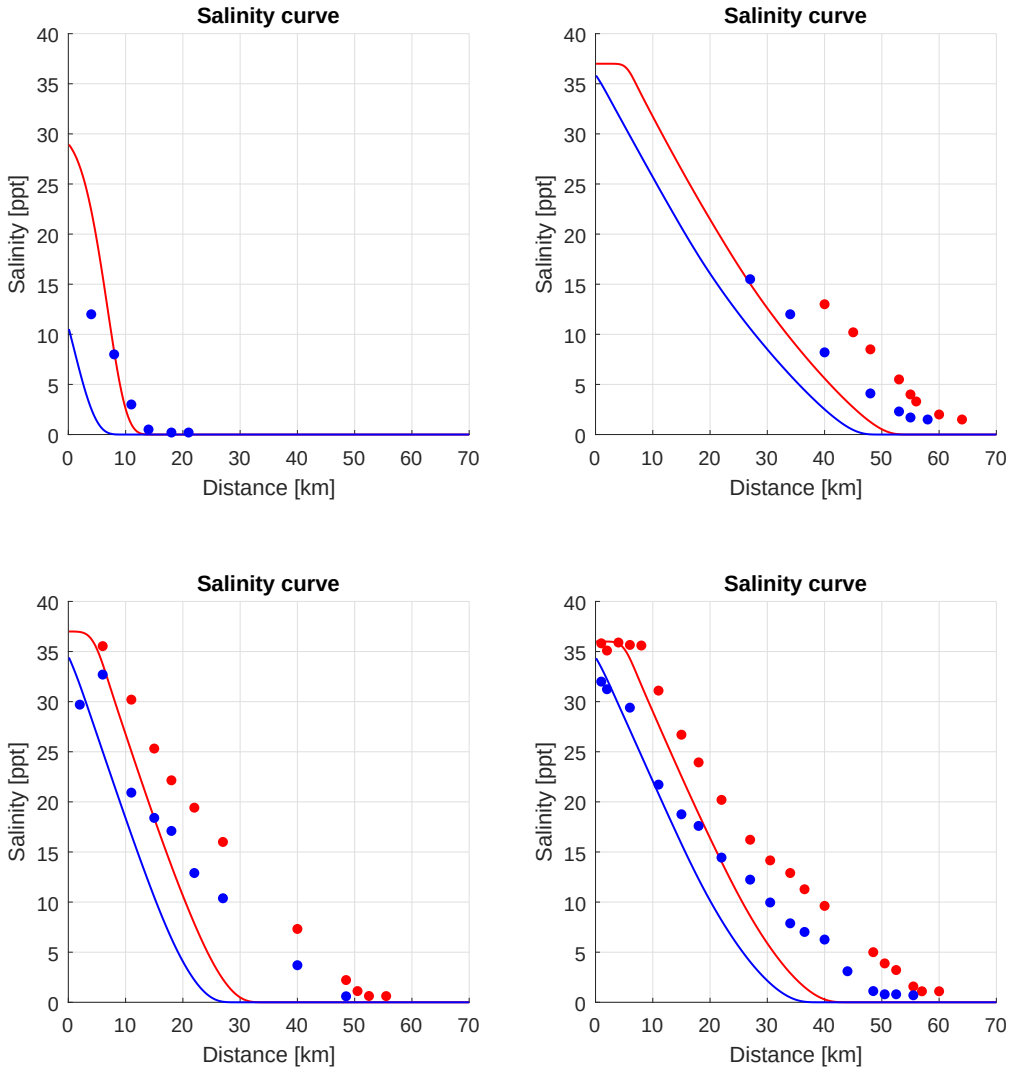

Figure D.68: *Salinity profile for the Limpopo estuary*

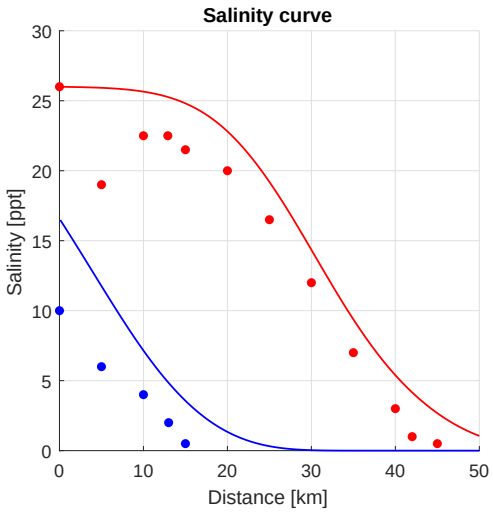

Figure D.69: *Salinity profile for the Lalang estuary*

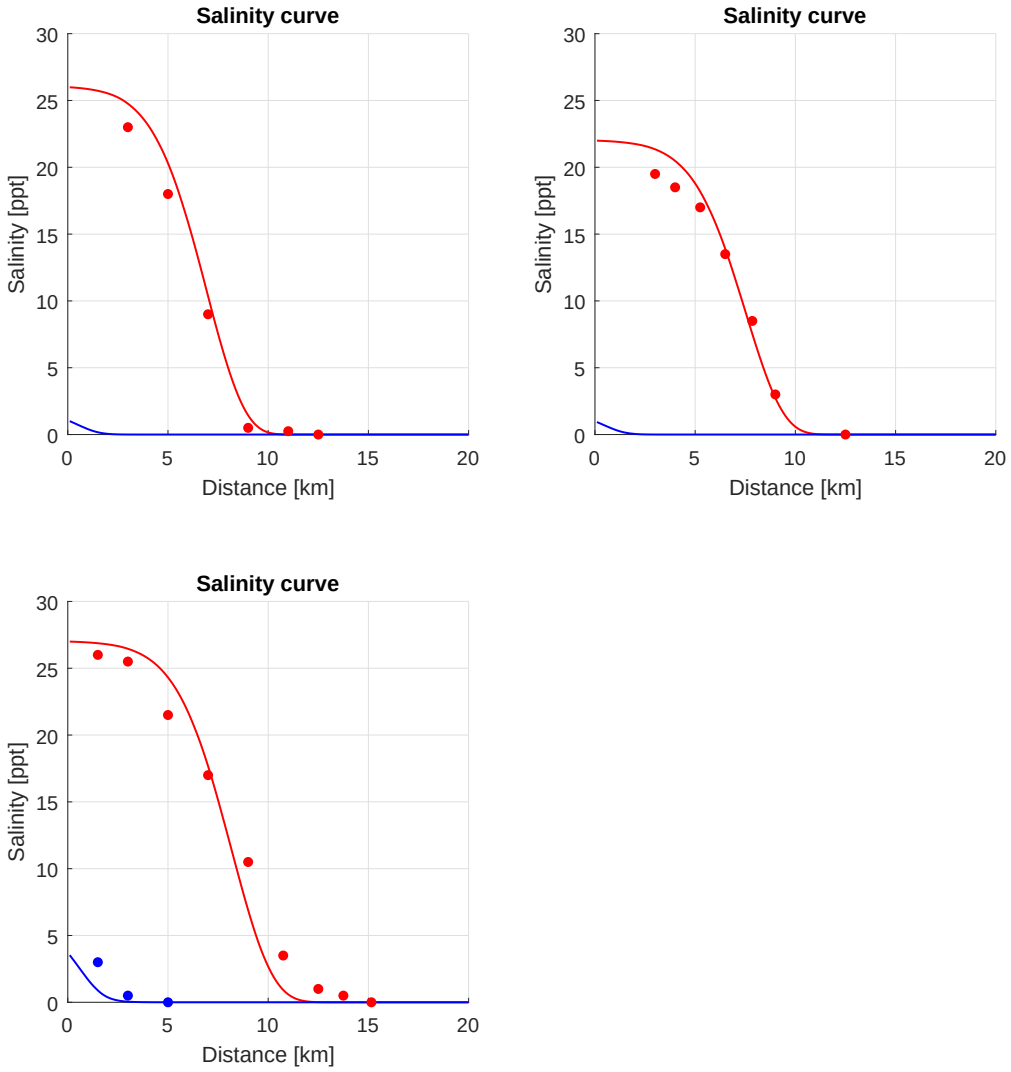

Figure D.70: *Salinity profile for the Sinnamary estuary*

D.8 Kuijper and van Rijn, Dispersion for prismatic channels

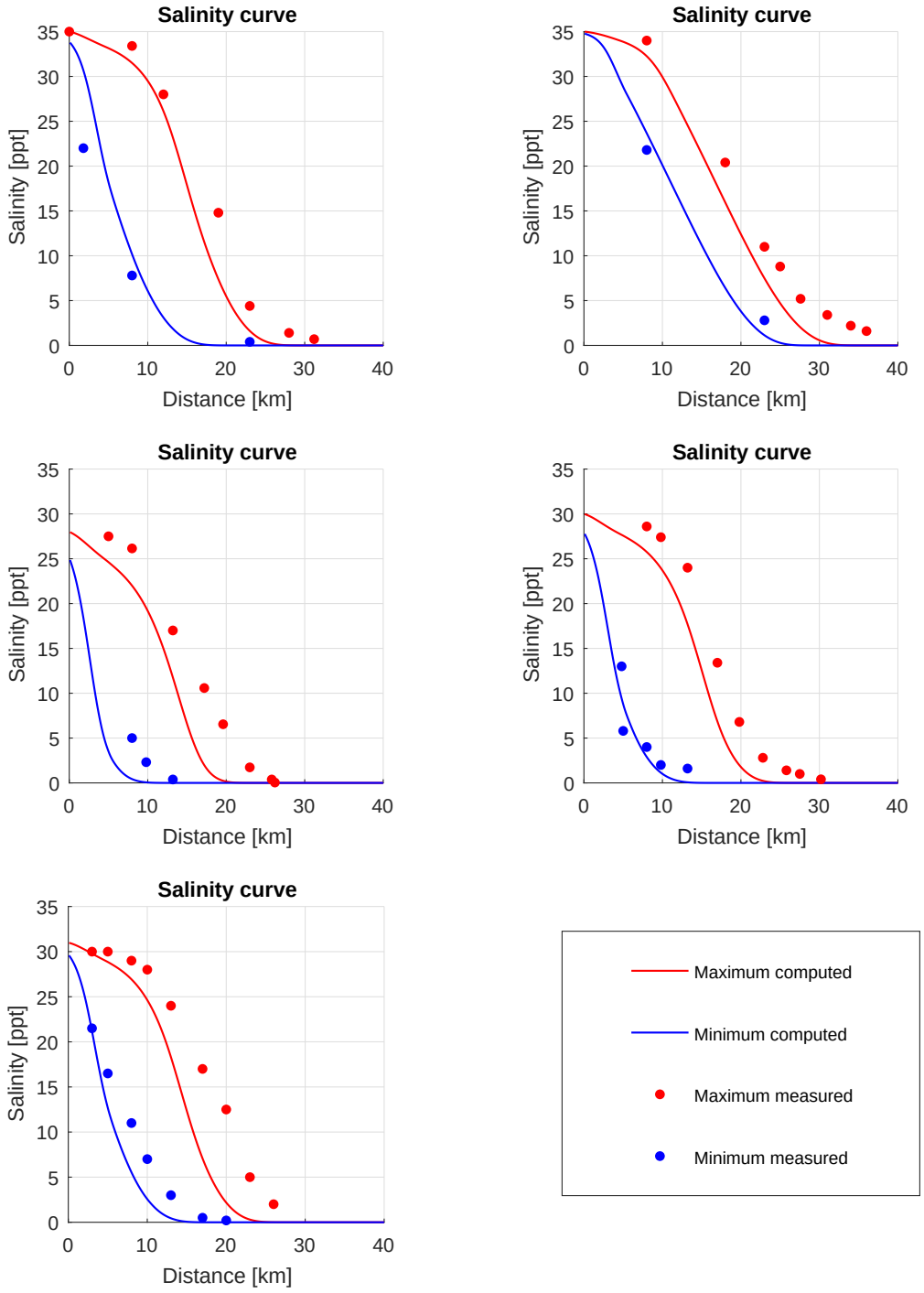

Figure D.71: *Salinity profile for the Maputo estuary*

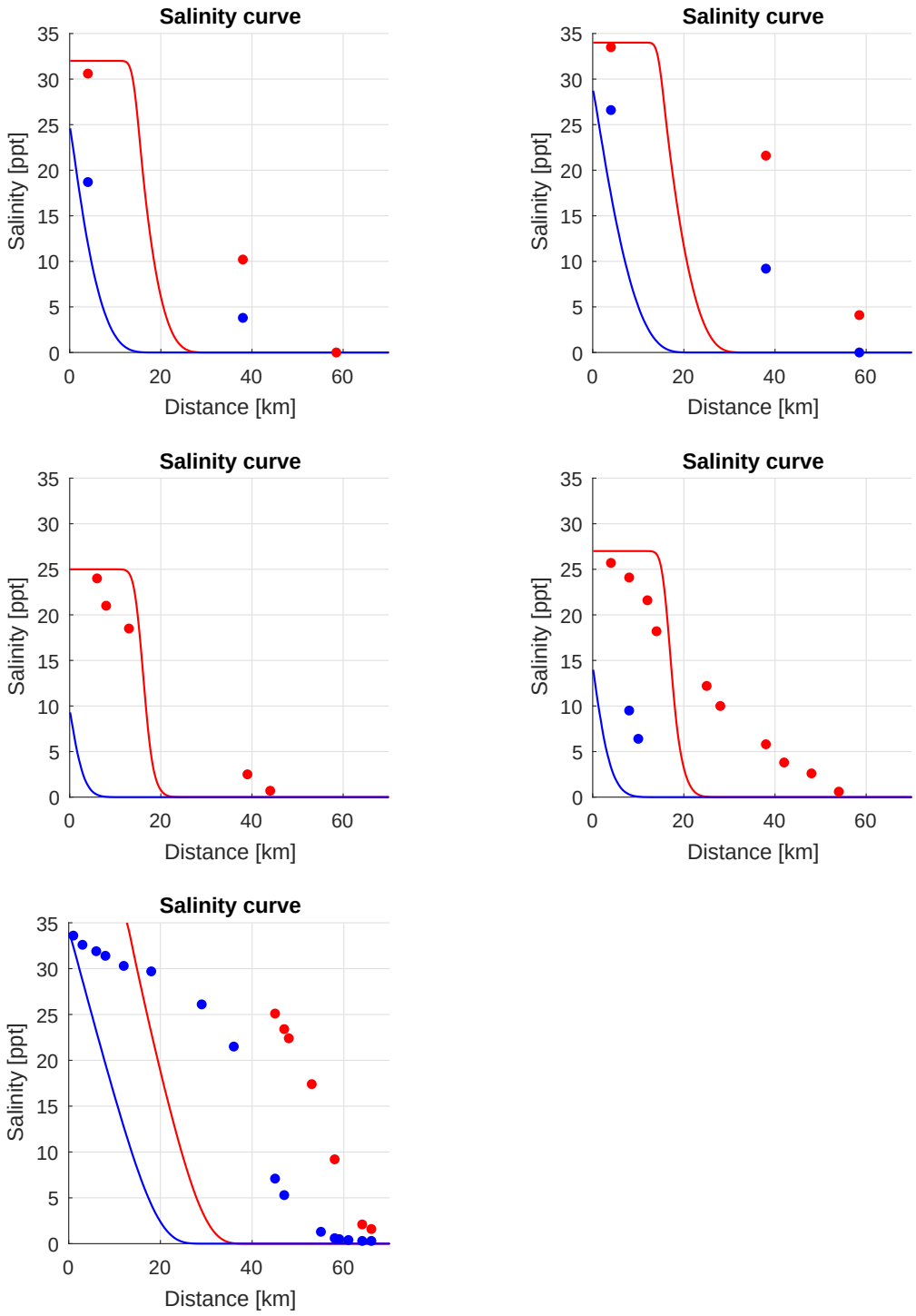

Figure D.72: *Salinity profile for the Pungue estuary*

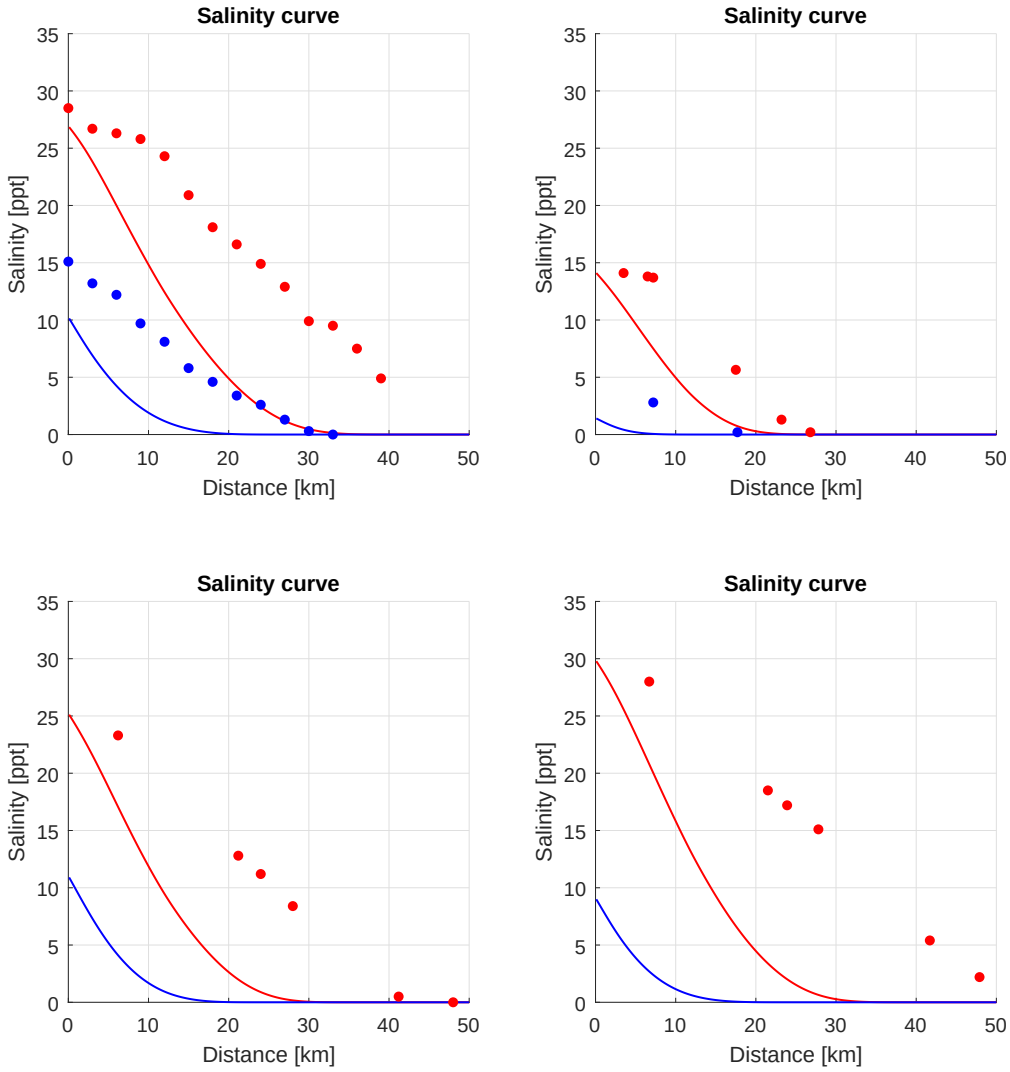

Figure D.73: *Salinity profile for the ChaoPhya estuary*

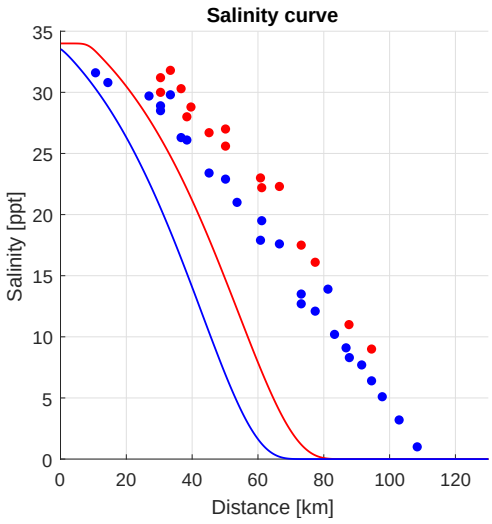

Figure D.74: *Salinity profile for the Westerschelde estuary*

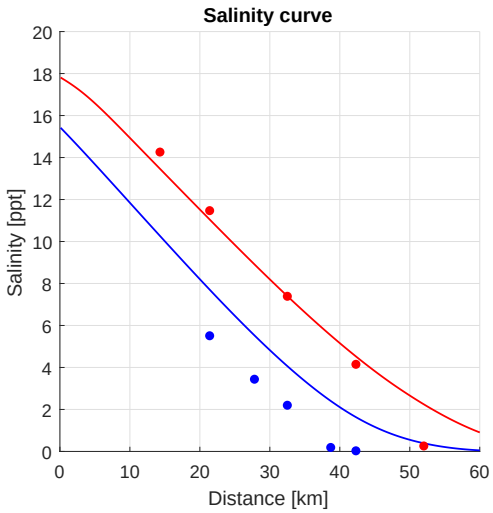

Figure D.75: *Salinity profile for the Landak estuary*

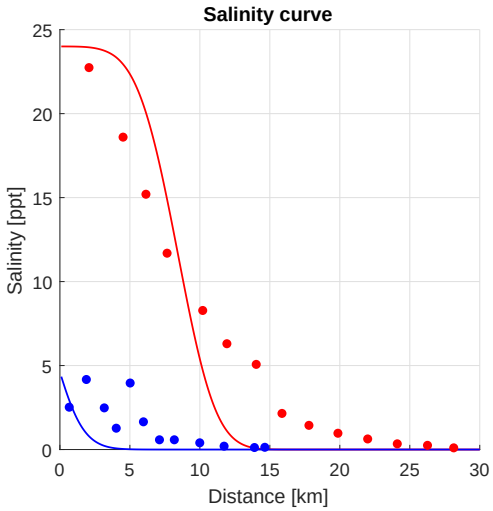

Figure D.76: *Salinity profile for the Perak estuary*

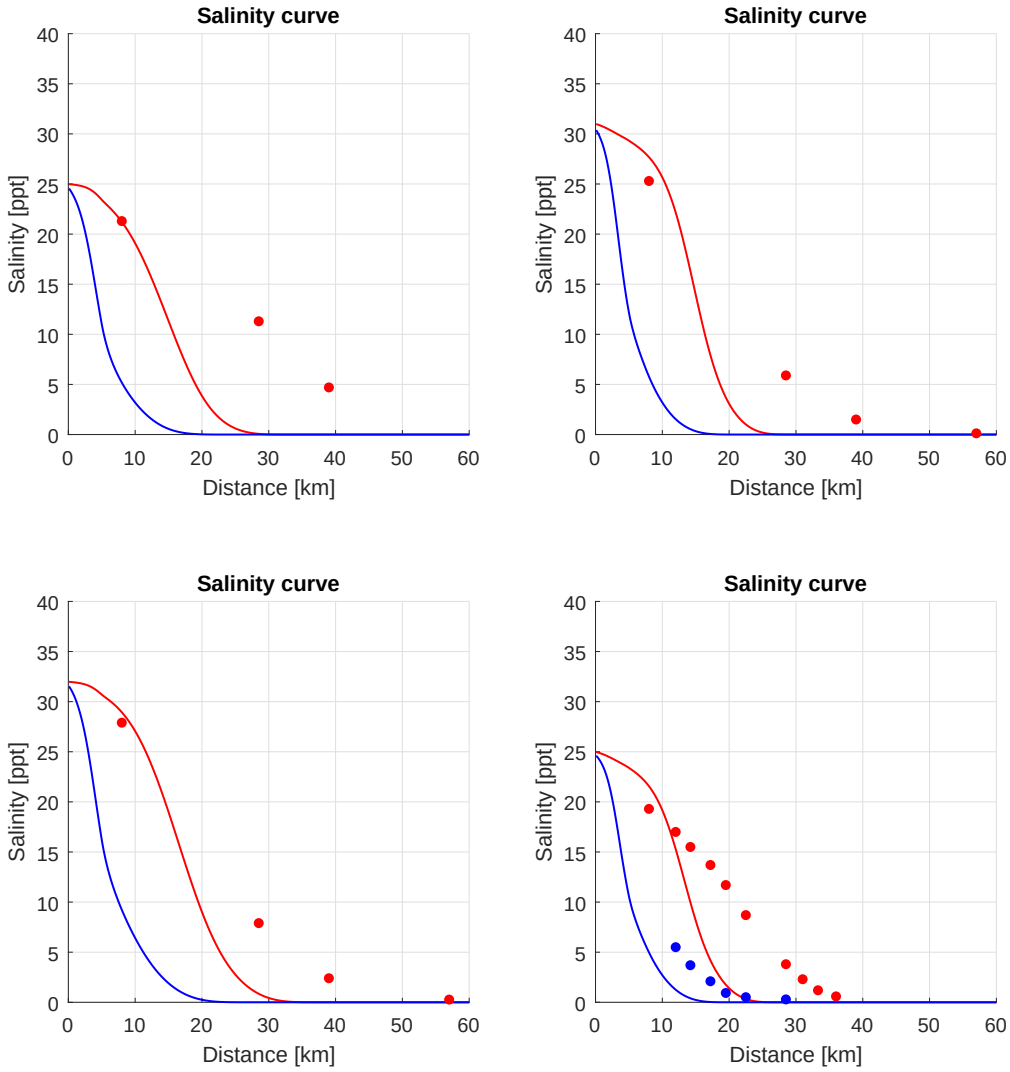

Figure D.77: *Salinity profile for the ThaChin estuary*

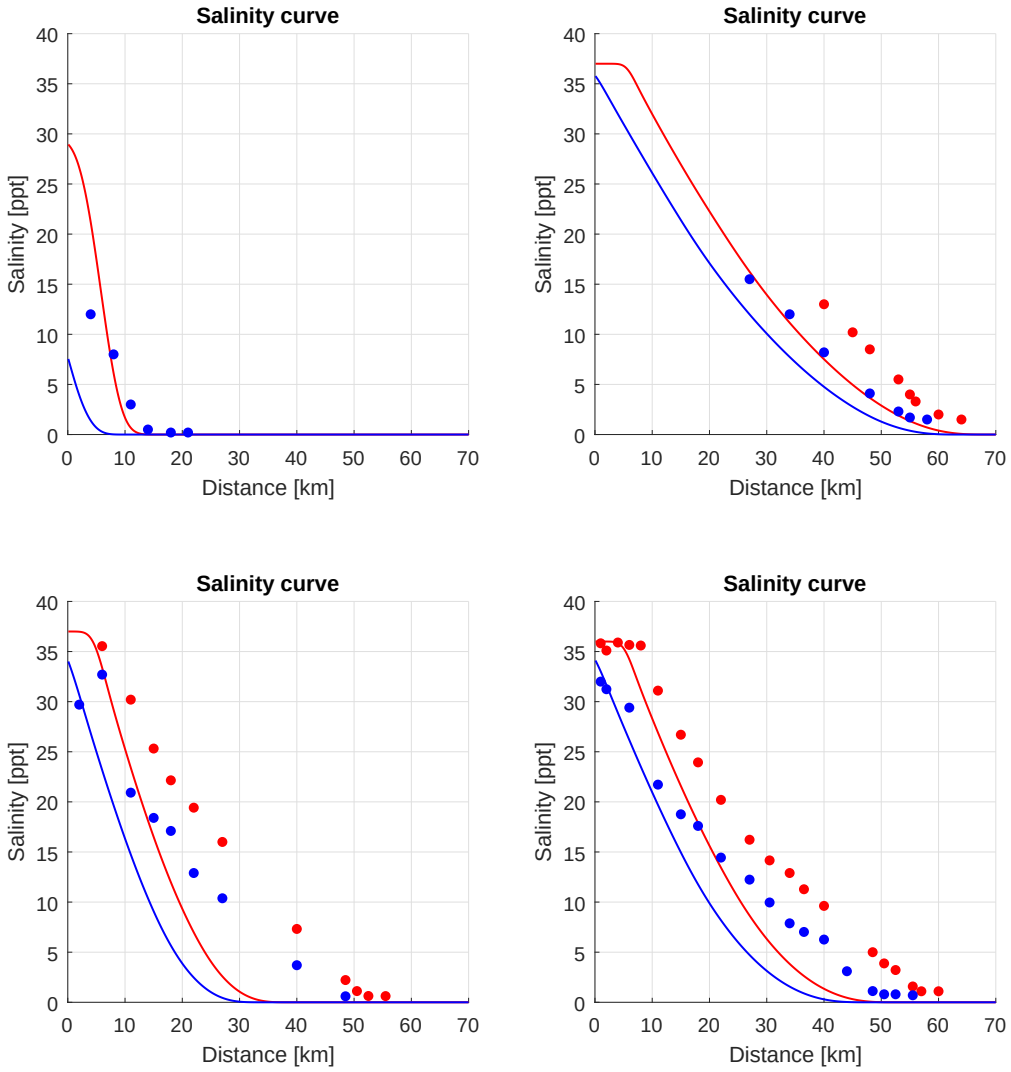

Figure D.78: *Salinity profile for the Limpopo estuary*

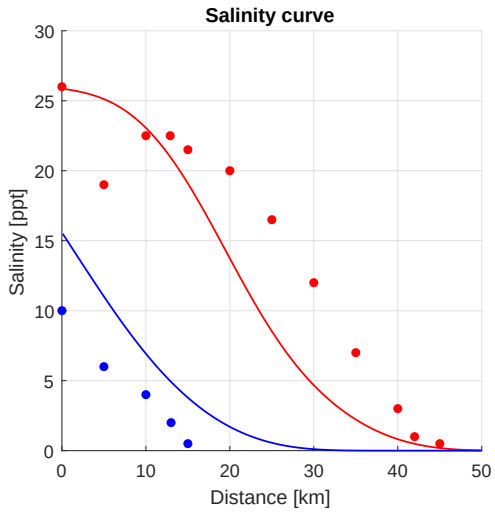

Figure D.79: *Salinity profile for the Lalang estuary*

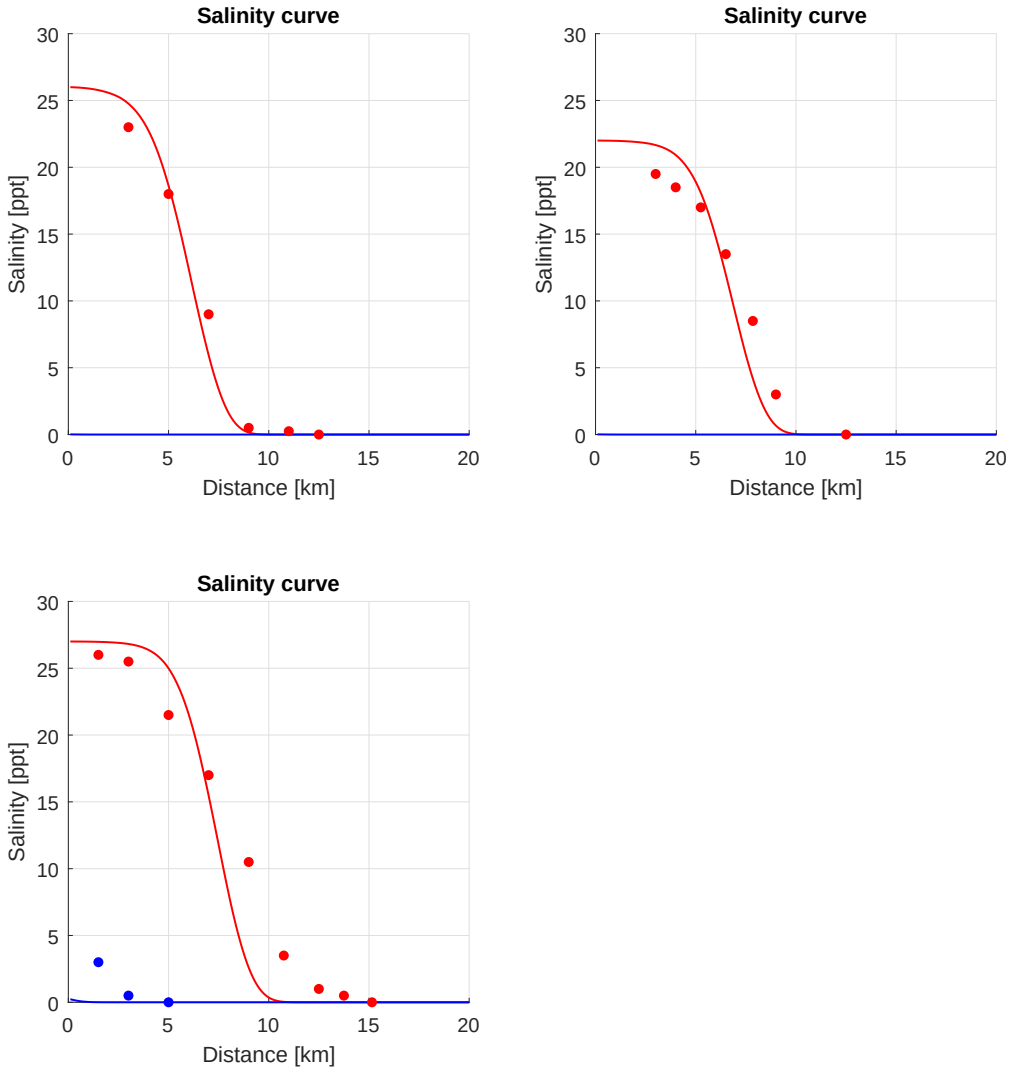

Figure D.80: *Salinity profile for the Sinnamary estuary*

E Effect of individual adjustments

Original TH-formulation:

$$D = \alpha(\frac{\Delta\rho}{\rho})^{\frac{1}{4}} Q_f^{\frac{1}{4}} B_0^{-\frac{1}{4}} u_0^{-\frac{3}{4}} < \frac{S}{S_0}\frac{\partial S}{\partial x} > \qquad \alpha = f_4 \frac{u_0^*}{S_0^*} L_e^2 (g\pi)^{\frac{1}{4}} \tag{E.1}$$

Adjusted formulations make use of the six additions or changes listed below. In addition also the relation with the salinity and salinity gradient is changed from $< \frac{S}{S_0}\frac{\partial S}{\partial x} >$ to $< \frac{S}{S_0} >< \frac{\partial S}{\partial x} >$, and in one case to $< \frac{S}{S_0} >^{\frac{1}{4}}$.

1 $+\frac{C}{\sqrt{g}}$
2 $+\frac{h}{E}$
3 $L_e \rightarrow E_0$
4 $N_R^{\frac{1}{4}} \rightarrow N_R^{\frac{1}{2}}$
5 $< \frac{S}{S_0}\frac{\partial S}{\partial x} > \rightarrow < \frac{S}{S_0} >^{\frac{1}{4}}$
6 $u_0^* \rightarrow u_0$

Since it is previously shown neglecting hydraulic dispersion, the so called f_3 term, does not significantly affect the model results, here it is assumed that the model results from the original TH-formulation can be compared with the ones below.

In the remainder of this appendix figures include the maximum (red) and minimum (blue) measured (striped) and computed (solid) intrusion lengths.

E.1 $+\frac{C}{\sqrt{g}}$

$$D = \alpha(\frac{\Delta\rho}{\rho})^{\frac{1}{4}} Q_f^{\frac{1}{4}} B_0^{-\frac{1}{4}} u_0^{-\frac{3}{4}} C < \frac{S}{S_0} >< \frac{\partial S}{\partial x} > \qquad \alpha = f_4 \frac{u_0^*}{S_0^*} L_e^2 (\frac{\pi}{g})^{\frac{1}{4}} \tag{E.2}$$

Since C only varies in the test with variable bed roughness and g is a constant only a difference in model results is expected for this respective test. The general behavior for the other series is not much affected. For a changing bed roughness the model results are improved. An increasing maximum intrusion with increasing C is observed due to this change. The minimum intrusion shows also an improvement, but still decreases with increasing C which is in contradiction with the measurements.

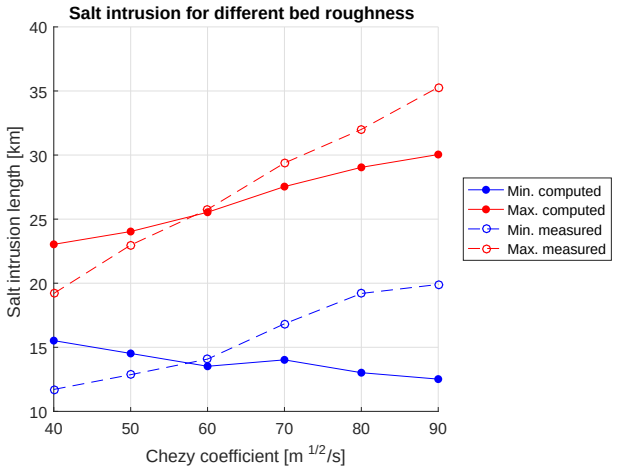

Figure E.1: *Effect of* $\frac{C}{\sqrt{g}}$

E.2 $+\frac{h}{E}$

$$D = \alpha(\frac{\Delta\rho}{\rho})^{\frac{1}{4}} Q_f^{\frac{1}{4}} B_0^{-\frac{1}{4}} u_0^{-\frac{7}{4}} h < \frac{S}{S_0} \frac{\partial S}{\partial x} > \qquad \alpha = f_4 \frac{u_0^*}{S_0^*} L_e^2 (\frac{g\pi^5}{T})^{\frac{1}{4}} \tag{E.3}$$

This term is added to better represent the effect of a changing water depth. It should be noted that this proposal was based on the work of Savenije and Kuijper, who both use the tidal excursion E instead of the estuary length L_e as a length scale. Now the tidal excursion introduces a stronger negative dependency on the maximum flood velocity u_0, which also affects the model results.
It was thus expected that by adding this term the results for the test series with different water depths should improve. In addition the proportionality to $u_0^{-\frac{7}{4}}$ is expected to affect the simulation. The variables W, C, h, L_e and Q_f do affect the maximum flood velocity, while for a variable $\Delta\rho/\rho$ the maximum flood velocity is almost constant. Here focus is on the h-series. What is observed in the results is that the simulation for variable h gives an almost equal result as the original formula. The effect of h is contradicted by the effect of u_0. The power of u_0 in this formulation is negative and bigger absolutely.

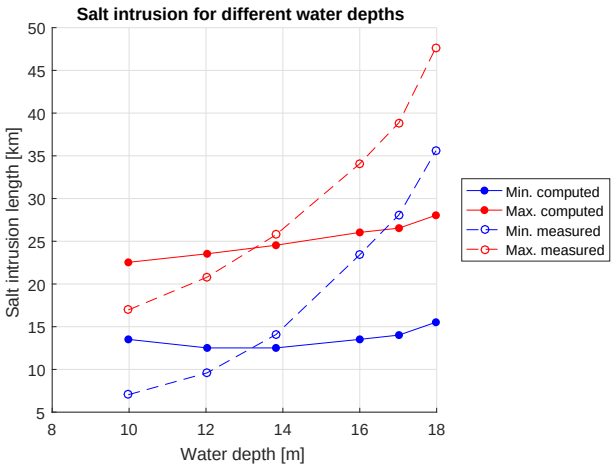

Figure E.2: *Effect of* $\frac{h}{E}$

E.3 $L_e \rightarrow E_0$

$$D = \alpha(\frac{\Delta\rho}{\rho})^{\frac{1}{4}} Q_f^{\frac{1}{4}} B_0^{-\frac{1}{4}} u_0^{\frac{5}{4}} < \frac{S}{S_0}\frac{\partial S}{\partial x} > \qquad \alpha = f_4 \frac{u_0^*}{S_0^*} T^2 (\frac{g}{\pi^7})^{\frac{1}{4}} \tag{E.4}$$

This change is introduced since the estuary length is hard to define and the tidal excursion is the actual length scale over which mixing occurs. The effect of this change is that power of the relation with u_0 changes from $-\frac{3}{4}$ to $\frac{5}{4}$. Therefore it is expected to see an improvement for C, h and Q_f, while a deterioration is expected for W and L_e.
Indeed a deterioration is observed for the series of W and L_e and an improvement for series C and h. The results for Q_f show improvements for small Q_f, but a too steep decline in intrusion length for large Q. The power of u_0 therefore seems to be to high, looking from this last perspective. As $\Delta\rho/\rho$ does not affect u_0 much its intrusion is not affected.

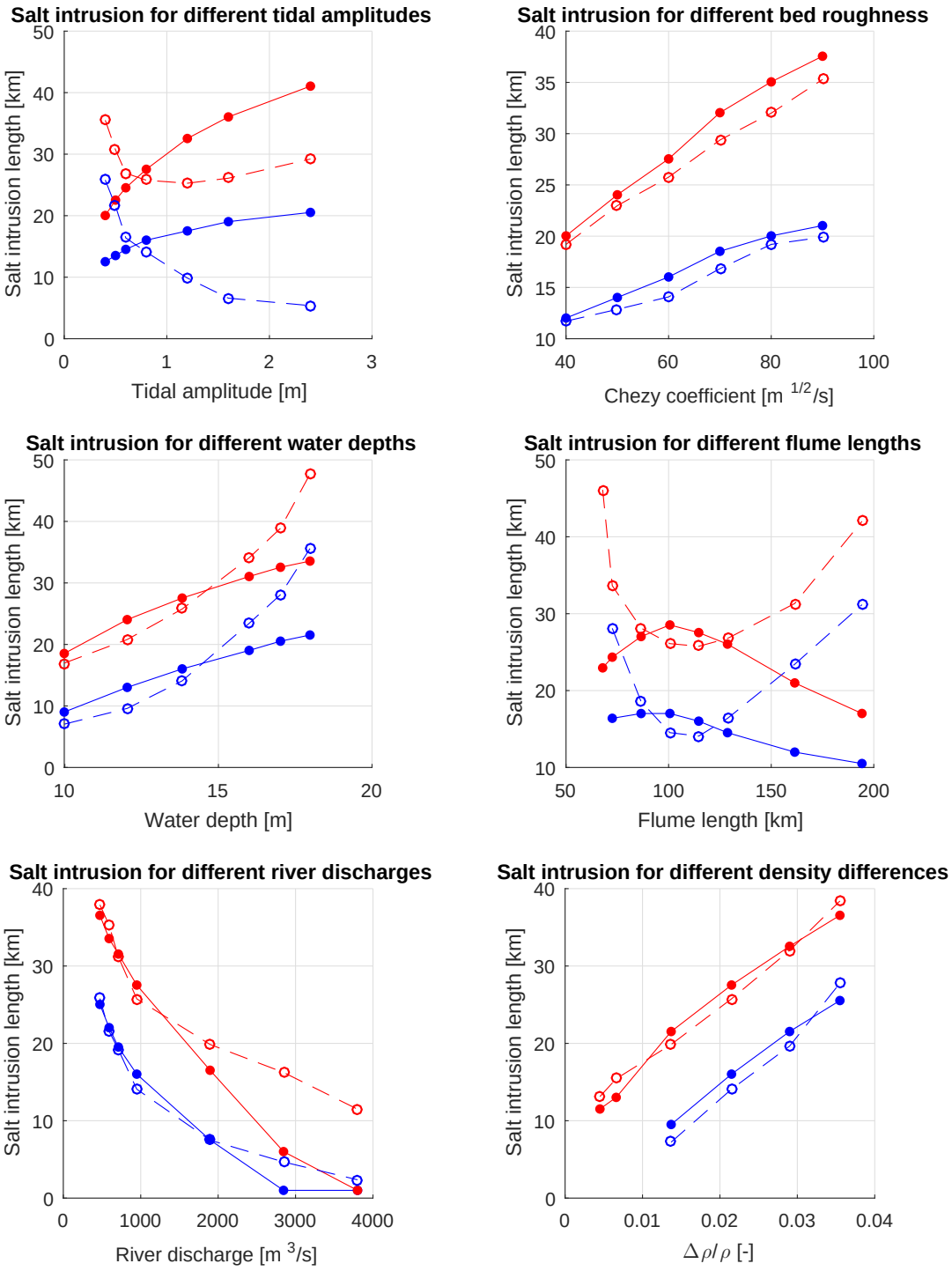

Figure E.3: *Effect of* $L_e \rightarrow E_0$

E.4 $N_R^{\frac{1}{4}} \rightarrow N_R^{\frac{1}{2}}$

$$D = \alpha(\frac{\Delta\rho}{\rho})^{\frac{1}{2}} Q_f^{\frac{1}{2}} B_0^{-\frac{1}{2}} u_0^{-\frac{3}{2}} < \frac{S}{S_0}\frac{\partial S}{\partial x} > \qquad \alpha = f_4 \frac{u_0^*}{S_0^*} L_e^2 \sqrt{g\pi} \tag{E.5}$$

By changing the power of the estuarine Richardson number N_R the dependency of the dispersion coefficient on $\Delta\rho/\rho$, Q_f, B_0 (but for this test it is constant) and u_0 change. Therefore changes are expected for all test series. Improvements are expected for W, L_e and $\Delta\rho/\rho$, deterioration is expected for C, h and Q_f.
Especially for small W there are improvements, only for the highest W the results are more off. For C the negative correlation increased. For low h the results deteriorated. For L_e the results show improvements. Those four effects can all be related to the change of the power of u_0.
The simulations of Q_f are affected by the change in the relation to both Q_f and u_0. There effects strengthen each other and the results are deteriorated. The strange increase for high discharges exploded and for low discharges the results are also off.
The simulations for $\Delta\rho/\rho$ show improvements. It is still doubtful if those improvements are the result of the higher power of N_R or the change from $< \frac{S}{S_0}\frac{\partial S}{\partial x} >$ to $< \frac{S}{S_0} >< \frac{\partial S}{\partial x} >$. In any case the higher power of N_R does help improve the results for changing densities.

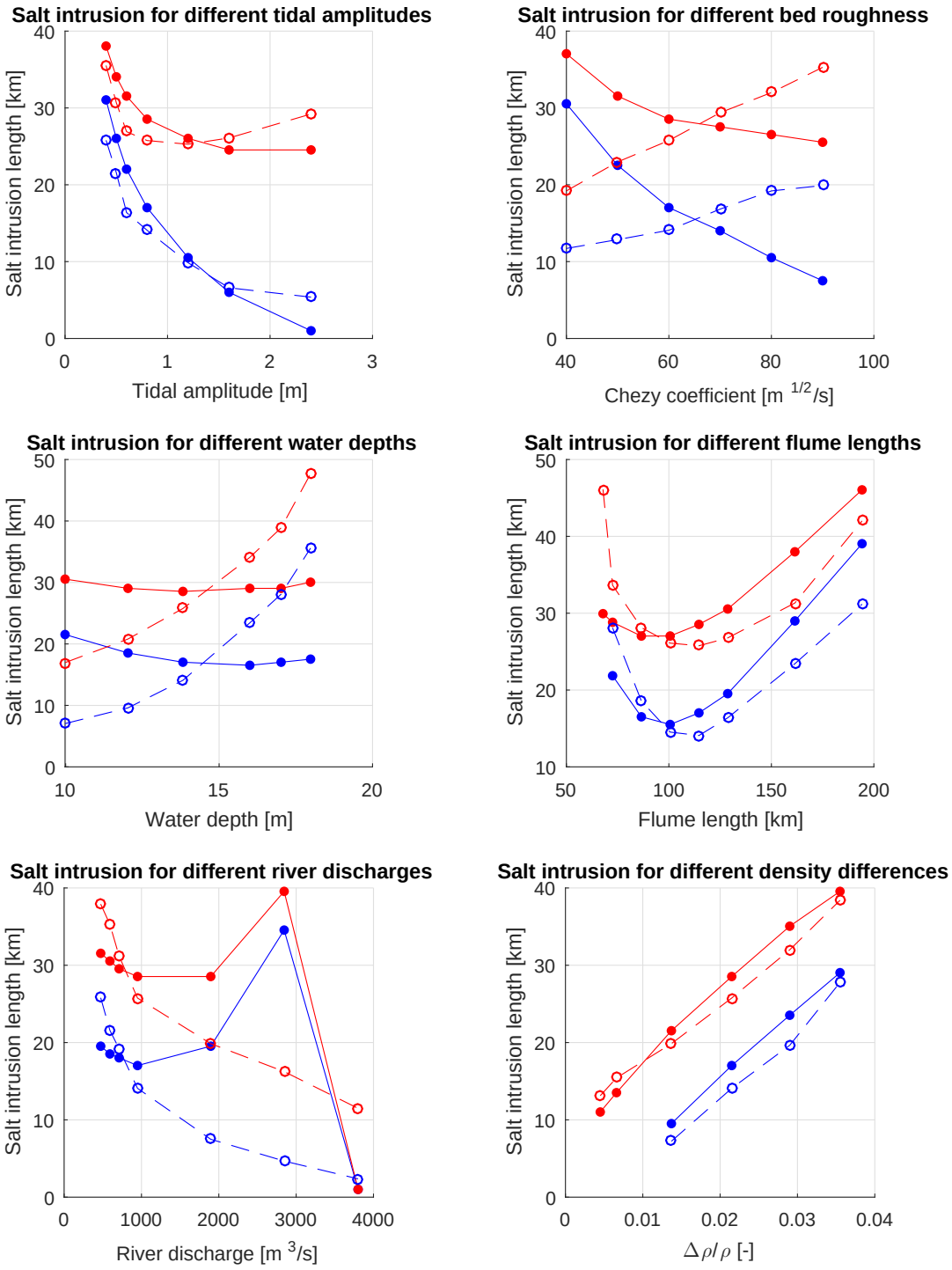

Figure E.4: *Effect of* $N_R^{\frac{1}{4}} \rightarrow N_R^{\frac{1}{2}}$

E.5 $< \frac{S}{S_0}\frac{\partial S}{\partial x} > \rightarrow < \frac{S}{S_0} >^{\frac{1}{4}}$

$$D = \alpha(\frac{\Delta\rho}{\rho})^{\frac{1}{4}} Q_f^{\frac{1}{4}} B_0^{-\frac{1}{4}} u_0^{-\frac{3}{4}} < \frac{S}{S_0} >^{\frac{1}{4}} \qquad \alpha = f_4 \frac{u_0^*}{S_0^*} L_e^2 (g\pi)^{\frac{1}{4}} \tag{E.6}$$

This adjustment to the formulation is expected to be most pronounced for convergent estuaries. As the flume test makes use of a prismatic channel it is hard to say what to expect.
What is observed is:
- W: very good simulation, behavior followed almost perfectly.
- C: deterioration, the inverse proportionality increased.
- h: minor improvement, there is now a increasing trend in intrusion with increasing water depth, however small.
- L_e: improved, however still quite off for low L, for higher flume lengths improved results.
- Q_f: improved, especially for low Q, the bump is still present (was expected as the dependency on u_0 did not change).
-$\Delta\rho/\rho$: improved, the slope is better approached but still underestimated.

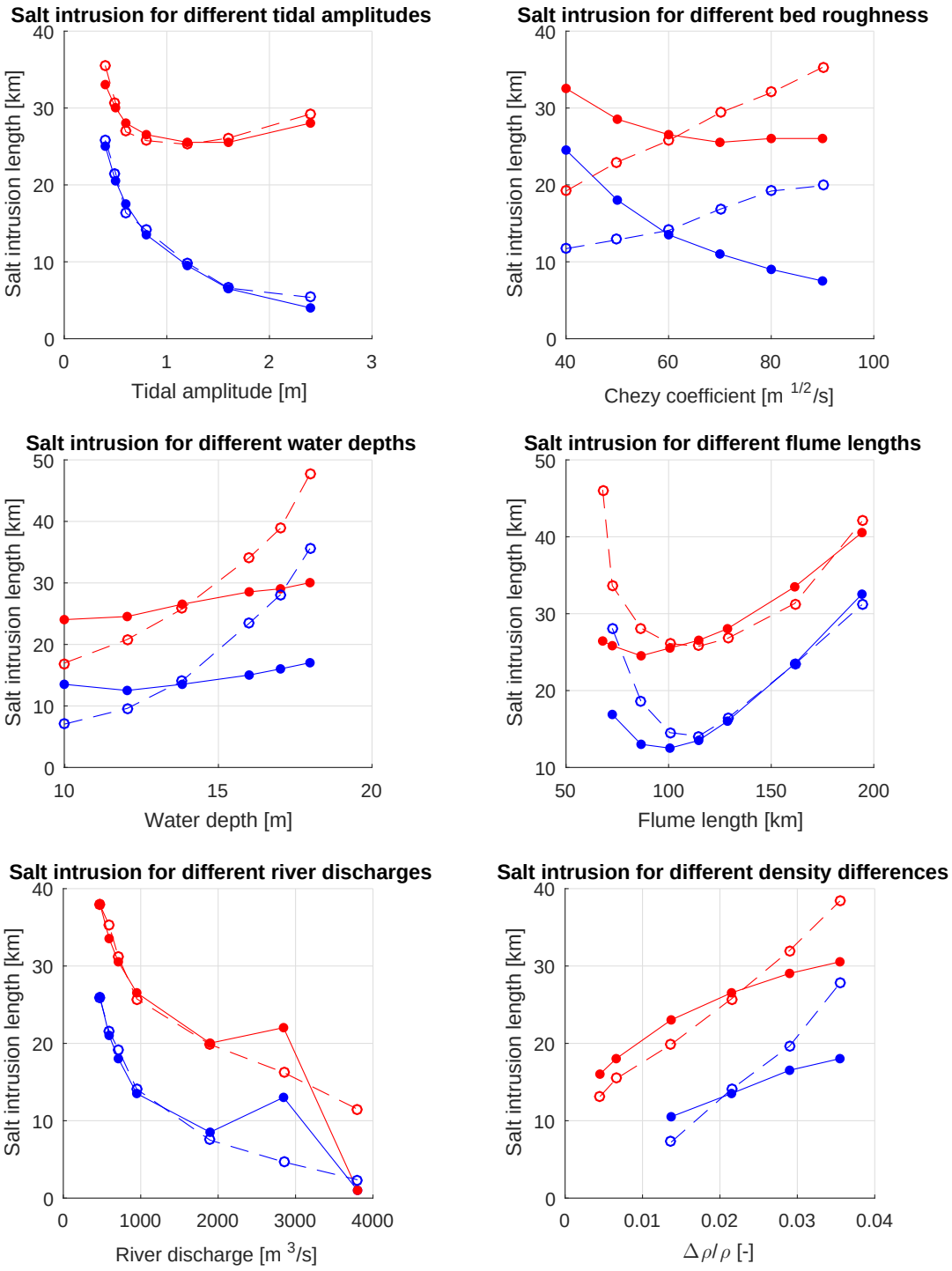

Figure E.5: *Effect of* $< \frac{S}{S_0} \frac{\partial S}{\partial x} > \rightarrow < \frac{S}{S_0} >^{\frac{1}{4}}$

E.6 $u_0^* \rightarrow u_0$

$$D = \alpha(\frac{\Delta\rho}{\rho})^{\frac{1}{4}} Q_f^{\frac{1}{4}} B_0^{-\frac{1}{4}} u_0^{\frac{1}{4}} < \frac{S}{S_0}\frac{\partial S}{\partial x} > \qquad \alpha = f_4 \frac{L_e^2}{S_0^*}(g\pi)^{\frac{1}{4}} \tag{E.7}$$

This adjustment only affects, again, the relation between D and u_0, the power changes from $-\frac{3}{4}$ to $\frac{1}{4}$. Improvements are expected for C, h and Q_f, while deterioration is expected for W and L_e.
Indeed the results for W and L_e are off. While improvements can be seen for C and h, however not sufficient yet. For increasing Q_f the intrusion decreases to fast, but at least the bump is gone. $\Delta\rho/\rho$ is only affected by the change from $< \frac{S}{S_0}\frac{\partial S}{\partial x} >$ to $< \frac{S}{S_0} >< \frac{\partial S}{\partial x} >$

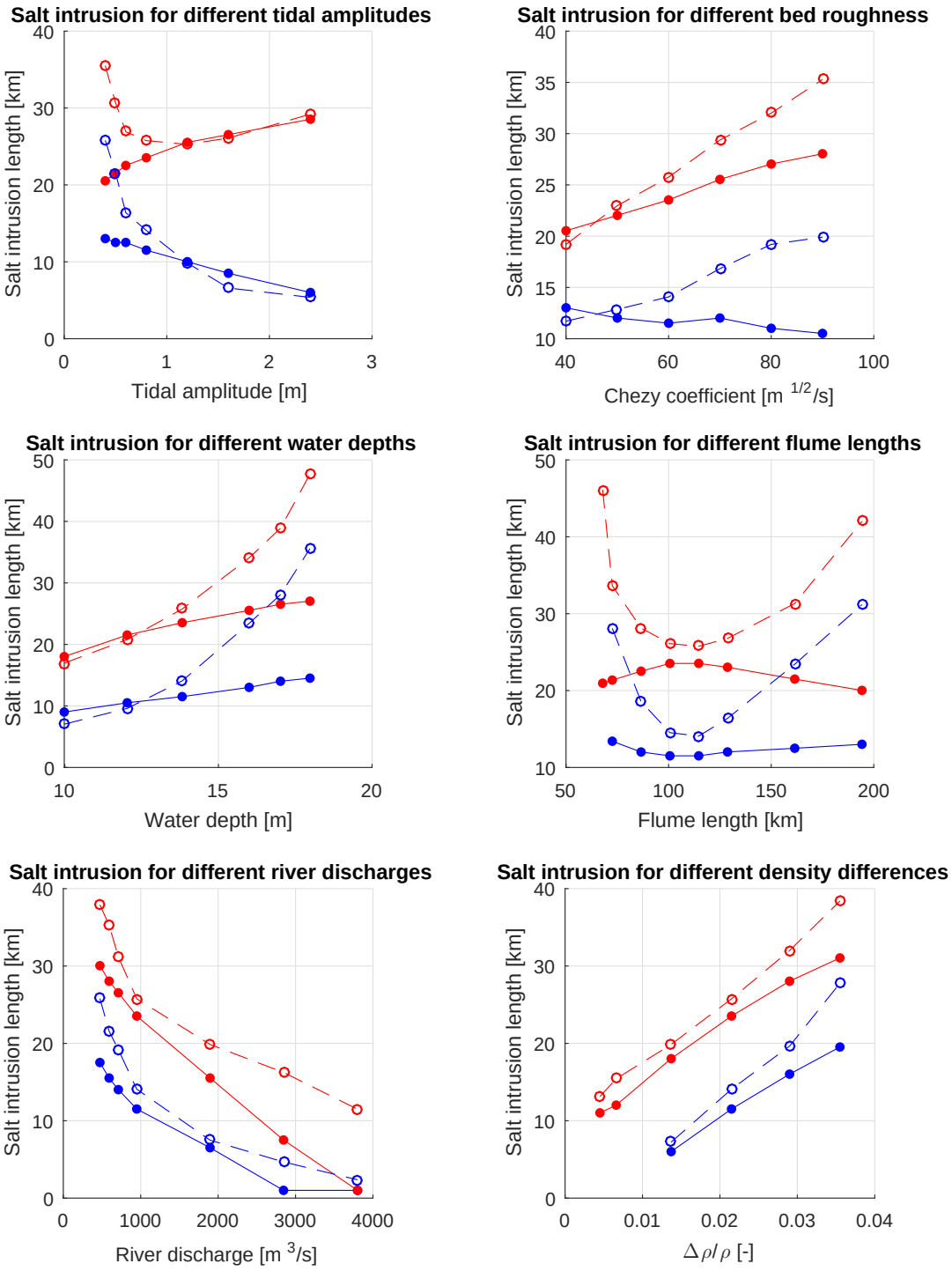

Figure E.6: *Effect of* $u_0^* \rightarrow u_0$

E.7 General conclusions

- $< \frac{S}{S_0} \frac{\partial S}{\partial x} >$ is not the same as $< \frac{S}{S_0} >< \frac{\partial S}{\partial x} >$. The change improves the results for the $\Delta\rho/\rho$ series.
- including $\frac{C}{\sqrt{g}}$ does improve the model results only for the C-series, it does not affect the others.
- including h will probably improve model results for h-series, here it is contradicted by the inclusion of E. This E also affects the other series, it improves the results for W and L_e while it deteriorates the results for C and Q_f.
- Changing estuary length L_e to tidal excursion E deteriorates the results for W and L_e, while it improves the results for C and h. For low Q_f the results also improve while for high Q_f the results are off, but so are the original ones.
- Enlarging the power of N_R results in a better simulation for W, L_e and $\Delta\rho/\rho$. At the same time it deteriorates the results for C and Q_f, and h only slightly.
- using $< \frac{S}{S_0} >^{\frac{1}{4}}$ should better represent convergent estuaries, however it also improves the results for the flume tests. The results for W, h, L_e, Q_f and $\Delta\rho/\rho$ are improved, while the results for C deteriorate.
- using u_0 instead of u_0^* deteriorates the model results for W and L_e, while the results for C improve and those for h and Q_f slightly.

F Improved definitions of P_e and $\hat{u}_0$

In this section the formula (Equation (F.1) for prismatic channels derived by Kuijper and Van Rijn (2011) is tested again for the tidal flume experiment[1]. Here P_e and $\hat{u}_0$ have been calculated based on the suggested adaptations in Chapter 7. One can see in Figure F.1 that the strange bump for the Q-series indeed disappeared. It should be noted that for extremely high discharges, where the direction of flow is only seaward salt does not intrude as an artifact of the boundary condition.

$$D_0^{TA} = 6\hat{u}_0 d_0 N_R^{0.5} \frac{C}{\sqrt{g}} \left(\frac{S_x^{TA}}{S_0^{TA}}\right)^K \tag{F.1}$$

Simulations for the C- and h-series slightly improve, while those for the A- and L-series slightly deteriorate. Table F.1 shows the values for R^2, $RMSE$ and σ for both the original series and the one using the improved values for P_e and $\hat{u}_0$. One can see that for the whole set the $RMSE$ and σ decrease significantly and also the reduced set gives slightly better results after implementing the improvements.

[1] Note: again the tidal averaged values for D and S are used.

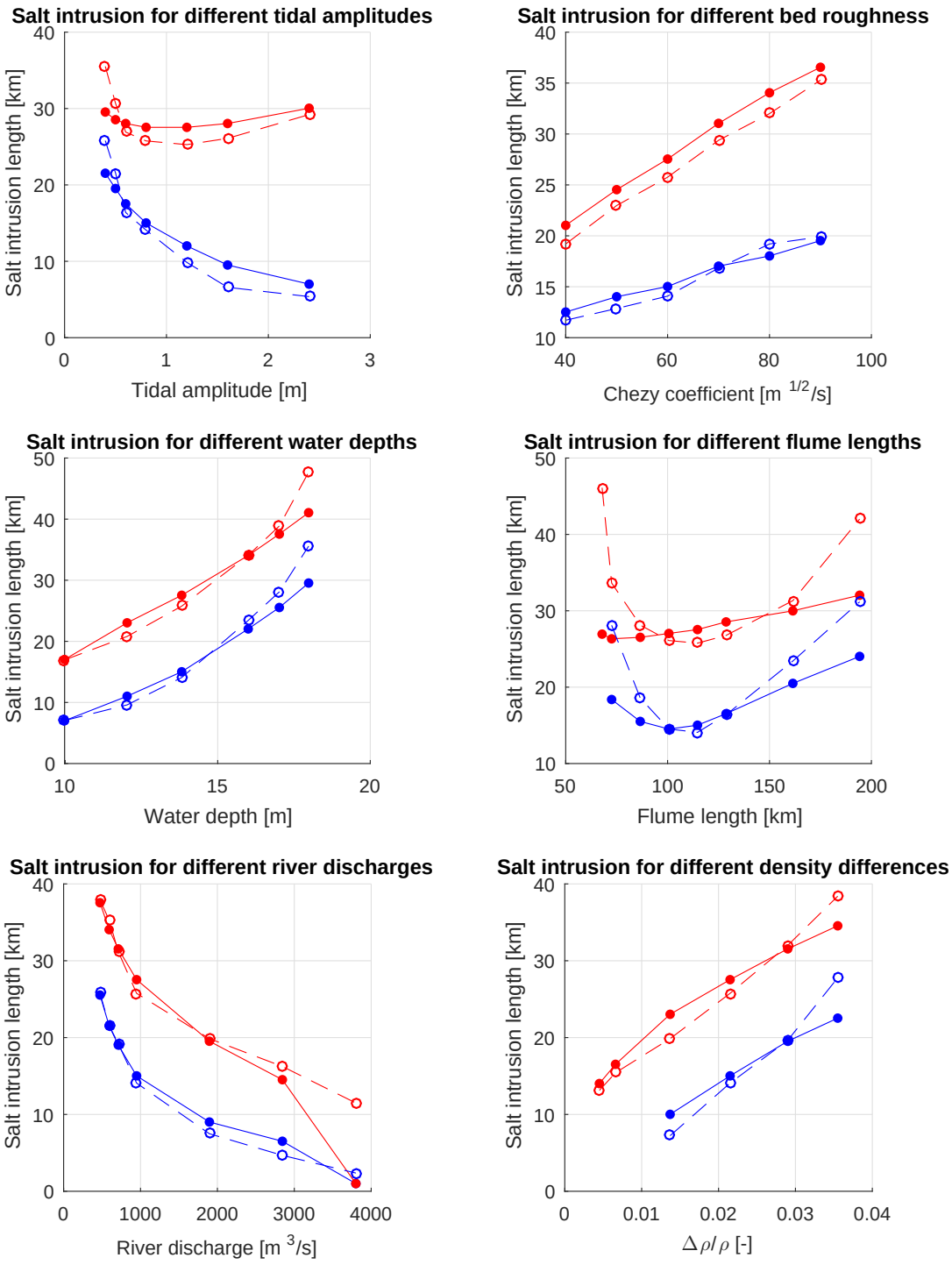

Figure F.1: *Measured and computed intrusion lengths for the tidal flume tests. Red indicates maximum intrusion, blue minimum intrusion. The solid line represents the model simulations and the dashed line the measurements.*

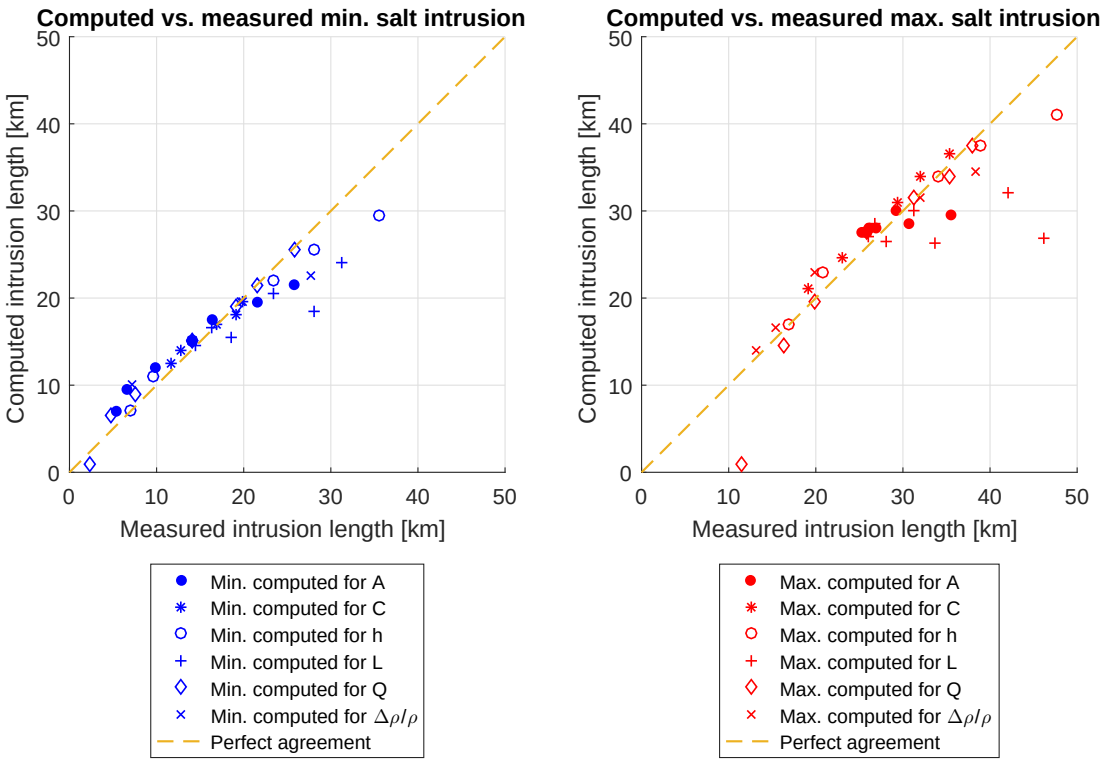

Figure F.2: *Measured vs. computed tidal intrusion lengths for the tidal flume test.*

Table F.1: *Quality criteria for model results*

	Original		Improved	
	All cases	Reduced set	All cases	Reduced set
R^2	0,82	0,87	0,86	0,87
$RMSE$	0,38	0,15	0,14	0,14
σ	0,39	0,15	0,14	0,14

G Predictive dispersion for prismatic channels by Kuijper and Van Rijn (2011) applied on real convergent estuaries

Equation (G.1) repeats the dispersion formulation for prismatic channels as described by Kuijper and Van Rijn (2011). Here this formulation is tested for real convergent estuaries, in order to research the effect of taking the depth as a length scale instead of the tidal excursion.

$$D_0^{HWS} = 6\hat{u}_0 d_0 N_R^{0.5} \frac{C}{\sqrt{g}} \left(\frac{S_x^{HWS}}{S_0^{HWS}}\right)^K \tag{G.1}$$

Simulations of salt intrusion in real convergent estuaries have been compared for both the maximum salt intrusion length and the salinity profiles along an estuary (Appendix D. In Figure G.1 measured and computed maximum intrusion lengths are plotted. Table G.1 shows the values for R^2, $RMSE$, σ_L, B_e and σ_p.

There is quite some correlation between measured and simulated maximum intrusion as can be seen from Figure G.1 and the R^2-value. However, in general the salt intrusion is underestimated as can be seen from Figure G.1 and the B_e-value. It is worth mentioning that the maximum intrusion lengths for the Landak and Lalang estuaries deviate from the general cloud of points. Those simulations are closer to the measurements than the others. The Landak and Lalang estuaries are narrow and have long intrusion lengths and are thus near prismatic.

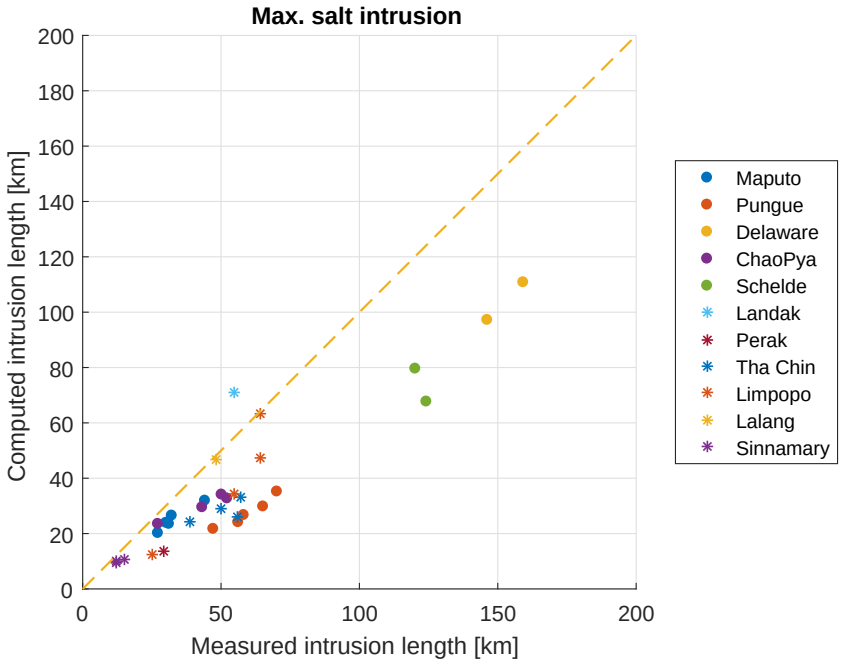

Figure G.1: *Measured vs. computed tidal intrusion lengths for real convergent estuaries. Dispersion is calculated with the dispersion formula for prismatic channels described by Kuijper and Van Rijn (2011).*

Table G.1: *Quality criteria for model results, in which σ_L and σ_p concern maximum intrusion and salinity profiles respectively.*

Criteria	Value
R^2	0,84
$RMSE$	0,37
σ_L	0,19
B_e	-3,49
σ_p	3,91